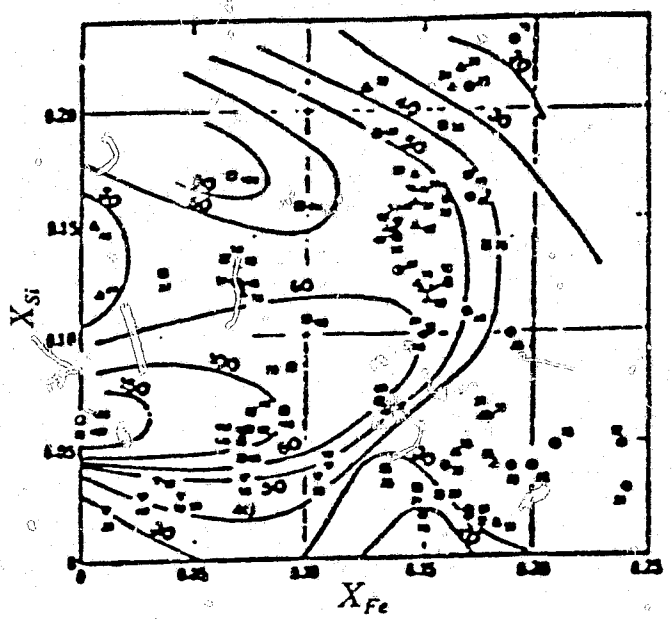

Figure 30 b. Isoactivity curves of Si in the Mn-Fe-Si-C melts saturated with C at 1500°C[119] ($\times 10^{-3}$). ▼, ▲, ■ and ● indicate the results in equilibrium with $MnO-SiO_2$, $CaO-MnO-SiO_2$, $CaO-MnO-Al_2O_3-SiO_2$ and $CaO-MnO-Al_2O_3-MgO-SiO_2$ slags respectively.

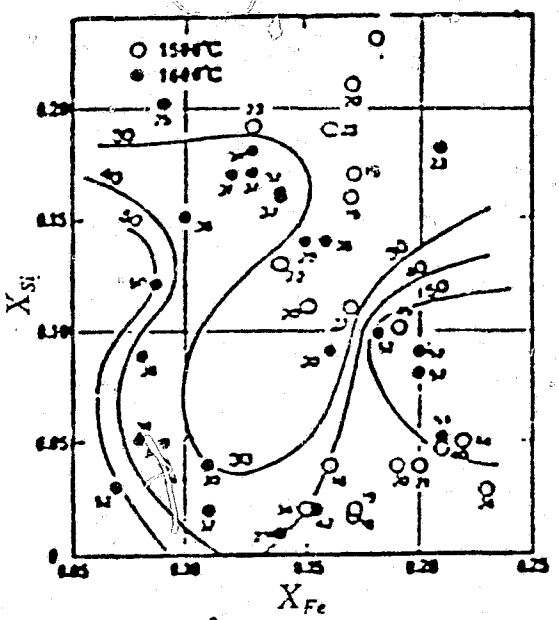

Figure 30 c. Values of a^2_{MnO}/a_{SiO_2} in the $CaO-MnO-Al_2O_3-MgO-SiO_2$ slags equilibrated with Mn-Fe-Si-C melts saturated with C ($\times 10^{-3}$). Contour lines are drawn by using the values at 1600°C[119].

is in low concentrations. There are very few studies on thermodynamics and metal-slag equilibria pertinent to high-carbon ferromanganese and silicomanganese smelting at typical process temperature of 1500°C. This work is directed to fill in some of these gaps.

3 EXPERIMENTAL TECHNIQUE AND PROCEDURE

3.1 Experimental technique

In this section a review of available experimental techniques for activity measurement and method adopted is presented.

3.1.1 Methods available for the measurements of activity of MnO in ferromanganese slags

The experimental techniques employed in the determination of thermodynamic properties of substances is very varied and diversified. These techniques can be summarized mainly in two groups as calorimetric methods and equilibration methods. Many methods are available for the determination of the activity of compounds in solution, but only some of them are suitable for determining the activity values of metal oxides in molten slags[121,122].

The thermodynamic functions like the heat (enthalpy) of formation at 298°K, the standard entropy, the heat capacity, the heats (enthalpy) of transition (fusion, evaporation, etc.) and enthalpies and entropies of solutions are the quantities for the thermodynamic description of substances. All of these thermodynamic functions can be used in the calculation of corresponding Gibbs free energies. Elevation of the boiling point and the depression of the freezing point can also be mentioned as a method in the determination of the thermodynamic functions of the substances. All these data can be obtained by means of suitable calorimeters.

However, these quantities can be measured with different type of apparatus employing different type of calorimeters[121,122]. Application of each calorimeter is restricted to a certain range of temperature and to a certain type of thermodynamic measurement. On the other hand, these methods rely on the accurate determinations of the thermodynamic data which are difficult to measure at the temperatures involved and the accurate temperature depression measurements may not be possible due to supercooling and superheating. There are many cases that the existence of metallic and covalent bonding prevents the determination of standard entropies, thus, the Gibbs free energies can not be calculated. Therefore, the methods of direct measurement of Gibbs free energy gain importance.

The Gibbs-Duhem equation can also be mentioned as a useful method to calculate the activity of one component of a solution where the activity of the other component is known experimentally.

The equilibration methods can in principle be broadly grouped under three sections:
-Vaporization techniques,
-Electromotive force measurement techniques,
-Gas equilibration techniques.
Vaporization and gas equilibration techniques involve static methods, dynamic methods, closed system techniques, open system techniques, direct measurement types, indirect measurement types, transportation types, recirculating types, and methods based on rates of evaporation. On the other hand, in electromotive force

measurement techniques solid and liquid electrolyte types and gas electrodes in oxygen concentration cells are employed.

In principle, the equilibration techniques are same for both the oxide and sulphide systems. However, they nee certain prerequisites as proper gas phases, etc. The crucible material chosen at high temperatures is also very important. Metal crucibles can easily be used to contain the oxides. Otherwise, the oxide system to be investigated must be saturated with respect to the crucible oxide in case of using an oxide refractory. As an example, a slag phase can be contained in a silica crucible if the slag is saturated with respect to silica.

Metals can easily be contained in oxide crucibles provided that the oxide crucible is not porous. In the case of containing both metal and oxide phases in the same crucible, the problem is more severe. In this case, carbon crucibles under reducing or inert atmospheres could be used, but the metal phase will usually be saturated with carbon. The sulphides are usually contained in proper oxide crucibles such as silica provided that sulphides are not oxidized.

The dew-point measurements are employed as a vaporization technique to obtain activities of components in solution by making use of an electric resistance furnace with two independently heated portions. This technique is suitable for systems where one of the components has a high vapour pressure compared

to others. For example, brass which is an alloy of Cu and volatile Zn and sulphide mixture containing volatile PbS or SnS may require the use of the dew-point technique. In this technique, the sample is placed in an evacuated long silica tube. Both ends of the silica tube are provided with measuring thermocouples. The temperature of the furnace is raised to the required value, and then the end away from the sample is slowly cooled. The coolest portion of the silica tube is observed through viewing windows. At a certain temperature at the cool end, measured by a thermocouple, for example if brass is used as a sample, pure zinc condenses in small droplets. Heating and cooling of this part of the tube is repeated and dew-point of zinc can be determined within ±1°C. The vapour pressure of zinc at the dew-point temperature equals the zinc partial pressure of the brass at the experimental temperature. This method can also be applied to other vapours.

Another similar vaporization method is the iso-piestic technique. The principle is the same as that of the dew-point technique. In this technique, the temperatures of the hot and cold ends of the tube are fixed and the equilibrium composition of the alloy is determined. The activity of the volatile component in the alloy at the temperature of the hot end can then be calculated provided the vapour pressure temperature relation for the volatile component is known. The hot end may also be supplied with a row of several alloy specimens held in a temperature gradient rather than at constant temperature as a time saving device. Subsequent

analysis of alloy specimens produce a number of results per run due to the fact that the activity of the volatile component in the alloy varies with temperature.

The vaporization techniques are not usually suitable for the measurement of the vapour pressure of slag components due to their too low vapour pressures in general, and the problem of finding a suitable crucible which must be able to contain the slag and which can be evacuated and sealed. Obviously pure silica which works well with sulphides will not work for oxides which are not saturated with respect to silica.

The electromotive force (emf) of a cell in which a chemical reaction or change occurs is also measured to yield thermodynamic data[121,122]. The chemical reaction to be investigated must be capable of being harnessed in a galvanic cell in such a way that its energy produces emf. The main problem in using this technique is to find a suitable electrolyte for the cell which is envisaged. The second most important aspect of these measurements is the identification of a single electrode process which occurs reversibly at each electrode. This method have proved to be a valid and accepted technique for obtaining thermodynamic data at moderate to high temperatures, especially in the solid state where other methods are either difficult to apply or are inaccurate. This technique, on the other hand, is not favourable for application to the complex slag systems at high temperatures since most of electrolytes available start electronic conduction at these temperatures yielding in

unreliable results. Due to these reasons, the classical gas-equilibration technique was chosen for this investigation which is described in the next section.

3.1.2 Method adopted for the measurement of MnO activity in ferromanganese slags

The gas equilibration technique was used for the determination of activity-composition relations both in Pt-Mn alloys and in ferromanganese slags in the present study. The activity of an oxide component in a liquid or solid oxide solution can be determined by monitoring the oxygen partial pressure over the oxide solution at a given temperature[121,122]. In this method, the required oxygen partial pressures are generated by the mixing of certain gases.

The principle can also be used to generate partial pressures of sulphur or chlorine when suitable gas mixtures are chosen. The samples can be heated in a vertical or horizontal furnace, the former being more preferable for quenching of the sample after equilibration. The oxygen partial pressures in equilibrium with the oxide samples can be generated by O_2-Ar, air-N_2, CO-CO_2, H_2-H_2O, H_2-CO_2 mixtures depending upon the range of p_{O_2} required. O_2-Ar and air-N_2 mixtures can generate p_{O_2} values down to approximately 10^{-3} atm. Other mixtures are essential for lower p_{O_2} values. The details of the experimental set-up employing gas equilibration technique will be explained in details in following sections.

The method adopted for the measurements of MnO activities in ferromanganese slags involved the equilibrium of platinum strips with slag in a platinum crucible, and a partial pressure of oxygen was imposed by gas mixtures of CO and CO_2. If initially pure MnO is used instead of a slag containing MnO, the equilibrium constant for the reaction will be given by

$$MnO(s) = \underline{Mn} + 1/2O_2(g) \quad \text{.....(18)}$$

$$K' = a'_{Mn} \sqrt{(p'_{O_2})} \; / \; a'_{MnO} \quad \text{.....(45)}$$

The bar under Mn indicates that it is in solution. If a slag containing MnO is used, the equilibrium constant will be

$$(MnO) = \underline{Mn} + 1/2O_2(g) \quad \text{.....(18)}$$

$$K = a_{Mn} \sqrt{(P_{O_2})} \; / \; a_{MnO} \quad \text{.....(46)}$$

Since activities are used, and not concentration terms, the equilibrium constants given by equations (45) and (46) will be the true equilibrium constants and will be equal. Equating and re-arranging gives

$$a_{MnO} = \sqrt{p_{O_2} / p'_{O_2}}\ a'_{MnO}\ \frac{a_{Mn}}{a'_{Mn}} \quad \text{.....(47)}$$

and, when $a_{Mn} = a'_{Mn}$ equation (47) becomes

$$a_{MnO} = \sqrt{p_{O_2} / p'_{O_2}}\ a'_{MnO} \quad \text{.....(48)}$$

Therefore, p_{O_2} is the partial pressure of oxygen prevailing at the time of the experiment, p'_{O_2} is the partial pressure of oxygen that would be in equilibrium with pure MnO and an alloy that contains the same amount of manganese as was formed in the slag experiment, and a'_{MnO} is the activity of the stoichiometric MnO in the non-stoichiometric oxide that would be in equilibrium with p'_{O_2}. In this work p'_{O_2} values were generated together with a_{Mn} values during experiments on the Pt-Mn binary system. The a'_{MnO} values corresponding to the p'_{O_2} values were obtained from the work of Davies and Richardson[15] (Appendix A). Equation (48) yields a_{MnO} values with pure solid MnO as the standard state. The standard state was changed to pure liquid MnO at 1500°C (hypothetical) by making use of the following equilibrium:

$$MnO(s) = MnO(l) \quad \text{.....(49a)}$$

and the free energy of transformation of MnO was calculated through the equation (49b):

$$\Delta G^0 = 43932 - 20.77T \; J/mole \quad \ldots\ldots(49b)$$

for which $\Delta G^0 = 7103.24 J/mole$ at 1500°C[123].

3.2 Experimental set-up

3.2.1 The furnace assembly

A gas-tight vertical molybdenum wound resistance furnace heated electrically has been assembled and employed for equilibration runs in the determination of the Mn activities in Pt-Mn binary alloys, the MnO activities in synthetic ferromanganese slags and the study of slag-metal equilibrium. Figures 31 and 32 show the outline of the reaction furnace employed throughout the experimental runs and the complete experimental set-up respectively. Although the figures are self-explanatory, further comments on construction and operating characteristics of the experimental system are as follows.

The furnace shell is of mild steel which is water-cooled at the top and bottom. It is 46 cm in both length and diameter. A recrystallized alumina tube with an inside diameter of 50 mm was used as the work (reaction) tube. The reaction tube, or, the work tube, was water-cooled at both ends with brass plates and tubing. Bostik silicon

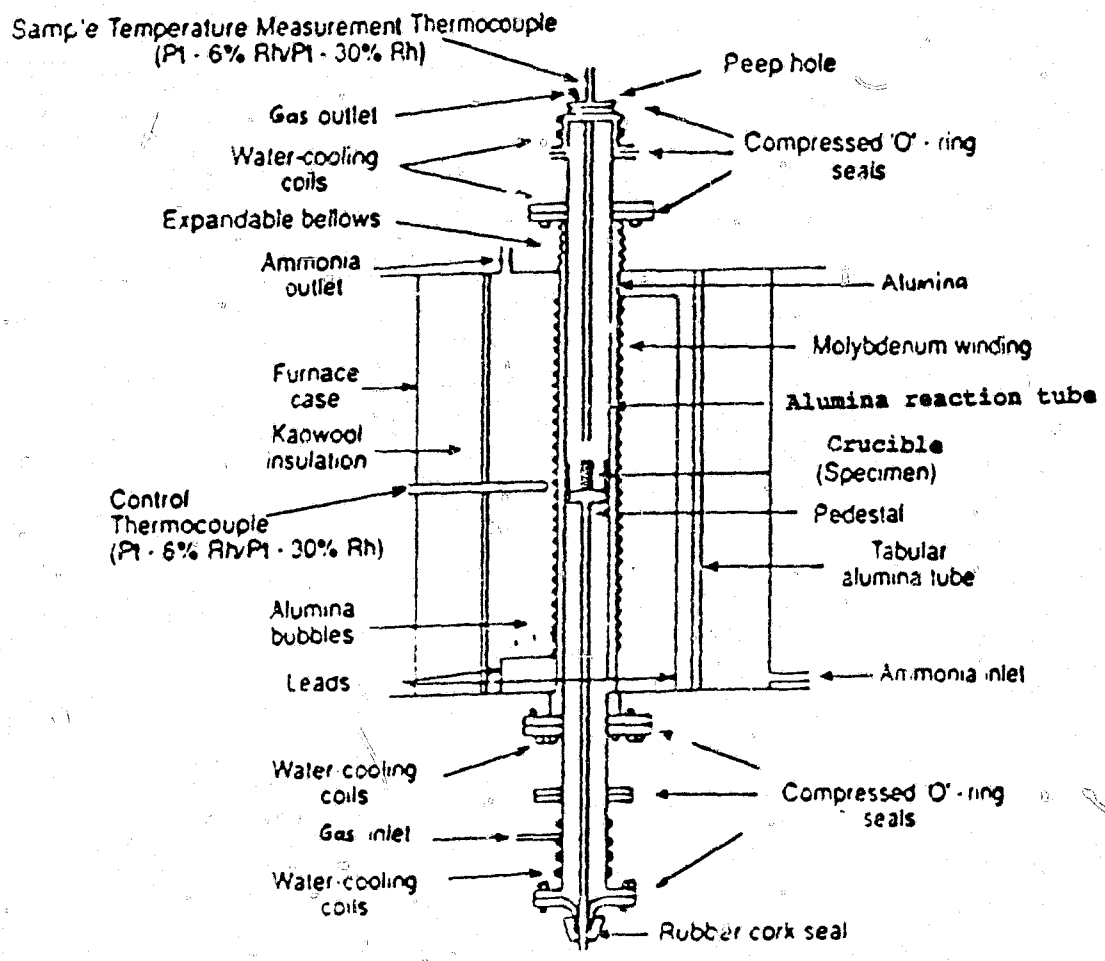

Figure 31. A cross-section of the vertical molybdenum wound resistance furnace.

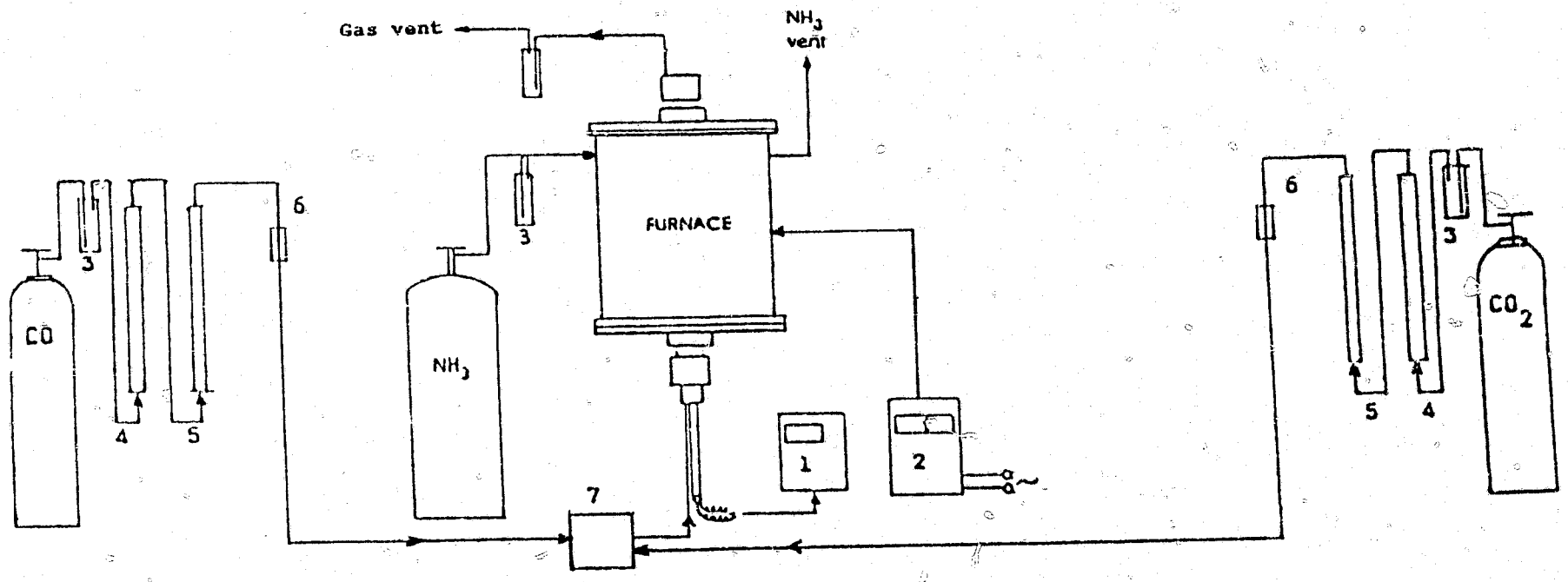

1. Digital temperature recorder
2. Eurotherm temperature controller
3. Gas bubbler
4. Silica gel drier
5. Magnesium perchlorate drier
6. Capillary flow-meters
7. Gas mixer

Figure 32. The complete experimental set-up.

seal was used as a sealent for the body of the furnace, and the work tube was fitted to the shell at the top and bottom with two compressed o-rings, which ensured gas-tight conditions. The top edge of the furnace was also additionally water-cooled with tubing in order to prevent the burning of silastic sealent due to the high temperature involved. Another alumina (heating) tube of a greater diameter was fitted around the work tube within the shell of the furnace. The molybdenum resistance elements were wound onto this alumina tube and were protected from oxidation by a reducing atmosphere provided by anhydrous ammonia which cracks into hydrogen and nitrogen at temperatures above 700°C. The cracking of anhydrous ammonia at higher temperatures (1300°, 1400°, and 1500°C) yields enough hydrogen to keep the oxygen potential below the equilibrium level needed for MoO formation. The anhydrous ammonia gas was introduced from the bottom end of the furnace through the ammonia inlet and, after passing through the furnace shell, was vented to the fume hood through the ammonia outlet at the top of the furnace shell. Similarly, the gas or gas mixture with which the reaction tube was continuously purged during operation was introduced from the bottom end of the furnace through the gas inlet which is on the bottom brass plate and, after passing through the reaction tube, was vented to the fume hood thrcugh the gas outlet which is on the top brass plate. For this reason, and also to avoid thermal shocks, the furnace was kept at 900°C and above when not in use. The molybdenum elements were covered by alumina cement for protection and embedded in a pool of spherical alumina bubbles (diameters in the range 1 mm to 3 mm) which served as thermal insulators. All this assembly, including the alumina bubbles was placed in a tabular alumina tube.

The space between the shell and the tabular alumina tube was filled with insulating wool. Two electrically insulated gas-tight terminals connected the windings to the electrical power cables.

A differential winding technique was used to obtain the desired temperature profile, which provided a 4 cm constant temperature zone at the centre. Approximately 22 meters of molybdenum resistance wire, 0.9 mm in diameter, were used for this purpose. The overall resistance was 1.65 ohm at room temperature. The normal current in the circuit was about 20 amperes when the furnace was operating at 1500°C.

3.2.2 The gas mixing system

The ancillary equipment for gas mixing purpose involved a gas purifying train and a mixer of conventional design. All the gases, before mixing, passed over drying columns of silica gel and anhydrous magnesium perchlorate and ascarite. In slag-metal distribution experiments, the CO gas was passed through ascarite and anhydrous magnesium perchlorate. For all experiments, the pressure in the system was equal to the ambient pressure. During the Pt-Mn binary system and ferromanganese slag experiments, the gas mixtures were obtained by means of the capillary tubes connected to U-tube manometers employing levelling bulbs and excess gas outlets. The gas mixing apparatus is shown in Figure 33.

The flow of each gas through capillaries was adjusted by the levelling bulbs containing a copper sulphate

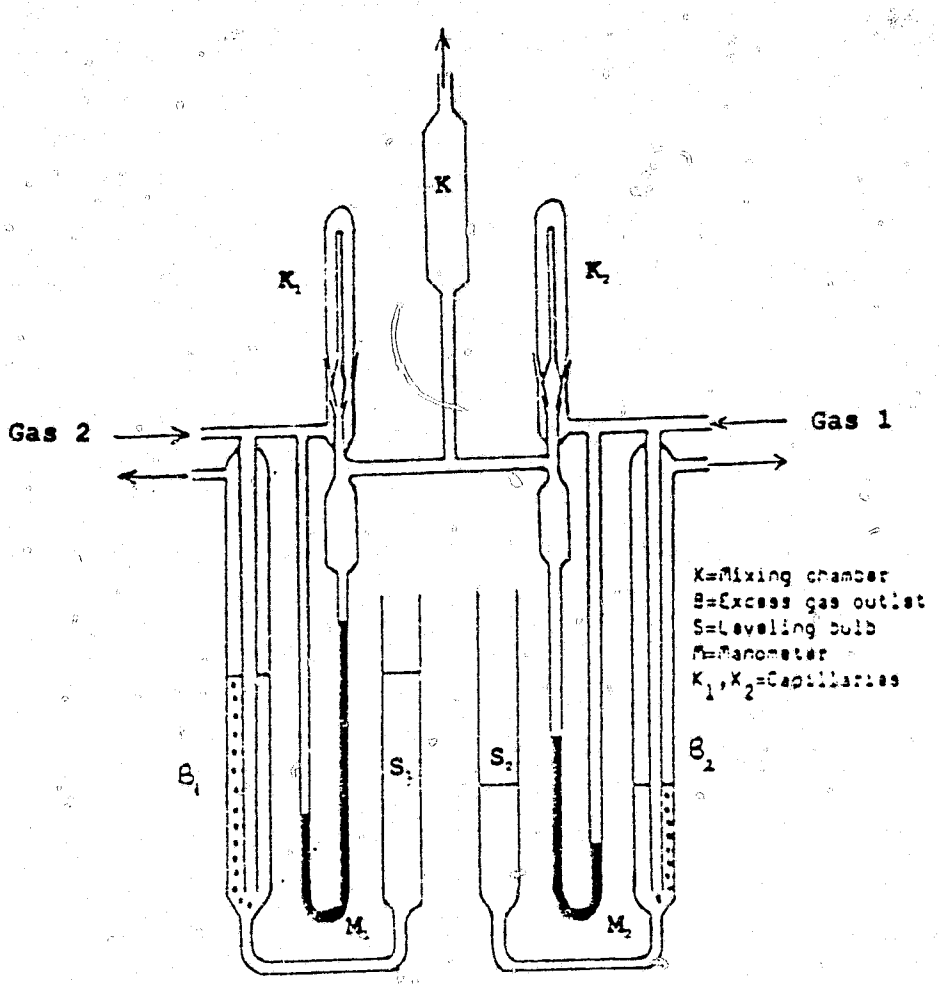

Figure 33. Gas mixing apparatus.

solution. The height of the levelling bulb determined the flow of the gas by adjusting the amount of flow of excess gas. This in turn determined the level of gas passing through the capillaries which was monitored by the U-tube manometers. Therefore, U-tube manometer-capillary combination was calibrated for both CO and CO_2 by the standard technique called bubble flow method. Details of gas mixing calibration, and the calculation procedure in obtaining desired partial pressures of oxygen are given in Appendix A.1.

Chemically pure CO and CO_2 gases were used (analysis given in Appendix B) in the experiments to determine the Mn activities in Pt-Mn binary system, the MnO activities in ferromanganese slags and the distribution of Mn between metal and slag phases.

3.2.3 Temperature control

Actual sample temperatures in the furnace were measured with a Pt-6%Rh/Pt-30%Rh (B-type) thermocouple which was calibrated against a standard thermocouple of the same composition, which was calibrated according to the melting points of gold, silver and copper. It is estimated that with this procedure the measured sample temperature were correct within ±2°C. The power unit of the furnace was a type 0703 25 A, 220 V, Eurotherm thyristor power pack which was connected to the furnace with a B-type thermocouple placed adjacent to the middle of the external surface of the heating windings. The unit was set according to the actual temperature readings registered by the previously mentioned thermocouple.

3.3 Sample preparation

The investigation was consisted of three stages which necessitated different sample preparation procedures to be applied for each stage.

3.3.1 Platinum strips and crucibles

The platinum specimens were 99.98 per cent pure and prepared as coupons with dimensions of 4 mm by 4 mm, cut from foil 0.025 mm thick.

The platinum crucibles were used in order to determine the Mn activities in Pt-Mn binary system and the MnO activities in synthetic ferromanganese slags. They were made by welding of platinum sheets (99.98 per cent pure) 0.125 mm thick with the following dimensions: 7 mm in diameter, 25 mm in depth, and a wall thickness of 0.125 mm. Prior to any experimental run with a platinum specimen, the platinum crucibles were equilibrated and thus saturated with pure MnO at the chosen gas mixture and the relevant experimental temperature, thus preventing the transfer of Mn into the platinum crucible instead of the platinum specimens.

In the slag-metal distribution experiments, graphite crucibles were used. They were produced from high purity graphite electrodes by cutting them into cylinders and drilling to give the final shape of a crucible with dimensions: 14 mm in internal diameter and 44 mm in height.

3.3.2 Preparation of synthetic MnO-CaO-MgO-SiO_2-Al_2O_3 slags

The slag was prepared as a homogeneous mixture made from its pure components. In total, 55 samples of slags of different compositions, containing MnO, CaO, MgO, SiO_2 and Al_2O_3 were prepared from analytical-reagent grade oxide powders. However, prior to use all the oxides except MnO, were first calcined in an electrical resistence-heated muffle furnace for about 24 hours at 1200°C. After cooling, the required amounts of CaO, MgO, SiO_2, and Al_2O_3 were carefully weighed and thoroughly mixed in the desired proportions to give slags of the designed compositions in an agate morter under a liquid blanket of acetone until all the acetone had vaporized. The dried mixtures were then pressed into disks by using an electro-servo hydraulic testing device (ESH), of the type used in material fatigue investigations. A cylindrical die of 20 mm in diameter was used to compress the mixtures by the ESH. The load employed for making the disks was about 4.5 tons. These disks were recalcined for 12 hours at about 1200°C in order to promote some useful sintering, and thereby homogenization, of the samples. On cooling, the homogenized disks were crushed and ground in an agate mortar and mixed with the required quantities of reagent-grade MnO in an agate mortar as described above before every individual run. The final product was heated at 110°C to drive off the acetone, cooled and charged into the MnO-saturated platinum crucibles. The rest of the disks were stored in sealed bottles for further experiments. As it was mentioned above, all the

mixing procedures were carried out under acetone in order to secure the best possible mixing of the oxide components.

The slag basicities ranged from about 0.4 to 1.2 and MnO contents ranged from 5 to 30 mass per cent. The initial Al_2O_3 content of slags were kept at 5 mass per cent level. After equilibration experiments there were slight deviations from this 5 mass per cent level for Al_2O_3 as reactions between the slag and platinum strips occurred. However, the data with values reasonably close to this level were treated as 5 mass per cent Al_2O_3 data. The initial slag compositions are shown in Table IV.

Table IV. The initial slag compositions.

Slag	MnO %	CaO %	MgO %	SiO_2 %
1	5.0	20.0	11.9	58.1
2	5.0	25.0	6.9	58.1
3	5.0	25.0	15.0	50.0
4	5.0	30.0	10.0	50.0
5	5.0	35.0	5.0	50.0
6	5.0	32.1	15.0	42.9
7	5.0	35.0	12.1	42.9
8	5.0	35.0	17.5	37.5
9	10.0	20.0	10.2	54.8
10	10.0	25.0	5.2	54.8
11	10.0	25.0	12.8	47.2
12	10.0	30.0	7.8	47.2
13	10.0	35.0	2.8	47.2
14	10.0	30.0	14.5	40.5
15	10.0	35.0	9.5	40.5
16	10.0	32.8	16.8	35.4
17	10.0	35.0	14.6	35.4
18	15.0	20.0	8.4	51.6
19	15.0	25.0	3.4	51.6
20	15.0	20.0	15.6	44.4
21	15.0	25.0	10.6	44.4
22	15.0	30.0	5.6	44.4
23	15.0	26.9	15.0	38.1
24	15.0	31.9	10.0	38.1
25	15.0	35.0	6.9	38.1
26	15.0	30.0	16.7	33.3
27	15.0	35.0	11.7	33.3
28	20.0	20.0	6.6	48.4
29	20.0	20.0	13.3	41.7
30	20.0	25.0	8.3	41.7
31	20.0	35.0	3.3	41.7

Table IV continued

Slag	MnO %	CaO %	MgO %	SiO_2 %
32	20.0	24.9	15.0	35.7
33	20.0	30.0	9.3	35.7
34	20.0	35.0	4.3	35.7
35	20.0	28.7	15.0	31.3
36	20.0	33.7	10.0	31.3
37	20.0	35.0	8.7	31.3
38	25.0	20.0	4.8	45.2
39	25.0	20.0	11.1	38.9
40	25.0	25.0	6.1	38.9
41	25.0	21.7	15.0	33.3
42	25.0	26.0	10.0	33.3
43	25.0	30.0	6.7	33.3
44	25.0	25.8	15.0	29.2
45	25.0	30.0	10.8	29.2
46	25.0	35.0	5.8	29.2
47	30.0	20.0	3.1	41.9
48	30.0	20.0	8.9	36.1
49	30.0	25.0	3.9	36.1
50	30.0	20.0	14.1	30.9
51	30.0	25.0	9.1	30.9
52	30.0	29.1	5.0	30.9
53	30.0	22.9	15.0	27.1
54	30.0	27.9	10.0	27.1
55	30.0	32.9	5.0	27.1

3.3.3 Preparation of Mn-Si-Fe-C alloys

In the slag-metal distribution experiments, the metal charge which consisted of Mn, Si, C and Fe was prepared from electrolytic manganese, iron, high-purity silicon and spectrographic-grade graphite powders. From these, a number of master alloys were prepared by melting the elements under an argon atmosphere in graphite crucibles. After the master alloys had been crushed and ground, they were stored in closed bottles in a vacuum desiccator. The composition of the alloys for the experimental runs were adjusted by adding the necessary pure elements in powder form to these master alloys. The ranges of initial alloy compositions as determined by chemical analysis are shown in Table V.

Table V. The initial metal-phase compositions.

Phase	Mn, %	Fe, %	Si, %	C, %
Ferromanganese	82.19	9.34	1.50	7
	79.77	11.73	1.50	7
	74.56	16.94	1.50	7
Silicomanganese	66.64	19.30	12.34	1.7
	62.55	19.30	16.46	1.7
	57.04	19.30	21.94	1.7

3.4 Preliminary experiments and equilibration time

A number of preliminary experiments were conducted in order to check that possible sources of systematic error were not causing significant inaccuracies.

Two separate samples of $CaO-MgO-SiO_2-Al_2O_3$, without MnO, were heated at 1500°C in a gas mixture of the same proportions as those used in the experiments, yielding an oxygen partial pressure of 5.80×10^{-8} atm at the temperatures involved. The samples were removed from the furnace and weighed after 5, 10 and 15 hours. The net average weight loss was found to be 0.18 mass per cent, 0.23 mass per cent and 0.28 respectively. Therefore, the loss of SiO_2 and MgO from the melt at this temperature and oxygen partial pressure was considered insignificant.

Another well known phenomena is the thermal diffusion of hydrogen molecules to the hot zone of the furnace. This will cause to the alteration of the desired oxygen

partial pressure in the furnace and it is well known where mixed gases are present across a temperature gradient. The lighter molecules tend to migrate to the hot zone and the heavier ones to the cooler zone of the furnace. This was predicted by number of investigators[9]. On the other hand, abnormal activity values were obtained from the use of the low flow rates (100 ml/min) in a previous study[9] and 400 ml/min and 600ml/min flow rates was found to be a safe lower limit. The high values resulting from the slower flow rate were probably due to the thermal diffusion of hydrogen molecules to the hot zone of the furnace. Since gaseous reactions, at the high temperatures involved during the experiments, are extremely rapid, gaseous equilibrium is almost certain to be attained at the flow rates, being higher than 600 ml/min, used in the present work. However, the reaction tube was also chosen as thick as possible in order to prevent the diffusion of hydrogen from cracked ammonia molecules to the hot zone of the furnace.

In a recent study[12] on the activities of manganese in Pt-Mn binary system it was shown that platinum coupons of thickness of 0.005 in. (0.127 mm) reached equilibrium with MnO within 8, 12, 24 and 80 hours at 1600°, 1500°, 1400° and 1300°C respectively and coupons of thickness of 0.002 in. (0.051mm) reached equilibrium within 48 hours at 1300°C. In the present study, the Pt strips used in Pt-Mn and ferromanganese slag experiments were 0.001 in. (0.025 mm) thick. Obviously, the thickness of the Pt strips used in the present study is the half of those used in the previous study. However, preliminary experiments were carried out to determine the

equilibration time for 1300°, 1400° and 1500°C in Pt-Mn system. The pure MnO was equilibrated with platinum strips at an experimental p_{O_2} value of 4.17×10^{-9} at 1300° for 7, 14, 21, 28, 35 hours. The results showed that equilibrium had been reached by 28 hours at 1300°C (Appendix B.1, Figure B.1.1). Therefore, the preliminary experiments in order to determine the equilibration time at 1400°C were carried out for 1, 7, 14, 21 and 28 hours considering improved kinetic conditions at higher temperatures. The results showed that equilibrium had been reached by 18 hours at 1400°C (Appendix B.1, Figure B.1.2). Finally, the equilibrium experiments were conducted for 1, 5, 9, 13, 17, 21 hours at 1500°C and it was found that the equilibrium was attained after 10 hours at 1500°C (Appendix B.1, Figure B.1.3). The analysis of platinum specimens and hence Mn activities were the same after about 28 hours at 1300°C, 18 hours at 1400°C and 10 hours at 1500°C. Therefore, it was assumed that equilibrium was reached at these temperatures with the relevant periods of time. On the other hand, a cross sectional examination of the Pt-Mn binary alloy samples which were obtained at 1300°C, 1400°C and 1500°C at different p_{O_2} values were performed by means of scanning electron microscopy (SEM) in combination with an EDAX (X-ray energy-dispersive analysis) facility. Concentration profiles of manganese on platinum strips were constructed by line scans using EDAX and each sample was analysed at 10 different points along a line across uhe platinum strip. The profiles of manganese on platinum strips verified that equilibrium had been attained that the profiles were very smooth. The results of these analysis for each sample are tabulated in Appendix B.3 (Tables B.3.1 to B.3.9). Nevertheless, for sake of insuring equilibrium to be

reached, the platinum strips were equilibrated with MnO for 48 hours at 1300°C and 24 hours both at 1400° and 1500°C.

In a previous study[9], the equilibration time for ferromanganese slags and Pt strips of 0.05 mm thickness was found to be 8 hours. In the present study, the preliminary experiments were also carried out for 1, 3, 5, 7 and 9 hours in order to determine the equilibration time for this stage and the same method as described above was applied and the same slag composition was used. It was found that equilibrium was reached in 6 hours for the thinner strips used (Appendix B.1, Figure B.1.4). The SEM-EDAX investigations were also carried out for number of Pt-Mn strips obtained at 1500°C and two different p_{O_2} values. Once again, very smooth concentration profiles were obtained that showed the attainment of equilibrium. These results are also tabulated in Appendix B.3 (Tables B.3.10 and B.3.11). However, once again the experiments were allowed to run about 24 hours each to ensure equilibrium.

In slag-metal equilibrium distribution experiments, the equilibration time was determined after a series of metal-slag equilibria experiments. The time varied from 3 to 15 hours and the initial compositions were kept the same. The approach to equilibrium was established by analysing the silicon dissolved in the metal as a parameter. It was found that a minimum of 10 hours was necessary for equilibration (Appendix B.1, Figure B.1.5). However, again a 24 hour period was employed for equilibration. The choice of 24 hours for experiments

was not purely on grounds of ensuring equilibrium but also due to practical reasons in the operation of laboratories.

3.5 The procedure of Mn and MnO activity measurements

The slag samples to be used in the experiments to determine the MnO activities in ferromanganese slags and the pure MnO sample to be used to determine the Mn activities in Pt-Mn binary system were charged, in 1 to 1.5 g quantities, into MnO-saturated platinum crucibles. Seven platinum strips were immersed in the slag (or pure MnO) sample at different levels. In the case of MnO activity measurements in ferromanganese slags, several platinum crucibles charged with slag of different compositions were placed in an A1-size alumina crucible surrounded by alumina bubbles, so that it was possible to run four or five different experiments at a time. However, in the case of Mn activity measurements, only one experimental run could be carried out at a time due to the unique requirement in partial pressure of oxygen. The alumina crucible was placed on the pedestal and raised slowly into the even temperature region of the furnace over a period of about 40 minutes. The reaction tube of the furnace was flushed for about 15 minutes with spectrographically pure argon before the mixed gases were purged. In the measurement of activities of MnO or Mn, the experiments were conducted at low p_{O_2} values obtained by the mixing of chemically pure CO and CO_2 gases. At the end of the equilibration, the mixed gases were turned off and argon only was allowed to pass and the samples were rapidly withdrawn to the water-cooled bottom end of the furnace from where they were removed quickly and quenched in water. After equilibration, the

platinum specimens were too brittle to permit mechanical removal of any adhering particles of MnO, and therefore, any such particles were removed by solution of 1:1 HCl. On the other hand, the edges of the platinum-manganese alloy coupon were sheared off to eliminate edge effects. Rao and Gaskell[12] reported that Mn in solution was not removed from the alloy during the chemical cleaning. This has also been verified in the present study by means of the microprobe analysis of manganese of the chemically cleaned and uncleaned pieces of the same platinum specimen which gave identical results within maximum 2 per cent. In microprobe analysis, the beam was directed to areas free from adhered particles on the uncleaned platinum specimen. Finally, the manganese content of equilibrated Pt-Mn specimens were determined by chemical analysis. In the case of MnO activity measurements in ferromanganese slags, the whole composition of slag was also analyzed and the total composition was found to be within 98 and 101 mass per cent. Occasionally, the manganese distribution profile along the length and thickness of the platinum strips were determined by microprobe analysis to ensure that equilibrium is fully attained.

3.6 The procedure of slag-metal equilibrium experiments

In the slag-metal equilibrium distribution experiments, the charge consisted of about 6 g of metal and 4 g of slag of selected compositions and were contained in graphite crucibles (Appendix B). Three graphite crucibles containing metal and slag samples of different compositions were placed in a larger graphite crucible, so that it was possible to run three different experiments at a time. The large graphite crucible was

placed on the pedestal and raised up slowly into the even-temperature region of the furnace over a period of about 40 minutes. The reaction tube of the furnace was flushed for about 15 minutes with spectrographically pure argon before the CO atmosphere was employed.

In manufacturing high-carbon ferromanganese and silicomanganese, the factor which determines the quality of product and the final recovery rate of manganese is the distribution reactions of components between alloy and molten slags in the refining furnace. Although many reactions are involved, the most important one in respect to the distribution of Mn and Si is considered to be the reaction (22) whose equilibrium condition had been examined in the past by various studies[119]. However, besides the reaction (22), the reaction (18) and the following one also occur in ferromanganese and silicomanganese production:

$$2(MnO) + [Si] = 2[Mn] + (SiC_2) \quad \text{.....(22)}$$

$$(MnO) + C = [Mn] + CO \quad \text{.....(18)}$$

$$(SiO_2) + 2C = [Si] + 2CO \quad \text{.....(50)}$$

As the reactions (18) and (50) are CO gas producing reactions, if the partial pressure of the ambient CO gas is low, the reduction of MnO and SiO_2 in molten slag will

proceed almost with no limit, thus the reaction (22) will not reach equilibrium even after these substances have disappeared. Therefore, all the experiments were done in a pure CO gas atmosphere. The flowrate of CO was kept at 600 cm^3/min. After equilibration at 1500°C for 24 hours, the CO gas was turned off and the argon was allowed to pass through the reaction tube and the crucibles were lowered to the bottom water-cooled end of the furnace quickly. The apparatus was opened from the bottom, and the graphite crucibles with their contents were immediately quenched in water. The crucible was broken and the slag and metal phases were removed from the crucible and separated. The graphite that had stuck onto both phases was removed with emery paper or a wire wheel. In general, it was easy to separate the slag and the metal phase as they came out in two separate and distinct layers. Both phases were crushed, ground, pulverized and were kept in sealed bottles in a dessicator until their contents were analysed. The analysis of alloys were done for Mn, Si, Fe and C. The whole composition of slag was analyzed and the total composition amounted to within 98 and 101 mass per cent.

3.7 Chemical analysis

The analytical work was done at Mintek. The manganese contents of the equilibrated Pt-Mn coupons were determined by the atomic absorption method, the final constituents of the slag were analysed by X-ray fusion, and the iron content of the slag was determined by the o-pheanthroline colorimetric method. The carbon content of the metal was analysed by means of a Leco analyser, and the other constituents of the metal by the

inductively coupled plasma (ICP) method. More information on the above-mentioned analytical methods can be found in Appendix B.2.

4 RESULTS AND DISCUSSIONS

Results of the experimental work with relevant discussions are gathered in two subsections of this chapter. The first part summarizes the results of activity measurements both in the Pt-Mn binary system and in the $CaO-MgO-SiO_2-Al_2O_3-MnO$ slags. The gas equilibration technique was used to determine the Mn and MnO activities in the Pt-Mn binary and the slag system respectively. The measured values were fitted into empirical model equations in order to predict the respective activities as a function of composition at the given temperature. In the case of Pt-Mn binary system, a simple linear equation was satisfactory, whereas in the slag system a multi-coefficient-multivariable quadratic equation was needed.

The second part summarizes the results gathered in experiments where the slag phase was equilibrated with molten Mn-Si-Fe-C alloys contained in graphite crucibles (carbon saturation) under a CO atmosphere. Combining some of the information from the first section on MnO activities, literature values on SiO_2 activities and compositional data from slag-metal equilibrium experiments, it was possible to calculate Mn and Si activities in molten Mn-Si-Fe-C alloys. The activity coefficients of manganese and silicon were fitted into multi-coefficient-multivariable quadratic equations in order to predict the respective activities as a function of composition at the given temperature. In addition, the iso-activity contours of silicon and manganese in silicomanganese and ferromanganese compositions were derived through the respective model equations.

4.1 Results of activity measurements

4.1.1 Activity composition relations in Pt-Mn system

Activity-composition relations in the solid-solution region of the Pt-Mn system were determined at 1300°, 1400° and 1500°C and p_{O_2} values between about 10^{-6} and 10^{-11} atm. The different p_{O_2} values used in these experiments and the calculated activity coefficients are given in Tables VI, VII and VIII.

Linear regression model was derived to predict the activity coefficients of manganese in Pt-Mn system at 1300°, 1400° and 1500°C. The results are summarized in Table IX.

In Figure 34, the logarithm of the activity coefficient of manganese, γ_{Mn}, is plotted against its mole fraction at 1300°C. In Figure 34, the dashed line represents the results of a previous study carried out by Rao and Gaskell[12], the solid line represents the predicted values calculated through the simple linear regression model and the symbols represent the experimental values. As it is seen from the Figure 34, the results of the present work are in reasonable agreement with those obtained by Rao and Gaskell[12]. At this temperature, the linear regression equation for activity coefficient of manganese is:

$$\ln\gamma_{Mn} = 19.087X_{Mn} - 13.475 \quad \text{.....(51)}$$

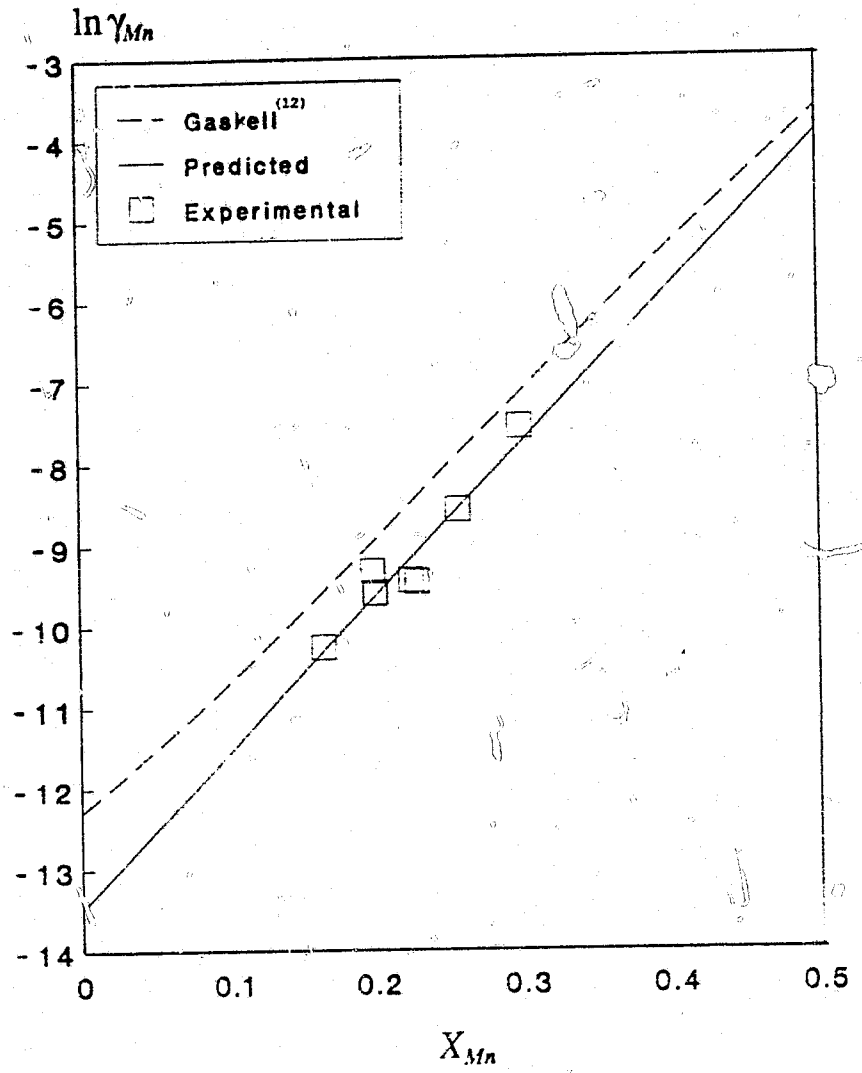

Figure 34. The change of activity coefficient of Mn with composition in Pt-Mn binary alloys at 1300℃.

In Figure 35, the logarithm of γ_{Mn} is plotted against its mole fraction at 1400°C and the lines and symbols represent the same as in the previous figure. The good agreement between experimental values and the previous study[12] is quiet obvious. At this temperature the regression equation for activity coefficient of manganese is:

$$\ln\gamma_{Mn} = 15.834X_{Mn} - 11.911 \quad \text{.....(52)}$$

Figure 36 shows the same relation between γ_{Mn} and its mole fraction in Pt-Mn binary alloys at 1500°C. This stage of the experimental runs were very important for calibration of the experimental set-up and also for using the calculated a_{Mn} values in the calculation of MnO activities in synthetic ferromanganese slags. Therefore the number of experiments conducted were more than those conducted at the two lower temperatures. The results show that the agreement between the present and Rao and Gaskell's[12] work is excellent at this temperature. The regression equation for activity coefficient of manganese at 1500°C is given below:

$$\ln\gamma_{Mn} = 14.470X_{Mn} - 10.793 \quad \text{.....(53)}$$

From the linear regression equation it is possible to obtain the Henrian activity coefficient; γ^{o}_{Mn} and self interaction parameter, ε^{Mn}_{Mn} of manganese in dilute

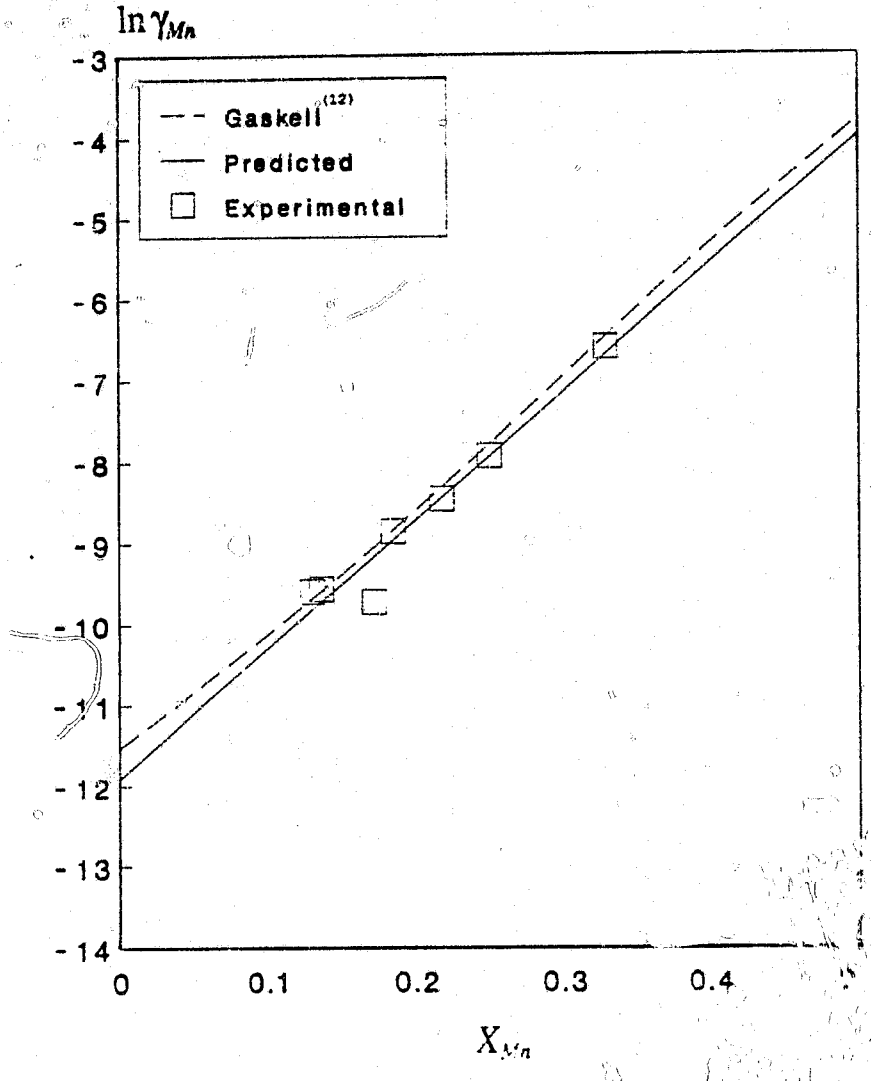

Figure 35. The change of activity coefficient of Mn with composition in Pt-Mn binary alloys at 1400°C.

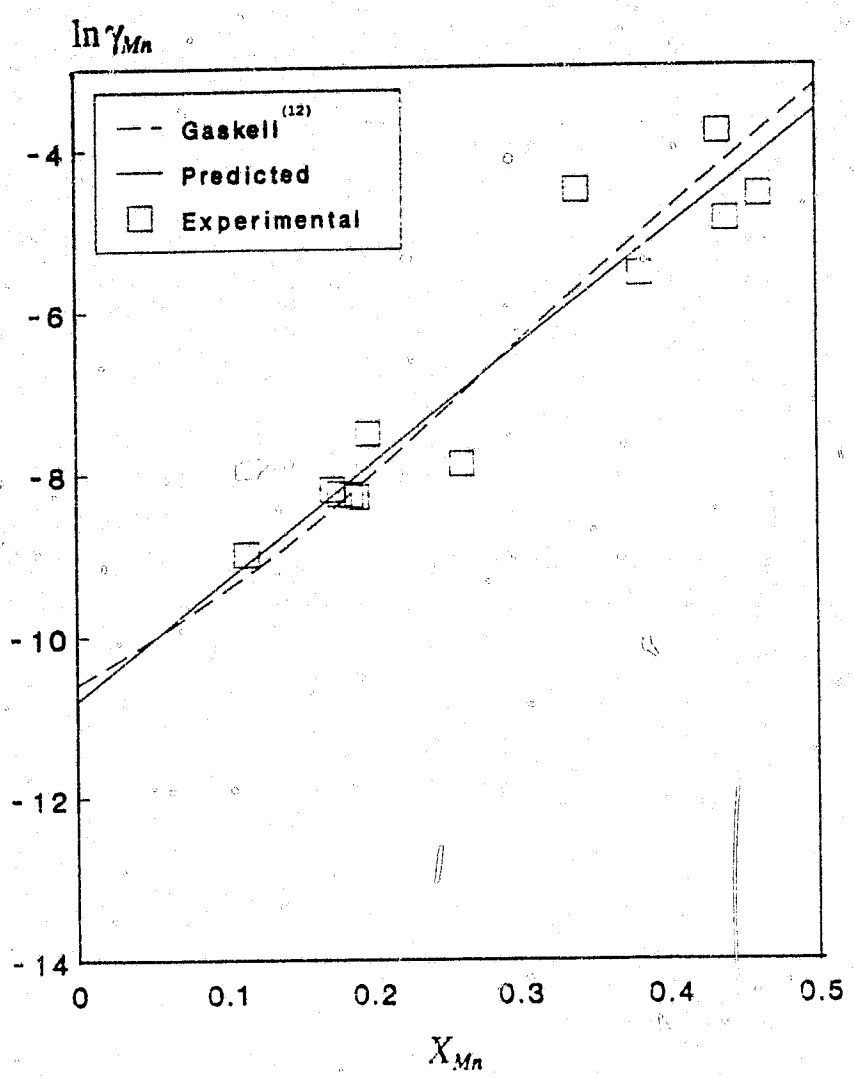

Figure 36. The change of activity coefficient of Mn with composition in Pt-Mn binary alloys at 1500°C.

solutions in platinum. The Henrian activity coefficient γ^{o}_{Mn} would be equal to 1.41×10^{-6}, 6.72×10^{-6} and 2.05×10^{-5} at 1300°, 1400° and 1500°C respectively. The self interaction parameter for manganese ϵ^{Mn}_{Mn} is; 19.087, 15.834 and 14.470 at 1300°, 1400° and 1500°C respectively. The Henrian activity coefficient values are in excellent agreement with those of Rao and Gaskell[12]. As it is seen from the three figures, there are a few data points showing a slight scatter and it is believed that this was due to some furnace failures experienced during some of the experimental runs. The failures were due to electrical cut-offs and increased water pressures especially during evenings and nights. These might have resulted in cracked reaction tubes which might have permitted hydrogen gas to enter the reaction zone and alter the equilibrium and also molybdenum wire failures. In almost each case, the furnace had to be re-constructed and re-wound. These problems were overcome by repeating the experimental runs which were unsuccessful. Another problem faced occasionally was the difficulties in obtaining the desired p_{O_2} values due to the pressure drops in the gas cylinders of CO and CO_2 especially in long term runs (48 and 24 hours).

Table VI. The compositions, the activity and the activity coefficients of Mn in Pt-Mn binary alloys at 1300°C.

p_{O_2}	X_{Mn}	$\ln\gamma_{Mn}$	γ_{Mn}	a_{Mn}
7.34×10^{-9}	0.201	-9.6028	6.75×10^{-5}	1.36×10^{-5}
4.17×10^{-9}	0.230	-9.4536	7.84×10^{-5}	1.80×10^{-5}
3.98×10^{-8}	0.166	-10.2575	3.51×10^{-5}	5.83×10^{-6}
4.17×10^{-9}	0.226	-9.4361	7.98×10^{-5}	1.80×10^{-5}
5.70×10^{-10}	0.258	-8.5735	1.89×10^{-4}	4.88×10^{-5}
5.54×10^{-11}	0.299	-7.5545	5.24×10^{-4}	1.57×10^{-4}
7.10×10^{-9}	0.202	-9.5925	6.82×10^{-5}	1.38×10^{-5}
4.17×10^{-9}	0.200	-9.3156	9.00×10^{-5}	1.80×10^{-5}

Table VII. The compositions, the activity, and the activity coefficients of Mn in Pt-Mn binary alloys at 1400°C.

p_{O_2}	X_{Mn}	$\ln\gamma_{Mn}$	γ_{Mn}	a_{Mn}
6.04×10^{-7}	0.138	-9.5712	6.97×10^{-5}	9.62×10^{-6}
6.77×10^{-7}	0.132	-9.5961	6.80×10^{-5}	8.98×10^{-6}
6.77×10^{-8}	0.186	-8.8608	1.42×10^{-4}	2.64×10^{-5}
5.07×10^{-9}	0.251	-7.9342	3.58×10^{-4}	8.99×10^{-5}
2.19×10^{-10}	0.219	-8.4774	2.12×10^{-4}	4.65×10^{-5}
2.35×10^{-10}	0.330	-6.5990	1.36×10^{-3}	4.49×10^{-4}
4.47×10^{-7}	0.173	-9.7342	5.92×10^{-5}	1.02×10^{-5}

Table VIII. The compositions, the activity, and the activity coefficients of Mn in Pt-Mn binary alloys at 1500°C.

p_{O_2}	X_{Mn}	$\ln\gamma_{Mn}$	γ_{Mn}	a_{Mn}
5.19×10^{-6}	0.116	-8.9992	1.24×10^{-4}	1.43×10^{-5}
4.99×10^{-7}	0.179	-8.2484	2.62×10^{-4}	4.68×10^{-5}
9.30×10^{-8}	0.199	-7.5092	5.48×10^{-4}	1.09×10^{-4}
1.14×10^{-7}	0.263	-7.8908	3.74×10^{-4}	9.84×10^{-5}
4.76×10^{-7}	0.191	-8.2892	2.51×10^{-4}	4.80×10^{-5}
4.76×10^{-7}	0.187	-8.2681	2.57×10^{-4}	4.80×10^{-5}
4.76×10^{-7}	0.174	-8.1960	2.76×10^{-4}	4.80×10^{-5}
4.98×10^{-10}	0.383	-5.5453	3.97×10^{-3}	1.50×10^{-3}
1.00×10^{-10}	0.440	-4.8794	7.60×10^{-3}	3.34×10^{-3}
4.99×10^{-11}	0.462	-4.5822	1.02×10^{-2}	4.73×10^{-3}
5.78×10^{-8}	0.341	-4.5175	1.09×10^{-2}	3.72×10^{-3}
4.86×10^{-9}	0.435	-3.8120	2.21×10^{-2}	9.62×10^{-3}

Table IX. Model parameters for activity coefficient of manganese.

°C	Correlation coefficient R^2	Coefficient a	Coefficient b
1300°C	0.919	-13.47497	19.08735
1400°C	0.947	-11.9113	15.83359
1500°C	0.901	-10.79273	14.46966

4.1.2 Activity of MnO in $CaO-MgO-SiO_2-Al_2O_3-MnO$ slags and modelling of results

Extensive experimental runs were carried out in order to determine MnO activities in slags at 1500°C. The Al_2O_3 content of the slags was kept at about 5 per cent by mass. The basicity ratios of the slags varied between 0.41 and 1.18. The initial compositions of the slags used in the experiments are shown in Table IV. A recent study by Eric, Hejja and Stange[50] have shown that all those slags were fully molten at temperatures greater than 1400°C. Therefore at 1500°C the slags formed a homogeneous liquid phase. The results of the experimental runs are summarized in Table X including the equilibrium composition of the slag, its basicity, CaO-to-MgO ratio and activity of MnO with respect to pure liquid MnO as the standard state.

Regression models, based on the data of the present work were developed to predict the activities of MnO as a function of slag composition. From the practical point of view, it was necessary to develop empirical models which will be valid in the particular composition range of the present study to predict the MnO activities. Satisfactory results were obtained for ferromanganese slags in predicting the electrical conductivities and the liquidus temperatures employing multi-coefficient quadratic equations in a previous study[50]. Since electrical conductivity of a slag is related especially to activities of metal oxide species, it was decided that the models should be quadratic in form. For example, if

Table X. Activity of MnO in $CaO-MgO-SiO_2-Al_2O_3-MnO$ slags at 1500°C with pure liquid MnO as the standard state.

Exp.No.	p_{O_2}	Equilibrium Compositions of the Slag (Mass Percentages)					a_{MnO}	Basicity	CaO:MgO
		MnO%	CaO	MgO%	SiO_2%	Al_2O_3%			
1		6.07	26.08	12.29	50.26	5.27	0.013	0.76	2.12
2		6.96	31.70	3.92	51.85	5.60	0.018	0.69	8.08
3		5.27	29.38	14.27	45.45	5.61	0.012	0.96	2.06
4		10.00	17.18	9.39	57.41	5.99	0.019	0.46	1.83
5		10.15	21.45	4.33	58.18	5.94	0.016	0.44	4.96
6		11.33	21.05	11.96	49.70	5.95	0.035	0.66	1.76
7		10.75	25.74	7.15	50.55	5.86	0.025	0.65	3.60
8		29.37	22.59	9.82	33.63	4.55	0.172	0.96	2.30
9		33.83	25.97	4.08	31.79	4.30	0.248	0.94	6.37
10		35.26	25.32	10.09	25.18	4.17	0.364	1.41	2.51
11		17.36	16.84	6.86	53.36	5.60	0.042	0.44	2.46
12		21.24	17.84	4.65	50.45	5.79	0.036	0.45	3.84
13	$4.76x10^{-7}$	15.91	20.56	3.62	55.61	4.29	0.035	0.43	5.69
14		10.90	29.99	1.85	51.13	6.14	0.030	0.62	16.21
15		10.59	26.40	13.15	43.94	5.93	0.045	0.90	2.01
16		10.46	30.97	7.36	45.50	5.72	0.038	0.84	4.21
17		9.36	28.91	16.95	39.24	5.54	0.057	1.17	1.71
18		9.02	28.92	13.64	41.13	7.28	0.047	1.03	2.12
19		15.63	21.41	9.52	47.68	5.76	0.043	0.65	2.25
20		15.64	25.72	4.88	47.91	5.85	0.051	0.64	5.27
21		13.74	26.66	16.72	36.92	5.96	0.085	1.18	1.59
22		14.13	30.44	12.16	37.42	5.85	0.077	1.14	2.50
23		20.46	21.38	7.86	44.47	5.84	0.051	0.66	2.72
24		20.99	25.34	2.57	45.23	5.87	0.052	0.62	9.86
25		19.83	21.69	13.84	38.83	5.81	0.104	0.92	1.57

Table X continued

Exp.No.	p_{O_2}	Equilibrium Compositions of the Slag (Mass Percentages)					a_{MnO}	Basicity	CaO:MgO
		MnO%	CaO	MgO%	SiO_2%	Al_2O_3%			
26	4.76×10^{-7}	19.18	26.03	8.79	40.03	5.97	0.076	0.87	2.96
27		19.65	29.99	3.84	40.29	6.23	0.079	0.84	7.80
28		18.50	25.44	15.16	35.99	4.91	0.121	1.13	1.68
29		18.17	29.86	10.11	36.50	4.86	0.113	1.10	2.95
30	5.80×10^{-6}	6.32	17.73	10.90	59.77	5.28	0.011	0.48	1.63
31		5.69	23.86	6.08	59.34	5.03	0.013	0.50	3.93
32		5.52	25.77	12.99	50.84	4.87	0.015	0.76	1.98
33		5.46	27.59	9.30	52.50	5.15	0.013	0.70	2.97
34		5.63	31.76	4.56	52.81	5.25	0.014	0.69	6.97
35		5.24	29.22	14.25	46.05	5.24	0.017	0.94	2.05
36		5.44	30.69	11.47	47.17	5.24	0.017	0.89	2.68
37		5.63	30.60	16.10	42.11	5.56	0.028	1.11	1.90
38		10.59	16.99	9.60	57.14	5.68	0.017	0.47	1.77
39	5.80×10^{-6}	10.98	21.57	4.25	57.51	5.69	0.018	0.45	5.07
40		9.75	21.06	12.50	51.69	5.00	0.017	0.65	1.68
41		10.67	25.15	7.84	51.30	5.04	0.021	0.64	3.21
42		10.38	29.82	2.65	52.07	5.08	0.021	0.62	11.28
43		10.02	25.95	13.29	45.11	5.63	0.032	0.87	1.95
44		8.08	28.51	17.44	40.72	5.25	0.039	1.13	1.63
45		8.33	30.89	14.77	40.68	5.34	0.039	1.12	2.09
46		15.19	16.65	7.89	54.45	5.82	0.021	0.45	2.11
47		16.78	20.85	2.54	54.16	5.68	0.038	0.43	8.21
48		16.82	16.51	15.13	46.02	5.53	0.038	0.69	1.09
49		13.62	21.69	10.14	48.75	5.80	0.028	0.65	2.14
50		15.21	22.74	15.02	41.46	5.57	0.057	0.91	1.51

Table X continued

Exp.No.	p_{O_2}	Equilibrium Compositions of the Slag (Mass Percentages)					a_{MnO}	Basicity	CaO:MgO
		MnO%	CaO	MgO%	SiO_2%	Al_2O_3%			
51		14.59	27.84	9.37	42.44	5.76	0.046	0.88	2.97
52		15.14	30.12	6.42	42.76	5.56	0.055	0.85	4.69
53		13.86	26.06	16.96	37.54	5.58	0.085	1.15	1.54
54		14.18	30.40	11.66	38.22	5.55	0.090	1.10	2.61
55		19.97	16.93	5.16	51.94	6.01	0.034	0.43	3.28
56		19.54	17.41	12.63	44.56	5.87	0.059	0.67	1.38
57		21.17	20.99	7.71	44.50	5.62	0.064	0.65	2.72
58		21.13	25.34	2.49	45.41	5.64	0.047	0.61	10.19
59		19.16	21.36	14.42	39.37	5.69	0.071	0.91	1.48
60		20.54	25.71	8.61	39.43	5.72	0.078	0.87	2.99
61		20.44	30.16	3.70	40.03	5.67	0.083	0.85	8.15
62	5.80×10^{-8}	18.38	29.32	10.40	35.96	5.93	0.078	1.10	2.82
63		17.31	31.64	8.61	36.53	5.91	0.067	1.10	3.67
64		9.23	25.02	11.44	48.86	5.45	0.030	0.75	2.19
65		8.68	25.90	11.54	48.59	5.29	0.030	0.77	2.25
66		16.35	21.28	11.24	45.41	5.72	0.047	0.72	1.89
67		13.97	21.01	12.13	47.06	5.82	0.035	0.70	1.73
68		7.59	19.47	10.33	56.98	5.64	0.020	0.52	1.89
69		7.41	19.26	10.37	57.34	5.63	0.019	0.52	1.86
70		9.52	18.21	9.75	56.82	5.70	0.022	0.49	1.87
71		8.94	16.66	9.92	58.49	5.99	0.024	0.45	1.68
72		19.13	21.90	14.25	38.70	6.02	0.090	0.93	1.54
73		18.49	22.58	14.18	38.96	5.80	0.079	0.94	1.59
74		25.04	19.10	14.20	35.84	5.82	0.107	0.93	1.34
75		21.57	23.40	15.31	33.68	6.05	0.161	1.15	1.53

Table X continued

Exp.No.	p_{O_2}	Equilibrium Compositions of the Slag (Mass Percentages)					a_{MnO}	Basicity	CaO:MgO
		MnO%	CaO	MgO%	SiO_2%	Al_2O_3%			
76		16.19	25.56	16.53	35.95	5.77	0.105	1.17	1.55
77		14.77	25.26	16.89	37.02	6.06	0.081	1.14	1.50
78		7.39	23.62	5.77	57.68	5.55	0.019	0.51	4.10
79		7.47	23.84	5.64	57.92	5.13	0.020	0.51	4.22
80		23.43	17.38	4.18	48.90	6.12	0.039	0.44	4.16
81		10.68	26.21	7.52	49.68	5.92	0.032	0.68	3.49
82		14.29	24.86	6.95	48.06	5.84	0.041	0.66	3.58
83		12.62	25.33	7.73	48.45	5.87	0.043	0.68	3.28
84		19.60	23.53	6.41	44.49	5.98	0.054	0.67	3.67
85		23.68	22.54	5.60	41.85	6.33	0.079	0.67	4.03
86		11.06	30.49	7.40	44.95	6.10	0.039	0.84	4.12
87	5.80×10^{-8}	9.43	29.44	8.98	46.94	5.20	0.022	0.82	3.28
88		12.64	28.50	8.07	42.25	5.54	0.034	0.87	3.53
89		15.32	27.51	8.13	43.55	5.49	0.046	0.82	3.38
90		14.09	27.30	8.52	44.56	5.45	0.041	0.81	3.21
91		18.21	28.35	9.51	38.40	5.54	0.098	0.99	2.98
92		19.22	27.19	10.71	37.30	5.58	0.087	1.02	2.54
93		18.58	28.74	8.67	38.25	5.77	0.098	0.98	3.32
94		14.78	19.38	3.38	57.31	5.15	0.028	0.40	5.73
95		12.69	20.92	3.80	56.72	5.87	0.020	0.44	5.50
96		9.42	28.74	5.22	50.82	5.80	0.024	0.57	5.50
97		7.62	30.41	5.50	50.88	5.60	0.018	0.71	5.53
98		16.47	26.60	4.74	46.40	5.79	0.036	0.68	5.62
99		25.34	22.82	3.82	41.87	6.15	0.065	0.64	5.97
100		17.96	29.78	5.69	40.73	5.84	0.048	0.87	5.24

Table X continued

Exp.No.	p_{O_2}	Equilibrium Compositions of the Slag (Mass Percentages)					a_{MnO}	Basicity	CaO:MgO
		MnO%	CaO	MgO%	SiO_2%	Al_2O_3%			
101		31.85	27.90	6.20	31.95	2.70	0.211	1.07	4.50
102		23.78	14.07	6.99	51.41	3.74	0.041	0.41	2.01
103		10.65	16.03	8.23	59.11	5.99	0.016	0.41	1.95
104		30.31	12.90	6.34	47.57	2.87	0.049	0.40	2.03
105		31.90	6.43	14.63	43.46	3.58	0.064	0.48	0.44
106		33.34	5.69	14.96	43.69	2.32	0.064	0.47	0.38
107		29.87	27.93	6.90	31.77	3.53	0.290	1.10	4.05
108		17.88	20.58	10.15	46.48	4.92	0.057	0.66	2.03
109		22.43	21.42	7.46	44.19	4.51	0.056	0.65	2.87
110		29.78	17.24	9.04	40.59	3.36	0.068	0.65	1.91
111		21.77	23.09	10.71	39.11	5.32	0.096	0.86	2.16
112	5.80×10^{-9}	26.34	22.00	11.00	36.63	4.03	0.088	0.90	2.00
113		4.42	11.84	36.41	40.99	6.35	0.020	1.18	0.33
114		15.16	23.80	12.35	43.54	5.14	0.033	0.83	1.93
115		12.09	29.95	13.99	38.70	5.27	0.071	1.14	2.14
116		11.70	11.12	34.63	37.88	4.68	0.068	1.21	0.32
117		17.26	27.01	13.74	37.14	4.86	0.101	1.10	1.97
118		20.90	25.84	13.36	35.31	4.60	0.130	1.11	1.93
119		26.49	24.73	12.44	32.47	3.87	0.230	1.14	1.99
120		12.44	4.79	21.49	56.42	4.86	0.022	0.47	0.22
121		11.26	19.36	5.42	58.92	5.05	0.028	0.42	3.57
122		14.21	16.42	8.95	55.79	4.63	0.028	0.45	1.83
123		14.37	19.14	5.55	56.09	4.84	0.027	0.44	3.45
124		20.85	16.95	5.24	52.97	4.00	0.039	0.42	3.23
125		25.94	15.81	5.55	49.11	3.59	0.055	0.43	2.85

Table X continued

Exp.No.	p_{O_2}	Equilibrium Composition of the Slag (Mass Percentages)					a_{MnO}	Basicity	CaO:MgO
		MnO%	CaO	MgO%	SiO_2%	Al_2O_3%			
126		12.10	25.03	7.13	50.92	4.82	0.035	0.63	3.51
127		18.01	5.88	25.24	46.44	4.44	0.030	0.67	0.23
128		17.35	23.12	7.23	47.96	4.44	0.031	0.63	3.20
129		20.74	21.82	7.25	46.11	4.08	0.042	0.63	3.01
130		30.20	19.95	6.22	40.35	3.28	0.094	0.65	3.21
131		9.51	7.61	33.96	43.92	5.01	0.018	0.95	0.22
132		10.37	8.26	31.82	44.37	5.19	0.025	0.90	0.26
133		13.50	28.07	8.69	44.64	5.10	0.041	0.82	3.23
134		16.72	28.64	8.00	42.07	4.57	0.059	0.87	3.58
135		22.97	25.94	8.36	38.71	4.02	0.088	0.89	3.10
136		25.40	6.32	28.69	36.69	2.90	0.101	0.95	0.22
137	5.80×10^{-8}	6.17	8.15	38.74	41.82	5.13	0.022	1.12	0.21
138		9.28	7.82	38.21	39.99	4.71	0.036	1.10	0.20
139		18.00	31.16	8.97	37.11	4.75	0.085	1.08	3.47
140		21.25	29.38	8.85	35.59	4.94	0.130	1.07	3.32
141		22.65	28.71	8.75	34.86	5.03	0.133	1.07	3.28
142		24.46	7.17	31.67	32.03	4.67	0.171	1.21	0.23
143		10.68	4.62	22.34	56.61	5.76	0.017	0.48	0.21
144		11.60	20.27	4.93	57.91	5.29	0.022	0.44	4.12
145		14.33	18.20	5.37	56.88	5.23	0.025	0.41	3.39
146		19.72	17.79	4.42	53.46	4.61	0.044	0.42	4.02
147		10.54	24.91	6.38	52.48	5.68	0.020	0.60	3.90
148		29.35	3.80	19.32	43.79	3.74	0.074	0.53	0.20
149		8.21	6.06	28.53	51.16	6.04	0.017	0.68	0.21
150		26.90	10.91	4.90	48.21	4.08	0.051	0.43	3.25

Table X continued

Exp.No.	p_{O_2}	Equilibrium Compositions of the Slag (Mass Percentages)					a_{MnO}	Basicity	CaO:MgO
		MnO%	CaO	MgO%	SiO_2%	Al_2O_3%			
151		14.86	23.90	6.37	49.72	5.15	0.038	0.61	3.75
152		17.37	22.44	6.52	48.61	5.06	0.049	0.60	3.4
153		20.73	21.74	5.92	46.94	4.66	0.056	0.59	3.67
154		25.04	21.93	5.78	43.07	4.19	0.074	0.64	3.79
155		29.16	5.10	21.41	40.01	4.33	0.090	0.66	0.24
156		15.52	4.44	35.72	40.82	3.50	0.057	0.98	0.12
157		26.06	5.78	26.68	35.86	5.62	0.130	0.91	0.22
158		13.07	16.48	26.21	36.67	5.58	0.076	1.10	0.63
159		1[illegible]	9.70	0.31	52.11	5.10	0.028	0.58	97.38
160		16	.19	0.30	49.41	5.42	0.039	0.58	93.35
161		20.02	26.20	0.79	47.16	5.83	0.049	0.57	33.25
162	5.80×10^{-8}	26.17	24.78	0.30	43.59	5.16	0.068	0.58	81.79
163		27.74	24.08	0.30	42.43	5.45	0.096	0.57	79.75
164		21.74	18.54	15.04	39.19	5.49	0.096	0.86	1.23
165		13.96	35.17	0.31	45.42	5.14	0.039	0.78	114.57
166		15.68	34.03	0.58	44.46	5.25	0.047	0.78	58.46
167		19.47	32.59	0.31	42.34	5.29	0.053	0.78	105.48
168		22.60	31.08	0.30	40.74	5.28	0.071	0.77	102.25
169		23.55	28.71	1.57	40.08	6.09	0.079	0.76	18.28
170		27.87	28.58	0.30	37.34	5.92	0.127	0.77	94.91
171		35.26	12.56	5.24	42.43	4.51	0.103	0.42	2.40
172		32.68	13.12	5.59	43.66	4.94	0.064	0.43	2.35
173		40.85	11.36	4.90	38.45	4.43	0.114	0.42	2.32
174		21.99	19.74	8.34	45.94	4.00	0.048	0.61	2.37
175		29.53	22.77	8.93	32.21	6.57	0.235	0.98	2.55

Table X continued

Exp.No.	P_{O_2}	Equilibrium Compositions of the Slag (Mass Percentages)					a_{MnO}	Basicity	CaO:MgO
		MnO%	CaO	MgO%	O_2%	Al_2O_3%			
176		13.03	24.54	7.19	50.01	5.25	0.028	0.63	3.41
177		11.06	30.70	7.65	45.35	5.24	0.028	0.85	4.01
178		21.83	26.56	6.58	39.76	5.28	0.074	0.83	4.04
179		29.35	23.28	5.72	36.29	5.36	0.161	0.80	4.07
180		11.74	34.16	8.78	39.80	5.54	0.056	1.08	3.89
181		16.88	34.17	7.68	36.23	5.05	0.081	1.15	4.45
182		27.10	28.06	6.70	32.69	5.46	0.211	1.06	4.19
183		12.87	19.75	3.92	56.83	6.62	0.022	0.42	5.04
184	5.80×10^{-8}	32.21	14.84	2.73	43.34	6.89	0.085	0.41	5.44
185		13.52	24.65	4.99	49.73	7.12	0.028	0.60	4.94
186		32.43	18.91	3.82	39.49	5.35	0.112	0.58	4.95
187		12.73	30.29	6.82	45.18	4.98	0.037	0.82	4.45
188		16.34	29.20	5.95	43.16	5.36	0.046	0.81	4.91
189		11.83	34.88	7.46	40.68	5.16	0.056	1.04	4.68
190		11.18	34.93	7.41	40.99	5.49	0.045	1.03	4.72
191		17.54	32.27	7.02	37.80	5.37	0.096	1.04	4.60
192		29.22	26.63	5.55	30.26	8.34	0.266	1.06	4.80
193		28.59	24.51	0.31	41.48	5.11	0.101	0.60	79.83
194		25.53	30.61	0.31	38.20	5.36	0.138	0.81	98.74

two components are present in the slag, and their concentrations are X_1 and X_2 then the activity Y could be correlated using a model of the form:

$$Y = a_0 + a_1X_1 + a_2X_2 + a_3X_1^2 + a_4X_1X_2 + a_5X_2^2 \quad \text{.....(54)}$$

Two quadratic multi-variable regression models were derived for predicting the MnO activities in ferromanganese slags. The first was based on the complete data containing 220 data points and it was referred to as data set 1. The second set was consisted of 194 data points and was referred to as data set 2. The choice of the number of data points in the second set were determined by the results of the previous regression. For the complete set involving 220 data points called data set 1, the regression analysis predicted that 26 experimental points were, from statistical point of view, out of the 90 per cent confidence level. When these experimental points were ignored resulting in data set 2 with 194 points, very high correlation coefficients were obtained indicating an excellent fit with all points within the confidence level. The results shown in Table X include these 194 reliable experimental points.

The independent variables were the mass percentages of MnO, CaO, MgO, SiO_2 and Al_2O_3 in the slag as well as the basicity ratio, B, defined as $B = (CaO + MgO)/SiO_2$ and the CaO-to-MgO ratio (denoted by CaO:MgO), a total of seven variables. The dependent variable was the activity of

MnO. The regressions using experimental data were carried out using routines from the SAS (Statistical Analysis Software) system. The first step was to use the SAS procedure RSREG which fits a complete quadratic response surface to the data. For a seven variable model, including quadratic and cross product terms, the analysis resulted in two models for the two data groups each having 36 parameters which were regarded as too many. The SAS procedure RSQUARE was then used. This procedure selects the optimum combination of independent variables to produce the best fit for a given number of independent variables in the model. With this approach, it was found that essentially similar fits could be obtained from a model with far fewer parameters and this was referred as the reduced model. The analysis resulted in two different reduced models for the two data groups. The results of statistical analysis are summarized in Table XI.

As it is seen from Table XI, it may appear that the complete quadratic model provides a slightly better fit than the reduced model, it was found that the errors in the points calculated using the reduced model were not significantly different to those calculated using the complete quadratic model. On the other hand, the reduced model contains less than half the number of parameters than the complete model does, thus making the reduced model a better choice from practical point of view.

When the two different data sets are considered, the reduced model representing the data set 1 containing 220 points has the lowest correlation coefficient (R^2). On

Table XI. Results for MnO activity model.

	Data set 1		Data set 2	
	Complete Quadratic Model	Reduced Model	Complete Quadratic Model	Reduced Model
Correlation Coefficient R^2	0.7751	0.7580	0.9636	0.9587
Number of parameters in model	36	16	36	16

the other hand, the complete quadratic model representing the data set 2 containing 194 data points has the highest correlation coefficient. However, the correlation coefficient for reduced model of data set 2 is not significantly different from that of complete quadratic model. Therefore, the reduced model representing the data set 2 containing 194 points were preferred to predict the activity of MnO in ferromanganese slags. The set of model equation parameters for both the complete quadratic and reduced models for data set 2 are collected in Table XII. The model equation used can be written as:

$$a_{MnO} = 0.7265 - 0.0249\ (\%SiO_2) - 2.3115\ (B)^2 + 0.0619\ (\%MnO \times B) - 0.0003\ (\%MnO)^2 + 0.1451\ (\%CaO \times B) - 0.0018\ (\%CaO \times \%MnO) - 0.0023\ (\%CaO)^2 + 0.1439\ (\%MgO \times B) - 0.0019\ (\%MgO \times \%MnO) - 0.0045\ (\%MgO \times \%CaO) - 0.0022\ (\%MgO)^2 - 0.0506\ (\%SiO_2 \times B) + 0.0005\ (\%SiO_2 \times \%MnO) + 0.0015\ (\%SiO_2 \times \%CaO) + 0.0015\ (\%SiO_2 \times \%MgO) \quad \ldots\ldots(55)$$

Thus, if the slag composition falls within the range as illustrated in Table X, this model can be confidently used to predict the MnO activities in ferromanganese slags at 1500°C. Due to the nature of the model, it is not advisable to use the model if the slag composition falls outside the range of data set 2. It is apparent from equation(55)and Table XII that basicity is the most important parameter affecting the activity of MnO in the slag which is in accord with the depolymerization of the slag as the concentration of basic oxides increase freeing Mn^{2+} ions.

Table XII. Model parameters for MnO activities and coefficients for MnO activity models.

Data set 2			
	Coefficient	Complete Quadratic Model	Reduced Model
Intercept	a_0	355.580207	0.7265
B	a_1	370.948910	-
CaO_MgO	a_2	-15.264099	-
MnO	a_3	-10.317808	-
CaO	a_4	-12.315650	-
MgO	a_5	-28.813727	-
SiO_2	a_6	-1.095937	-0.02494
Al_2O_3	a_7	-38.087350	-
$(B)^2$	a_8	-2.543098	-2.31152
CaO_MgO x B	a_9	-0.000671	-
$(CaO\_MgO)^2$	a_{10}	-0.000004203	-
MnO x B	a_{11}	-3.6640144	0.061891
MnO x CaO_MgO	a_{12}	0.152682	-
$(MnO)^2$	a_{13}	0.067401	-0.00025538
CaO x B	a_{14}	-3.552170	0.14512
CaO x CaO_MgO	a_{15}	0.152707	-
CaO x MnO	a_{16}	0.152727	-0.0018256
$(CaO)^2$	a_{17}	0.084619	-0.0022844
MgO x B	a_{18}	-3.555340	0.14394
MgO x CaO_MgO	a_{19}	0.208931	-
MgO x MnO	a_{20}	0.318260	-0.0018543
MgO x CaO	a_{21}	0.334965	-0.0045093

Table XII continued

$(MgO)^2$	a_{22}	0.250289	-0.0022426
SiO_2 x B	a_{23}	-3.761755	-0.05055
SiO_2 x CaO_MgO	a_{24}	0.152664	-
SiO_2 x MnO	a_{25}	0.043500	0.0005164
SiO_2 x CaO	a_{26}	0.063932	0.0015194
SiO_2 x MgO	a_{27}	0.229481	0.0015104
$(SiO_2)^2$	a_{28}	-0.024803	-
Al_2O_3 x B	a_{29}	-3.697481	-
Al_2O_3 x CaO_MgO	a_{30}	0.152249	-
Al_2O_3 x MnO	a_{31}	0.412971	-
Al_2O_3 x CaO	a_{32}	0.432341	-
Al_2O_3 x MgO	a_{33}	0.597451	-
Al_2O_3 x SiO_2	a_{34}	0.320847	-
$(Al_2O_3)^2$	a_{35}	0.3446666	-

The results of the present work were also fitted, by making use of the equilibrium slag compositions, to one of the most attractive slag models developed by Gaye[89-92,124]. The model is based on the description of the liquid slag in terms of cells composed of an oxygen anion surrounded by two cations, and makes use of only binary parameters (2 to 3 per binary system).

4.1.2.1 Description of the slag model applied to the liquid mixture of an arbitrary number of oxides

A liquid mixture of m oxides is considered in which X_i represents the mole fraction of oxide $(M)_{u_i}O_{v_i}$ $(i = 1 \text{ to } m)$. The assumptions made in this model were as follows:
-An anionic sublattice without vacancies filled with oxygen ions and a cationic sublattice,
-The cationic sublattice is filled with the cations in the decreasing order of their charge,
-The structure is described in terms of symmetric (i-O-i) and asymmetric (i-O-j) cells (i and j being two different atoms), in numbers R_{ii}, ..$2R_{ij}$.., and the energy parameters consist of parameters for asymmetric cells formation, and parameters of interaction between cells. R_{ij} refers to the fraction of i-O-j cells for a random distribution of cations on their sub-lattice.
Although it is an oversimplification of the actual polymeric structure of the melt, in the $CaO-SiO_2$ system, a Si-O-Si cell represents a doubly bonded oxygen (O°), a Si-O-Ca cell represents a singly bonded oxygen (O^-) and a Ca-O-Ca cell represents a free oxygen ion (O^{2-}). Thus, the computed numbers R_{Si-Si} and $2R_{Si-Ca}$, of Si-O-Si and Si-O-Ca cells reflects the degree of polymerization of the melt. The very complex equations developed permit

the calculation of the thermodynamic activities of the all oxide components and the phase diagrams. In addition, experimental runs were done for systems containing up to six components chosen among $MnO-CaO-MgO-SiO_2-Al_2O_3-Fe_2O_3-FeO$. A very satisfactory agreement between the experimental data and the calculated values was found.

(i) Energy of cells formation

To each asymetric cell, is associated its energy of formation W_{ij}, from the symetric cells constituting the limiting pure liquid oxides:

$$i-O-i \;+\; j-O-j \;=\; 2i-O-j \quad (\Rightarrow 2W_{ij}) \qquad \ldots\ldots(56)$$

In order to obtain a satisfactory representation of one of the binary systems studied ($CaO-Al_2O_3$), it was necessary to consider a linear variation of W_{ij} with composition. The general formalism adopted thus provides for the possibility of using two cell formation parameters:

$$W_{ij} \;=\; (W_{ij})_1 \;+\; (W_{ij})_2 X_i \qquad \ldots\ldots(57)$$

where i is the cation of highest charge.

(ii) Energy of cells interaction

The various cells constituting the multicomponent melt are assumed to be distributed at random and interaction energies between them are considered (E_{ij-kl} to represent the interaction between cells i-O-j and k-O-l). Several further assumptions are made which allow the consideration of only binary interaction parameters:
-Interaction between alike cells is neglected (these terms are included in the W_{ij} parameter, assuming that they are independent of the environment of the given cells).
-Additivity rules are assumed, such as:

$$E_{jj-ii} = 2E_{ij-ii} \quad \text{.....(58)}$$

$$E_{ij-kk} = E_{ik-kk} + E_{jk-kk} \quad \text{.....(59)}$$

The only remaining type of interaction parameter (E_{ij-ij}) will be called E_{ij} for simplicity of notation.

For strongly interactive systems (SiO_2-CaO, SiO_2-MgO), it was necessary to consider a variation of the interaction parameter with composition, in order to obtain a satisfactory description of the thermodynamic properties over the whole composition range (occurrence of a miscibility gap in the acid domain, fit of silicates or

lime saturation and oxide activities in the middle range and in the basic domain of related ternary systems). As for the W_{ij} parameters, a linear relationship:

$$E_{ij} = (E_{ij})_1 + (E_{ij})_2 X_i \quad \ldots\ldots\ldots\ldots\ldots\ldots (60)$$

was used, where i is the cation of highest charge.

Therefore, the model was designed with the objective of describing multicomponent systems in terms of only a few binary parameters. In the applications which will be shown later, these parameters were taken as temperature independent, so that for the 19 limiting binary systems investigated, an average of 2.2 non-zero coefficients are used. The values selected for these parameters are given in Table XIII.

(iii) Expression of the thermodynamic functions of the liquid mixture of oxides

Before giving the final expressions, the definition of the various symbols will be given in Table XIV.

Table XIII. Energy parameters used in the model[89].

System	Cation		Cells Formation (Joule)		Cells Interaction (joule)	
	i	j	$(W_{ij})_1$	$(W_{ij})_2$	$(E_{ij})_1$	$(E_{ij})_2$
SiO_2-Al_2O_3	Si	Al	8368.0	0	-12552.0	0
SiO_2-Fe_2O_3	Si	Fe^{3+}	4184.0	0	6694.4	0
SiO_2-CaO	Si	Ca	-52300.0	0	-18828.0	31380.0
SiO_2-FeO	Si	Fe^{2+}	-6276.0	0	8786.4	4184.0
SiO_2-MgO	Si	Mg	-33472.0	0	5020.8	12552.0
SiO_2-MnO	Si	Mn	-18828.0	0	-4184.0	21756.8
Al_2O_3-CaO	Al	Ca	-35564.0	12552.0	-23012.0	-20920.0
Al_2O_3-FeO	Al	Fe^{2+}	-1673.6	0	-9623.2	0
Al_2O_3-MgO	Al	Mg	-14.6	0	-29288.0	0
Al_2O_3-MnO	Al	Mn	-5020.8	0	-13388.0	0
Fe_2O_3-CaO	Fe^{3+}	Ca	-30961.6	0	-8368.0	0
Fe_2O_3-FeO	Fe^{3+}	Fe^{2+}	-2092.0	0	-2092.0	0
Fe_2O_3-MnO	Fe^{3+}	Mn	-2092.0	0	-2092.0	0
CaO-FeO	Ca	Fe^{2+}	-12552.0	0	2092.0	0
CaO-MgO	Ca	Mg	4184.0	0	0	0
CaO-MnO	Ca	Mn	-2092.0	0	-3347.2	0
FeO-MgO	Fe	Mg	-2092.0	0	0	0
FeO-MnO	Fe	Mn	-2092.0	0	0	0
MgO-MnO	Mg	Mn	-2092.0	0	-3347.2	0

Table XIV. Nomenclature for the definition of the various symbols used in the expression of the thermodynamic functions of the liquid mixture of oxide[99].

m	Number of oxides $(M_i)_{u_i}.O_{v_i}$
u_i, v_i	Stoichiometric indexes of oxides
X_i	Molar fractions of oxides
R_{ii}, $2R_{ij}$	Numbers of i-O-i, i-O-j cells
$W_{ij}=(W_{ij})_1+(W_{ij})_2.X_i$	Energy parameters for asymetric cells formation
$E_{ij}=(E_{ij})_1+(E_{ij})_2.X_i$	Energy parameters for cells interactions
$D_i=\sum_{k=i}^{m} v_k X_k$	Summation of stoichiometric indexes of oxides multiplied by mole fractions
$R_{ij}=(v_i v_j X_i X_j)/D_1$	Fraction of i-O-j cells for a random distribution of cations on their sublattice
$Q_i=\sum_{k=i+1}^{m} (v_k X_k/D_1).(E_{ik}/RT)$	Summation of fraction of i-O-j cells for a random distribution of cations on their sublattice multiplied by energy parameters for cells interactions

(iv) Free energy of mixing

The free energy of mixing, G_M, can be calculated once the cell fractions, R_{ij}, which indicate the degree of polymerisation is known. The cell fractions have to satisfy the two sets of constraints, namely a linear sets of equations which are material balances and a set of quadratic equations which come from maximizing the partition function. The expression for the mixing free energy of the melt, with reference to the liquid pure oxides, is as follows:

$$G^M = 2\sum_{i=1}^{m-1}\sum_{j=i+1}^{m}\left[R_{ij}W_{ij} + R_{ii}\frac{v_j X_j}{D_1}E_{ij}\right]$$

$$-RT\sum_{i=1}^{m-1}\frac{u_i}{v_i}\left[D_i \ln\left(\frac{D_i}{v_i X_i}\right) - D_{i+1}\ln\left(\frac{D_{i+1}}{v_i X_i}\right)\right]$$

$$-RT\sum_{i=1}^{m}\sum_{j=1}^{m}[\Gamma_{ij}^{*}\ln R_{ij}^{*} - R_{ij}\ln(R_{ij})] \quad \text{.....(61)}$$

where the cell fractions, R_{ij} satisfy a system of $m(m+1)/2$ constrains, that is, i=1 to m:

$$\sum_{j=1}^{m} R_{ij} = v_i X_i \quad \text{.....(62a)}$$

$$R_{ii}.R_{ij} - R_{ij}^2/P_{ij}^2 = 0 \quad (j = i+1 to m) \ldots\ldots\ldots\ldots\ldots\ldots\ldots\ldots\ldots\ldots\ldots\ldots (62b)$$

The equation (62a) shows the linear equations which are material balances whereas the equation (62b) shows the quadratic equations which come from the maximization of the partition function.

The only numerical difficulty lies in the resolution of the system of equations (62a) and (62b), in particular for systems having a large number of components (10 equations in a 4-component system; 21 equations in a 6-component system). A particularly efficient technique was devised for this resolution. Computer time on IRSID's VAX 11/780 is about 0.3 seconds CPU for one composition in a 6 component system and this time is approximately proportional to the number of components.

(v) Numerical scheme for the solution of constraint equations

If it is noted that $y_i \equiv (R_{ii})^{1/2}$, the system of equations (62a) and (62b) is transformed into:

$$y_i . \sum_{1}^{m} P_{ij} . y_j = v_i X_i \quad (i = 1 \quad to \quad m) \ldots\ldots\ldots\ldots\ldots\ldots\ldots\ldots\ldots\ldots (63a)$$

$$R_{ij} = P_{ij}.y_i.y_j \quad (i,j = 1 \quad to \quad m).....(63b)$$

Once the values of the y_i's have been obtained from the system of m quadratic equations (63a), the calculation of the R_{ij}'s through the equation (63b) is straightforward. For the resolution of equations (63a), a scheme using a succession of Taylor's series expansions in terms of the variable $z \equiv T/\sigma$ varying between z=0 ($\sigma \to \infty$) and z=1 ($\sigma \to T$) has been devised. The variations of y_i between $\sigma \to \infty$ (random distribution of cations, that it is $y_i^* = V_i X_i / D_i$) and $\sigma \to T$ are thus described. For any intermediate temperature σ, equations (63a) are written:

$$y_i . \sum_{j=1}^{m} (P_{ij})^z . y_j = v_i X_i \quad (i = 1 \quad to \quad m).....(64)$$

and the Taylor's series expansions have the form:

$$[y_i]_{z+\Delta z} = [y_i]_z + [y']_z . \Delta z + [y'']_z . \Delta z^2/2, ...(65)$$

expressions in which the first and second order derivatives of y_i's are obtained through differentiation of the system of equations (63a).

The only numerical difficulty in the resolution of the system of equations (62a) and (62b) is thus reduced to the solution of two systems of m linear equations:

$$(A).(y') = (B') \quad \text{.....(66)}$$

$$(A).(y'') = (B'') \quad \text{.....(67)}$$

where

$$a_{ij} = (p_{ij})^{z}.y_i \quad if\ j \neq i \quad \text{.....(68)}$$

$$a_{ij} = y_i + \sum_{k=1}^{m} (P_{ik})^{z}.yk \quad if\ j \neq i \quad \text{.....(69)}$$

$$b'_i = -y_i \sum_{j=1}^{m} (P_{ik})^{z}.\ln P_{ij}.y_j \quad \text{.....(70)}$$

$$b''_i = -\sum_{j=1}^{m} (P_{ij})^{z}[2y'_i y'_j + 2(y'_i y_j + y_i y'_j)\ln P_{ij} + y_i y_j (\ln P_{ij})^2] \quad \text{.....(71)}$$

(vi) Enthalpy and entropy of mixing

The free energy of mixing having been computed for a given composition at temperatures T, $T-\Delta T$ and $T+\Delta T$, the enthalpy and entropy of mixing are obtained using Gibbs-Helmotz equation:

$$H^M = \delta(G^M/T)/\delta(1/T) \quad \text{.....(72)}$$

$$H^M = [G^M(T+\Delta T)/(T+\Delta T) - G^M(T-\Delta T)/(T-\Delta T)]/[1/(T+\Delta T) - 1/(T-\Delta T)] \quad \text{.....(73)}$$

$$S^M = (H^M - G^M)/T \quad \text{.....(74)}$$

When the W_{ij} and E_{ij} parameters are assumed temperature independent, the mixing entropy is identical to the configurational entropy.

(vii) Component activities

By incrementing to various sides of the composition of which the activities are needed, the derivative of free energy with composition, $\delta G^M/\delta X_j$, is obtained. The activities of the components with liquid state references are calculated numerically from the computed free energy of mixing and its derivatives with respect to composition through equation (75).

$$RT\ln a_i = G^M + \sum_{j=2}^{m} (\delta_{ij} - X_j)\frac{\delta G^M}{\delta X_j} \quad \ldots\ldots i = 1 \quad to \quad m \ldots\ldots\ldots\ldots\ldots\ldots\ldots\ldots (75)$$

where δ_{ij} = Kronecker's symbol

T = absolute temperature

R = universal gas constant

a_i = activity of component a

m = number of compounds

For this calculation, the derivatives of the free energy of mixing are computed numerically:

$$\delta G^M/\delta X_j = [G^M(X_k, X_j + \Delta X_j) - G^M(X_k, X_j - \Delta X_j)]/2\Delta X_j \ldots\ldots\ldots\ldots\ldots\ldots\ldots\ldots (76)$$

Changes of reference state can then be made to express the activities with respect to the classically used reference states. For instance, the ratio of activities referenced to solid and liquid states is given by (neglecting the differences in heat capacity):

$$(a_{MO})_s/(a_{MO})_l = \exp\left(\frac{\Delta H_m - T\Delta S_m}{RT}\right) \ldots\ldots\ldots\ldots\ldots\ldots\ldots\ldots\ldots\ldots\ldots\ldots (77)$$

where ΔH_m and ΔS_m are the enthalpy and entropy of melting of the pure component. The values of ΔH_m and ΔS_m for the various oxides studied are given in Table XV.

Table XV. Enthalpy and entropy of change of reference state for the various components[89].

Component	Classical reference	ΔH_{ref} (joule/mole)	ΔS_{ref} (joule/mole/K)
SiO_2	Solid (cristobalite)	9539.5	4.770
Al_2O_3	Solid	110876.0	47.698
Fe_2O_3	"	86776.2	46.024
CaO	"	80332.8	28.242
MnO	"	50208.0	23.472
MgO	"	77404.0	25.020
FeO	"FeO" liquid in equilibrium with Fe	8221.6	4.184

(viii) Use of the model for the description of phase diagrams-Liquid miscibility gaps

The determination of the miscibility gaps existing in the acid domain of silicate melts was made graphically, for the binary systems. As the inflexions on the free energy curves are not pronounced, the determination of equilibrium compositions, for a series of temperatures, was made from the computed activities of both components.

The good agreement obtained between experimental and computed miscibility gaps, which cover a temperature span of 400 to 600 K can be considered as a conclusive test that the effect of temperature on the free energy is properly represented by the model, using temperature-independent parameters.

(ix) Equilibrium of liquid slag with stoichiometric compounds

Equilibrium of liquid slag with stoichiometric compounds is the most common situation for oxide systems. For any composition, it is possible to express the activity in the liquid phase, taking as reference a given stoichiometric compound. For instance, in any melt containing SiO_2 and CaO, the activity of the compound 2CaO-SiO2 (solid) is given by:

$$a_{2CaO-SiO_2} = (a_{CaO})^2 . a_{SiO_2} . \exp(-\Delta G_f / RT) \quad \ldots\ldots\ldots\ldots\ldots\ldots (78)$$

where a_{CaO} and a_{SiO_2} are the activities of solid CaO and SiO_2, and ΔG_f is the free energy of formation of $2CaO-SiO_2$ from CaO (solid) and SiO_2 (solid).

The compositions for which the activity of the stoichiometric compound is unity represent its saturation limit at the given temperature.

The values used to represent the free energy of formation ($\Delta G_f = A - BT$) of the various compounds of interest for the systems studied are listed in Table XVI. For most of the compounds, the values were taken from the SGTE data bank. For some of the compounds, it was necessary to alter significantly the value of the enthalpy and entropy terms (while keeping the value of the free energy well within domain of reported uncertainty), in order to obtain the best fit of the phase diagram. This was also the case, in particular, for the compounds $2CaO-SiO_2-Al_2O_3$ and $CaO-Al_2O_3-2SiO_2$, for which values of 60.25 and 55.23 joule/mole.°K (B or ΔS values used to represent the free energy of formation, Table XVI) had to be used instead of the values of 15.06 and 19.67, respectively, found in the tables of thermochemical values.

(x) Equilibrium of liquid slag with ideal solution of stoichiometric compounds

Table XVI **Free energy of formation of stoichiometric compounds from pure components taken in the reference state of Table XV values used in the model[89].**

Component	$\Delta G^0_{form} = A - BT$	
	A (joule/mole)	B (joule/mole.K)
$CaO-SiO_2$	-77069.28	3.38
$3CaO-2SiO_2$	-202924.00	12.9
$2CaO-SiO_2$	-79705.20	35.56
$3CaO-SiO_2$	-115060.00	23.01
$2FeO-SiO_2$	-97487.20	-52.72
Wustite (FeO)	-31338.16	-19.00
$MgO-SiO_2$	-41254.24	-4.18
$2MgO-SiO_2$	-50919.28	9.62
$MnO-SiO_2$	-26777.60	-2.09
$2MnO-SiO_2$	-61295.60	-12.55
$3CaO-Al_2O_3$	-23430.40	33.89
$CaO-Al_2O_3$	-23012.00	18.83
$CaO-2Al_2O_3$	-23012.00	25.94
$CaO-6Al_2O_3$	-22593.60	31.80
$FeO-Al_2O_3$	-64015.20	-23.43
$MgO-Al_2O_3$	-6108.64	25.94
$MnO-Al_2O_3$	-47823.12	-11.72
$2SiO_2-3Al_2O_3$	-76564.48	26.36
$2CaO-SiO_2-Al_2O_3$	-61923.20	60.25
$CaO-2SiO_2-Al_2O_3$	-13807.20	55.23
$CaO-MgO-2SiO_2$	-75583.96	29.71
$CaO-MgO-SiO_2$	-83219.76	16.11
$2CaO-MgO-2SiO_2$	-128950.88	42.26
$3CaO-MgO-2SiO_2$	-205016.00	31.80

In the general case of extended solid solutions, the phase diagram calculation would require a precise estimation of the free energy of the solid phase. In some cases, however, the assumption of an ideal solid solution of two compounds can be applied. With this assumption, the condition of saturation in, for instance, (Fe-Mn)O solid solution, for a melt containing among other components FeO and MnO, is expressed as:

$$a_{FeO}(solid) + a_{MnO}(solid) = 1 \quad \text{.....(79)}$$

a_{FeO} and a_{MnO} being the activities of FeO and MnO in the ideal solid solution of these two compounds.

This assumption leads to a fairly accurate estimation of liquidus temperatures for the (Fe-Mn)O, (Ca-Mn)O solid solutions, as well as for olivine phases and melilite[89].

In a six component system, a set of 21 simultaneous equations have to be solved. The present time of calculation on an AT computer is about 20 seconds. A decrease in calculating time reduces the accuracy. The advantages of this model is that it can be applied to complex slag systems with great reliability, it represents a large basicity range and it is very efficient for the numerical treatment with regard to its short computing time. These set of simultaneous equations were solved by making use of a computer software developed at MINTEK[125].

4.1.2.2 Discussion on activity of MnO in ferromanganese slags

Another important concept in analysing the behaviour of slags is the basicity and it was given due consideration in the present study. Since the concept of basicity of slags is such a useful and important one, various different ways of expressing it have been derived over the years. The most common approach was the use of basicity ratio or basicity index in which the basic oxides were placed on the numerator and acid oxides on the denominator. Different forms of classical basicity ratio have been derived. The simplest one expressed as (CaO% / SiO_2%) was useful as a first approximate guide. In slags containing appreciable quantities of components other than CaO and SiO_2, it was an imperfect measure of basicity. Since most blast furnace slags tend to contain significant amounts of MgO and Al_2O_3, the ratio (CaO% + MgO%) / (SiO_2% + Al_2O_3%) has found some application in industrial practise. This expression, however, implies that MgO is equivalent to CaO as a basic oxide and that Al_2O_3 is equivalent to SiO_2 as an acid oxide on a mass per cent basis, and clearly neither of these equivalences is accurate. Various other more complex ratios have appeared in the literature from time to time, but none has demonstrated any significant improvement over that of Bell, to exhibit an accurate linear relationship with the logarithm of the sulphide capacity of these slags[126]. Bell et al. suggested the ratio[126]

$$\frac{X_{CaO} + 0.5X_{MgO}}{X_{SiO_2} + 0.33X_{Al_2O_3}} \quad \text{.....(80)}$$

where X was the mole fraction of the component concerned. This expression implies that MgO is half as effective as CaO as a base on a molar basis, while Al_2O_3 is one third as effective as SiO_2 as an acid, again on a molar basis.

The other approach adopted has been the use of excess base expressions, of the form $\Sigma Basic oxides - \Sigma Acid oxides$, where the concentration units can be either mass per cent, molar per cent or mole fraction. This approach has not been widely used, though fairly recently Brown has suggested what is perhaps the most interesting form of this expression from a fundamental point of view[126]. Brown suggested the relation[126]

$$Excess \quad base = \frac{X_{CaO}}{I_{CaO}} + \frac{X_{MgO}}{I_{MgO}} - \frac{X_{SiO_2}}{I_{SiO_2}} - \frac{X_{Al_2O_3}}{2I_{Al_2O_3}} \qquad (81)$$

where I is the ion-oxygen attraction of the cation involved. The expression he used has been shown to exhibit an excellent linear correlation with the logarithm of the sulphide capacity of blast furnace slags[126].

The main problem with these expressions for both basicity index and excess base, is that, they involve an arbitrary decision as to whether a component is a basic or acidic oxide, so that they can be assigned to the numerator or denominator in a basicity ratio, or assigned a positive or negative sign in an excess base relation,

respectively. For most components the situation is clear and this poses no real problem, however, for intermediate oxides, such as TiO_2, this can indeed pose some difficulty. A secondary problem with ratios is that the assessment of basicity becomes impossible in slags free of any recognized acid components, such as that might be used in secondary processing of iron and steel.

An alternative approach is the use of optical basicity which has been pioneered and developed in the field of glass chemistry[126]. In this approach, basicities are regarded in terms of the electron donor power of the oxygen ions present. This can be measured experimentally by introducing trace quantities of metal ions which respond directly to the degree of electron donation experienced from the oxides of the glass. From a large number of measurements of the optical basicity of glasses, mainly using Pb^{2+} as the probe ion, Duffy and Ingram discovered the optical basicity of an oxide, λ, is related to the Pauling electronegativity, x of the cation involved by the expression[126]:

$$\lambda = 0.74/(x - 0.26) \quad \text{.....(82)}$$

Use of this relation allows calculation of the optical basicity for any main group element oxide in which the cation has an inert gas electron configuration and which does not display any transition metal behaviour in a slag. Hence, by use of the relationship:

$$\Lambda = X_A\lambda_A + X_B\lambda_B + \ldots\ldots\ldots\ldots\ldots\ldots(83)$$

it is possible to calculate the bulk or average optical basicity value, Λ, for a slag of any composition involving these oxides. In this equation, X is the equivalent cation fraction, based on the fraction of negative charge neutralized by the charge on the cation concerned. For any component, X can be evaluated in various ways. Where the composition is expressed in terms of mole fractions, the most convenient relation is:

X = (*Mole fraction of component . number of oxygen atoms of oxide molecule*) / Σ*Mole fraction of component . number of oxygen atoms of oxide molecule*.....(84)

A correlation has been established[126] between optical basicity values for slags and their sulphide capacities at 1500°C, from data in seven systems not containing any transition metal oxide. By fitting data for fourteen other systems containing transition metal oxides to this relationship, effective optical basicity values have been deduced[126] for the four oxides concerned, FeO, Fe_2O_3, MnO and TiO_2.

In the present work, optical basicity values were also calculated along with the classical basicity for every individual slag composition making use of the data of Sommerville and Sosinsky[126]. However, due to problems in expressing the optical basicity of MnO (transition metal oxide) accurately, the average optical basicity values

of slags were not employed in regression models. Furthermore an acceptable relationship between optical and classical basicity could not be found for the present slags. The data employed for CaO, MgO, SiO_2, Al_2O_3 and MnO in order to calculate the average optical basicity of the slags in present study are given in Tables XVII and XVIII. In Table XVIII Λ_s represents the apparent or effective optical basicity values for transition metal oxides.

In Figures 37 to 42, the MnO activities are plotted against its mass per cent. The symbols represent the experimental values, the solid line and the dashed line represent the predicted values through the empirical formula and slag model respectively. As it is seen from the figures, the basicity and CaO-to-MgO ratios of these individual groups are different. The alumina content is constant at around 5 mass per cent. The basicity and CaO-to-MgO ratios of the slags chosen from the experimental values are given with error ranges. This was due to selecting the experimental points which have very similar basicity and CaO-to-MgO ratios in order to form individual experimental groups with different basicity and CaO-to-MgO ratios with the error limits not exceeding $\pm$ 0.05.

As it is seen from Figures 37 to 42, there is excellent agreement between the predicted activity values from the empirical model equation and the values obtained from the slag model with the maximum difference being below 20 per cent, which also shows that, the agreement between the theoretical activity values obtained from the slag model

Table XVII. Optical basicity of various oxides[126].

Oxide	Electronegativity of cation	Lambda
K_2O	0.8	1.04
Na_2O	0.9	1.15
BaO	0.9	1.15
Li_2O	1.0	1.00
CaO	1.0	1.00
MgO	1.2	0.78
Al_2O_3	1.5	0.61
SiO_2	1.8	0.48
B_2O_3	2.0	0.42
P_2O_5	2.1	0.40
CO_2	2.5	0.33
SO_3	2.5	0.33

Table XVIII. Optical basicity values calculated from sulphide capacity data[126].

Oxide	Λ_S	Standart Deviation, %	Number of Data Points
TiO_2	0.61	11.0	136
Fe_2O_3	0.70	4.4	17
FeO	1.03	10.0	87
MnO	1.21	8.0	73

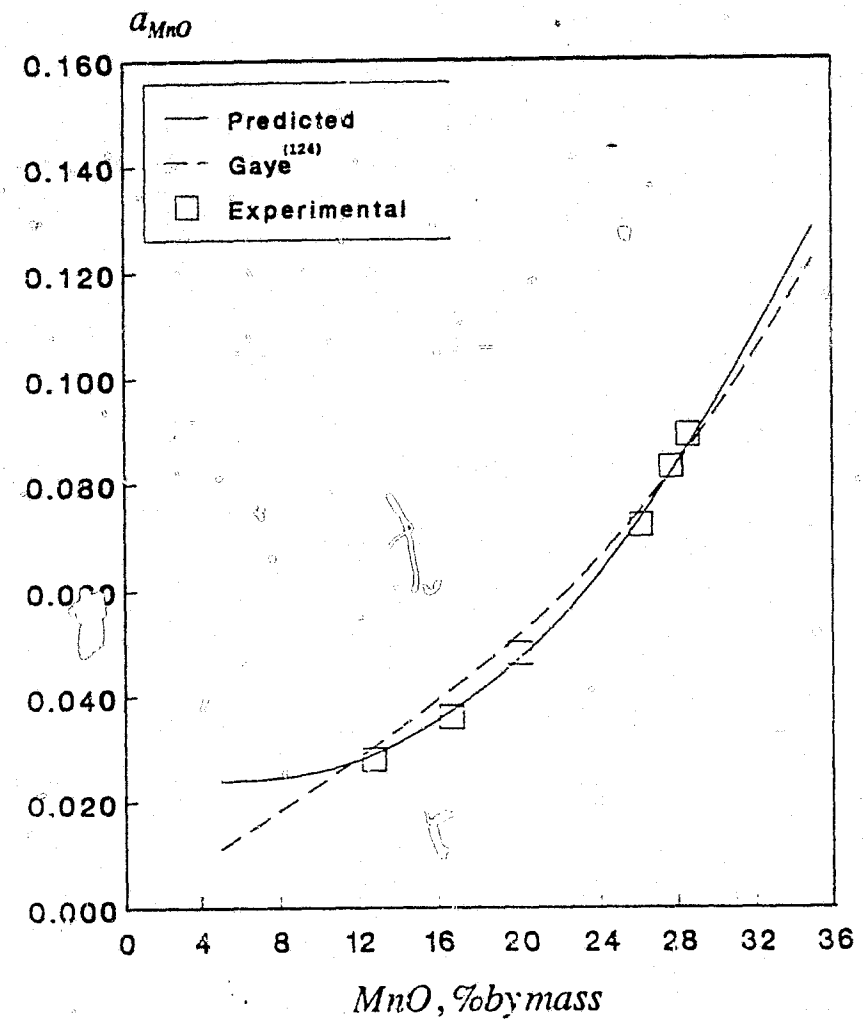

Figure 37. Activities of MnO in MnO-CaO-MgO-SiO_2-Al_2O_3 slags at 1500°C, B=0.58±0.02, CaO:MgO=∞, % Al_2O_3=5, optical basicity=0.68.

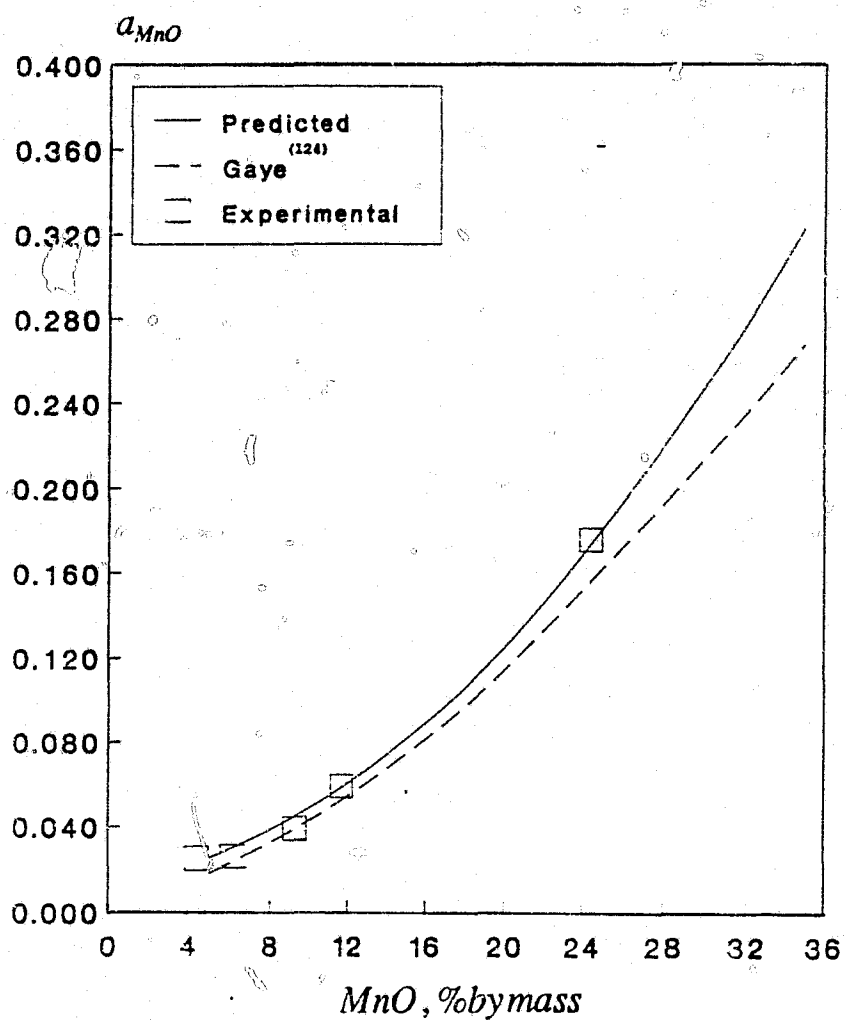

Figure 38. Activities of MnO in $MnO-CaO-MgO-SiO_2-Al_2O_3$ slags at 1500°C, B=1.17±0.05, CaO:MgO=0.26±0.04, % Al_2O_3=5, optical basicity=0.66.

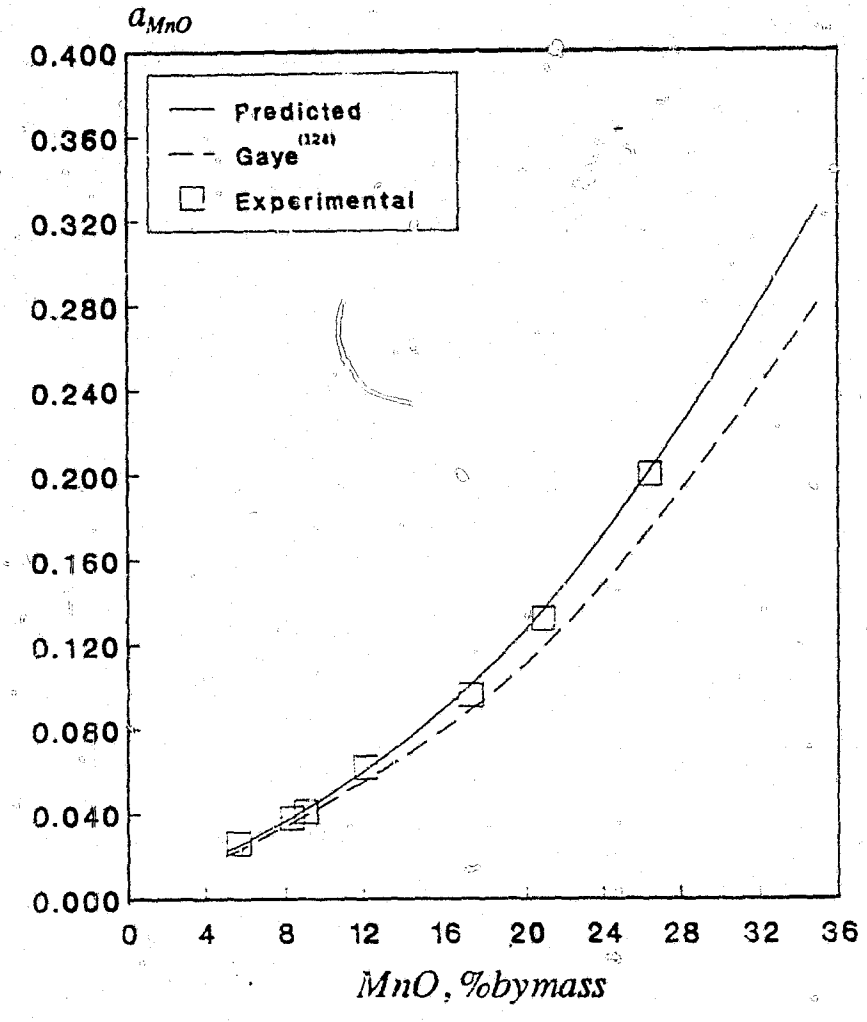

Figure 39. Activities of MnO in MnO-CaO-MgO-SiO_2-Al_2O_3 slags at 1500°C, B=1.11±0.06, CaO:MgO=2.02±0.04, % Al_2O_3=5, optical basicity=0.70.

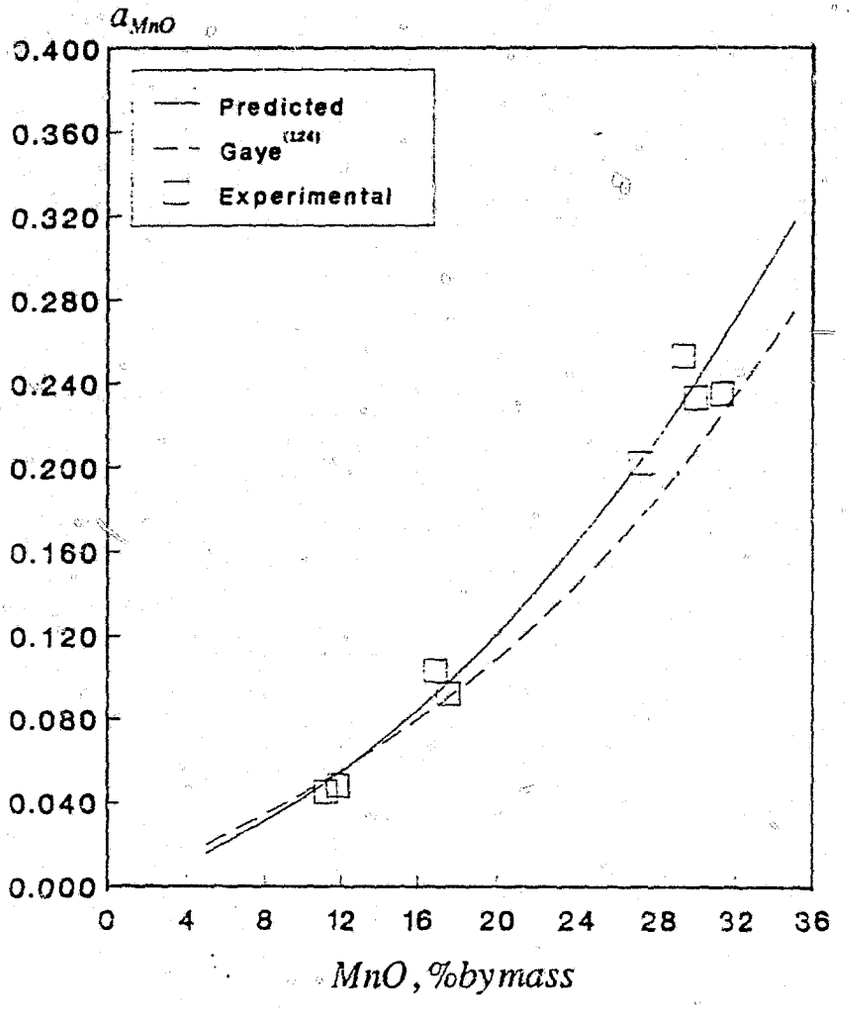

Figure 40. Activities of MnO in MnO-CaO-MgO-SiO_2-Al_2O_3 slags at 1500°C, B=1.07±0.05, CaO:MgO=4.50±0.06, % Al_2O_3=5, optical basicity=0.73.

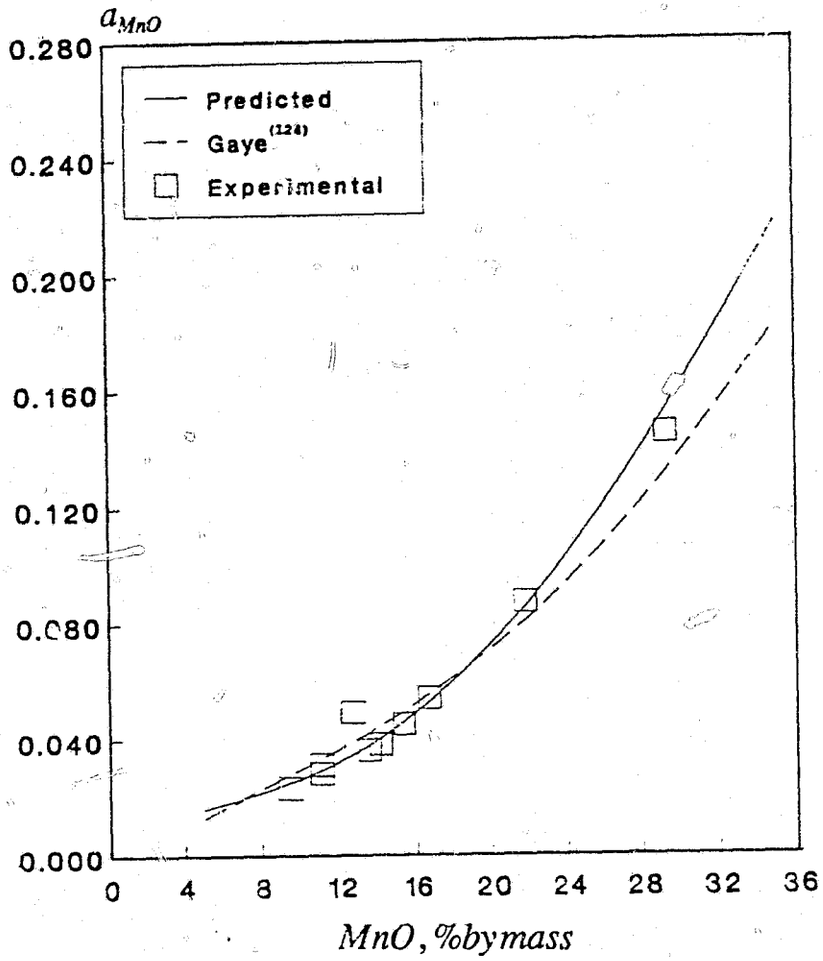

Figure 41. Activities of MnO in $MnO-CaO-MgO-SiO_2-Al_2O_3$ slags at 1500°C, B=0.83±0.04, CaO:MgO=3.65±0.06, % Al_2O_3=5, optical basicity=0.67.

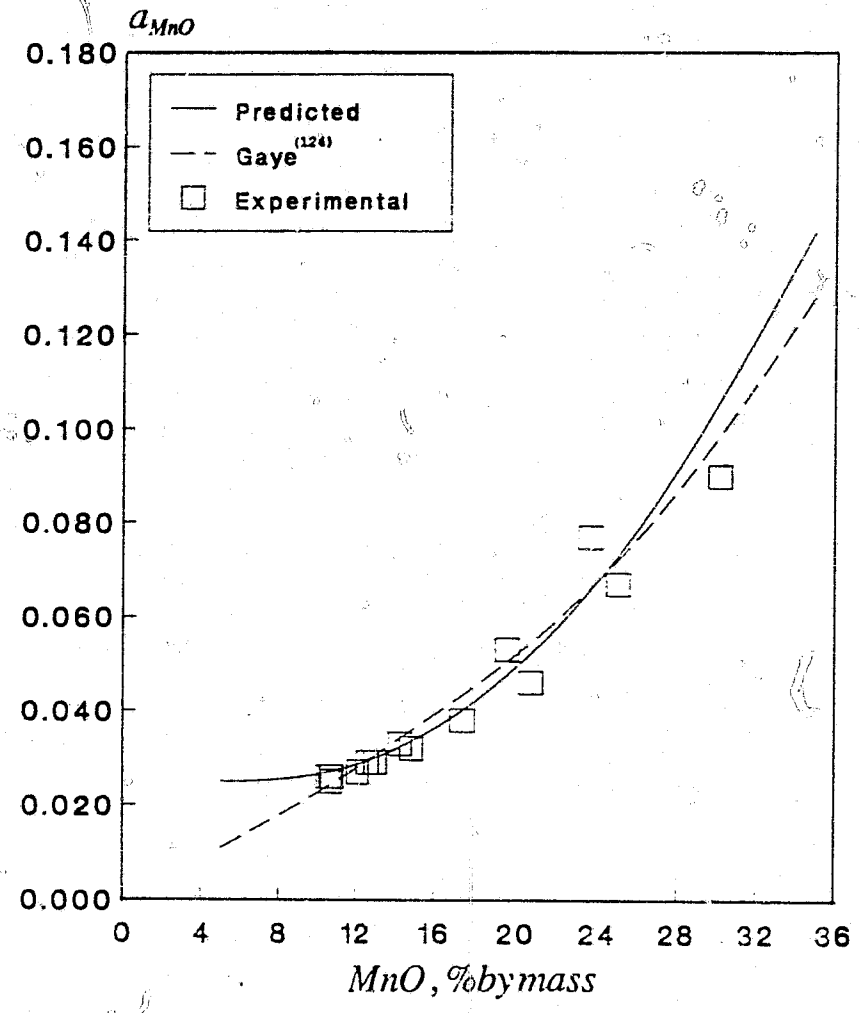

Figure 42. Activities of MnO in MnO-CaO-MgO-SiO_2-Al_2O_3 slags at 1500°C, B=0.64±0.05, CaO:MgO=3.57±0.06, % Al_2O_3=5, optical basicity=0.65.

and the experimental values determined in the present study is satisfactory. It can be stated that the synthetic ferromanganese slag behaviour can be approximated to Gaye's[124] slag model successfully. (The figures showing the relationship between the MnO content and the activities of MnO at various basicity and CaO-to-MgO ratios are collected in Appendix C, through Figures C.1 to C.15)

Evidently an increase in the mass concentration of MnO in the slag increases its activity. The increase in the activity of MnO with increasing concentration can be explained in terms of the principle of the ionic structure in liquid slags. At a given concentration of MnO in the slag, a certain proportion of Mn^{2+} ions will be associated with the silicate and aluminate anions, and a certain portion of them will be associated with free oxygen ions. An increase in the mass concentration of MnO in the slag will further break down the network structure causing an increase in the number of free oxygen ions. Silicate anionic groups are preferentially associated with Ca^{2+} and Mg^{2+} ions and metal ions such as Mn^{2+}, due to their preference for free oxygen ions, will be associated with free oxygen ions which will be reflected as an increase in MnO activity.

The regression model adopted was used in order to predict the activities of MnO in the slag in the experimental composition range and at various basicity and CaO-to-MgO ratios in order to analyse the effect of these parameters on the activity of MnO as a function of its concentration. Various curves were plotted at constant

basicity ratio with various CaO-to-MgO ratios, and similarly at constant CaO-to-MgO ratio with various basicity ratios. In Figure 43, the effect of CaO-to-MgO ratio on the activity of MnO at constant basicity ratio is seen. According to this figure, CaO has a slight effect in increasing the MnO activities. Figures 44 to 46 illustrate the same effect of CaO on MnO activity at different basicity ratios. This result is also in agreement with the work of Warren[9]. Other plots showing the same effect of CaO on the MnO activities are also given in Appendix C, in Figures C.16 to C.21.

In order to measure and compare the action of various oxides in silicate and aluminate melts, an adequate measuring standard or criteria must be established. The modern slag theory proposes the disintegration of the silica network and the formation of a number of different anionic groups. The extent to which this phenomena happens has been shown to be dependent upon the free energy of interaction between metal oxide and silica. Therefore, an attempt in order to explain the results of the present study must also consider the free energy of formation of certain orthosilicates and metasilicates. At metasilicate composition the network r[illegible] not be modified significantly due to the lower free energy of formation of $MgSiO_3$ and $CaSiO_3$ than those of Mg_2SiO_4 and Ca_2SiO_4[121,123,127,128] respectively. This results in a less disrupted silica network. When the free energy of formation of the orthosilicates Ca_2SiO_4, Mg_2SiO_4, and $CaMgSiO_4$ are taken into consideration, it can easily be seen that Ca_2SiO_4 has the most negative free energy of formation[121,123,127,128]. Furthermore, the free energy of formation of $CaMgSiO_4$ is more negative[121,123,127,128] than that

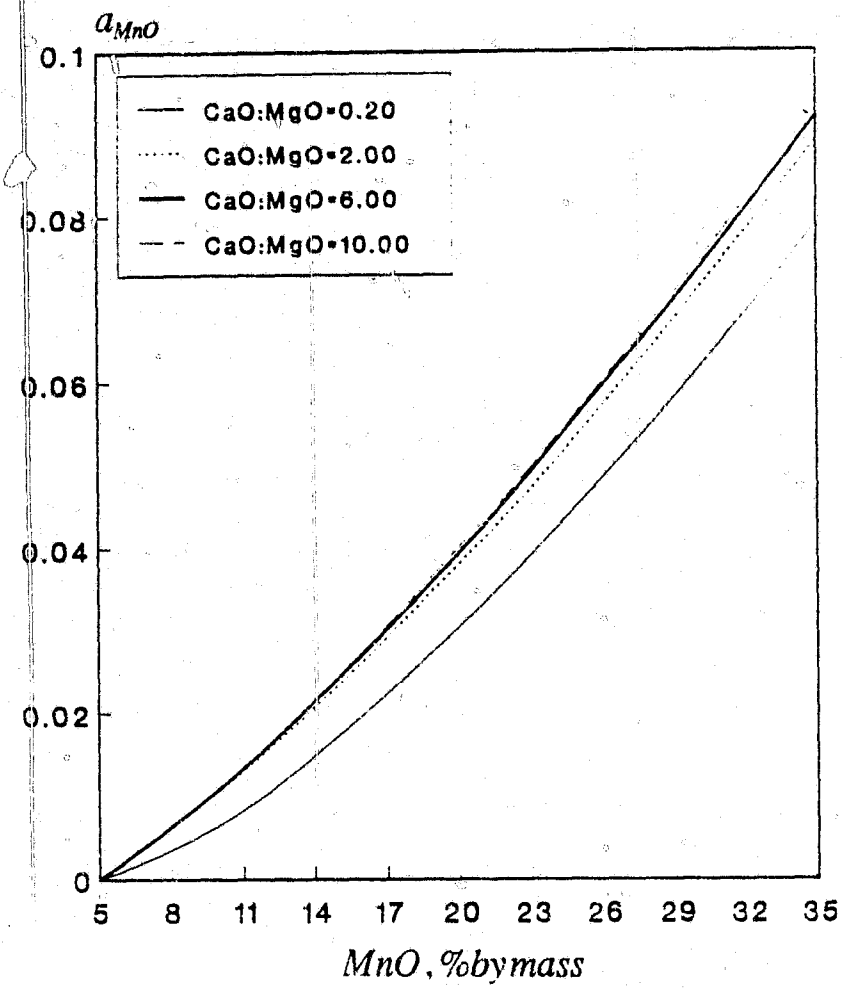

Figure 43. Activities of MnO in MnO-CaO-MgO-SiO_2-Al_2O_3 slags at 1500°C for various CaO-to-MgO ratios with B=0.40.

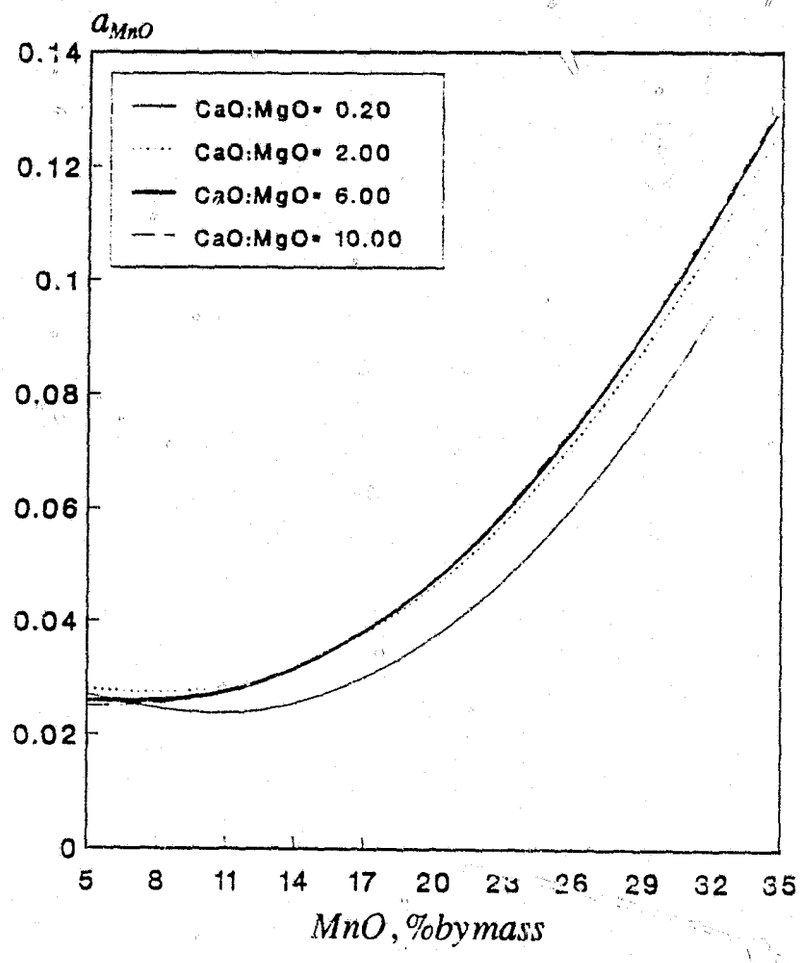

Figure 44. Activities of MnO in MnO-CaO-MgO-SiO_2-Al_2O_3 slags at 1500°C for various CaO-to-MgO ratios with B=0.60.

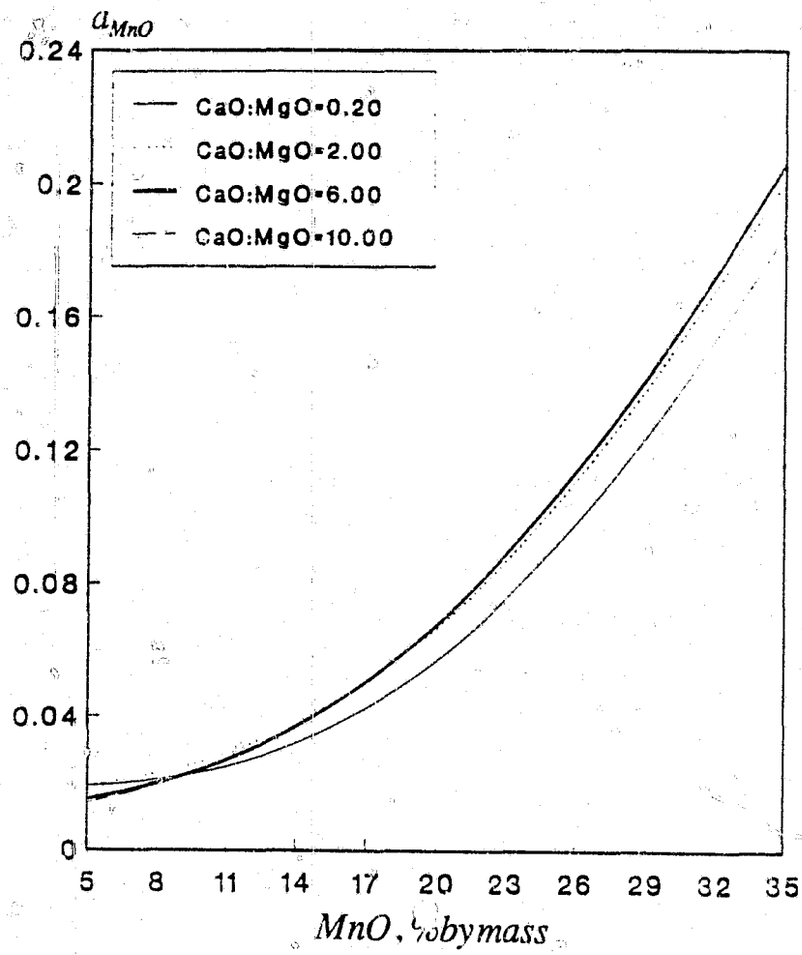

Figure 45. Activities of MnO in MnO-CaO-MgO-SiO_2-Al_2O_3 slags at 1500°C for various CaO-to-MgO ratios with B=0.80.

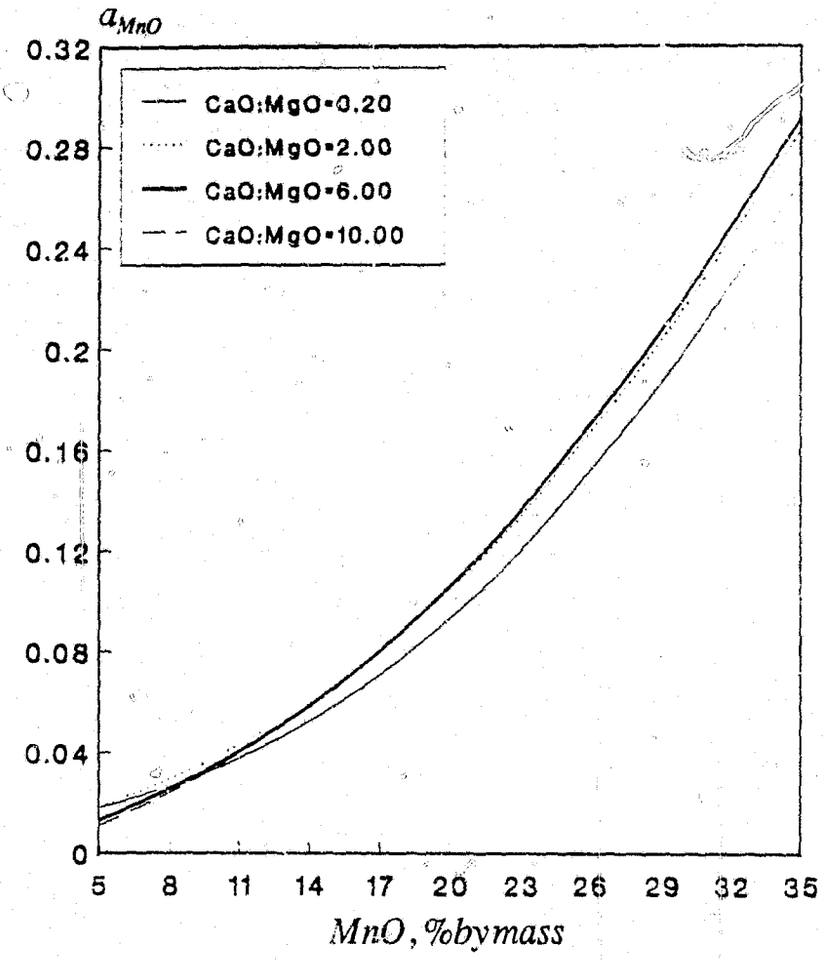

Figure 46. Activities of MnO in $MnO-CaO-MgO-SiO_2-Al_2O_3$ slags at 1500°C for various CaO-to-MgO ratios with B=1.00.

of $MgSiO_4$. In other words, this can be interpreted as meaning that the interaction of Ca^{2+} ions with SiO_2 is stronger than those of mixed Ca^{2+} and Mg^{2+} ions and individual Mg^{2+} ions. Thus, one can conclude that an increase in the amount of CaO can lead to an increased tendency for the formation of Ca_2SiO_4 orthosilicate, leading to higher MnO activities in the slags. Because of the interaction of Ca^{2+} with silica, Mn^{2+} ions gain more freedom, i.e. become less associated with the silica network, and therefore the MnO activities increase.

Figures 47 to 50 illustrate the effect of basicity ratio on the MnO activities when CaO-to-MgO ratio remains constant. An increase in the basicity ratio clearly increases the MnO activity. This can be explained in a very similar way in terms of modern slag theory. At low basicities almost all the metal cations, viz. Ca^{2+}, Mg^{2+}, Mn^{2+} are associated with the large silicate anionic groups and only very a few free O^{2-} ions exist. In other words, at low basicities, the silica network is not disrupted. The activity of MnO in such melts is thus low. As the concentration of the basic oxides increases, the silica network is broken up into smaller anionic groups which refers to lower slag viscosity and the proportion of free oxygen ions begins to increase. Thus, an equal number of divalent cations, which were associated with silicate anions, associate with free oxygen anions. At this point, divalent cations like Ca^{2+}, Mg^{2+} because of their higher interaction with silicate ions, are preferentially associated with silicate ions, and thus Mn^{2+} ions will have less degree of association with silicate ions. In other words, the free energy of formation of $MnSiO_3$ is less negative than that of $MgSiO_3$

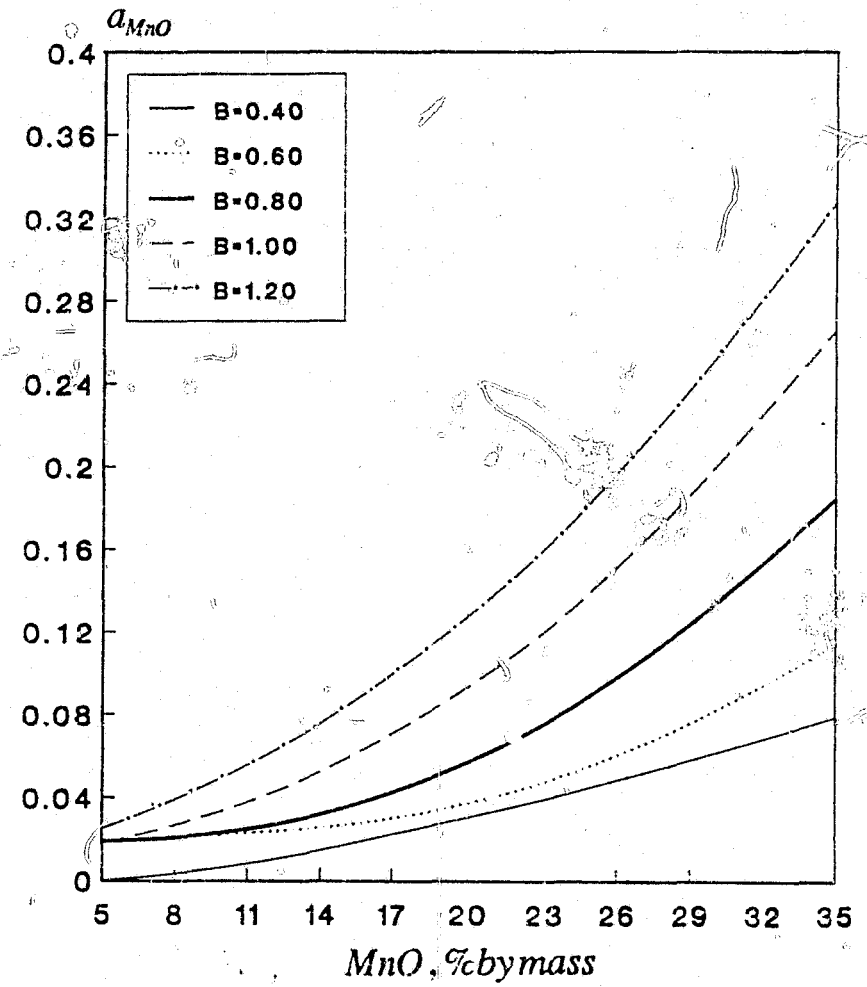

Figure 47. Activities of MnO in $MnO-CaO-MgO-SiO_2-Al_2O_3$ slags at 1500°C for various basicity ratios with CaO:MgO=0.20.

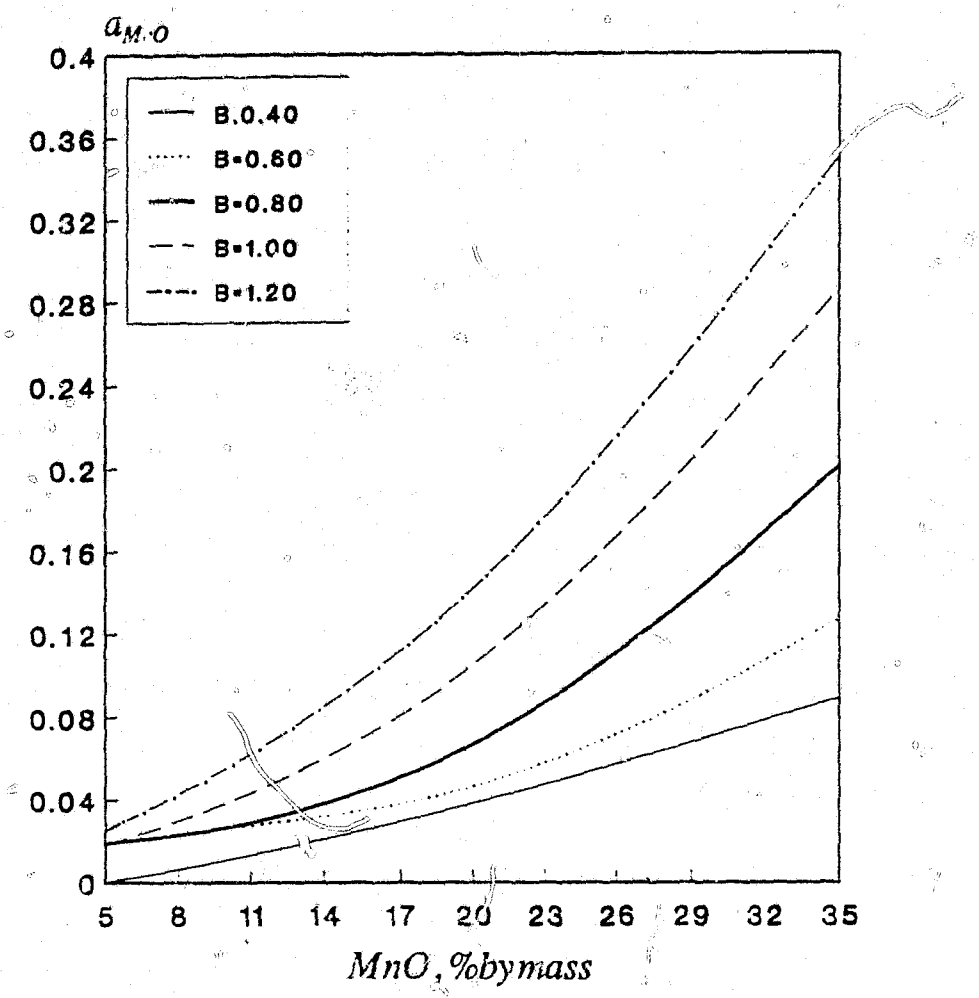

Figure 48. Activities of MnO in MnO-CaO-MgO-SiO_2-Al_2O_3 slags at 1500°C for various basicity ratios with CaO:MgO=2.00.

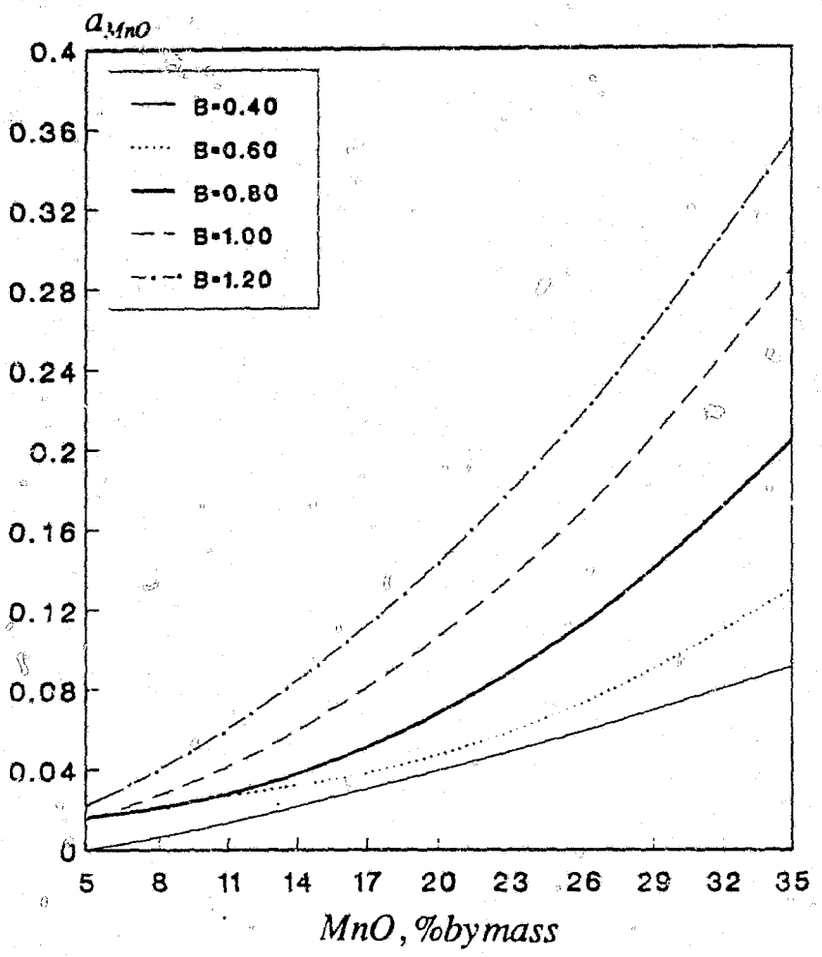

Figure 49. Activities of MnO in $MnO-CaO-MgO-SiO_2-Al_2O_3$ slags at 1500°C for various basicity ratios with CaO:MgO=4.00.

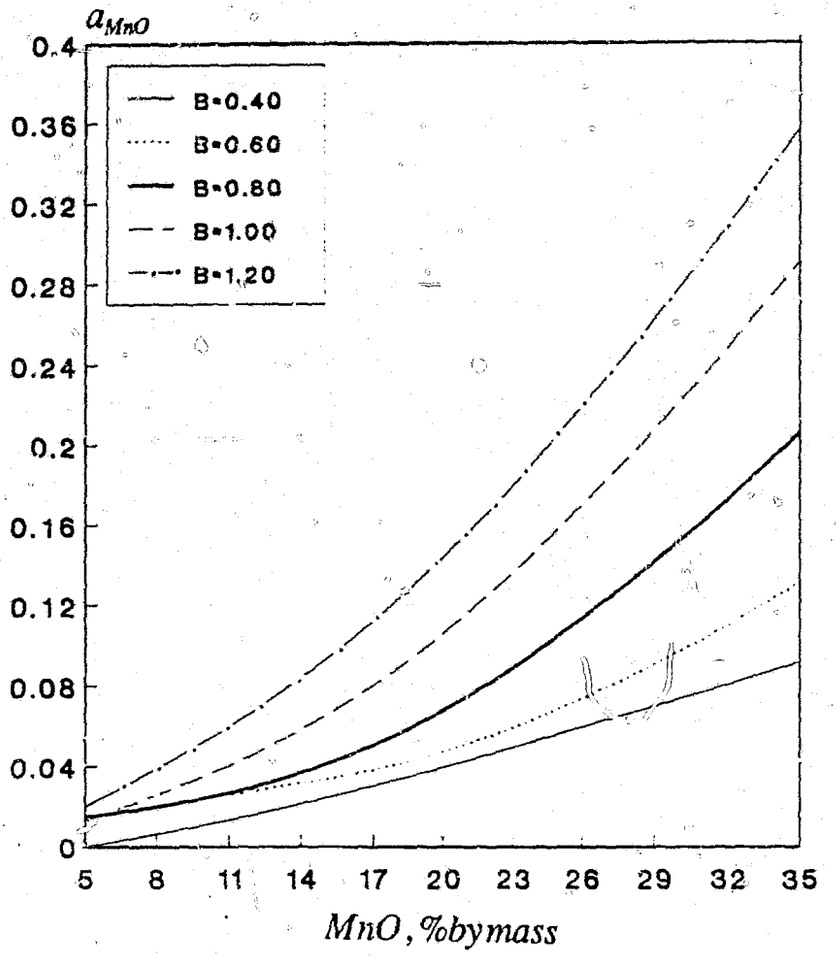

Figure 50. Activities of MnO in MnO-CaO-MgO-SiO_2-Al_2O_3 slags at 1500°C for various basicity ratios with CaO:MgO=6.00.

and $CaSiO_3$[121,123,127,128]. Thus, Mn^{2+} ions can not overcome the interaction between these metal cations and silicate ions, and therefore an increase in basicity increases the MnO activities in the slag. (Other plots showing the effect of basicity ratio on the MnO activities are given in Appendix C, in Figures C.22 to C.24). There is also the fact that at high basicity values, the slag liquidus temperatures tend to increase which would also result in an increase in MnO activity.

Figures 51 and 52 were plotted to illustrate respectively the effect of CaO-to-MgO and Basicity ratio on the activity of MnO at a constant MnO concentration of 15 mass per cent. Figure 51 proves, as shown earlier, the fact that as CaO replaces MgO in the slag, activity of MnO is slightly increased. Figure 52, on the other hand, demonstrates the dominant effect of basicity in changing the activity of MnO. The activity of MnO (at 15 mass per cent MnO) raises four-fold from about 0.08 at basicity ratio of 0.4 to about 0.32 at basicity ratio of 1.2.

4.1.3 Activity coefficient of MnO in $CaO-MgO-SiO_2-Al_2O_3-MnO$ slags

In figures 53 to 59, the activity of MnO was plotted against its mole fraction at constant basicity and CaO-to-MgO ratios. An increase in the mole fraction of MnO in the slag increases its activity. Turkdogan[57] found that the activity coefficient of MnO was not affected by its concentration. Therefore, the activity coefficient of MnO was plotted against its mole fraction in Figures 60 to 65 in order to compare the results of the present study to the previous study[57]. As it is seen in

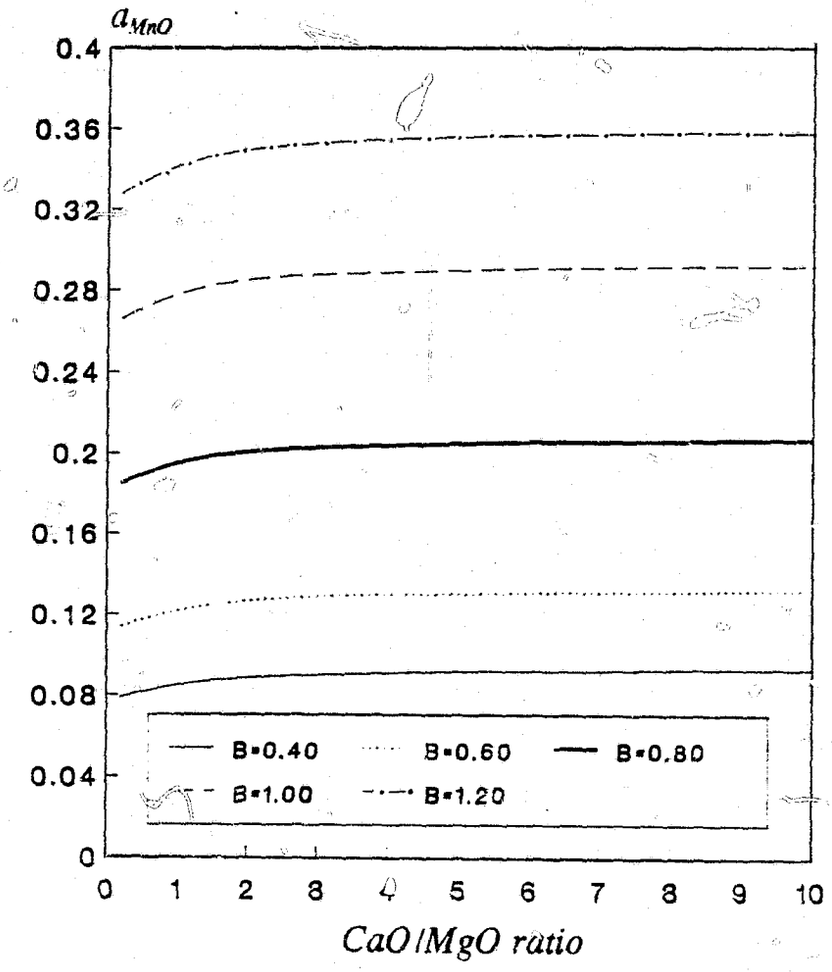

Figure 51. The effect of different basicity ratios on the activities of MnO in $MnO-CaO-MgO-SiO_2-Al_2O_3$ slags at 1500°C with % MnO=15.

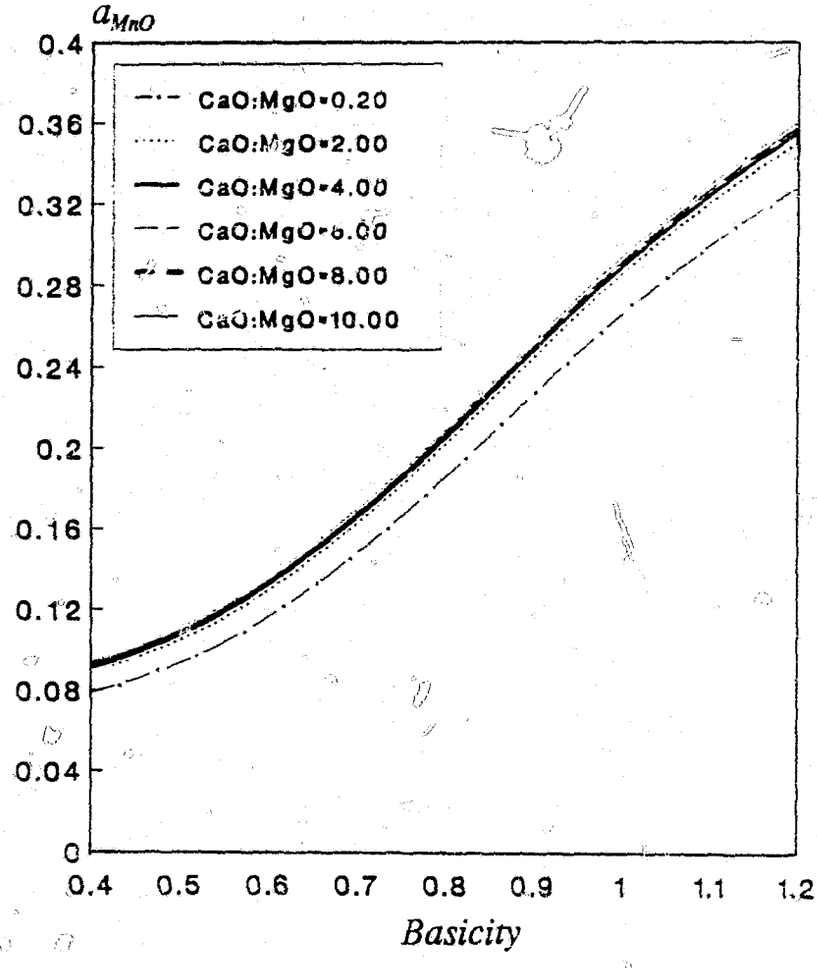

Figure 52. The effect of different CaO-to-MgO ratios on the activities of MnO in $MnO-CaO-MgO-SiO_2-Al_2O_3$ slags at 1500°C with % MnO=15.

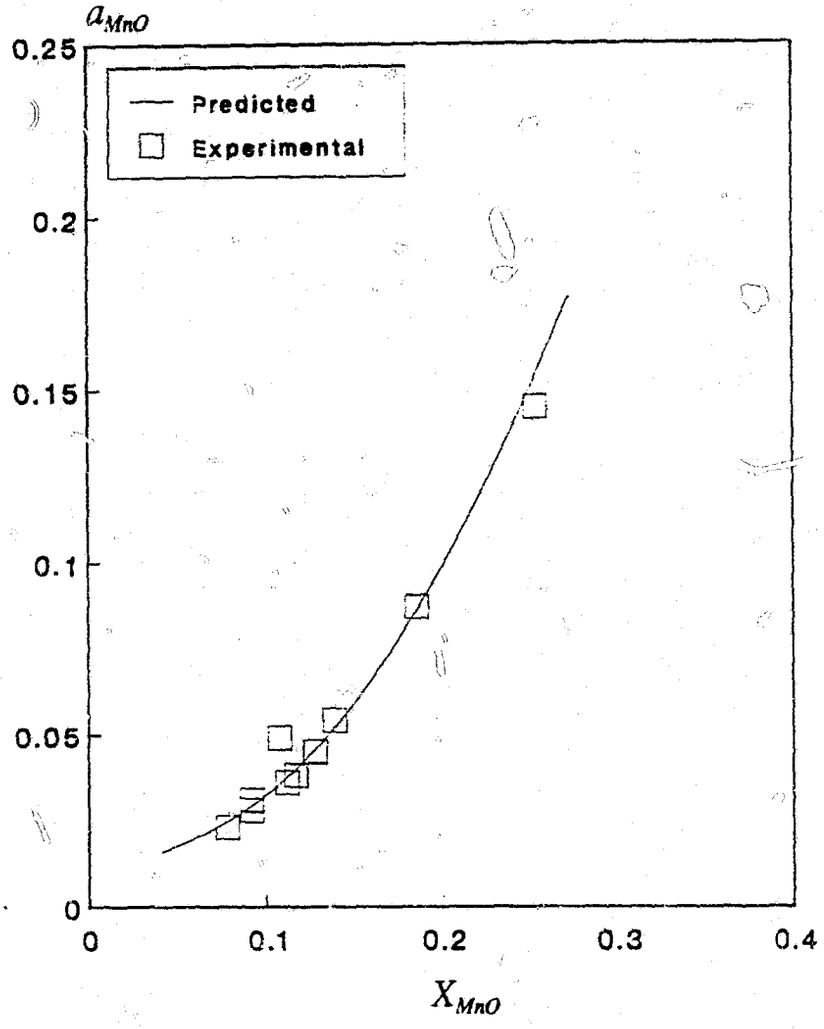

Figure 53. The variation of MnO activity with composition in $MnO-CaO-MgO-SiO_2-Al_2O_3$ slags at 1500°C, B=0.83±0.04, CaO:MgO=3.65±0.46, % Al_2O_3=5.

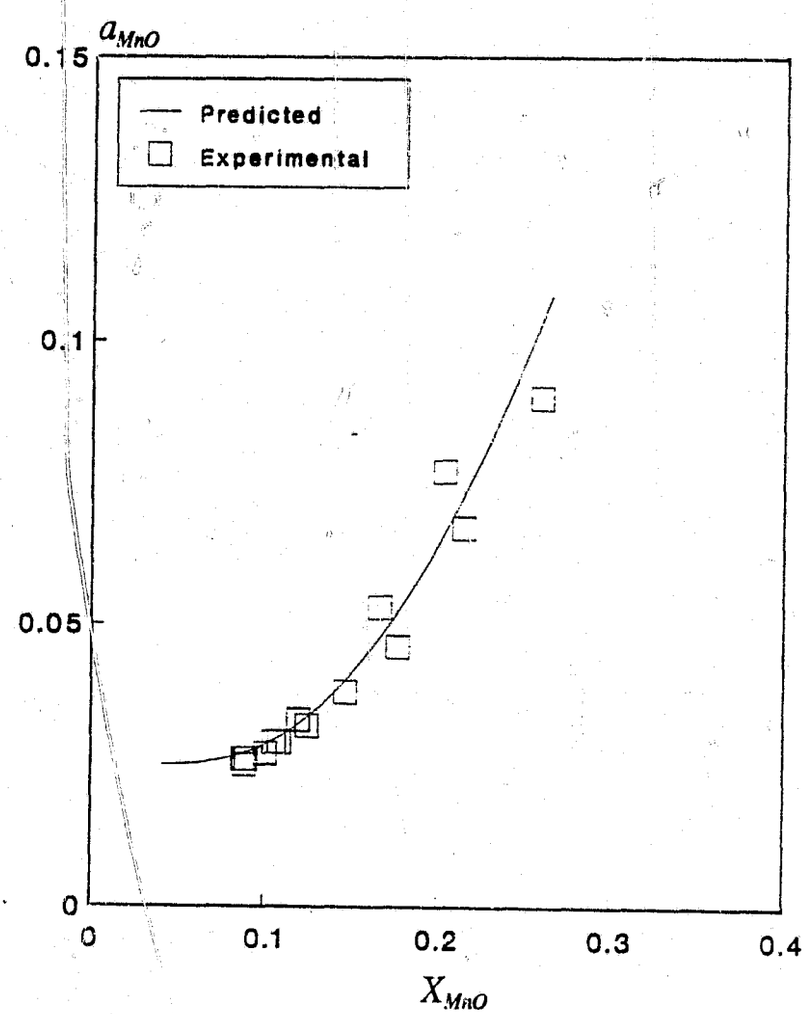

Figure 54. The variation of MnO activity with composition in MnO-CaO-MgO-SiO_2-Al_2O_3 slags at 1500°C, B=0.64±0.05, CaO:MgO=3.57±0.41, & Al_2O_3=5.

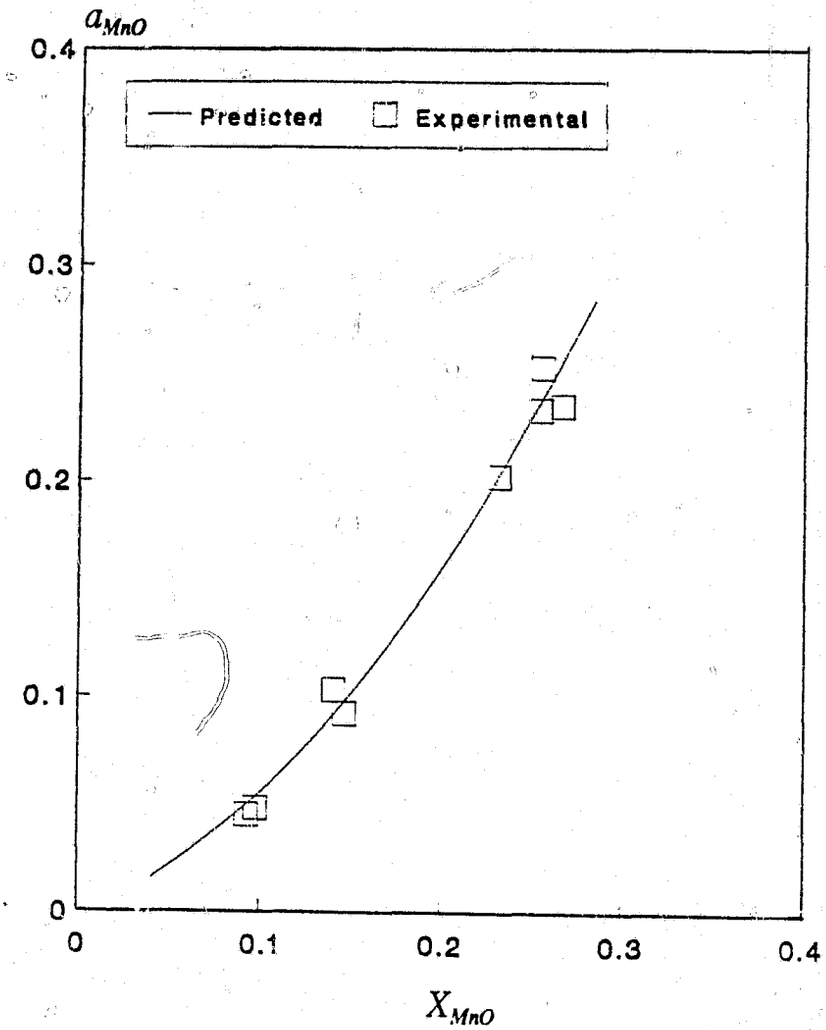

Figure 55. The variation of MnO activity with composition in $MnO-CaO-MgO-SiO_2-Al_2O_3$ slags at 1500°C, B=1.07±0.06, CaO:MgO=4.50±0.38, % Al_2O_3=5.

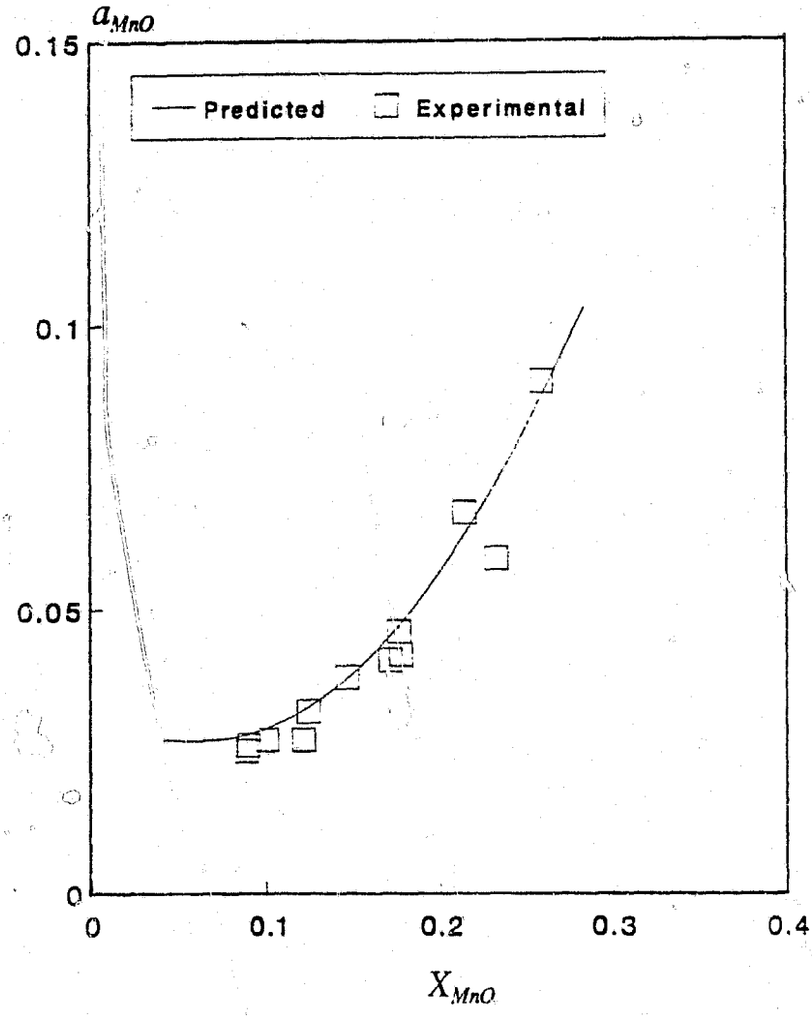

Figure 56. The variation of MnO activity with composition in $MnO-CaO-MgO-SiO_2-Al_2O_3$ slags at 1500°C, B=0.48±0.08, CaO:MgO=4.00±0.16, % Al_2O_3=5.

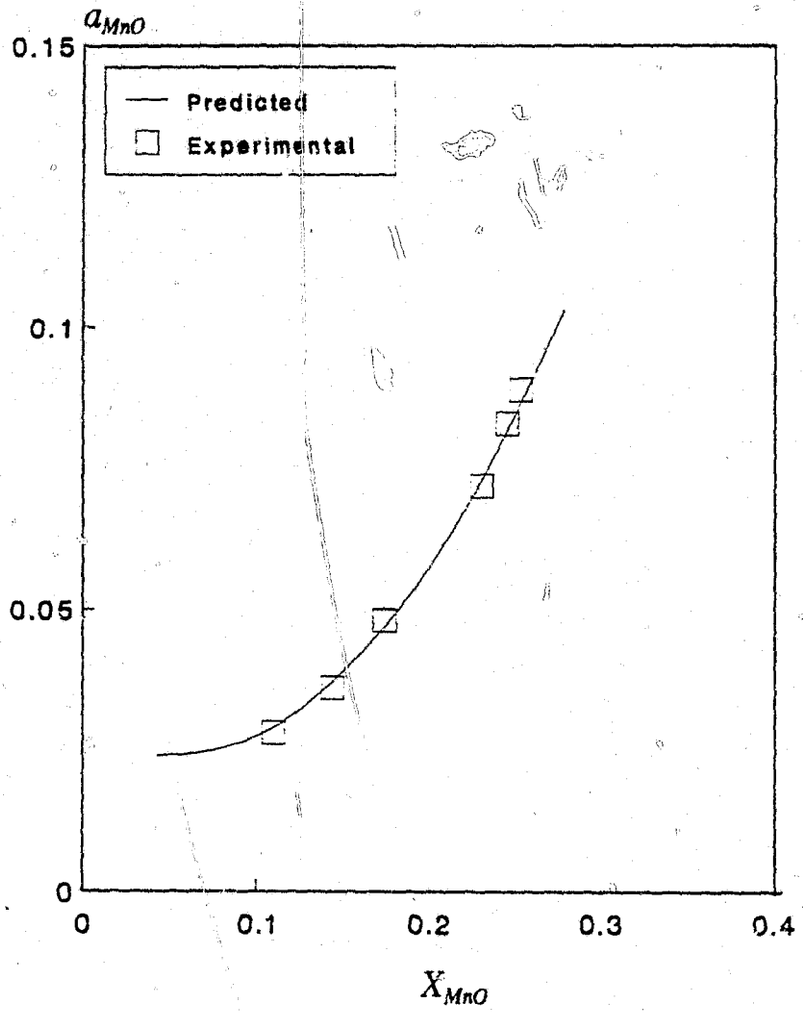

Figure 57. The variation of MnO activity with composition in $MnO-CaO-MgO-SiO_2-Al_2O_3$ slags at 1500°C, B=0.58±0.02, CaO:MgO=∞, % Al_2O_3=5.

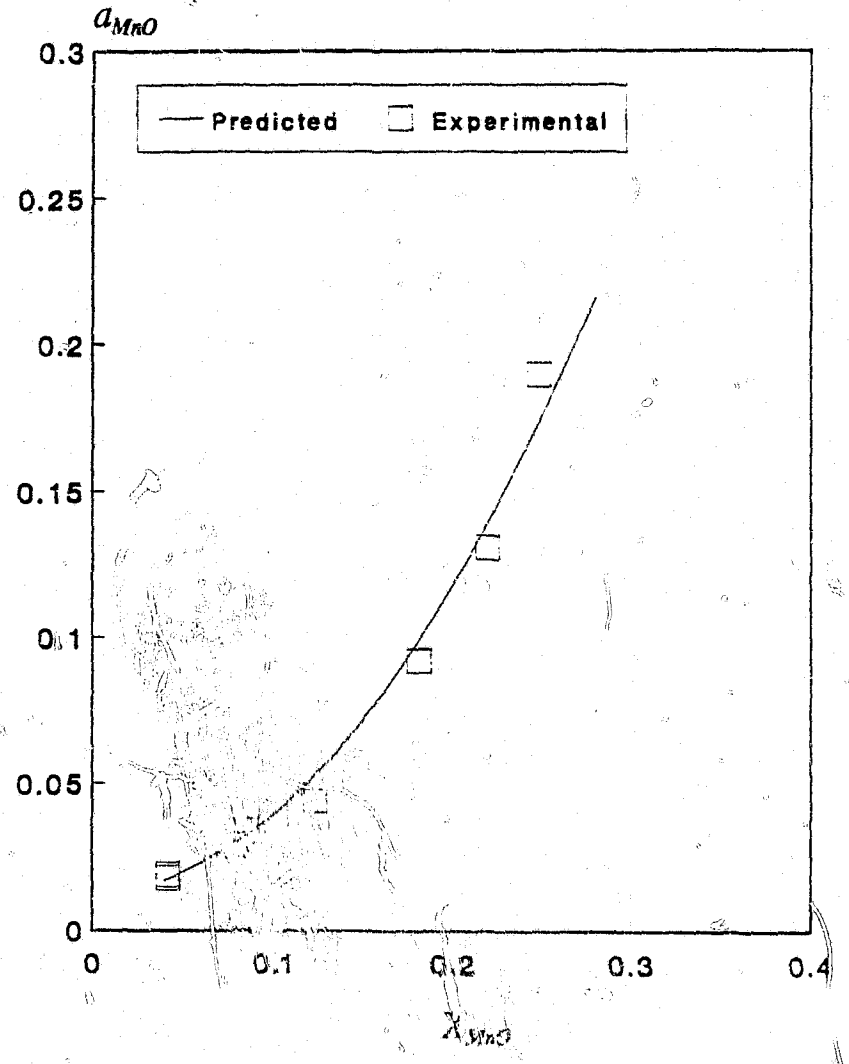

Figure 58. The variation of MnO activity with composition in MnO-CaO-MgO-SiO_2-Al_2O_3 slags at 1500°C, B=0.90±0.07, CaO:MgO=2.06±0.19, & Al_2O_3=5.

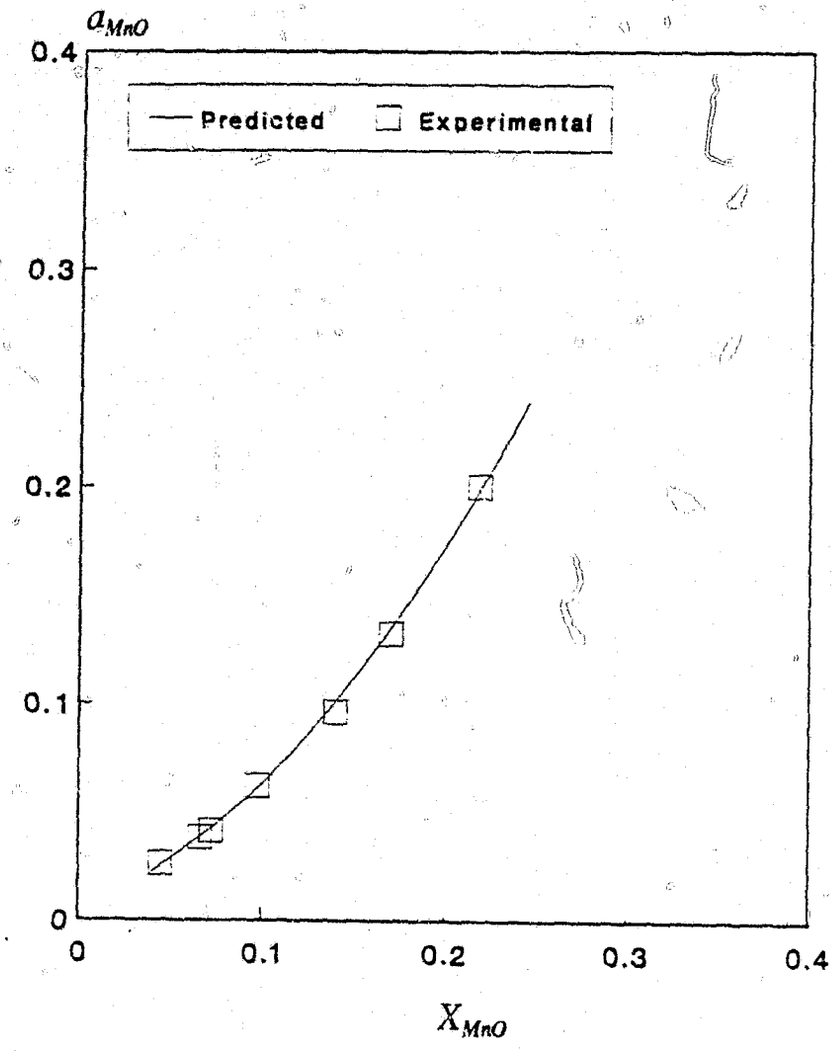

Figure 59. The variation of MnO activity with composition in $MnO-CaO-MgO-SiO_2-Al_2O_3$ slags at 1500°C, B=1.11±0.06, CaO:MgO=2.02±0.12, % Al_2O_3=5.

Figures 60 to 65, the concentration of MnO in the slag affects its own activity coefficient within the compositional limits of the present study and the activity coefficient of MnO increases with an increase in its mole fraction. The results of the present investigation show greater differences from those of Turkdogan[57]. In Warren's study[9], the slag compositions were more basic than those of Turkdogan. In present study the slags are even more acidic than those of Turkdogan. The results of Turkdogan are also out of line with those calculated from the results of Filer and Darken[55] by Abraham and his co-workers[52] and with slag-metal relationships in ferromanganese practice. Apart from that, Turkdogan, in his results, was also unable to show the temperature dependence of activity of MnO shown subsequently by the previously named authors[52,53]. The activity coefficient being also a measure or indicator of interactions between ions or atoms, in principle, should be affected by composition. In the present study, activity coefficient of MnO is generally less than one indicating negative deviations from ideality and tendency towards compound formation in the slag. This tendency is not great however, due to the relatively high magnitude of γ_{MnO}. It is evident that, on a molecular base, MnO in the slag would favour to surround itself with other components. This tendency would probably increase as its own concentration increases, and there would be more and more competing MnO molecules for less and less other oxides. Thus inevitably, individual MnO molecules will find themselves surrounded with relatively less other oxides but with relatively more like molecules-MnO. This will

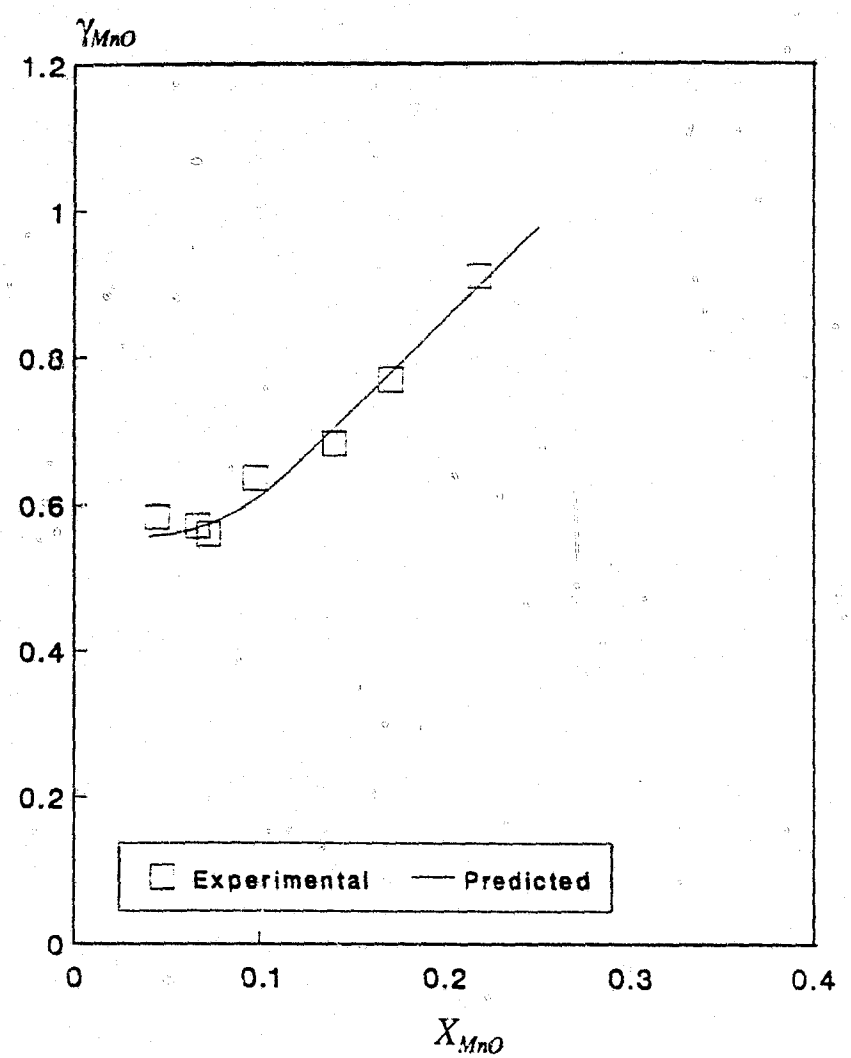

Figure 60. The variation of activity coefficient of MnO with composition in $MnO-CaO-MgO-SiO_2-Al_2O_3$ slags at 1500°C, B=1.11±0.06, CaO:MgO=2.02±0.12, % Al_2O_3=5.

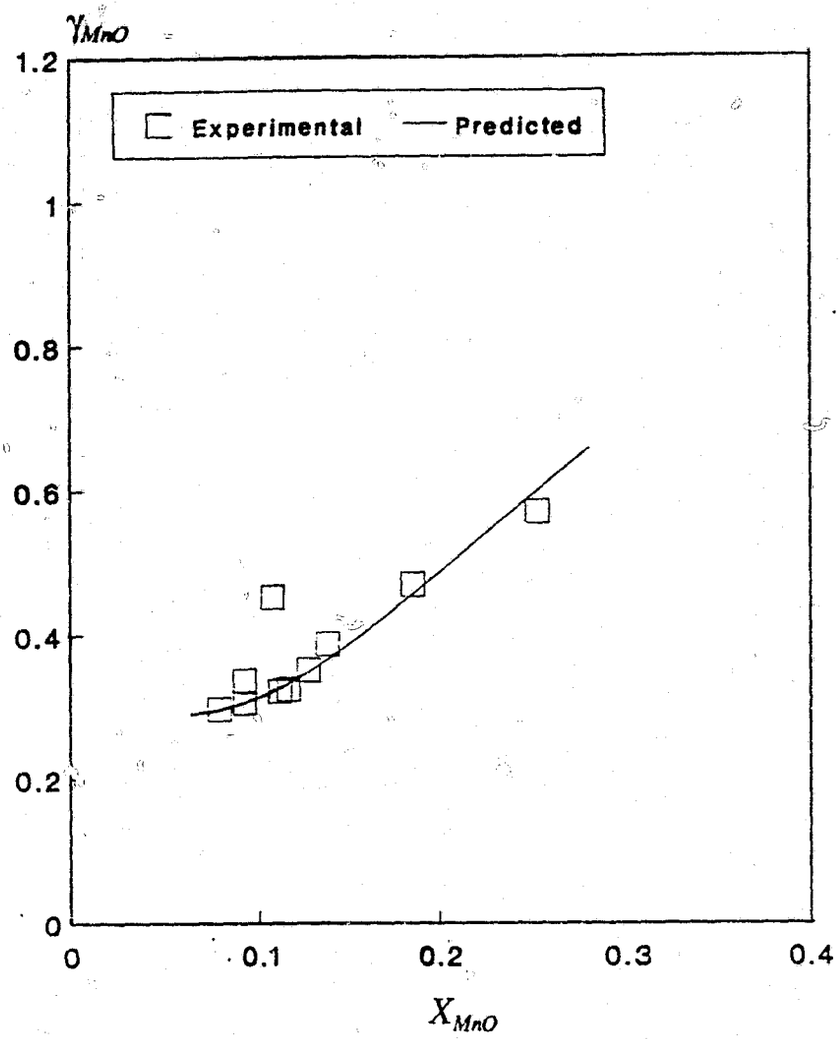

Figure 61. The variation of activity coefficient of MnO with composition in $MnO-CaO-MgO-SiO_2-Al_2O_3$ slags at 1500°C, B=0.83±0.04, CaO:MgO=3.65±0.46, % Al_2O_3=5.

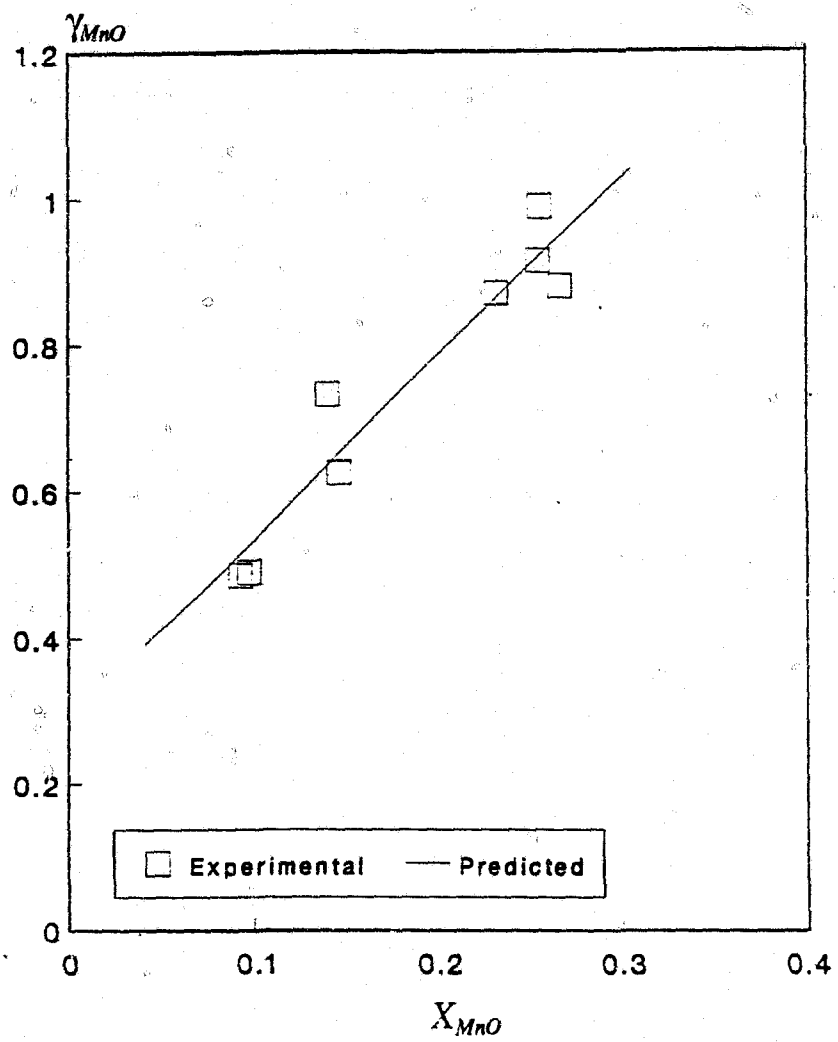

Figure 62. The variation of activity coefficient of MnO with composition in $MnO-CaO-MgO-SiO_2-Al_2O_3$ slags at 1500°C, B=1.07±0.06, CaO:MgO=4.50±0.38, % Al_2O_3=5.

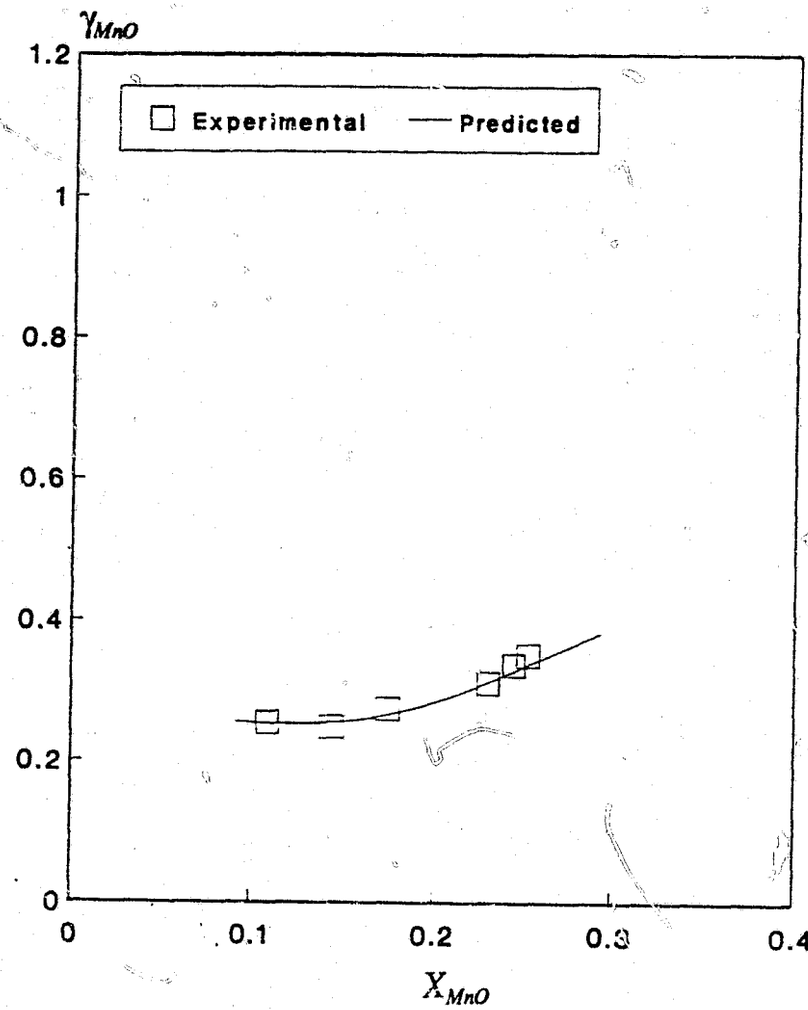

Figure 63. The variation of activity coefficient of MnO with composition in MnO-CaO-MgO-SiO_2-Al_2O_3 slags at 1500°C, B=0.58±0.02, CaO:MgO=∞, % Al_2O_3=5.

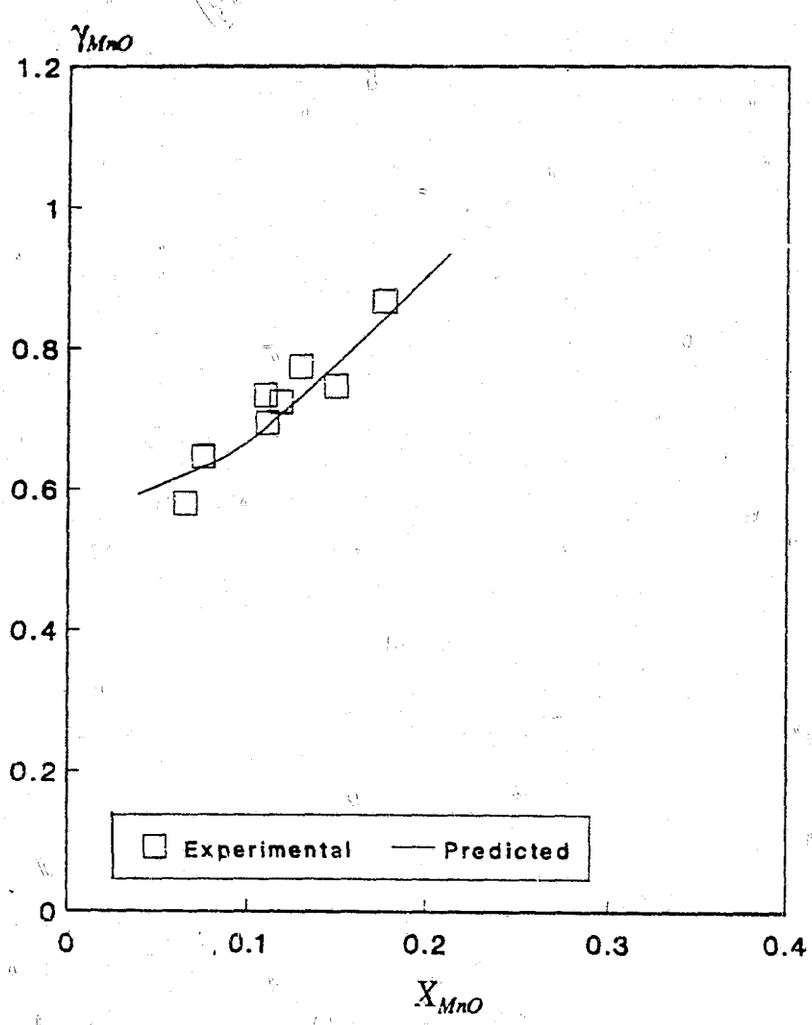

Figure 64. The variation of activity coefficient of MnO with composition in $MnO-CaO-MgO-SiO_2-Al_2O_3$ slags at 1500°C, B=1.15±0.03, CaO:MgO=1.59±0.11, % Al_2O_3=5.

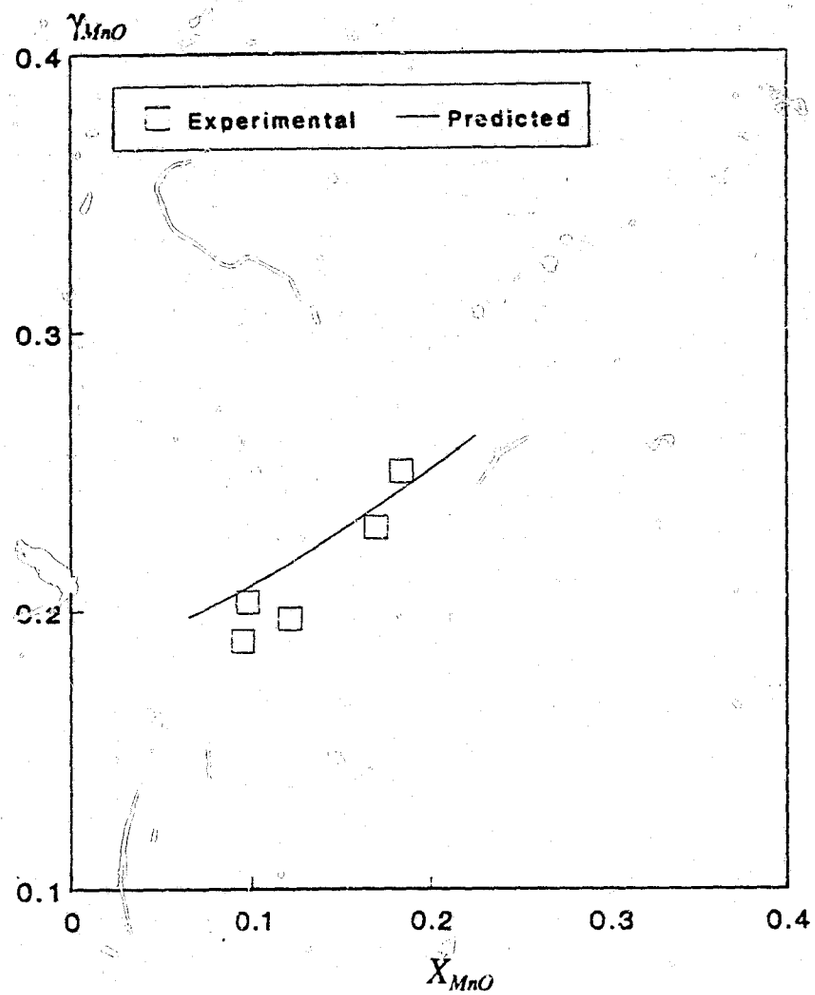

Figure 65. The variation of activity coefficient of MnO with composition in $MnO-CaO-MgO-SiO_2-Al_2O_3$ slags at 1500°C, B=0.43±0.02, CaO:MgO=3.79±0.37, % Al_2O_3=5.

probably be reflected as an increase in activity coefficient of MnO with an increase in its own concentration.

On the other hand, the results of present study is in good agreement with those of Warren[9] although, the sl... are more acidic in the present study. Using the same argument offered above, in more acidic slags, the concentration of MnO will inevitably be low and thus an increase in its concentration will affect its own activity coefficient more. The increase in the activity coefficient of MnO with increasing concentration can also be explained by the use of modern slag theory. At any one concen...ion of MnO, a certain number of Mn^{2+} ions will be a...ciated with the silicate and aluminate anions, and a certain number only with free oxygen ions. When MnO concentration increases, there will be a simultaneous increase in the number of free oxygen ions and in the number of manganese ions associated only with them. This increase will be more than the increase in manganese ions associated with the network, due to the further breakdown in network. Therefore the activity coefficient of MnO increases with an increase in its concentration as the interaction between free like ions/molecules increase. MnO can be also considered as a basic oxide but its basic strength is lower than those of CaO, MgO, BaO, etc. However, an increase in the concentration of MnO in the slag can still be considered as an increase in the amount of a basic oxide which will lead to a further break-up in the silica network. This will allow more O^{2-} and Mn^{2+} ions to be free from the

network and therefore the activity and activity coefficient of MnO will increase with an increase in its concentration.

4.2 The results of slag- metal equilibrium experiments

The slag-metal equilibrium experiments were carried out in graphite crucibles at 1500°C under a pure CO atmosphere. Thus, the metal phase was always saturated with respect to graphite. The actual basicity ratios of the slags ranged between 1.00 and 1.39 for different compositions. The equilibrium experiments were conducted in composition ranges simulating ferromanganese and silicomanganese compositions encountered in the industrial practice. Over 100 experiments were carried out, from which 71 successful ones were selected and sent for analysis. The results of the experimental runs are presented in tabular and graphical form in the following. All the data gathered are collected in Tables XIX and XX respectively for ferromanganese and silicomanganese compositions.

4.2.1 Manganese distribution

In Figure 66, the effect of basicity ratio on the logarithm of the distribution ratio of manganese is seen. The distribution ratio of a species "i" is defined as per cent of "i" in the slag divided by per cent of "i" in the metal phase. In all the figures, round and square brackets indicate the slag and metal phases respectively. An increase in basicity ratio decreases the manganese distribution ratio, in other words, an increase in basicity ratio causes an increase in the manganese content of the metal phase relative to that of

Table XIX. The results of the equilibrium experiments in ferromanganese composition at 1500°C and CO atmosphere.

Ex. No.	METAL PHASE					SLAG PHASE						
	Mn%	Si%	Fe%	C%	Mn:Fe	MnO%	CaO%	MgO%	Al_2O_3%	SiO_2%	CaO:MgO	B
1	77.03	4.39	11.40	7.18	6.76	9.97	27.55	14.79	5.56	41.93	1.86	1.01
2	78.20	3.53	10.96	7.31	7.14	10.99	25.55	16.19	5.74	41.33	1.58	1.01
3	78.19	3.65	10.83	7.33	7.22	10.30	24.75	17.10	6.05	40.85	1.45	1.04
4	78.54	3.45	10.65	7.36	7.37	10.43	23.63	18.61	6.42	40.70	1.27	1.04
5	79.06	3.38	10.21	7.36	7.74	11.43	22.76	18.33	6.81	40.27	1.24	1.02
6	73.61	4.77	14.49	7.14	5.08	9.44	28.10	15.27	5.24	41.74	1.84	1.04
7	74.90	4.04	13.80	7.27	5.43	10.32	27.27	15.32	5.42	41.47	1.78	1.03
8	75.50	3.69	13.70	7.12	5.51	11.32	25.37	16.48	5.69	40.94	1.54	1.02
9	76.16	3.34	13.18	7.32	5.78	12.44	24.07	17.34	5.76	39.98	1.39	1.04
10	76.36	3.16	13.04	7.44	5.86	11.35	23.11	18.71	6.34	40.28	1.24	1.04
11	77.08	2.70	12.55	7.68	6.14	11.58	22.71	18.60	6.82	40.09	1.22	1.03
12	69.09	3.84	20.64	6.43	3.35	8.07	28.20	14.86	5.56	43.11	1.90	1.00
13	69.20	4.29	19.44	7.08	3.56	9.09	27.57	15.36	6.17	41.61	1.79	1.03
14	70.20	4.02	18.84	6.95	3.73	9.69	26.13	16.67	5.94	41.36	1.57	1.03
15	70.66	3.37	18.50	7.48	3.82	10.62	24.95	17.43	6.27	40.52	1.43	1.01
16	71.68	3.19	17.71	7.42	4.05	10.77	23.08	18.93	7.06	39.96	1.22	1.05
17	70.70	3.51	18.51	7.27	3.82	9.79	23.83	19.08	6.71	40.38	1.25	1.06
18	78.23	2.04	11.44	8.30	6.84	4.11	35.53	15.58	4.98	39.60	2.28	1.29
19	78.19	1.82	11.30	8.69	6.92	5.50	33.91	15.88	5.47	39.00	2.14	1.20
20	78.29	1.98	10.81	8.92	7.24	4.76	35.29	15.32	5.22	39.22	2.30	1.27
21	78.48	2.29	10.54	8.70	7.45	7.94	31.87	15.16	5.64	39.19	2.10	1.20
22	78.65	2.58	10.34	8.43	7.61	9.03	30.01	16.12	6.02	38.62	1.86	1.19
23	78.94	2.23	10.15	8.68	7.78	8.06	29.18	17.69	6.54	38.33	1.65	1.22
24	75.19	2.61	13.91	8.28	5.41	5.64	33.78	15.47	4.98	39.74	2.18	1.24
25	75.61	2.55	13.65	8.19	5.54	6.25	33.50	15.74	5.24	39.07	2.13	1.26

Table XIX continued

Ex. No.	METAL PHASE					SLAG PHASE						
	Mn%	Si%	Fe%	C%	Mn:Fe	MnO%	CaO%	MgO%	Al_2O_3%	SiO_2%	CaO:MgO	B
26	75.42	2.48	13.75	8.36	5.49	6.53	32.27	16.34	5.50	39.17	1.97	1.24
27	75.24	2.46	13.19	9.11	5.70	5.09	33.87	16.22	5.95	38.67	2.09	1.30
28	75.30	2.61	13.20	8.90	5.70	5.17	33.24	16.42	6.64	38.34	2.02	1.30
29	75.82	2.42	13.23	8.54	5.73	4.90	31.90	18.12	7.10	37.77	1.76	1.32
30	68.35	4.23	20.30	7.12	3.37	3.76	36.81	15.85	5.43	37.94	2.32	1.39
31	68.48	3.61	20.39	7.53	3.36	9.68	32.80	14.74	5.28	35.51	2.23	1.34
32	69.91	3.43	19.60	7.05	3.57	4.38	34.36	16.80	6.33	37.94	2.05	1.35
33	69.22	3.52	20.00	7.25	3.46	3.53	35.79	15.38	6.94	38.15	2.33	1.34
34	70.50	3.31	18.69	7.50	3.77	3.94	34.28	16.94	7.33	37.31	2.02	1.37
35	70.68	3.13	18.82	7.37	3.76	4.04	32.44	17.72	7.86	37.78	1.83	1.33

Table XX. The results of the equilibrium experiments in silicomanganese composition at 1500°C and CO atmosphere.

Ex. No.	METAL PHASE					SLAG PHASE							
	Mn%	Si%	Fe%	C%	Mn:Si	MnO%	CaO%	MgO%	SiO_2%	Al_2O_3%	Fe_2O_3%	CaO:MgO	B
1	62.63	13.88	20.67	2.82	4.51	16.16	16.36	8.96	53.35	5.06	0.10	1.83	0.47
2	63.28	13.26	20.16	3.31	4.77	15.62	18.38	8.32	51.98	5.60	0.10	2.21	0.51
3	64.60	13.15	19.36	2.88	4.91	14.80	22.46	3.08	52.27	7.28	0.11	7.29	0.49
4	60.27	17.15	20.68	1.91	3.51	11.02	16.32	10.30	57.22	5.03	0.11	1.58	0.47
5	61.02	16.50	20.13	2.35	3.70	11.67	16.33	8.78	56.00	7.10	0.12	1.86	0.45
6	61.36	16.21	19.47	2.96	3.79	13.17	17.13	7.80	56.14	5.63	0.12	2.20	0.44
7	61.90	17.01	19.07	2.02	3.64	14.16	17.99	5.83	56.55	5.41	0.11	3.09	0.42
8	62.09	16.56	18.84	2.52	3.75	14.35	18.74	4.40	56.36	6.03	0.12	4.26	0.41
9	63.29	15.67	18.66	2.38	4.04	15.94	19.21	2.61	55.99	6.16	0.10	7.36	0.39
10	58.14	20.59	20.18	1.09	2.82	5.19	16.57	10.56	62.02	5.54	0.14	1.57	0.44
11	58.52	20.55	19.72	1.21	2.85	8.40	15.94	8.84	61.22	5.28	0.32	1.80	0.40
12	59.30	20.36	19.11	1.24	2.91	8.80	16.91	7.45	61.10	5.64	0.10	2.27	0.40
13	59.95	19.85	19.12	1.09	3.02	10.61	17.85	5.99	59.47	5.99	0.10	2.98	0.40
14	60.34	19.99	18.23	1.43	3.02	11.73	18.40	4.18	59.44	6.16	0.10	4.40	0.38
15	60.93	19.80	17.76	1.51	3.08	11.45	20.53	2.80	58.30	6.82	0.10	7.33	0.40
16	62.09	16.22	19.29	2.40	3.83	15.41	17.22	5.94	55.79	5.54	0.10	2.90	0.42
17	64.02	14.39	18.87	2.72	4.45	16.45	17.66	4.20	55.72	5.67	0.10	4.20	0.39
18	64.68	14.02	18.16	3.14	4.61	18.26	18.41	2.47	54.93	5.82	0.10	7.45	0.38
19	61.73	12.97	21.82	3.48	4.76	11.25	19.14	13.42	50.80	5.21	0.20	1.43	0.64
20	62.25	12.72	21.56	3.47	4.89	11.30	20.24	12.13	50.69	5.45	0.20	1.67	0.64
21	63.01	12.12	21.11	3.76	5.20	12.44	16.59	14.71	50.45	5.62	0.20	1.13	0.62
22	63.66	11.80	20.98	3.57	5.39	13.27	17.39	12.97	50.41	5.77	0.20	1.34	0.60
23	64.17	11.56	20.42	3.85	5.55	14.09	18.14	11.63	49.97	5.97	0.20	1.56	0.60
24	65.14	11.07	19.94	3.85	5.88	14.76	19.22	9.84	49.73	6.26	0.20	1.95	0.58
25	59.58	16.46	21.67	2.29	3.62	8.81	19.22	13.47	53.09	5.22	0.20	1.43	0.62

Table XX continued

Ex. No.	METAL PHASE					SLAG PHASE							
	Mn%	Si%	Fe%	C%	Mn:Si	MnO%	CaO%	MgO%	SiO_2%	Al_2O_3%	Fe_2O_3%	CaO:MgO	B
26	60.10	15.78	21.34	2.78	3.81	9.21	19.98	11.77	53.62	5.21	0.20	1.70	0.59
27	60.41	15.69	21.13	2.77	3.85	13.66	18.15	9.22	52.8	5.91	0.20	1.97	0.52
28	61.45	14.92	20.73	2.90	4.12	11.95	16.49	12.44	53.53	5.38	0.20	1.33	0.54
29	62.02	14.76	20.23	2.99	4.20	13.12	17.52	11.31	52.06	5.79	0.20	1.55	0.55
30	62.76	13.90	19.81	3.53	4.52	10.49	16.54	14.92	52.33	5.52	0.20	1.11	0.60
31	57.14	19.83	21.64	1.39	2.88	6.90	18.44	12.66	55.67	4.93	1.49	1.46	0.56
32	57.39	19.87	21.47	1.28	2.89	6.61	20.72	12.41	54.35	5.60	0.32	1.67	0.61
33	57.66	20.07	20.73	1.54	2.87	8.67	16.40	14.31	54.13	5.33	1.17	1.15	0.57
34	58.72	18.59	21.01	1.68	3.16	10.08	16.64	12.48	55.11	5.37	0.33	1.33	0.53
35	59.89	18.30	20.00	1.81	3.27	10.71	17.35	10.82	55.20	5.71	0.20	1.60	0.51
36	60.29	17.89	19.96	1.86	3.37	11.44	17.88	9.09	55.69	5.69	0.20	1.97	0.48

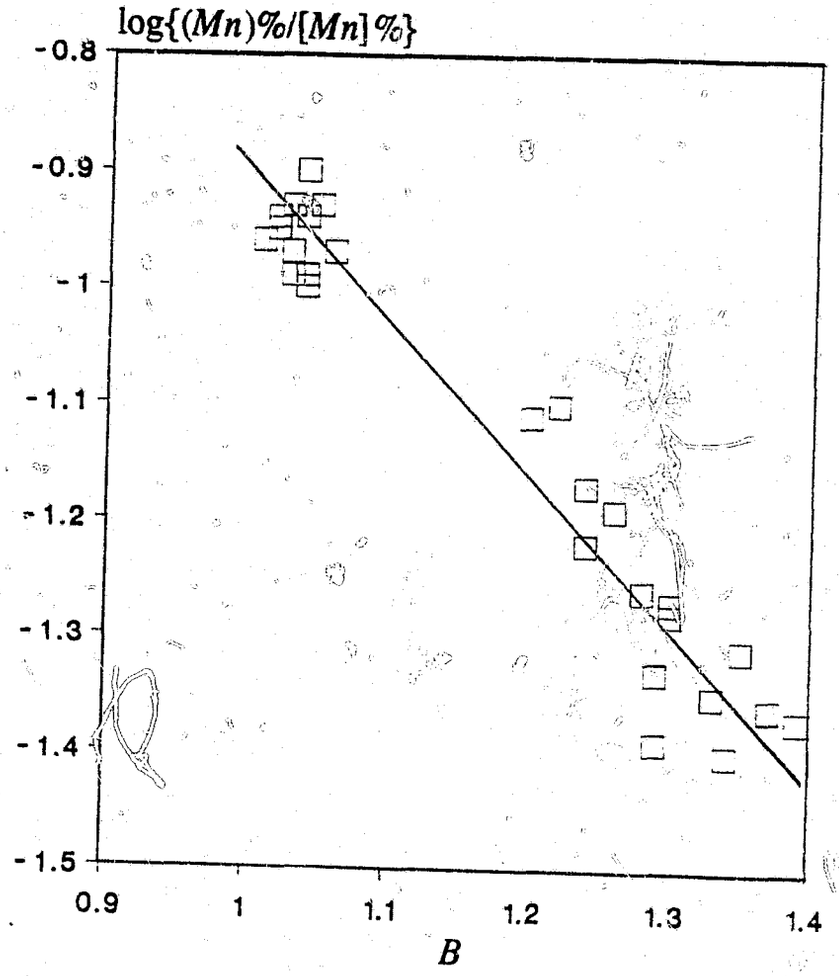

Figure 66. The effect of basicity ratio on the manganese distribution at 1500°C under CO atmosphere.

the slag. This can be explained in terms of the breakup of the silica network with the addition of basic oxides. Due to the strong interaction between divalent cations Ca^{2+}, Mg^{2+} and silicate ions, Mn^{2+} ions become freer and associate with free oxygen anions resulting in higher MnO activity in the slag, which favours the transfer of manganese into the metal phase. This result is in good agreement with those reported by Stukel and Cocubinsky[56] and Turkdogan and Hancock[62].

In Figure 67 and 68, the effect of silica concentration of the slag on the manganese distribution ratio is seen. An increase in the silica concentration increases the Mn distribution ratio which results in an increase of MnO concentration of the slag. An increase in silica concentration makes the slag less basic causing more Mn^{2+} ions associate with the silica network, thus, increasing the MnO concentrations in the slag. It also appears that at a given SiO_2 concentration in the slag, the distribution ratio of manganese is higher when the Si-to-Fe ratio in the metal phase is higher. This result is due to the fact that a relatively higher silicon concentration in metal means a relatively higher silica activity in slag and in accord with the above discussion, the manganese distribution ratio is higher.

Figure 69 shows the relation between CaO-to-Al_2O_3 ratio and the Mn distribution between slag and metal phases. The Si-to-Fe ratio is 0.23 in the metal phase. As it is seen in the figure, when CaO replaces Al_2O_3 in the slag, the Mn transfer to the metal phase increases. This can also be explained by referring to increased MnO

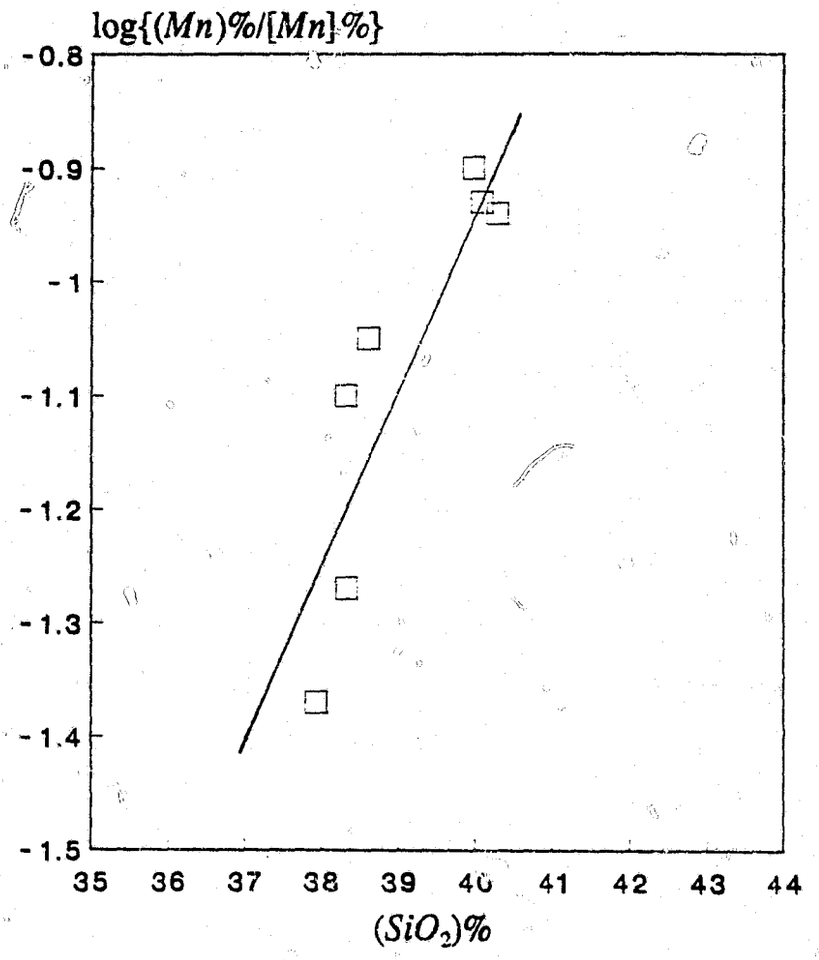

Figure 67. The effect of the SiO_2 content of the slag on manganese distribution with Si:Fe≅0.23 in the metal phase at 1500°C under CO atmosphere.

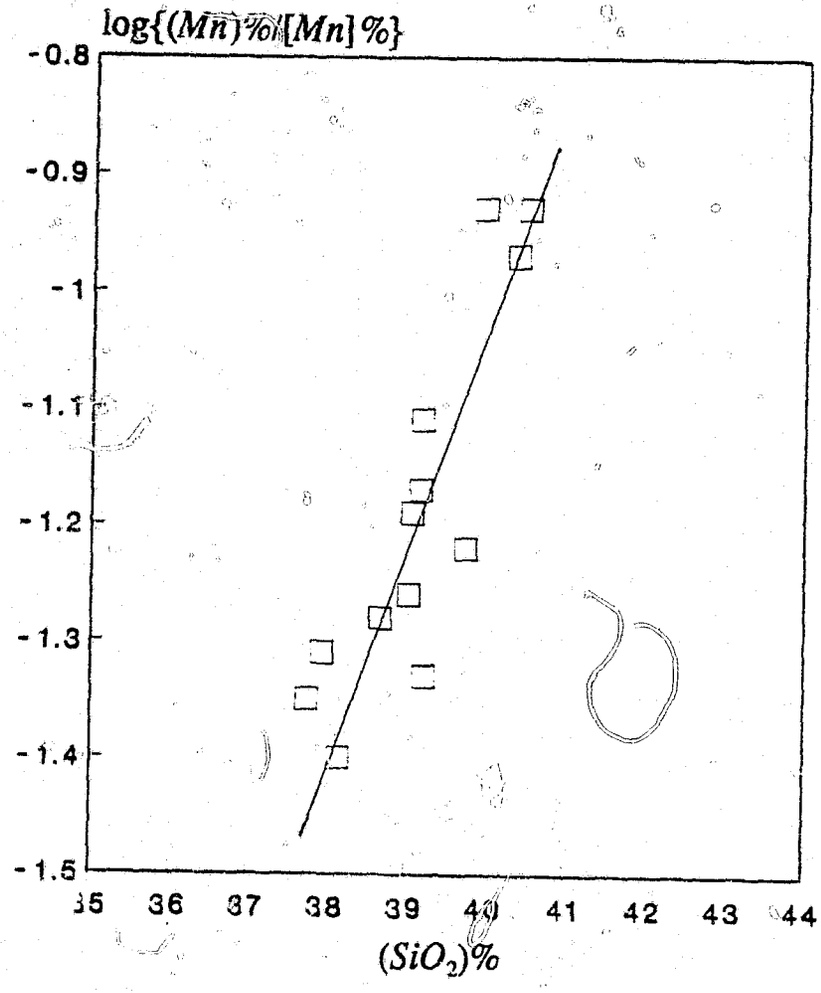

Ficure 68. The effect of the SiO_2 content of the slag on manganese distribution with Si:Fe≅0.18 in the metal phase at 1500°C under CO atmosphere.

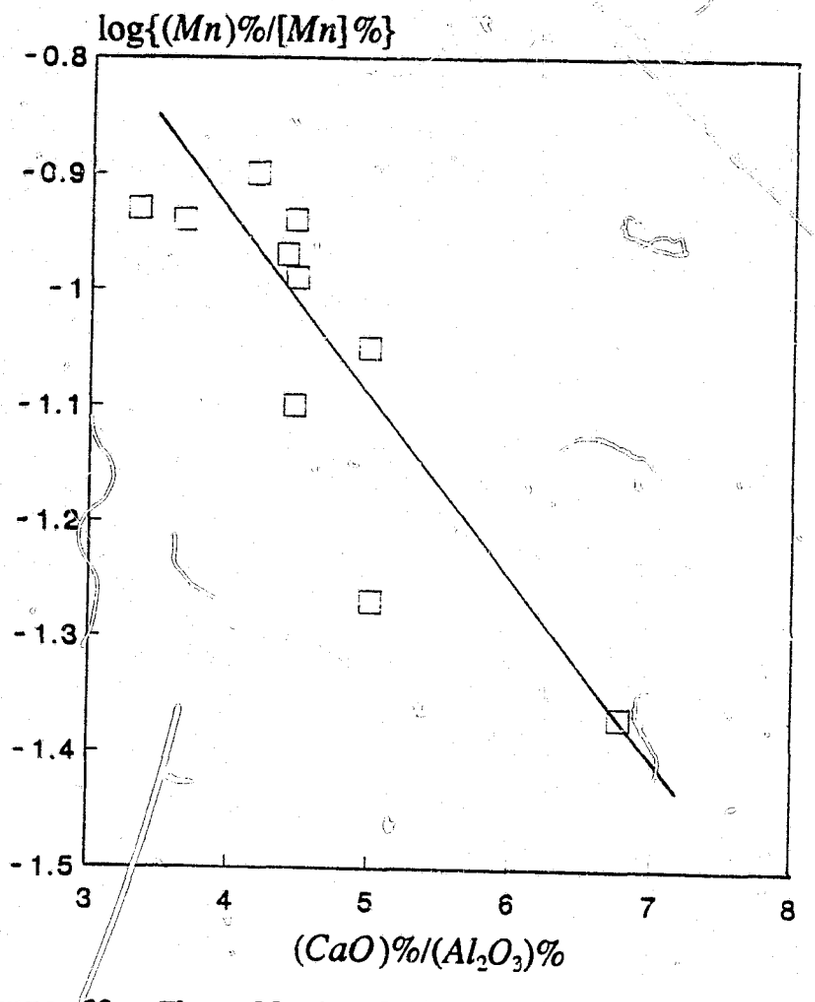

Figure 69. The effect of the CaO-to-Al_2O_3 ratio of the slag on manganese distribution with Si:Fe≅0.23 in the metal phase at 1500°C under CO atmosphere.

activities by an increase in the concentration of CaO in the slag. (Another figure showing this relationship is given in Appendix D, Figure D.1).

In Figure 70, the effect of MgO-to-CaO ratio on manganese distribution is illustrated where four different data groups with different MnO concentrations are superimposed (The individual data groups with the experimental points are given in Appendix D, Figures D.2 to D.5). It can be seen that the distribution ratio of manganese increases as MgO replaces CaO although the effect is slight. In other words, a decrease in the MgO-to-CaO ratio increases the transfer of Mn to the metal phase. As the MnO content of the slag increases, this effect is slightly more emphasized. As it was mentioned earlier, the free energy of formation of Ca_2SiO_4 is more negative than the free energy of formation of Mg_2SiO_4[121,123,127,128] which results in a stronger interaction between Ca^{2+} and silicate anions. This results in higher MnO activity values, thus, the Mn content of the metal phase increases. The slightly higher effect at lower MnO contents is due to the sufficient amount of CaO to form orthosilicates with silica network and freeing the respective amount of Mn^{2+} ions from the silica network. At higher MnO contents, the same CaO content might not be sufficient to free more Mn^{2+} ions from the silica network.

Compared to the initial values of the concentrations of the components of the alloy phases given in Table V, the composition of ferromanganese alloy phase given in Table XIX differ as far as the silicon content of the alloy phase is concerned. The reason to this fact is

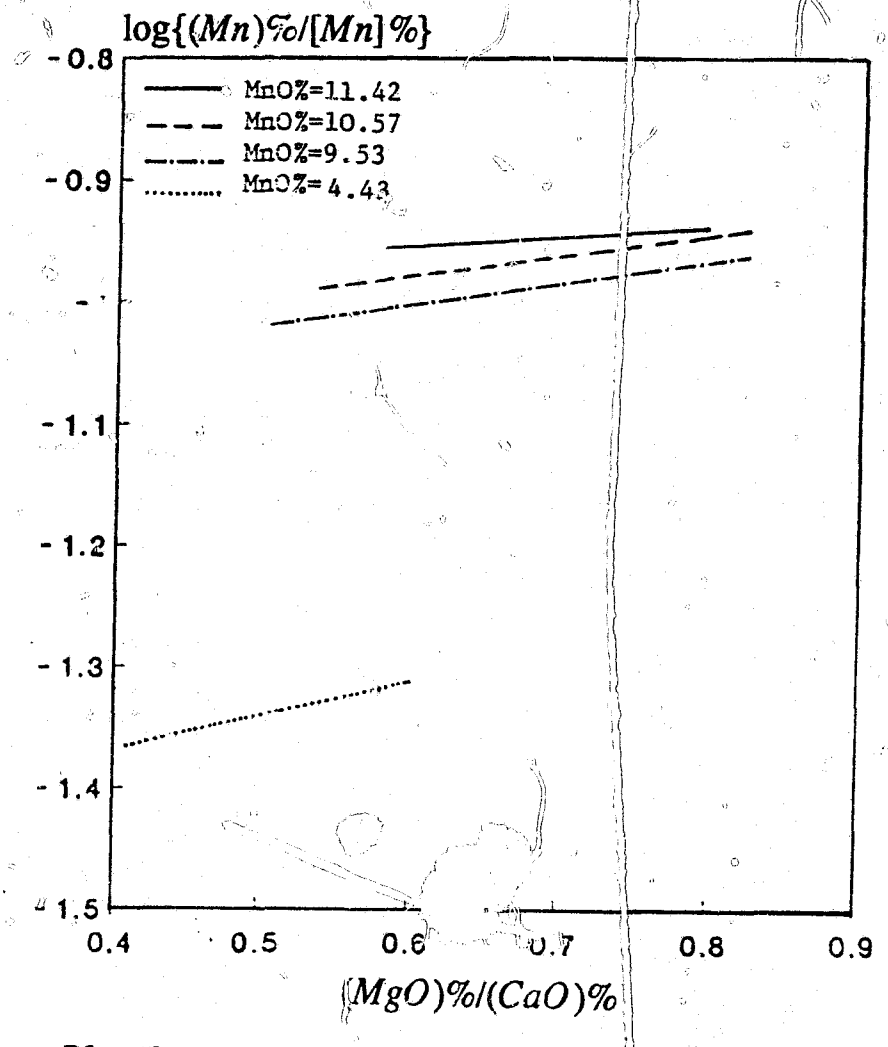

Figure 70. The effect of the MgO-to-CaO ratio of the slag on manganese distribution with different MnO concentrations at 1500°C under CO atmosphere.

attributable to the reducing power of the experimental system operating under a CO atmosphere and excess carbon (graphite crucible). Under such highly reducing conditions, SiO_2 in the slag phase is reduced to the metal phase especially at the temperatures as high as 1500°C if the system is given sufficient time such as it could reach to the equilibrium level.

In the metal phase, the carbon and manganese concentrations are directly proportional to each other which can be observed in Figure 71. Thus an increase in manganese concentration increases the saturation solubility limit of carbon in Mn-Fe-C-Si ferroalloys. Linear regression model equation was derived to predict the carbon concentration (mass per cent) and very high correlation coefficient (r^2=0.930) was obtained. At 1500°C, the regression equation is:

$$\%C = 30.6952 + 5.4453\ \%Mn \quad \text{.....(85)}$$

The relationship between the manganese content of the slag and the slag basicity is shown in Figure 72. As the slag basicity increases, the equilibrium manganese content of the slag decreases rapidly. This is again due to an increased MnO activity in the slag which favours reduction from slag.

4.2.2 Silicon distribution

The relationship between the equilibrium solubilities of carbon (at saturation) and silicon in Mn-Si-Fe-C alloys

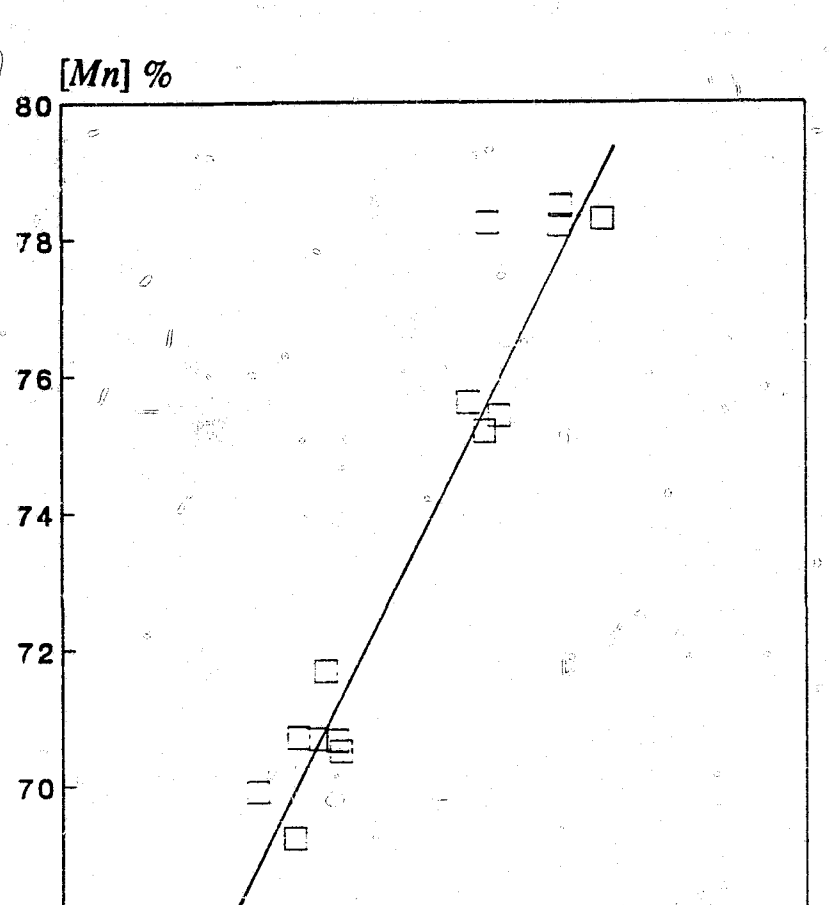

Figure 71. The effect of the Mn content on the C content of the metal phase with Si:Fe≅0.18 at 1500°C under CO atmosphere.

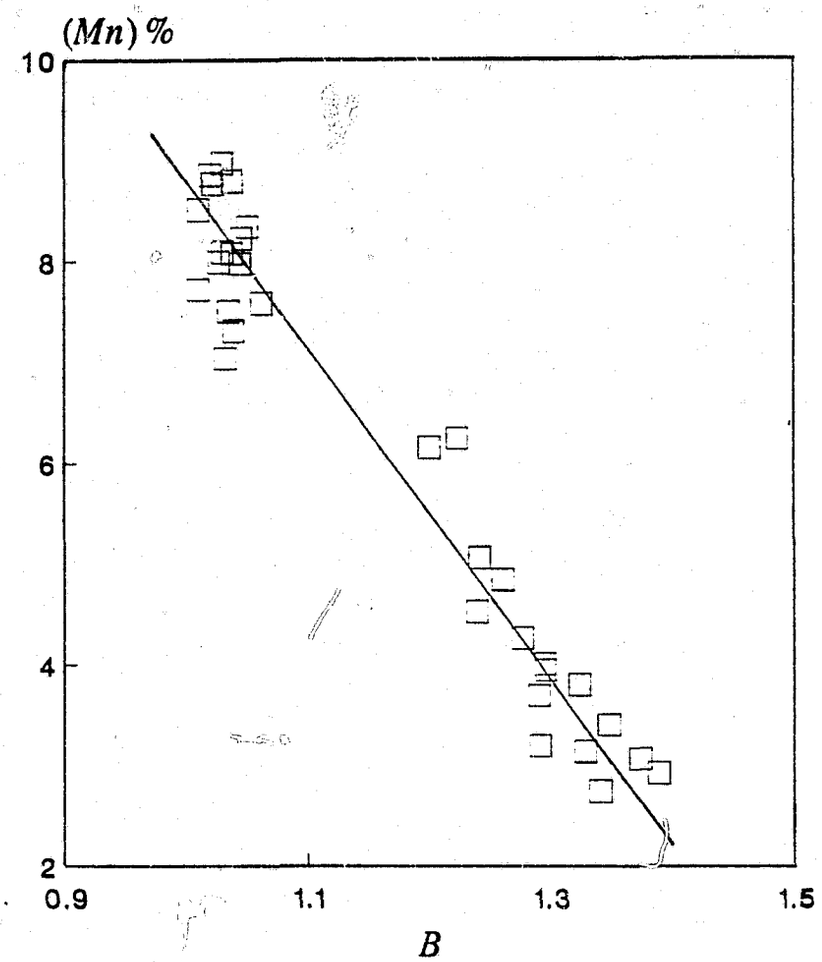

Figure 72. The effect of the basicity on the Mn content of the slags at 1500°C under CO atmosphere.

is illustrated in Figures 73 and 74. Figure 73 is applicable for ferromanganese alloys where three different data groups with different Mn-to-Fe ratios are plotted. Appendix D contains the individual data groups with the experimental points in Figures D.6 to D.8. It can be seen that, at constant silicon contents, as the Mn-to-Fe ratio increases, the carbon solubility in the metal phase increases. The carbon and silicon concentrations in the metal phase are inversely related as expected and this behaviour can be explained in terms of the stability of carbides. As silicon lowers the solubility of carbon, the conditions becomes less favourable for carbide formation. Thermodynamically, this is an indication that silicon decreases the activity of carbon.

For the silicomanganese metal phase, four different Mn-to-Si ratios were selected: 2.9, 3.5, 4.5, 5.6. In Figure 74, these four different data groups are superimposed. The Figure shows the relationship between dissolved carbon (at saturation) and silicon in the metal phase. As it was observed in Figure 73 for ferromanganese alloys, in silicomanganese composition, the carbon and silicon concentrations have an opposite effect on each other. It can be seen that, within these series of experiments, as the Mn-to-Si ratio increases, the curves shift down and to the right. Same interpretations can be made from this result that at constant silicon contents (on a line parallel to the x-axis), as the Mn-to-Si ratio increases, the carbon solubility in the metal phase increases, and secondly, at constant carbon content (on a line parallel to the y-axis) as the Mn-to-Si ratio increases, the silicon

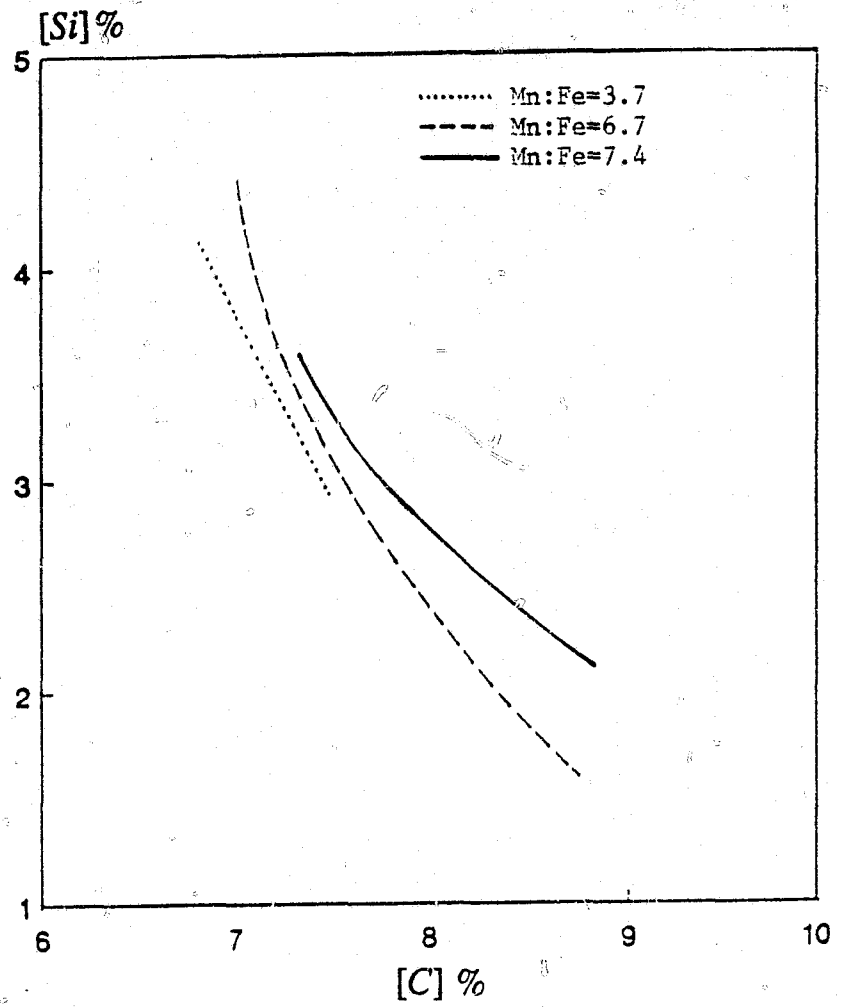

Figure 73. The effect of the Si content on the C content of the metal phase with different Mn-to-Fe ratios at 1500°C under CO atmosphere.

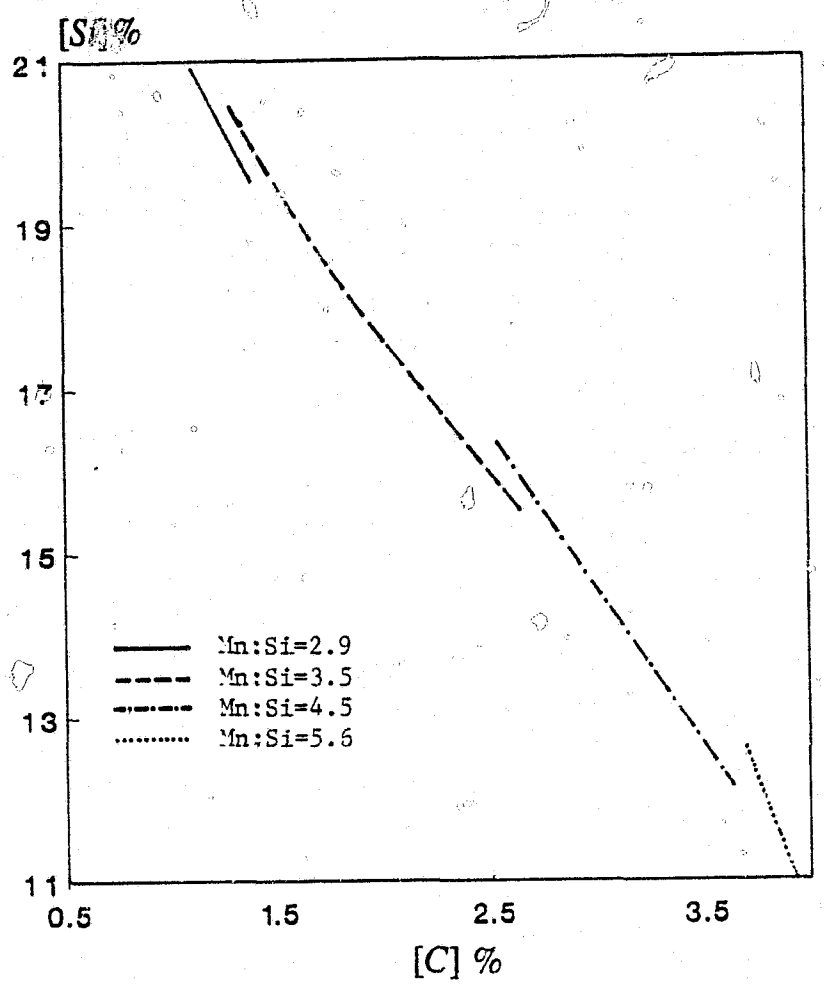

Figure 74. The effect of the Si content on the C content of the metal phase with different Mn-to-Si ratios at 1500°C under CO atmosphere.

solubility increases (the individual data groups with different Mn-to-Si ratios and experimental points are given in Appendix D, Figures D.9, D.10, D.11, D.12). This result also verifies the effect of manganese concentration on the saturation solubility limit of carbon in Mn-Fe-C-Si ferroalloys which is observed in Figure 73.

The silicon content of the metal phase in ferromanganese and silicomanganese compositions are to a great extent affected by the silica content of the slag with which they are in equilibrium. The Figures 75 and 76 show the effect of the Mn-to-Fe and Mn-to-Si ratios of the metal phase on the relationship between the silicon content of the metal and silica content of the slag in ferromanganese and silicomanganese compositions respectively. As the silica content of the slag increases, the silicon content of the metal phase increases and this effect is even more noticeable at the higher Mn-to-Fe and Mn-to-Si ratios. The increase in the silica activity in the slag with increasing silica concentration results in the transfer of silicon from the slag to the metal (The individual experimental groups with different Mn-to-Fe and Mn-to-Si ratios are given in Appendix D, Figures D.13 to D.19).

The CaO-to-Al_2O_3 ratio has also an effect on the reduction of silica from the slag. This effect is shown in Figures 77 and 78, in ferromanganese and silicomanganese compositions respectively. In Figure 77, two data groups with different Mn-to-Fe ratios are superimposed and in Figure 78, four data groups with different Mn-to-Si

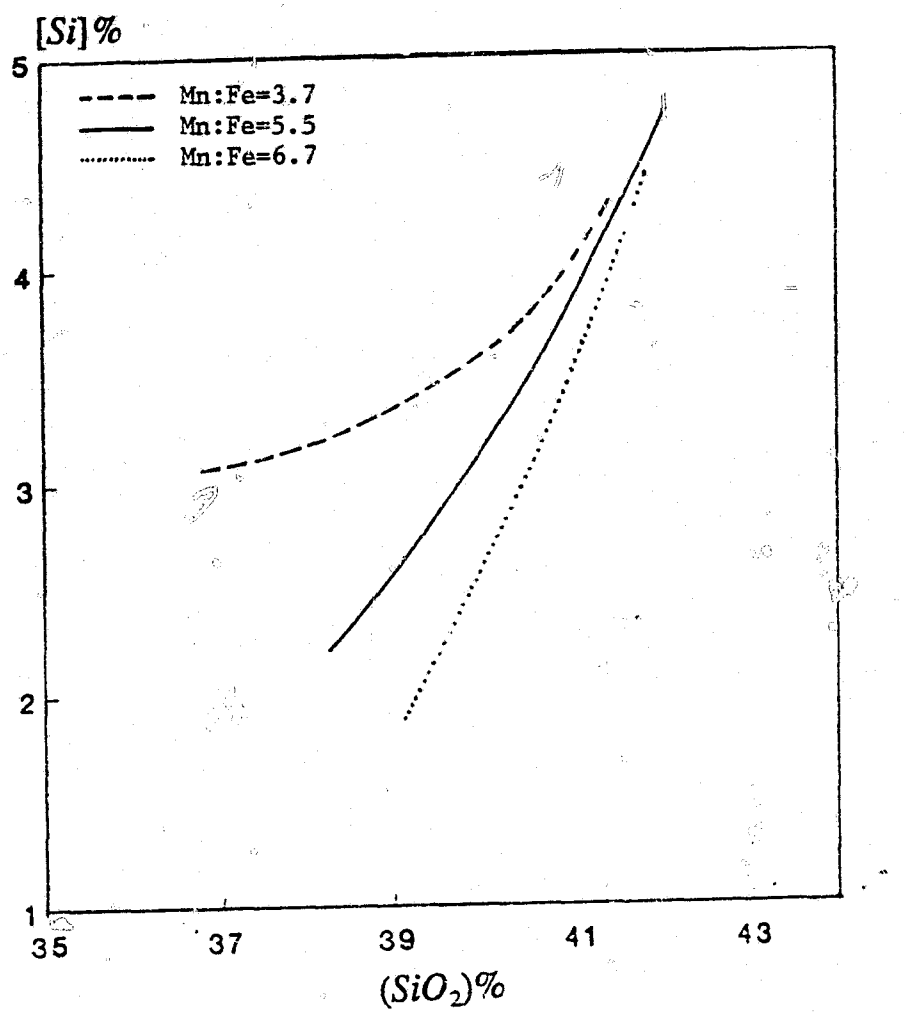

Figure 75. The effect of the SiO_2 content of the slag phase on the Si content of the metal phase with different Mn-to-Fe ratios at 1500°C under CO atmosphere.

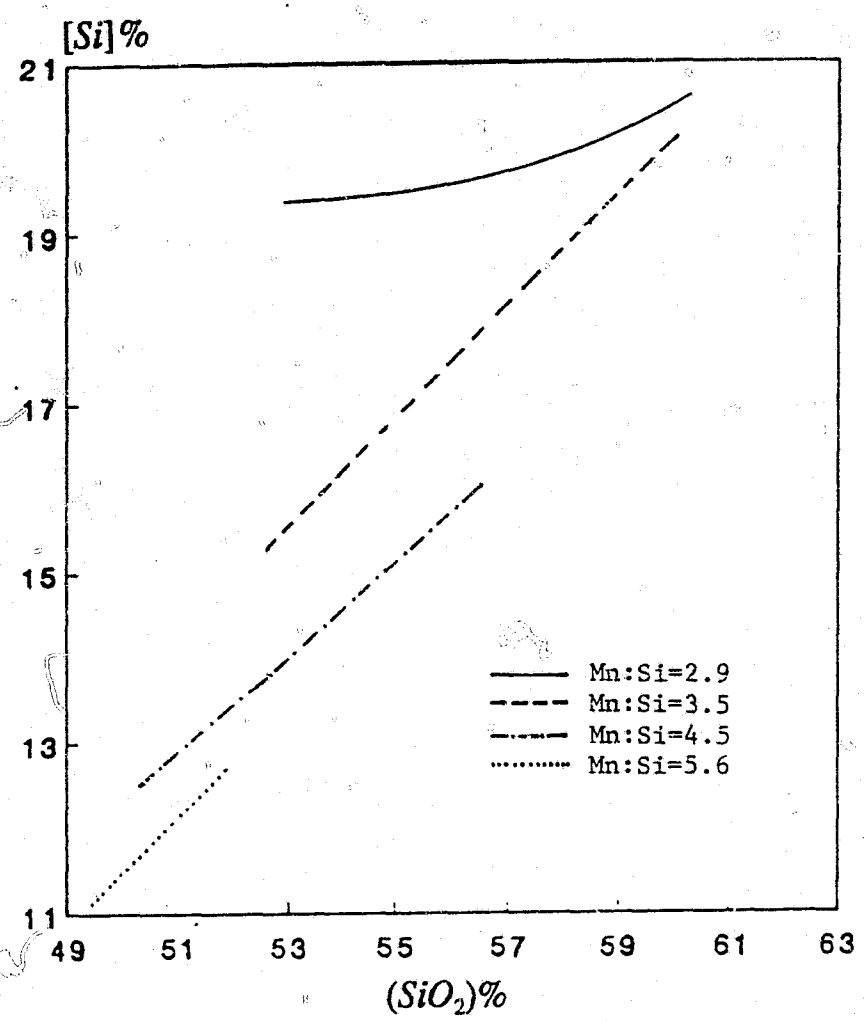

Figure 76. **The effect of the SiO_2 content of the slag phase on the Si content of the metal phase with different Mn-to-Si ratios at 1500°C under CO atmosphere.**

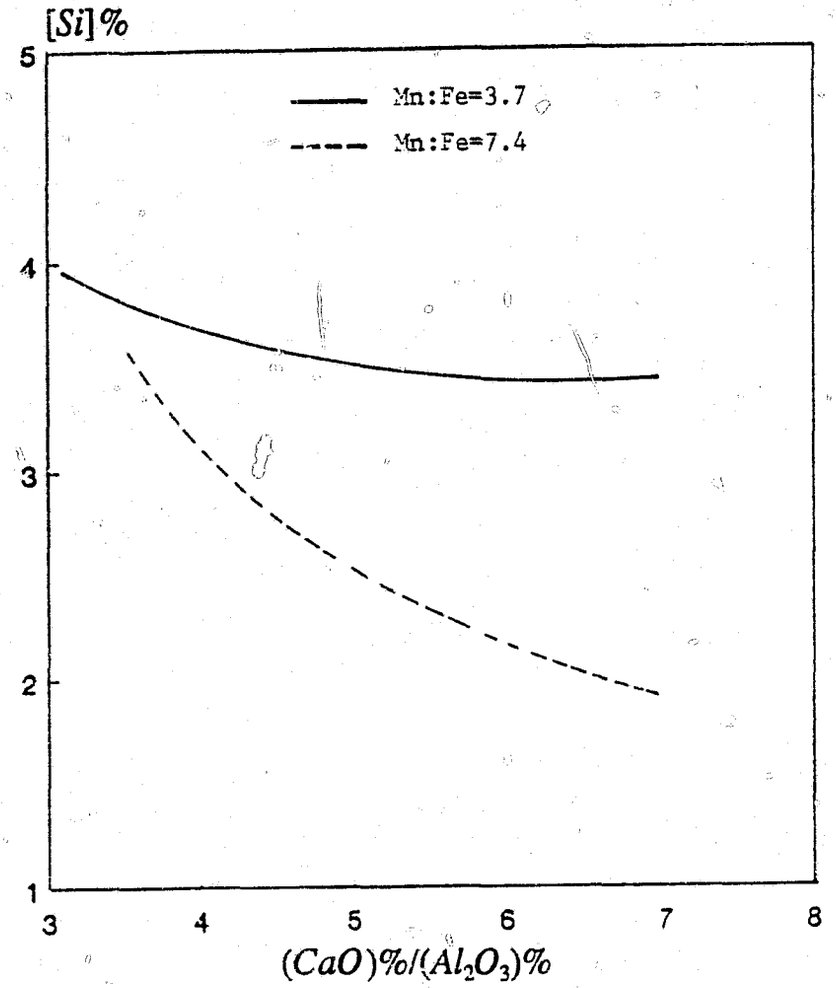

Figure 77. **The effect of the CaO-to-Al_2O_3 ratio of the slag phase on the Si content of the metal phase with different Mn-to-Fe ratios at 1500°C under CO atmosphere.**

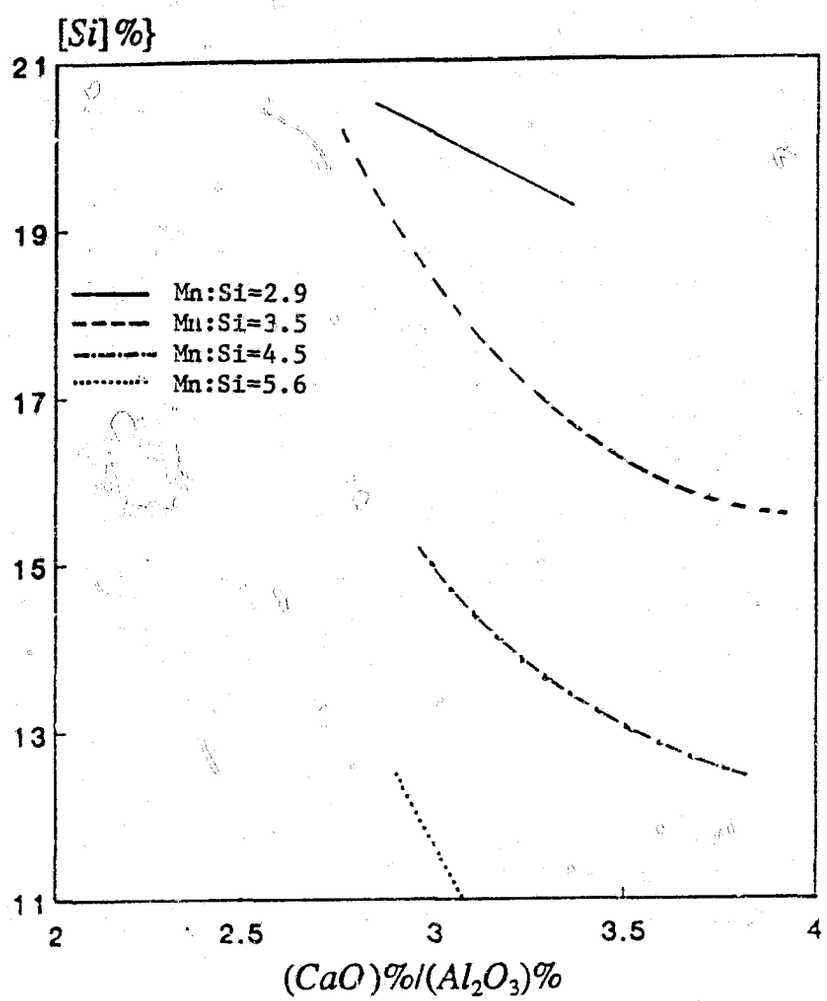

Figure 78. The effect of the CaO-to-Al_2O_3 ratio of the slag phase on the Si content of the metal phase with different Mn-to-Si ratios at 1500°C under CO atmosphere.

ratios are superimposed (the data individual groups with different Mn-to-Fe and Mn-to-Si ratios are given in Appendix D, Figures D.20 to D.25). As it is seen from the figures, as the CaO-to-Al_2O_3 ratio increases (at more or less constant Al_2O_3 content), the silicon content of the metal decreases. As the Mn-to-Fe ratio increases, the effect of increasing CaO-to-Al_2O_3 ratio on the silicon content of the metal is even greater. On the other hand, in Figure 78, the same relationship between the CaO-to-Al_2O_3 ratio and the silicon content of the metal phase is observed, although, the increasing effect of CaO-to-Al_2O_3 ratio is even more emphasized with increasing Mn-to-Si ratio. This indicates that the activity of silica in the slag is decreased by the substitution of CaO in accordance with the network modification power of CaO. This result is similar to the findings of Fulton and Chipman[129]. Another study[130] showed that, as Al_2O_3 was replaced with CaO in slags of low SiO_2 content, the equilibrium silicon content of the metal increased. In the case of slags with a high SiO_2 content, the opposite effect was observed[130]. This is also in agreement with the findings of the present study as the present slags had high SiO_2 contents.

In Figure 79, the effect of the MgO-to-CaO ratio of the slag on the silicon distribution between the slag and the metal phases is analysed at constant Al_2O_3 and SiO_2 levels. As MgO replaces CaO in the slag, the distribution ratio of silicon decreases and the silicon content of the metal increases relative to that of the slag. This can be explained with reference to the MnO activities. It was observed that CaO had a slight effect in increasing the MnO activities owing to the different

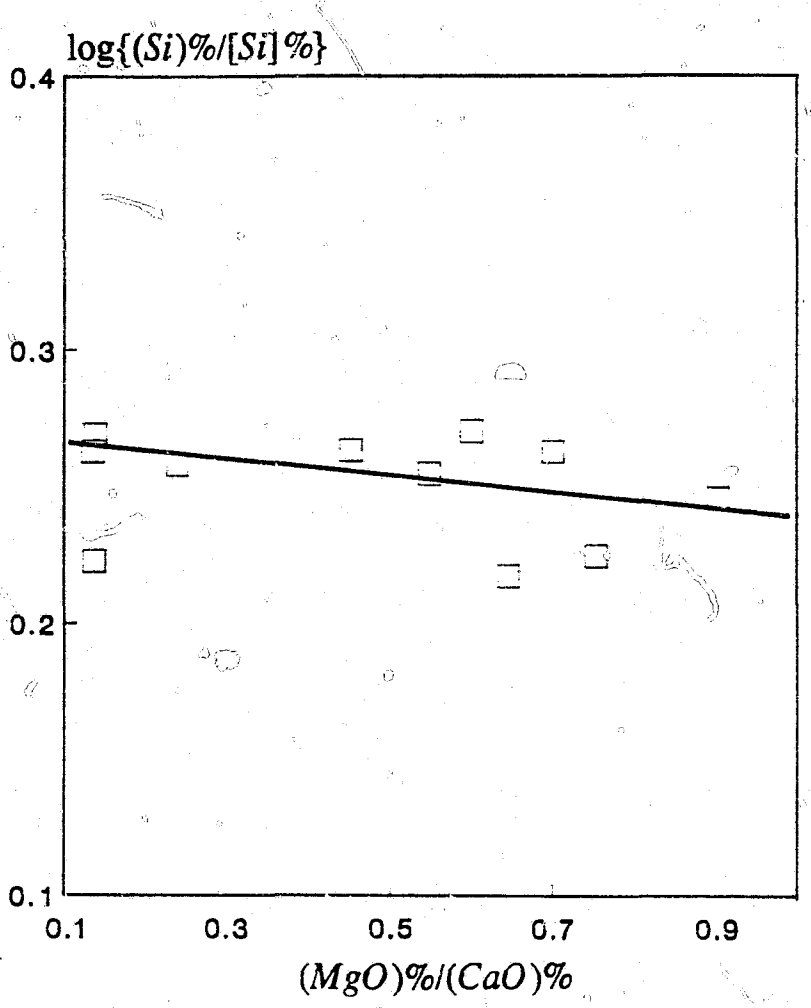

Figure 79. The effect of the MgO-to-CaO ratio of the slag on the Si distribution with 5% Al_2O_3 and 53.1% SiO_2 at 1500°C under CO atmosphere.

free energies of formation of the complex orthosilicates. As MgO replaces CaO, it may cause a decrease in MnO activity, and there is less tendency for Ca_2SiO_4 species to form in the slag. This may cause an increase in the activity of SiO_2 in the slag and therefore the silicon content of the metal increases.

In Figure 80, it can be seen that the silicon content of the metal phase decreases as the basicity ratio of the slag increases. This can also be explained in a very similar way in terms of the breakup of the silica network with the addition of basic oxides. Because of the strong interaction between divalent cations Ca^{2+}, Mg^{2+} and the silicate ions, the activity of silica in the slag decreases and the silicon content of the metal decreases with increasing basicity.

4.2.3 Manganese and silicon activities in Mn-Si-Fe-C melts

The results of this investigation on MnO activities in manganese slags were in excellent agreement with those predicted from the slag model developed by Gaye[124] using the compositional information gathered in the present work. Therefore SiO_2 activities in the slag were predicted through the slag model in order to calculate the Si activities in Mn-Si-Fe-C metal phase and the compositional information of the slag and metal phases were provided from the results of slag-metal equilibrium experiments by the equation:

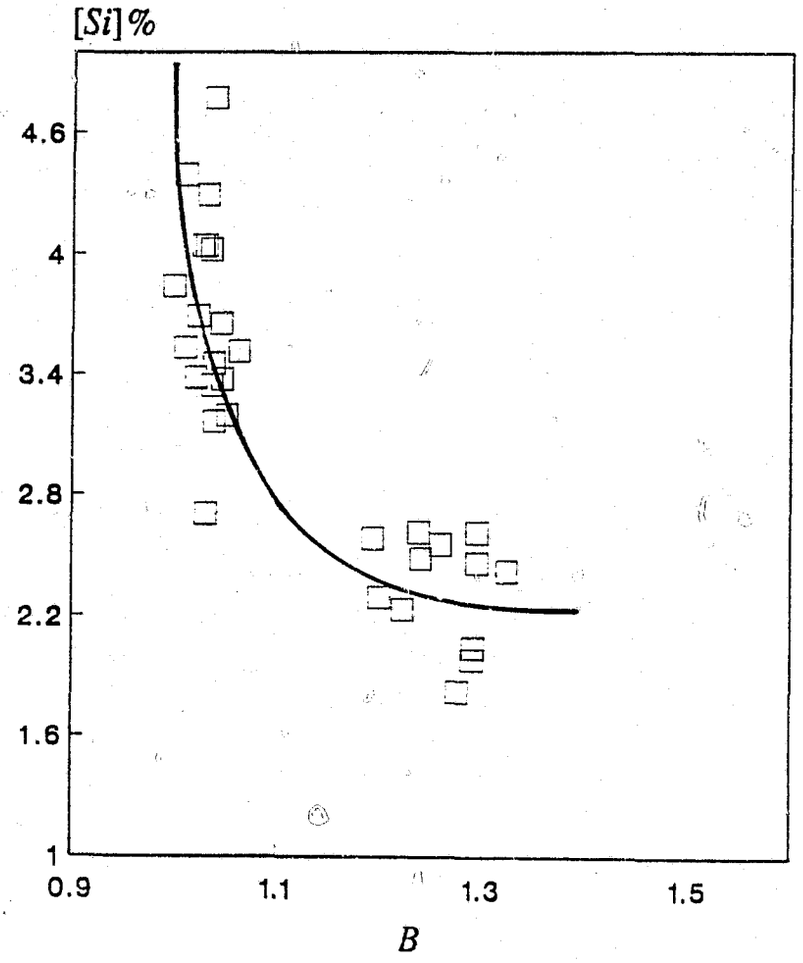

Figure 80. The effect of the basicity ratio of the slag on the Si content of the metal phase at 1500°C under CO atmosphere.

$$(SiO_2) + 2[C] = [Si] + 2CO \quad \Delta G^0 = 55968.28 J/mole \ldots\ldots\ldots\ldots (86)$$

the equilibrium constant of this reaction can be written as:

$$K = \frac{a_{Si} \times (p_{CO})^2}{a_{SiO_2} \times (a_C)^2} \ldots\ldots\ldots\ldots (87)$$

In equation (87), $a_C = 1$ and $p_{CO} = 1$ atm. Thus the equation (87) reduces to:

$$K = \frac{a_{Si}}{a_{SiO_2}} \ldots\ldots\ldots\ldots (88)$$

where K=0.02244.

The Mn activities were also calculated similarly using known activities of MnO in the slag through the equation

$$(MnO) + [C] = [Mn] + CO \quad \Delta G^0 = -23622.80 J/mole \ldots\ldots\ldots\ldots (89)$$

The equilibrium constant of this reaction can be written as:

$$K = \frac{a_{Mn} \times p_{CO}}{a_C \times a_{MnO}} \quad \text{.....(90)}$$

In equation (90), $p_{CO} = 1$ atm and $a_C = 1$, therefore, the equation (90) reduces to:

$$K = \frac{a_{Mn}}{a_{MnO}} \quad \text{.....(91)}$$

where K = 4.953.

As it is seen, the activities of Si and Mn can be easily calculated through the equations (88) and (91) and they are shown in Tables XXI and XXII. The compositions of the slag and the metal phases have been shown in section 4.2.1 in Tables XIX and XX with the same experimental numbers.

Quadratic multi-variable regression models were derived to predict the activity coefficient of silicon in silicomanganese and ferromanganese metal phase compositions by making use of the slag-metal equilibrium data in Tables XXIII to XXIV. As it is seen from the Tables XXIII to XXIV, silicon shows strong negative deviations from ideality in silicomanganese and ferromanganese compositions indicating a tendency towards order (compound formation).

Table XXI. Activities of silicon and manganese in silicomanganese metal phase in equilibrium with slag.

Exp.No.	a_{MnO}	a_{SiO_2}	a_{Mn}	a_{Si}
1	0.032	0.600	0.158	0.013
2	0.033	0.548	0.163	0.012
3	0.030	0.545	0.149	0.012
4	0.023	0.675	0.114	0.015
5	0.017	0.646	0.084	0.014
6	0.023	0.656	0.114	0.015
7	0.024	0.668	0.119	0.015
8	0.022	0.661	0.109	0.015
9	0.024	0.659	0.119	0.015
10	0.008	0.744	0.040	0.017
11	0.005	0.750	0.025	0.017
12	0.003	0.741	0.015	0.017
13	0.008	0.713	0.040	0.016
14	0.005	0.715	0.025	0.016
15	0.008	0.681	0.040	0.015
16	0.026	0.660	0.129	0.015
17	0.026	0.665	0.129	0.015
18	0.031	0 650	0.154	0.015
19	0.026	0.475	0.129	0.011
20	0.027	0.470	0.134	0.011
21	0.028	0.484	0.139	0.011
22	0.029	0.487	0.144	0.011
23	0.031	0.477	0.154	0.011

Table XXI continued

Exp.No.	a_{MnO}	a_{SiO_2}	a_{Mn}	a_{Si}
24	0.033	0.472	0.163	0.011
25	0.025	0.533	0.124	0.012
26	0.026	0.550	0.129	0.012
27	0.029	0.565	0.144	0.013
28	0.027	0.580	0.134	0.013
29	0.029	0.539	0.144	0.012
3	0.026	0.533	0.129	0.012
31	0.023	0.620	0.114	0.014
32	0.025	0.556	0.124	0.012
33	0.024	0.592	0.119	0.013
34	0.025	0.615	0.124	0.014
35	0.024	0.617	0.119	0.014
36	0.024	0.632	0.119	0.014

Table XXII **Activities of silicon and manganese in ferromanganese metal phase.**

Exp.No.	a_{MnO}	a_{SiO_2}	a_{Mn}	a_{Si}
1	0.039	0.159	0.193	0.004
2	0.045	0.152	0.223	0.003
3	0.051	0.137	0.253	0.003
4	0.047	0.142	0.233	0.003
5	0.053	0.144	0.263	0.003
6	0.038	0.146	0.188	0.003
7	0.042	0.147	0.208	0.003
8	0.048	0.143	0.238	0.003
9	0.057	0.128	0.282	0.003
10	0.052	0.135	0.258	0.003
11	0.054	0.138	0.267	0.003
12	0.030	0.181	0.149	0.004
13	0.039	0.153	0.193	0.003
14	0.042	0.148	0.208	0.003
15	0.048	0.136	0.238	0.003
16	0.052	0.133	0.258	0.003
17	0.047	0.134	0.233	0.003
18	0.022	0.069	0.109	0.002
19	0.028	0.069	0.139	0.002
20	0.025	0.067	0.124	0.002
21	0.042	0.083	0.208	0.002
22	0.050	0.081	0.248	0.002
23	0.046	0.077	0.228	0.002

Table XXII continued

Exp.No.	a_{MnO}	a_{SiO_2}	a_{Mn}	a_{Si}
24	0.030	0.078	0.149	0.002
25	0.033	0.072	0.163	0.002
26	0.035	0.075	0.173	0.002
27	0.026	0.066	0.129	0.001
28	0.026	0.067	0.129	0.002
39	0.027	0.061	0.134	0.001
30	0.016	0.046	0.079	0.001
31	0.054	0.039	0.267	0.001
32	0.021	0.055	0.104	0.001
33	0.016	0.061	0.079	0.001
34	0.017	0.053	0.084	0.001
35	0.018	0.064	0.089	0.001

Table XXIII. Activity coefficients of silicon in silicomanganese metal phase.

$\ln\gamma_{Si}$	X_{Mn}	X_{Si}	X_{Fe}
-2.832	0.509	0.221	0.165
-2.857	0.510	0.209	0.160
-2.862	0.527	0.210	0.155
-2.901	0.490	0.273	0.166
-2.924	0.493	0.261	0.160
-2.822	0.488	0.252	0.152
-2.891	0.503	0.270	0.152
-2.853	0.499	0.260	0.149
-2.809	0.514	0.249	0.149
-2.956	0.472	0.327	0.161
-2.951	0.473	0.325	0.157
-2.942	0.480	0.322	0.152
-2.986	0.489	0.317	0.153
-2.982	0.487	0.316	0.145
-3.036	0.491	0.312	0.141
-2.838	0.502	0.256	0.153
-2.724	0.520	0.229	0.151
-2.688	0.520	0.221	0.144
-2.919	0.496	0.204	0.172
-2.902	0.501	0.200	0.171
-2.850	0.505	0.190	0.167
-2.831	0.515	0.187	0.167
-2.804	0.516	0.182	0.161

Table XXIII continued

$\ln\gamma_{Si}$	X_{Mn}	X_{Si}	X_{Fe}
-2.764	0.525	0.175	0.158
-3.078	0.482	0.261	0.173
-3.027	0.482	0.248	0.168
-2.942	0.485	0.246	0.167
-2.894	0.494	0.235	0.164
-2.962	0.498	0.232	0.160
-2.893	0.500	0.216	0.155
-3.110	0.462	0.314	0.172
-3.269	0.466	0.315	0.171
-3.190	0.464	0.316	0.164
-3.046	0.476	0.295	0.167
-3.029	0.484	0.289	0.159
-3.008	0.488	0.283	0.159

Table XXIV. Activity coefficients of silicon in ferromanganese metal phase.

$\ln\gamma_{Si}$	X_{Mn}	X_{Si}	X_{Fe}
-2.807	0.594	0.066	0.086
-2.879	0.605	0.053	0.083
-2.911	0.604	0.055	0.082
-2.855	0.607	0.052	0.081
-2.835	0.611	0.051	0.079
-3.176	0.567	0.072	0.110
-3.012	0.578	0.061	0.105
-2.928	0.586	0.056	0.105
-2.825	0.590	0.051	0.100
-2.768	0.590	0.048	0.099
-2.607	0.594	0.041	0.095
-2.699	0.547	0.059	0.161
-3.076	0.536	0.065	0.148
-3.016	0.547	0.061	0.144
-2.720	0.595	0.030	0.086
-2.597	0.590	0.027	0.084
-2.674	0.586	0.029	0.080
-2.823	0.590	0.034	0.078
-2.947	0.594	0.038	0.077
-2.797	0.594	0.033	0.075
-2.963	0.570	0.039	0.104
-2.943	0.575	0.038	0.102
-2.911	0.571	0.037	0.102
-3.576	0.559	0.036	0.096
-2.946	0.562	0.038	0.097
-3.575	0.572	0.036	0.098
-3.958	0.546	0.052	0.150
-3.978	0.537	0.053	0.153
-3.860	0.548	0.047	0.143

In silicomanganese and ferromanganese compositions, $\ln\gamma_{Si}$ was fit into the equation (94) which is a multi-variable quadratic equation.

$$\ln\gamma_{Si} = a_0 + a_1X_{Mn} + a_2X_{Si} + a_3X_{Fe} + a_4X_{Mn}^2 + a_5X_{Si}^2 + a_6X_{Fe}^2 + a_7X_{Mn}X_{Si} + a_8X_{Mn}X_{Fe} + a_9X_{Si}X_{Fe} \quad \text{.....(92)}$$

In equation (92), for both compositions, the dependent variable was $\ln\gamma_{Si}$ and the independent variables were atomic fractions of manganese, silicon and iron. The atomic fraction of carbon was not included in the regression analysis due to lower correlation coefficients computed. The regression analysis were carried out using the SAS procedure RSREG and RSQUARE as explained in detail in section 4.1.2 and very high correlation coefficients were obtained.

The results of the statistical analysis are summarized in Tables XXV and XXVI. The set of model equation parameters for both the complete quadratic and reduced models for silicomanganese and ferromanganese compositions are shown in Table XXVII. In the case of ferromanganese, the choice of the number of data points were determined by the results of the previous regression. For the complete set involving 35 data points, the regression analysis predicted that 6 experimental points were, from statistical point of view, out of the 90 per cent confidence level. When these experimental points were ignored resulting in a set with 29 points, very high correlation coefficients were

Table XXV. Results for $\ln\gamma_{Si}$ model in silicomanganese metal phase.

	Complete Quadratic Model	Reduced Model
Correlation Coefficient R^2	0.8376	0.8098
Number of parameters in model	10	6

Table XXVI. Results for $\ln\gamma_{Si}$ model in ferromanganese metal phase.

	Complete Quadratic Model	Reduced Model
Correlation Coefficient R^2	0.8290	0.8169
Number of parameters in model	10	6

Table XXVII. Model parameters for $\ln\gamma_{Si}$ in both silicomanganese and ferromanganese compositions.

	Silicomanganese Composition		Ferromanganese Composition	
Coefficient	Complete Quadratic Model	Reduced Model	Complete Quadratic Model	Reduced Model
a_0	-16.126165	8.2237	74.713371	9.6390
a_1	69.939652	-	-196.397373	-14.4553
a_2	-15.806002	-13.4747	-557.148460	-108.7
a_3	-32.101573	-123.5	-310.476568	-247.9
a_4	-77.788858	-28.5236	126.833582	-
a_5	6.608401	-	195.632285	-
a_6	-75.342825	-	-25.099092	-
a_7	0.444770	-	648.491372	-
a_8	67.392607	199.7	433.944173	352.9
a_9	71.896112	79.5894	1634.189790	1106.0

obtained indicating an excellent fit with all points within the confidence limit. As it is seen in Tables XXV and XXVI, high correlation coefficients were obtained for both procedures indicating an excellent fit with all data points within the confidence limits.

The complete quadratic model equation for silicomanganese composition can be written as:

$$\ln\gamma_{Si} = -16.126165 + 69.939652\ X_{Mn} - 15.806002\ X_{Si} - 32.101573\ X_{Fe} - 77.788858\ X_{Mn}^2 + 6.608401\ X_{Si}^2 - 75.342825\ X_{Fe}^2 + 0.444770\ X_{Mn}\ X_{Si} + 67.392607\ X_{Mn}\ X_{Fe} + 7i.896112\ X_{Si}\ X_{Fe} \quad \text{.....(93)}$$

and the complete quadratic model equation for ferromanganese composition can be written as:

$$\ln\gamma_{Si} = 74.713371 - 196.397373\ X_{Mn} - 557.148460\ X_{Si} - 310.476568\ X_{Fe} + 126.833582\ X_{Mn}^2 + 195.632285X_{Si}^2 - 25.099092\ X_{Fe}^2 + 648.491372\ X_{Mn}\ X_{Si} + 433.944173\ X_{Mn}\ X_{Fe} + 1634.189790\ X_{Si}\ X_{Fe} \quad \text{.....(94)}$$

The reduced model equations can be very practical for calculating the activity coefficients of silicon in the

metal phase. Therefore, these equations are also given below. The reduced model equation for silicomanganese composition is:

$$\ln\gamma_{Si} = 8.2237 - 13.4747\ X_{Si} - 123.5\ X_{Fe} - 28.5236\ X_{Mn}^2 + 199.7\ X_{Mn}\ X_{Fe} + 79.5894\ X_{Si}\ X_{Fe} \quad \text{.....(95)}$$

The reduced model equation for ferromanganese composition is:

$$\ln\gamma_{Si} = 9.6390 - 14.4553\ X_{Mn} - 108.7\ X_{Si} - 247.9\ X_{Fe} + 352.9\ X_{Mn}\ X_{Fe} + 1106.0\ X_{Si}\ X_{Fe} \quad \text{.....(96)}$$

Quadratic multi-variable regression models were also derived to predict the activity coefficient of manganese in silicomanganese and ferromanganese metal phase compositions by making use of the slag-metal equilibrium data in Tables XXVIII to XXIX. As it is seen from the Tables XXVIII to XXIX, manganese shows strong negative deviations from ideality in silicomanganese and ferromanganese compositions indicating a tendency towards order (compound formation).

In both silicomanganese and ferromanganese compositions, in equation (97), the dependent variable was $\ln\gamma_{Mn}$ and the independent variables were atomic fractions of manganese, silicon and iron. Equation (97) is very

Table XXVIII. Activity coefficients of manganese in silicomanganese metal phase.

$\ln\gamma_{Mn}$	X_{Mn}	X_{Si}	X_{Fe}
.170	0.509	0.221	0.165
-1.140	0.510	0.209	0.160
-1.264	0.527	0.210	0.155
-1.459	0.490	0.273	0.166
-1.769	0.493	0.261	0.160
-1.454	0.488	0.252	0.152
-1.441	0.503	0.270	0.152
-1.520	0.499	0.260	0.149
-1.463	0.514	0.249	0.149
-2.468	0.472	0.327	0.161
-2.941	0.473	0.325	0.157
-3.465	0.480	0.322	0.152
-2.504	0.489	0.317	0.153
-2.969	0.487	0.316	0.145
-2.508	0.491	0.312	0.141
-1.358	0.502	0.256	0.153
-1.394	0.520	0.229	0.151
-1.217	0.520	0.221	0.144
-1.347	0.496	0.204	0.172
-1.319	0.501	0.200	0.171
-1.291	0.505	0.190	0.167
-1.274	0.515	0.187	0.167
-1.208	0.516	0.182	0.161

Table XXVIII continued

$\ln \gamma_{Mn}$	X_{Mn}	X_{Si}	X_{Fe}
-1.170	0.525	0.175	0.158
-1.358	0.482	0.261	0.173
-1.318	0.482	0.248	0.168
-1.214	0.485	0.246	0.167
-1.306	0.494	0.235	0.164
-1.241	0.498	0.232	0.160
-1.354	0.500	0.216	0.155
-1.400	0.462	0.314	0.172
-1.323	0.466	0.315	0.171
-1.360	0.464	0.316	0.164
-1.345	0.476	0.295	0.167
-1.404	0.484	0.289	0.159
-1.412	0.488	0.283	0.159

Table XXIX. Activity coefficients of manganese in ferromanganese metal phase.

$\ln\gamma_{Mn}$	X_{Mn}	X_{Si}	X_{Fe}
-1.124	0.594	0.066	0.086
-0.998	0.605	0.053	0.083
-0.870	0.604	0.055	0.082
-0.957	0.607	0.052	0.081
-0.843	0.611	0.051	0.078
-1.104	0.567	0.072	0.110
-1.022	0.578	0.061	0.105
-0.902	0.586	0.056	0.105
-0.738	0.590	0.051	0.101
-0.827	0.590	0.048	0.099
-0.799	0.594	0.041	0.095
-1.300	0.547	0.059	0.161
-1.021	0.536	0.065	0.148
-0.967	0.547	0.061	0.144
-1.697	0.595	0.031	0.086
-1.445	0.590	0.027	0.084
-1.553	0.586	0.029	0.080
-1.042	0.590	0.034	0.078
-0.873	0.594	0.038	0.077
-0.957	0.594	0.033	0.075
-1.342	0.570	0.039	0.104
-1.261	0.575	0.038	0.102
-1.194	0.571	0.037	0.102
-1.466	0.559	0.036	0.096
-1.471	0.562	0.038	0.097
-1.451	0.572	0.036	0.098
-1.657	0.546	0.052	0.150
-1.916	0.537	0.053	0.153
-1.817	0.548	0.047	0.143

useful in calculating $\ln\gamma_{Mn}$ values. The regressions were carried out using the SAS procedure RSREG and RSQUARE as explained in details in section 4.1.2.

$$\ln\gamma_{Mn} = a_0+a_1X_{Mn}+a_2X_{Si}+a_3X_{Fe}+a_4X_{Mn}^2+a_5X_{Si}^2+a_6X_{Fe}^2+a_7X_{Mn}X_{Si} +a_8X_{Mn}X_{Fe}+a_9X_{Si}X_{Fe} \quad (97)$$

In silicomanganese and ferromanganese compositions $\ln\gamma_{Mn}$ was fit into equation (97) by using the whole data points in Tables XXVIII and XXIX. The results of the statistical analysis are summarized in Tables XXX and XXXI. The set of model equation parameters for both the complete quadratic and reduced models for silicomanganese and ferromanganese compositions are shown in Table XXXII. In the case of ferromanganese, the choice of the number of data points were determined by the results of the previous regression. For the complete set involving 35 data points, the regression analysis predicted that 6 experimental points were, from statistical point of view, out of the 90 per cent confidence level. When these experimental points were ignored resulting in a set with 29 points, very high correlation coefficients were obtained indicating an excellent fit with all points within the confidence limit. The results shown in Table XXXI include these 29 reliable experimental points.

In both compositions, the reduced models were preferred for practical convenience and the reduced model for silicomanganese composition is:

Table XXX. Results for $\ln\gamma_{Mn}$ model in silicomanganese metal phase.

	Complete Quadratic Model	Reduced Model
Correlation Coefficient R^2	0.8369	0.8317
Number of parameters in model	10	6

Table XXXI. Results for $\ln\gamma_{Mn}$ model in ferromanganese metal phase.

	Complete Quadratic Model	Reduced Model
Correlation Coefficient R^2	0.8688	0.8409
Number of parameters in model	10	6

Table XXXII. Model parameters for $\ln\gamma_{Mn}$ and coefficients for $\ln\gamma_{Mn}$ models.

	Silicomanganese Composition		Ferromanganese Composition	
Coefficient	Complete Quadratic Model	Reduced Model	Complete Quadratic Model	Reduced Model
a_0	-194.957975	74.4176	-65.077416	-6.8048
a_1	565.763436	-300.1	203.675667	8.0995
a_2	281.796891	-	414.227457	30.2975
a_3	236.967381	-	-105.705933	-
a_4	-349.388607	320.5	-163.200905	-
a_5	-444.453738	-122.8	-526.908868	-1427.3
a_6	-197.398474	-	-1767.796475	-303.9
a_7	-697.525461	-	123.234109	-
a_8	183.752519	-143.8	847.903460	-
a_9	236.446432	332.3	-77.531731	1263.2

$$\ln\gamma_{Mn} = 74.4176 - 300.1\ X_{Mn} + 320.5\ X_{Mn}^2 - 122.8\ X_{Si}^2 - 143.8\ X_{Mn}\ X_{Fe} + 332.3\ X_{Si}\ X_{Fe} \quad \text{.....(98)}$$

For ferromanganese composition, the reduced model is:

$$\ln\gamma_{Mn} = -6.8048 + 8.0995\ X_{Mn} + 30.2975\ X_{Si} - 1427.3\ X_{Si}^2 - 303.9\ X_{Fe}^2 + 1263.2\ X_{Si}\ X_{Fe} \quad \text{.....(99)}$$

The iso-activity contours of silicon for silicomanganese and ferromanganese compositions were derived through the reduced model equations (95) and (96) at 1500°C and are shown in Figure 81 and 82. As it was mentioned before, the figures represent a carbon-saturated system and if atomic fraction of silicon, X_{Si}, increases, then, atomic fraction of carbon, X_C, decreases. Namely, the carbon concentration decreases as it goes up to the top part of the figure. In this system, X_C takes a certain value if the atomic fraction of iron, X_{Fe}, and X_{Si} are given, and therefore, the compositions of all carbon-saturated alloy melts of the Mn-Si-Fe-C system can be represented on a plane with X_{Fe} and X_{Si} on both axes as shown in Figures 81 and 82.

In silicomanganese composition (Figure 81), the predicted iso-activity contour values vary between 0.012-0.021. However, in ferromanganese composition (Figure 82), the silicon activities are even smaller (between 5×10^{-4} and 3×10^{-3}). The difference between the

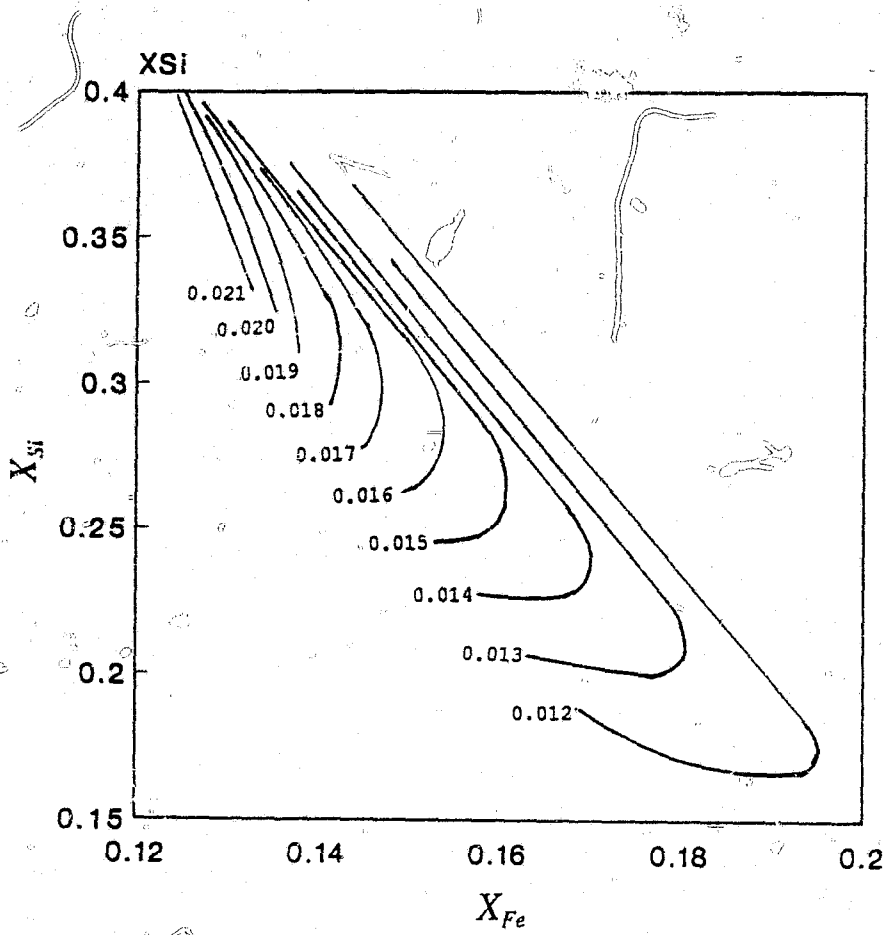

Figure 81. Iso-activity lines of Si in silicomanganese melts saturated with C at 1500°C.

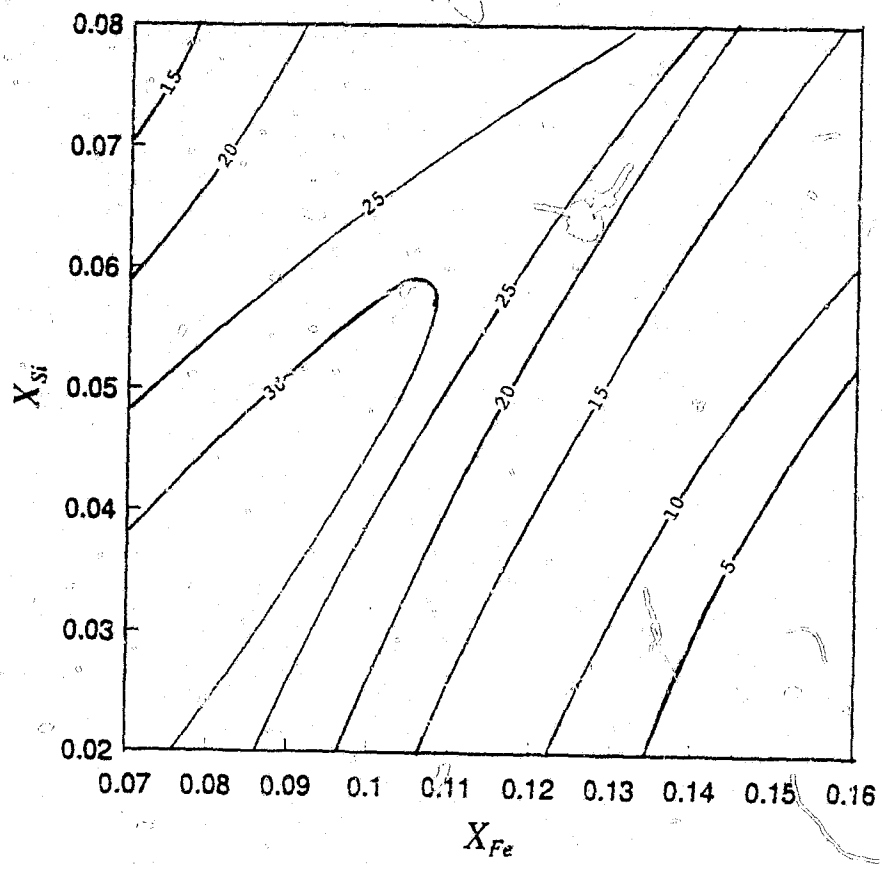

Figure 82. Iso-activity lines of Si in ferromanganese melts saturated with C at 1500°C ($\times 10^{-4}$).

silicon activities in these two compositions can, to a certain extent, be explained according to the difference in silicon concentrations (being higher in silicomanganese composition) in these compositions. Concerning the carbon-saturated system Mn-Si-Fe-C, the related thermodynamic data is very scarce. Therefore, it is difficult to explain the order of magnitude change in iso-activity curves by estimation from the stable phases in the liquid state. However, liquid-solid equilibria of Fe-Mn-C ternary system has been studied by Vogel and Doring[132], and in great detail, by Isobe[131]. Schurmann and Geisler[132] revised the liquidus surface in the light of the solid phases in the binary C-Mn system and established that between 0 and 3 mass per cent manganese, graphite separates as the stable phase. The primary crystallization surfaces shown in Figure 83[132] are for δMn, δFe, γFe which is continuous with γMn, M_3C, ε, M_5C_2, M_7C_3 and graphite.

As it is seen in Figure 81, the iso-activity contours show a maximum in the high Si region of silicomanganese composition where X_{Fe} is between 0.12 and 0.14. In other words, silicon activities increase with a decrease in X_{Fe} and increase in X_{Si}. An increase in a_{Si} can be explained by an increase in its atomic fraction. However, in Fe-Mn-C ternary system, if the silicon content is ignored for an approach in interpreting the increase in silicon activity, the composition range falls into the liquid region in Fe-Mn-C ternary system at 1500°C which disfavours the SiC formation. This can also increase the silicon activity in the melt. Another factor leading to an increase in silicon activities can be the strong

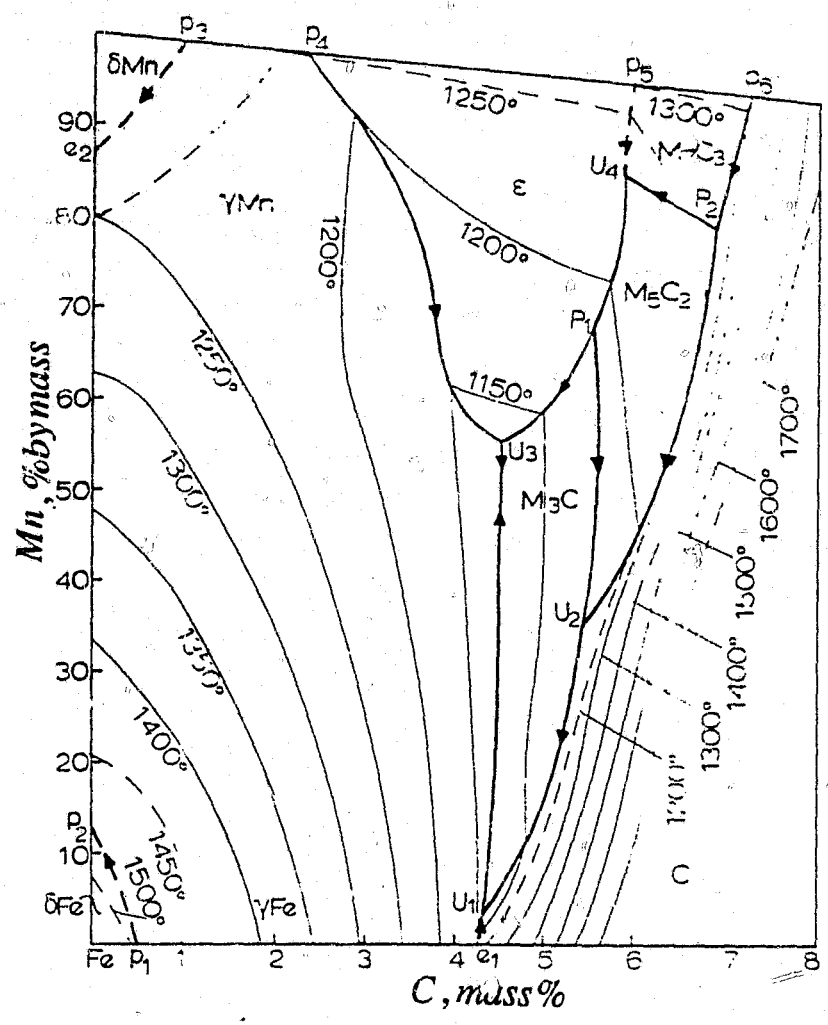

Figure 83. Liquidus projection of Fe-Mn-C system[131].

inter-atomic attraction between Mn, Fe and C, even in liquid phase[119] freeing some of the silicon atoms in the melt.

In Figure 82, the iso-activity contours of silicon in ferromanganese composition are shown. The curves indicate a maximum in the low X_{Fe} and X_{Si} region, at the lef bottom of the figure. In other words, the activity of silicon decreases with an increase in X_{Si} and X_{Fe}. In ferromanganese composition, the silicon content is very low (1.82-4.77 mass per cent) and Fe-Mn-C ternary system (Figure 83) can be used more safely. The ferromanganese compositions studied fall into the M_3C_2 carbide primary crystallization field. The free energy of formation of SiC and Mn_3C_2 carbide from their elements were calculated[132] at 1100 K (827°C) as it is seen below:

$$Si + C = SiC \quad \Delta G^0 = -62708.42 J/mole \qquad (100)$$

$$5Mn + 2C = Mn_5C_2 \quad \Delta G^0 = -74058.6 J/mole \qquad (101)$$

It is clear from equations (100) and (101) that Mn_5C_2 is thermodynamically more stable than SiC. Therefore, Mn_5C_2 formation is favoured with respect to SiC formation leading to higher silicon activities even at lower silicon concentrations. The activity of silicon is, however, far smaller in ferromanganese compositions. The decreasing atomic fraction of silicon and the

increasing atomic fraction of manganese also play a role on the lower silicon activities in comparison to silicomanganese compositions.

The Figures 84 and 85 shows the iso-activity contours of manganese which are derived through the reduced model equations (98) and (99) in silicomanganese and ferromanganese compositions respectively. In Figure 84, in silicomanganese composition, an increase in X_{Fe} decreases a_{Mn} values. A decrease in X_{Fe} will increase X_{Mn} and X_{Si} in carbon-saturated system and this will lead to higher a_{Mn} values.

In Figure 85, a decrease in X_{Si} at constant X_{Fe} first increases and then decreases the a_{Mn} values in the ferromanganese composition. The increase in a_{Mn} is clear due to increase in X_{Mn} at fixed X_{Fe} and X_C values. However, even a further decrease in X_{Si} causes a_{Mn} to start decreasing which may be due to the fact that at very low silicon concentrations, the saturation solubility limit of carbon increases substantially favouring stronger Mn-C interactions and a tendency for Mn_3C_2 formation which will tend to decrease a_{Mn} values.

When the results of the present study are compared to the results of Tanaka[117,119] who studied the same system (Figures 30a and 30b), it is seen that the iso-activity contours of silicon and manganese have very similar patterns but represent different activity values. As far as a_{Mn} values are concerned, Tanaka's study[117] was

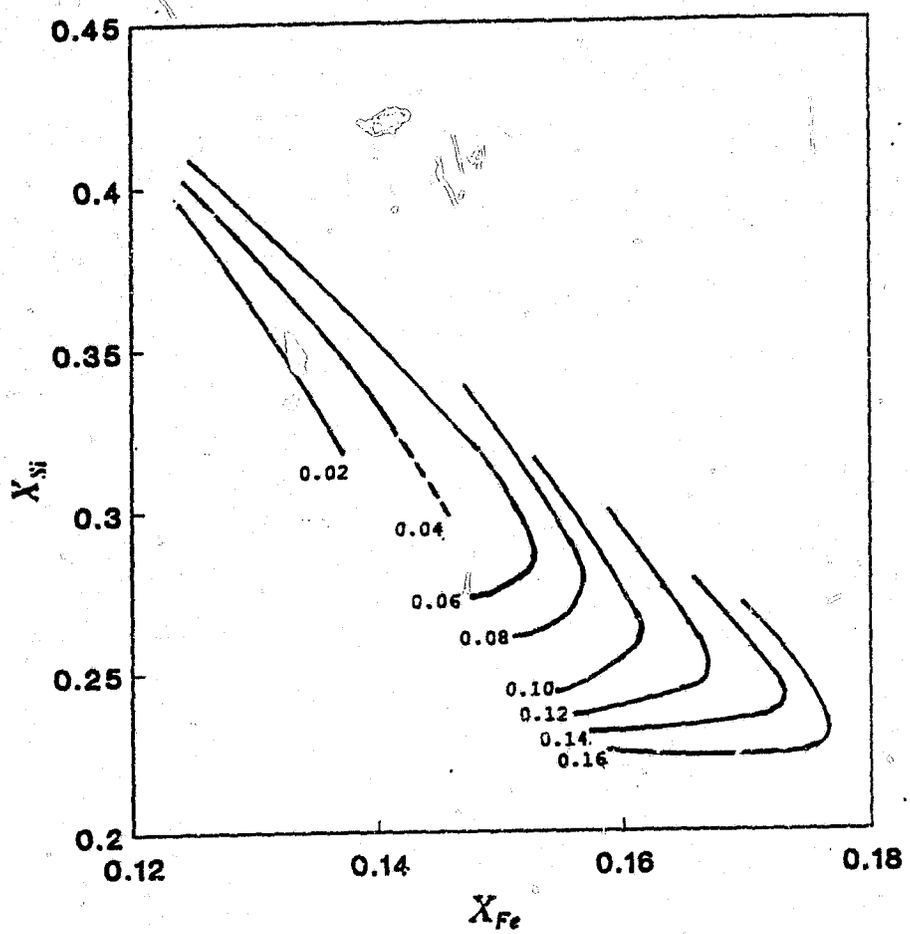

Figure 84. Iso-activity lines of Mn in silicomanganese melts saturated with C at 1500°C.

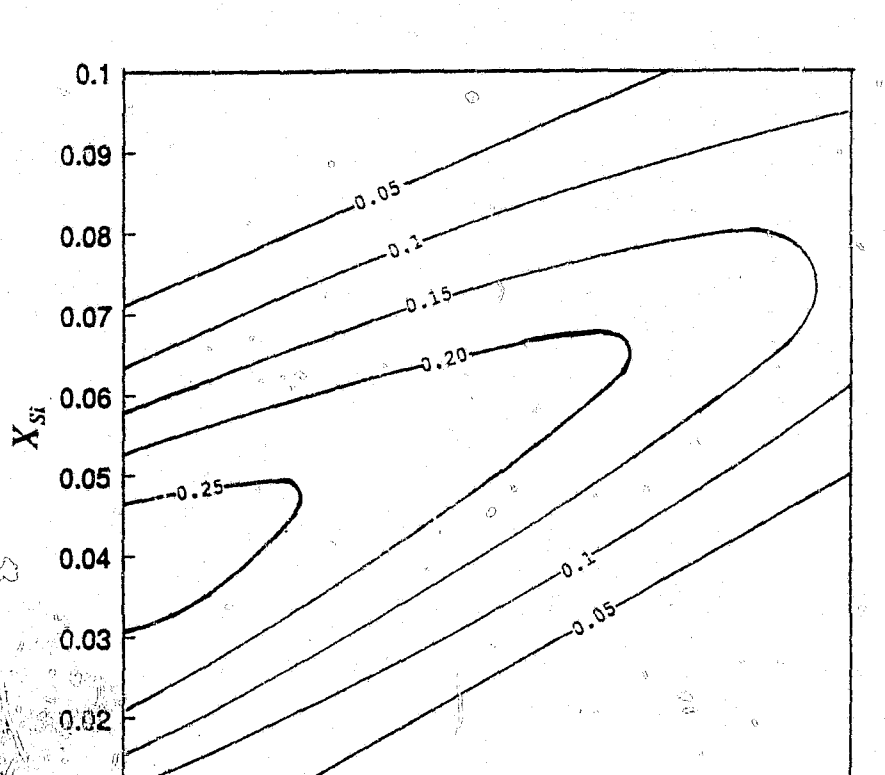

Figure 85. Iso-activity lines of Mn in ferromanganese melts saturated with C at 1500°C.

conducted at 1400°C. The 100°C temperature difference between two studies might result in different a_{Mn} values. On the other hand, Tanaka[117] determined the manganese activities in carbon-saturated Mn-Si-Fe-C melts by the measurement of vapour pressures by the transportation method. However, in the present study, a_{Mn} values in Mn-Si-Fe-C melts were calculated through equation (91) by making use of the MnO activities in ferromanganese slags which were measured by gas equilibration technique. Another difference between the present and Tanaka's study is that the equilibration time is significantly different in two studies. Tanaka concluded that 120 minutes was sufficient to attain the equilibrium. However, in the present study, the slag-metal samples were kept for 24 hours in the even temperature zone of the reaction furnace. As far as the high viscosity of ferromanganese slags are concerned, the equilibrium time established by Tanaka might be insufficient in order to allow the components in the slag to overcome diffusional barriers. Another important difference between two studies is the method of cooling the samples. In Tanaka's work, after 120 minutes, the power supply was cut off, the flow rates of circulation water and CO gas inside the coil and at the surface of the furnace cover were increased, the sample was rapidly cooled in the original state of crucible. It was considered that after a few seconds, the slag phase was solidified and after about 2 minutes the alloy of low melting point composition was solidified and during this period of time, any shift of manganese and silicon between the two phases was ignored. However, in the present study, after 24 hours, the samples were rapidly drawn to the bottom end of the furnace and immediately quenched in water. Therefore, the cooling time was much

shorter and it is believed that, in Tanaka's work, there might be some deviation from equilibrium. Furthermore, in Tanaka's study, the analysis of alloys were done for iron, silicon and carbon and the residual was given to manganese. Occasionally, manganese was also analyzed to confirm the results. In the present work, all metallic elements in alloy phase were analyzed. This might cause some errors in analytical results.

Briefly, during the course of calculation of Tanaka's study, due to lack of known data, it was necessary to use activities of temperature significantly different from his experiments or to use extrapolated values of known data. Therefore, if there is any change in the thermodynamic data which was used in his study such as those seen in Rankin's example[59], the values of activities which were obtained by his study will vary significantly. Tanaka[117] himself considered his experimental values as approximate and differences exist between the calculations and experiments in his work. These differences between the two studies can lead to differences in a_{Mn} and a_{Si} values.

5 SUMMARY AND CONCLUSIONS

This research work was carried out to determine the activity of manganese oxide in synthetic $MnO-CaO-MgO-SiO_2-Al_2O_3$ slags that are typical of the production of ferromanganese in submerged arc electric furnaces in South Africa. The procedure followed in this study consists of:

-The redetermination of the activity composition relationship in the Pt-Mn binary alloys at 1300°, 1400° and 1500°C and at p_{O_2} values between about 10^{-6} and 10^{-11} atm. The results of these experiments were utilized in MnO activity measurements.

-The determination of MnO activities in $MnO-CaO-MgO-SiO_2-Al_2O_3$ slags at 1500°C and at two different p_{O_2} values: 4.76×10^{-7} and 5.80×10^{-8} atm.

-The investigation of manganese and silicon distribution between carbon-saturated Mn-Si-Fe-C alloys and $MnO-CaO-MgO-SiO_2-Al_2O_3$ slags under 1 atmosphere of CO gas at 1500°C.

The project was initiated in an attempt to help to reduce MnO losses from the slag and to find an optimum slag composition for practical implication during the production of ferromanganese alloy. The main objectives of this study were:

-To investigate the effect of concentration, basicity ratio and CaO-to-MgO ratio on MnO activities in above mentioned slags,

-To develop a statistical model equation which represents the activity data successfully and which can be used to predict the MnO activities in the composition range of this work,

-To fit the activity data to a slag model which will

describe the thermodynamic properties of the slag successfully.
-To study Mn and Si equilibrium distributions between the slag and the metal,
-To develop statistical model equations which represent $\ln\gamma_{Mn}$ and $\ln\gamma_{Si}$ data successfully and which can be used to predict the activity coefficients of Mn and Si in the compositional range of this work,
-To derive the iso-activity contours of Si and Mn in silicomanganese and ferromanganese compositions

In the light of the experimental procedure explained above, the conclusions are outlined as follows:
-Activity of MnO in the slag increases with increasing concentration of MnO in the slag,
-Activity of MnO in the slag tends to increase with an increasing CaO-to-MgO ratio of the slag,
-Activity of MnO in the slag increases with an increasing basicity ratio of the slag,
-An increase in basicity ratio of the slag decreases the Mn distribution ratio,
-An increase in silica concentration of the slag increases the Mn distribution ratio,
-An increase in CaO-to-Al_2O_3 ratio of the slag decreases the Mn distribution ratio,
-An increase in MgO-to-CaO ratio of the slag increases the Mn distribution ratio,
-The carbon and manganese contents of the metal phase are directly proportional,
-The carbon and silicon concentrations in the metal phase are inversely related and, as the Mn-to-Fe or Mn-to-Si ratio increases, the carbon solubility in the metal phase decreases,
-An increase in the silica content of the slag phase

increases the silicon content of the metal phase and this effect is more pronounced at the higher Mn-to-Fe or Mn-to-Si ratios,

-An increase in the basicity of the slag decreases the silicon content of the metal phase.

The practical value of the investigations performed on slags will depend how far the results could be translated into usable form for industrial furnace operation. A quadratic multi-variable regression model was derived by using the SAS system for predicting the MnO activities in $MnO-CaO-MgO-SiO_2-Al_2O_3$ slags at 1500°C. The empirical model represents the MnO activity data successfully. The activity data have been interpreted in terms of the statistical slag model developed by Gaye[124] and there is an excellent agreement between the measured activities and the derived values through the slag model.

The composition of a slag determines its general physico-chemical properties and offers an important tool in order to control the smelting process due to its influence on furnace operation. The slag properties which are the most influential on a metallurgical operation are the activity of the slag components, the viscosity, electrical conductivity (for an electric furnace) and the liquidus temperature of a slag. On the other hand, the nature of the formation and subsequent behaviour of the slag phase as the charge descends in the furnace as well as the kinetics of reaction are also very important. Other slag properties like density, surface tension and heat conductivity are somewhat less important in their influence on the process and the influence of the slag composition on these properties is still not well known.

As far as the behaviour of slag in the ferromanganese operations is concerned, the most important factors are the MnO content and the basicity ratio, as has been clearly demonstrated in this work. It was shown in a recent work[50] that an increase in MnO concentration decreases the viscosity and increases the electrical conductivity.

In ferromanganese production, the activity of MnO should be as high as possible in order to obtain better recoveries of manganese. On the other hand the viscosity of the liquid slag should be low and the diffusivity of the slag components high. The electrical conductivity of the slag should be reasonably high in order to maintain the cost-effectiveness. It must be pointed out that the liquidus temperature of the slag should be low in order to minimise manganese losses by vaporisation but should be high so as to improve the conditions for the kinetics of MnO reduction.

From the results of the present study it can be seen that high MnO activity values are achieved with more basic slags for a given MnO concentration. However, basic slags often have high liquidus temperatures, thus, the smelting temperature must be high in order to obtain a fluid slag. The slag must be fluid enough so that the sub-liquidus operation which will result in the presence of crystalline material which could lead to high viscosities and sticky furnace operation must be avoided.

On the other hand, high temperatures also increase the rate of reduction of MnO from the slag and also the degree of reduction. The high temperature also increases

the MnO activities[9]. High MnO activities lead to improved kinetics. For example, if the liquid slag composition is monitored to obtain higher MnO activity values, the viscosity is decreased[43]. However, high basicities may lead to manganese metal losses due to quite considerable volatilization of that component as temperature increases. The manganese metal which volitilizes is of extremely small particle size, practically in fume form and it is carried over with the gas and lost before it is condensed in the cooler regions higher up in the furnace[133]. High temperature also lead to an increased silica reduction[52] and the MnO reduction is directly related to silica reduction[57]. But several studies have shown that manganese was close to equilibrium in ferromanganese practice and silicon was further removed from equilibrium[55,56]. Nevertheless, for better recoveries of manganese, the activity of MnO should be high and the silica activity should be low. This can only be achieved with higher basicities.

The viscosity of the slag is an important property in order to have a smooth operation of a ferromanganese furnace. The viscosities of the final slags in ferromanganese production are generally low, and in most cases, the flow difficulties are not encountered. However, the mobility of alloy droplets through the slag and the mobility of constituents in the slag can be improved by decreasing or minimising the viscosity of the final slag. A fluid slag results in better flow and smoother heating in the furnace and an alloy with more even composition and higher quality can be produced. The viscosity of a slag is affected by two major factors which are the composition of the slag and the superheat in the slag above its liquidus temperature. As mentioned

before, the anions are the flow units of a molten slag and the silicate network is further broken down with the addition of basic oxides like CaO, MgO and MnO. Therefore the viscosity of the molten slag decreases. However, MnO can not be considered as an agent to decrease the viscosity.

Another important factor in the ferromanganese production is the rate of reduction of metal from slag. A higher rate will result in a faster production and a closer approach to equilibrium. The kinetics of the reduction of MnO could involve a number of rate limiting steps that include transport of the reactants or products from the bulk phase to the slag-metal interface, the phase boundary reaction itself, which may involve several steps, and finally the nucleation of the gas bubbles. Also a role being played by electrochemical exchanges is possible. The rate of reduction is temperature dependant and an increase in temperature increases the rate of reduction. Several authors[134,135] showed that the rate of reduction of MnO in slags by graphite, at below 10 per cent MnO, is very slow compared to carbon dissolved in liquid iron. This can be explained by a decrease in the activity of MnO in the slag. On the other hand, a diffusion controlled mechanism limited by manganese transport in the slag was proposed by Tarby and Philbrook[135] and Yagi and Ono[136]. In another work[137] it was shown that the rate of reduction from basic slags with 45 per cent CaO, 10 per cent MgO, 10 per cent Al_2O_3 and 35 per cent SiO_2 is controlled by chemical reaction. The elimination of diffusion as the rate limiting step was also supported by other experimental runs, including the geometry and concentration of the melt and it was found that the rate

of reduction of MnO in ferromanganese furnaces is also controlled by interfacial chemical reaction rather than diffusion. Thus, one can easily say that the nucleation of CO bubbles in the molten slag is not the rate limiting step. When conclusions of Daines and Pelke[137] and the approach above are considered, the rate of reduction of MnO in the furnace will depend on the surface area of the reducing media in contact with the slag and the activity of the oxygen ions in the slag. Toop and Samis[79] suggested that the activity of oxygen ions increase with increasing MnO activity. Therefore it can be concluded that the rate of reduction increases in proportion to the MnO activity. This is borne out by the fact that the rate of reduction of MnO increases with increasing basicity of the slag[135,136] and concluded from the theory of absolute reaction rates that the difference in reaction rates for different compositions may be attributed to the difference in the activity of MnO in the different slags.

The electrical conductivity of slags in ferromanganese production is affected mainly by the MnO content and the basicity ratio similar to activity of MnO. As MnO content increases the electrical conductivity decreases and an increase in basicity decreases the viscosity and increases the electrical conductivity. In fact, viscosity and electrical conductivity are inversely related.

The slag-to-metal ratio is an important aspect that the ratio should be kept as low as possible. The smaller the ratio, the less power will be required to melt the burden and the larger ratio does not decrease the lost MnO in the slag. The final slag composition, therefore, is dependent on the quality of the manganese ore used and

the type and quantity of gangue minerals present. On the other hand the price of the raw materials required to obtain the more suitable slag compositions may inhibit their use[9].

The high basicity is desirable to achieve high MnO activities, but it increases the power input due to the high liquidus temperature in order to obtain a fluid slag. An investigation[138] about the effect of MgO on the slag basicity and the liquidus temperature showed that when MgO replaces CaO (3-13 per cent MgO), the basicity can be increased from 1.4-1.6 to between 1.7 and 2.8 without a substantial increase in the liquidus temperature, resulting in an increased recovery of manganese.

In summary, the desirable features of slag composition can be stated in broad overall context. The slags with high basicity is an important choice which will result in improved kinetic conditions, higher MnO activities, low slag viscosity and increased rate of reduction. The extent to which the basicity can be increased depends on the liquidus temperature of the slag and can be obtained roughly from the phase diagrams determined by Osborn et al.[74] and more precisely from the liquidus temperature determinations of Eric, Hejja and Stange[50].

In order to improve the recovery of manganese, its activity in the slag should be maximized without increasing its concentration. The activity of MnO can be increased by employing slags of higher basicities as mentioned above. However, this also results in higher liquidus temperatures of slag[50], requiring higher power input in the furnace. Therefore, an optimum must be

reached. Both the manganese content of the slag and the silicon content of the metal phase decrease rapidly as the basicity of the slag increases. It appears that a basicity ratio of around 1.0 to 1.2 results in reasonably optimum conditions where the silicon content of the metal is low and the manganese content of the slag is around 9 per cent (about 12 per cent MnO). In the previous work[50], it was suggested that a slag composition having an optimum around 15 per cent would be the range for the furnace operation. In terms of optimum electrical conductivities, viscosities and liquidus temperatures, this is in excellent agreement with the findings of the present work, where activity of MnO can be maximized without an increase in its concentration in the slag by operating the slags at a basicity ratio of about 1.0 to 1.2 and MnO content of approximately 12 per cent. When this is done, better recoveries of manganese will be achieved with reasonably high MnO activities in the slag, with low viscosity, low liquidus temperature, and reasonable slag resistivity.

In the present study, the activities of MnO were measured in synthetic $MnO-CaO-MgO-SiO_2-Al_2O_3$ slags that are typical of the production of high-carbon ferromanganese in submerged arc electric furnaces in South Africa. The future work may include the MnO activity measurements in medium-carbon and low-carbon ferromanganese slag compositions in order to gather further data to improve manganese recovery from the slag in these operations. The liquidus temperatures and the electrical conductivities of synthetic $MnO-CaO-MgO-SiO_2-Al_2O_3$ slags were measured in the same composition range in a previous study[50], therefore, their viscosities should also be

measured in order to have an useful tool, in combination with the activity data of the present work, to maximize the efficiency of the process.

6 APPENDICES

APPENDIX A

APPENDIX A.1 Calibration of flowrates of CO and CO_2

The calibration involves the timing of the rate of progress of a soap bubble up an inverted burette. In other words, the calibration technique involved adjustment of Δh value which is the difference between liquid levels in the u-tubes at evenly graduated values ranging from low to high. Thus, the velocity of the air bubbles were measured in cm^3/sec. These measurements were repeated for at least six times, so that the mean value of gas flowrate was calculated with error analysis. The values of velocities were plotted against Δh values as it is seen in Figures A.1 and A.2 for CO and CO_2 respectively.

Thus, the desired flowrate of CO and CO_2 through capillary tubes could be obtained by making use of these curves. Linear regression analysis were performed on the data generated to obtain two regression in Figures A.1 and A.2 for establishing gas flowrates :

$$f(CO) = 0.41(\Delta h) + 2.39 \quad \text{.....(A.1)}$$

$$f(CO_2) = 0.28(\Delta h) + 3.60 \quad \text{.....(A.2)}$$

The correlation coefficients were found to be equal to 0.9985 and 0.9987 for CO and CO_2 respectively. As it is seen from Figures A.1 and A.2 and the equations (A.1) and (A.2), the relation between flowrates and Δh values is linear to a certain point. The Δh values were calculated

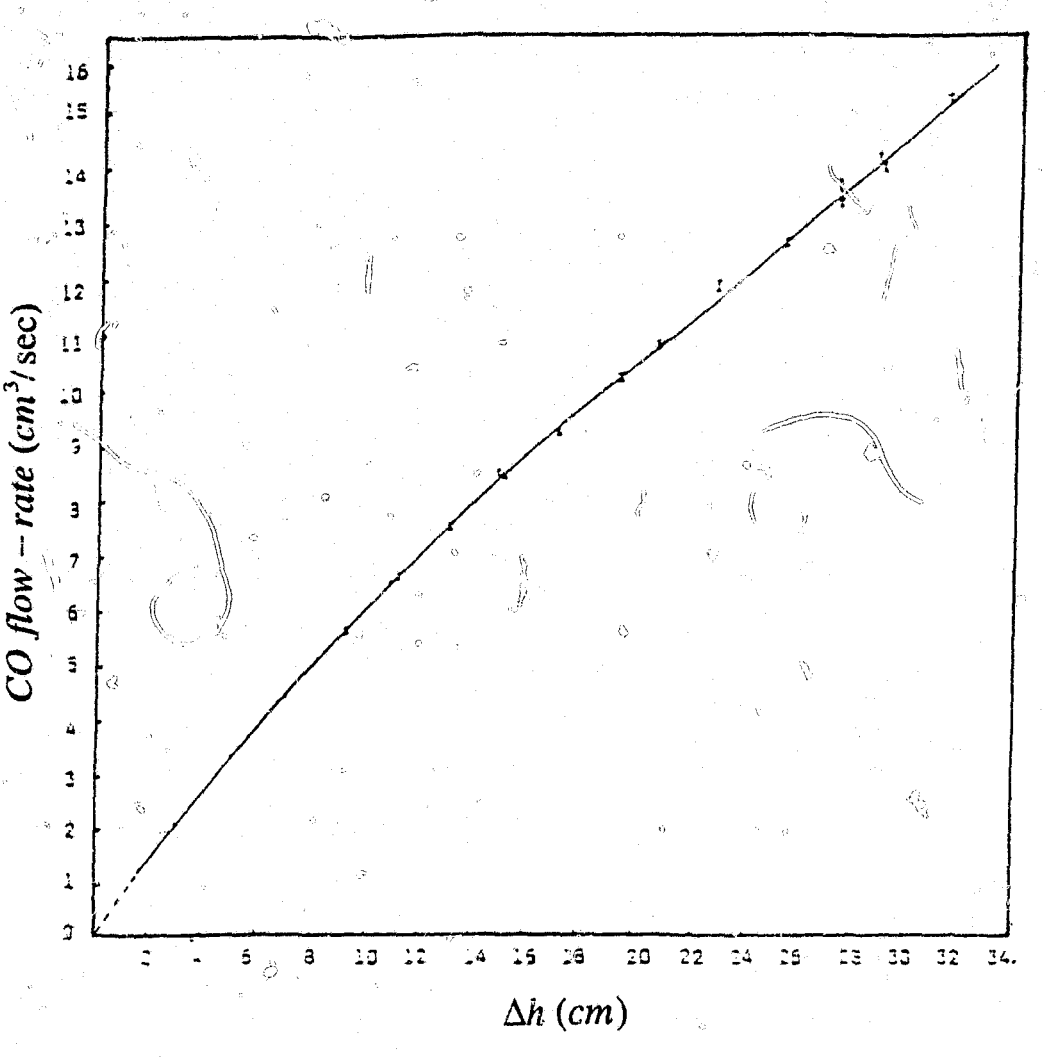

Figure A.1. Flowrate of CO through capillary tube.

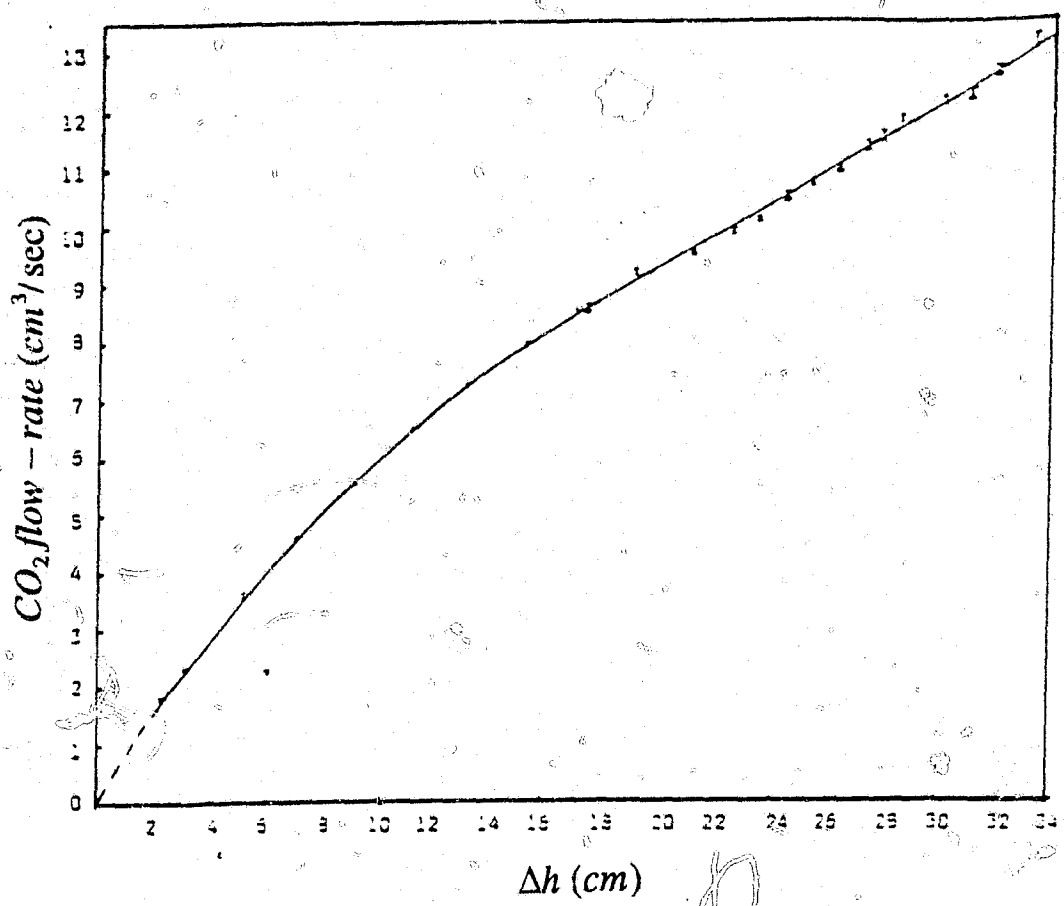

Figure A.2. Flowrate of CO_2 through capillary tube.

by making use of the equations (A.1) and (A.2) when the desired flowrates of CO and CO_2 fell into the linear portion of the curves. The non-linear portion of the curves were used to read the Δh values corresponding to desired values of CO and CO_2 flowrates when the flowrates were not in the linear portion of the curves.

When CO_2-CO mixtures are used, the following equilibrium can be written at 1500°C,

$$CO(g) + \frac{1}{2}O_2(g) = CO_2(g) \quad \text{.....(A.3)}$$

and from literature[123],

$$\Delta G^0 = -279175.97 + 84.60T \ J/mole \quad \text{.....(A.4)}$$

and the K value for this reaction can be written through:

$$r = K \cdot (p_{O_2})^{\frac{1}{2}} = p_{CO_2} / p_{CO} \quad \text{.....(A.5)}$$

and:

$$lnK = \frac{33577.81}{T} - 10.18 \ J/mole \quad \text{.....(A.6)}$$

At total pressure of 1 atm, the partial pressures of CO and CO_2 can be replaced by their flowrates, and r is simply the ratio of the flowrate of the gases through the capillary tubes determined by calibration previously. In this regard, K values of this reaction at different temperatures can be calculated by equation (A.6) and if

the K value obtained and known p_{O_2} value is substituted in equation (A.5), r can be calculated. The Δhvalues which are related to this ratio can also be obtained from the curves in figure A.1 and A.2. Consequently, the desired CO_2/CO values can be obtained through capillary tubes by establishing known Δh values in gas mixing system. The Figure A.3 shows[122] the p_{O_2} values that can be obtained by various r ratios as a function of temperature. The region below the hatched line can not be used due to the precipitation of carbon.

APPENDIX A.2 Oxygen partial pressure-a_{MnO} relationship for solid non-stoichiometric MnO

In the study carried out by Richardson and Davies[15], measurements were made of the extent to which manganous oxide departs from the stoichiometric composition as the partial pressure of oxygen is raised at temperatures between 1500° and 1650°C. The ratio N(O):N(Mn) which is the ratio of number of atoms of oxygen to manganese in the non-stoichiometric oxide was found to increase from 1.0 to 1.045 as the oxygen partial pressure was raised from 10^{-10} or 10^{-11} atm to 10^{-2} atm. The compositions at fixed oxygen partial pressures were found to be independent of temperature. The departures from stoichiometry were smaller than for ferrous oxide, but the form of the relationship between composition and oxygen pressure was similar and the results could have been interpreted reasonably in terms of cation vacancies in a manner suggested by Wagner[15]. In Figure A.4, non-stoichiometry of MnO as a function of oxygen pressure is shown. Broken line is theoretical curve and N_O/N_{Mn} values were obtained at 1500°-1600°C. As it is seen from

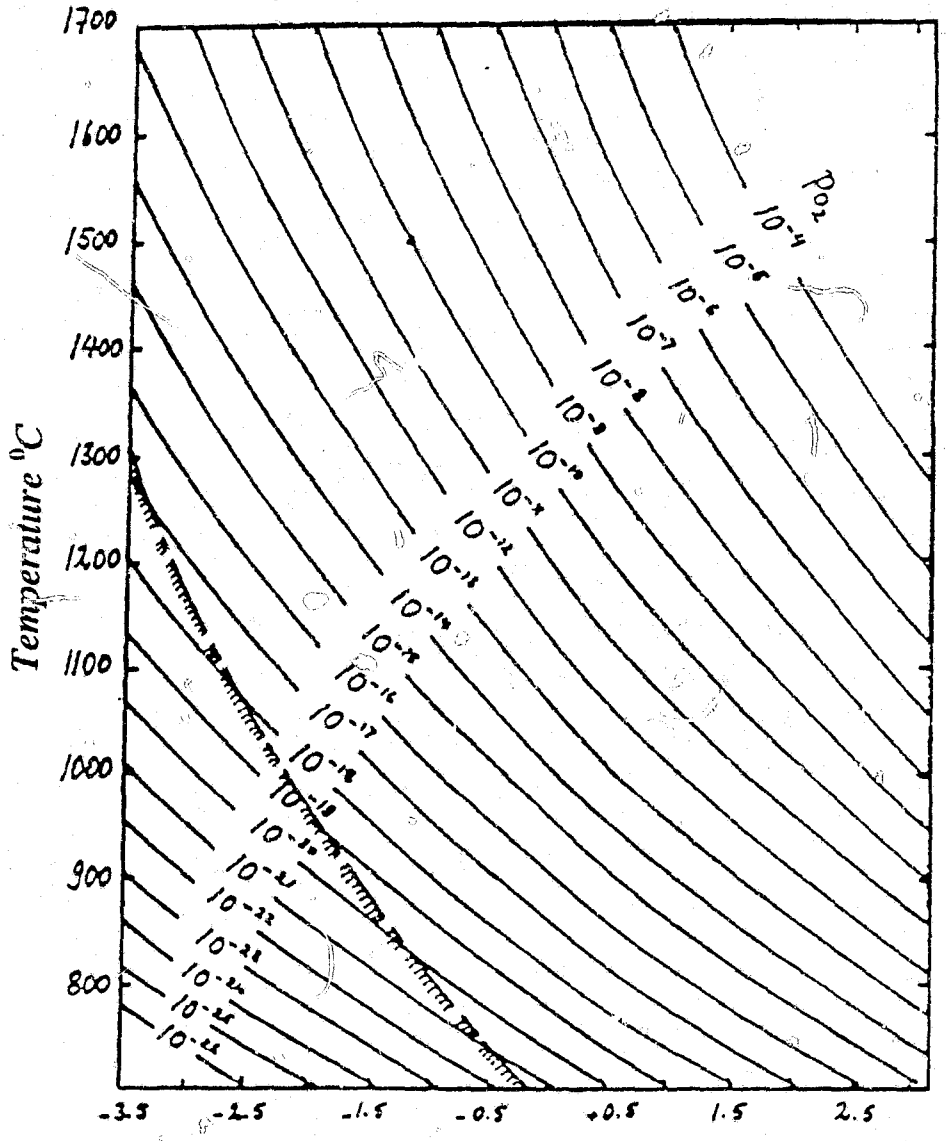

Figure A.3. p_{O_2} **values that can be obtained by various CO_2-to-CO ratios at different temperatures**[122].

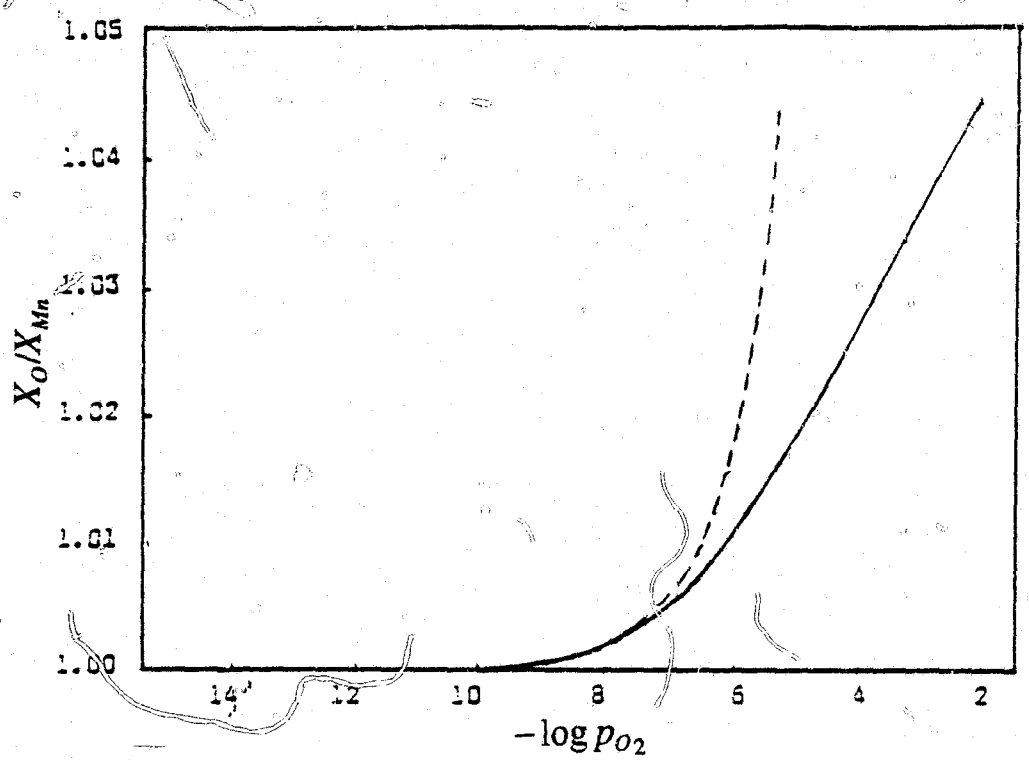

Figure A.4. Non-stoichiometry of MnO[15] as a function of oxygen pressure (between 1500°-1650°C). Broken line is theoretical curve.

Figure A.4, non-stoichiometry of MnO increases as p_{O_2} increases. In figure A.5, activities of stoichiometric MnO in non-stoichiometric oxide as a function of oxygen pressure ar shown. During this study, a_{MnO}' values were read from Figure A.5 for experimentally known p_{O_2}' values corresponding to Pt-Mn system for calculating the activity of MnO in ferromanganese slags through the equation below, where p_{O_2} was fixe y the $CO-CO_2$ gas mixture during a run:

$$a_{MnO} = \sqrt{(p_{O_2} \ / \ p'_{O_2})} \cdot a'_{MnO} \qquad \text{.....(A.6)}$$

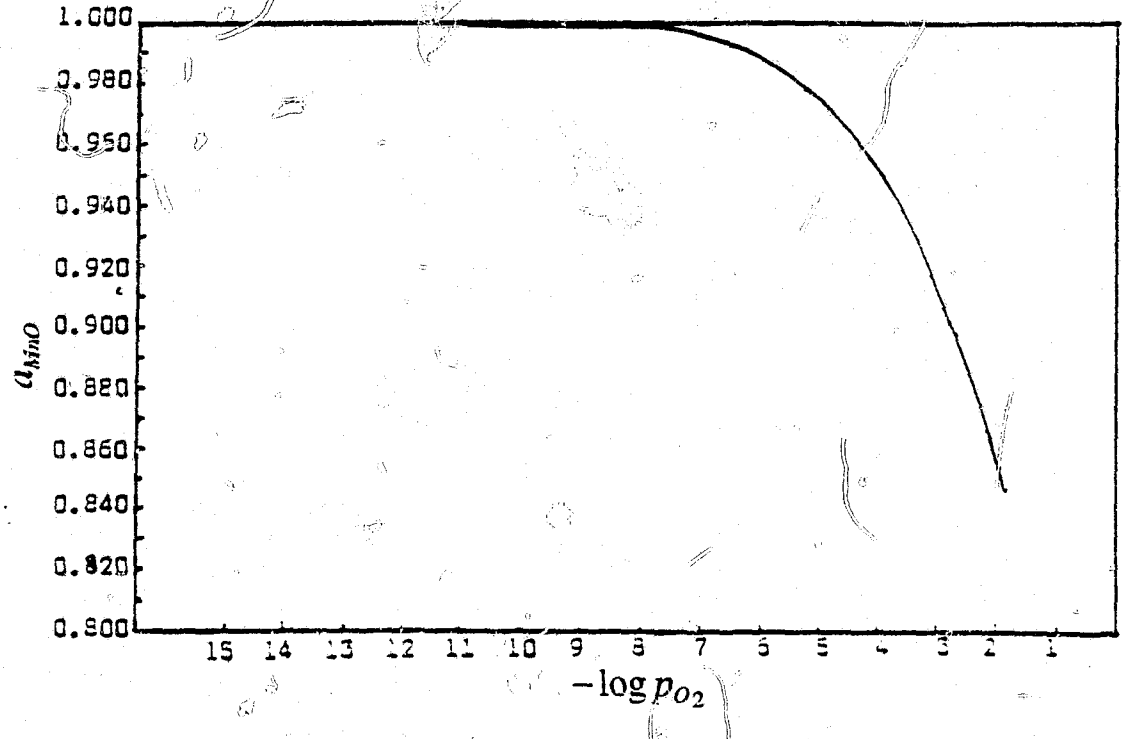

Figure A.5. Activity of stoichiometric MnO[15] in the non-stoichiometric oxide as a function of oxygen pressure.

APPENDIX B

APPENDIX B.1 The determination of equilibration time

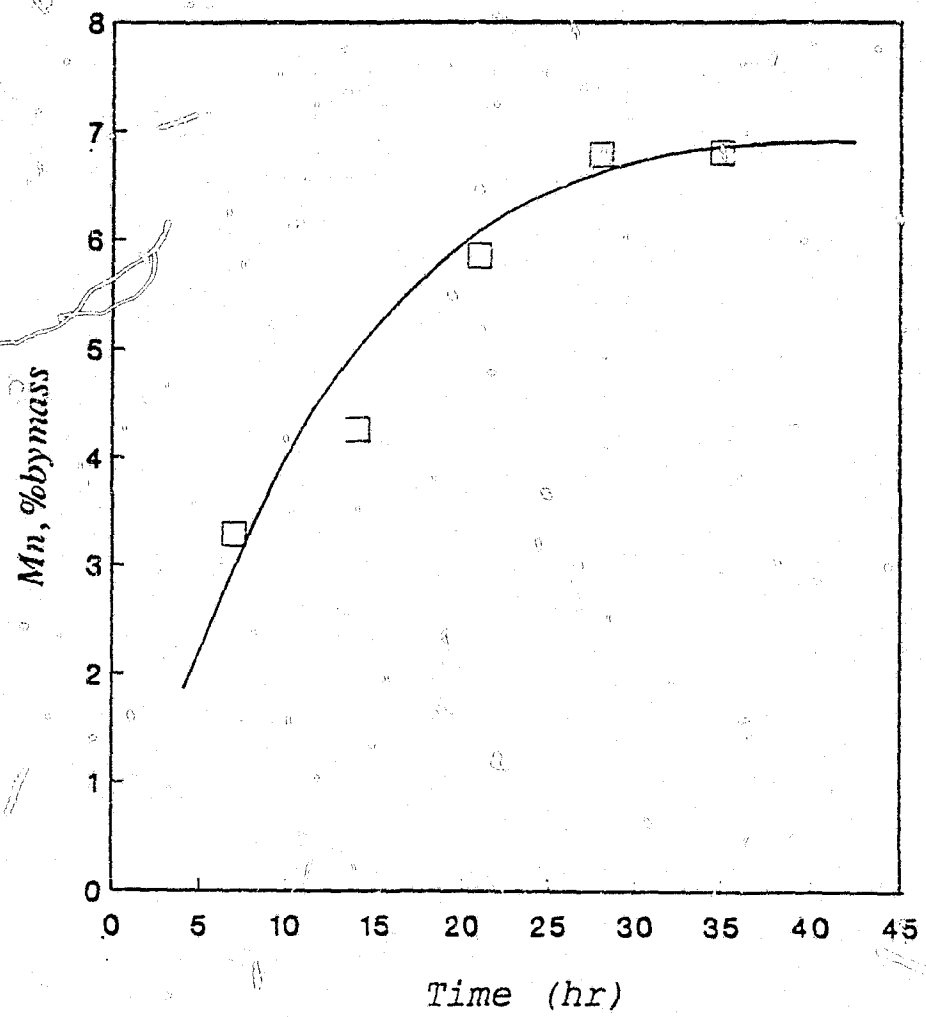

Figure B.1.1. Manganese picked up by platinum from pure MnO as a function of time at 1300°C.

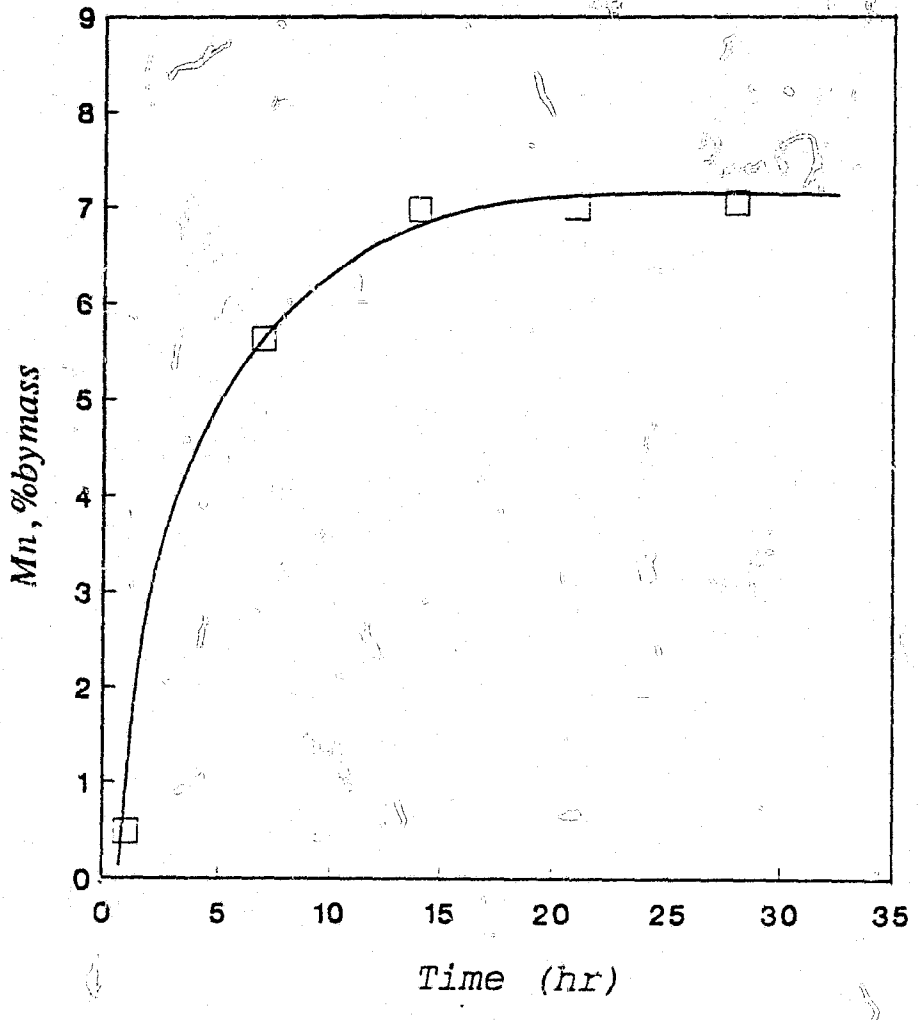

Figure B.1.2. Manganese picked up by platinum from pure MnO as a functicn of time at 1400°C.

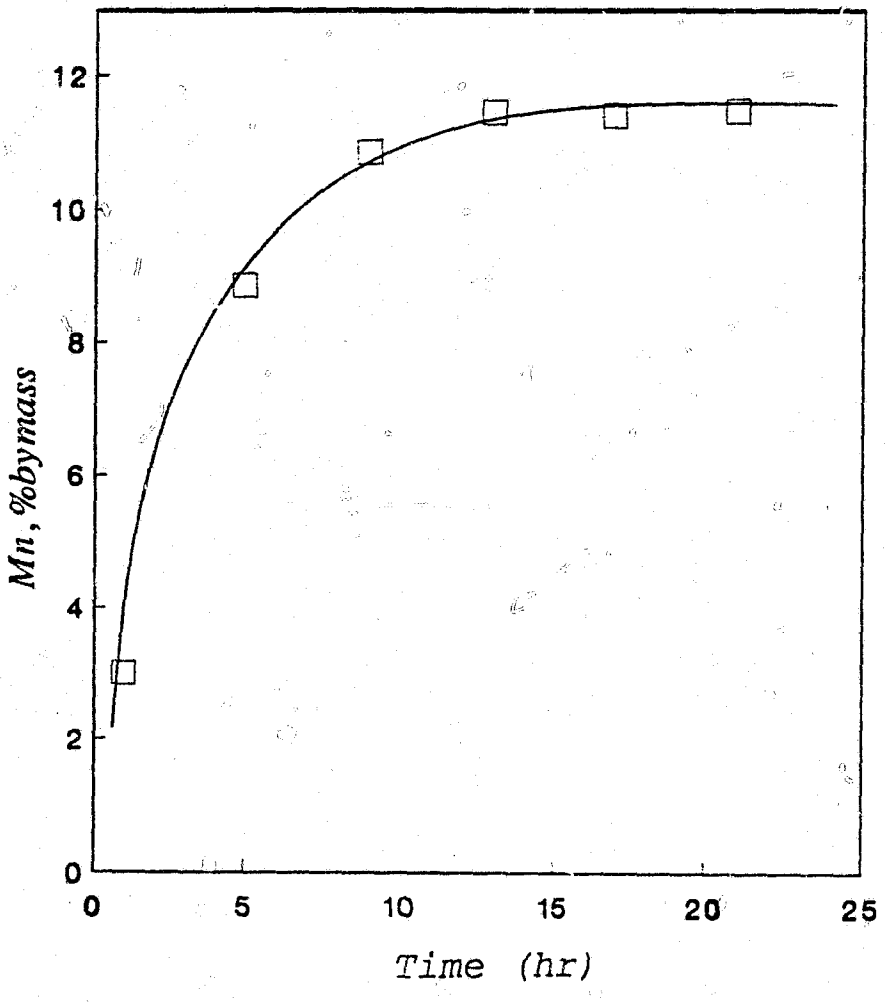

Figure B.1.3. Manganese picked up by platinum from pure MnO as a function of time at 1500°C.

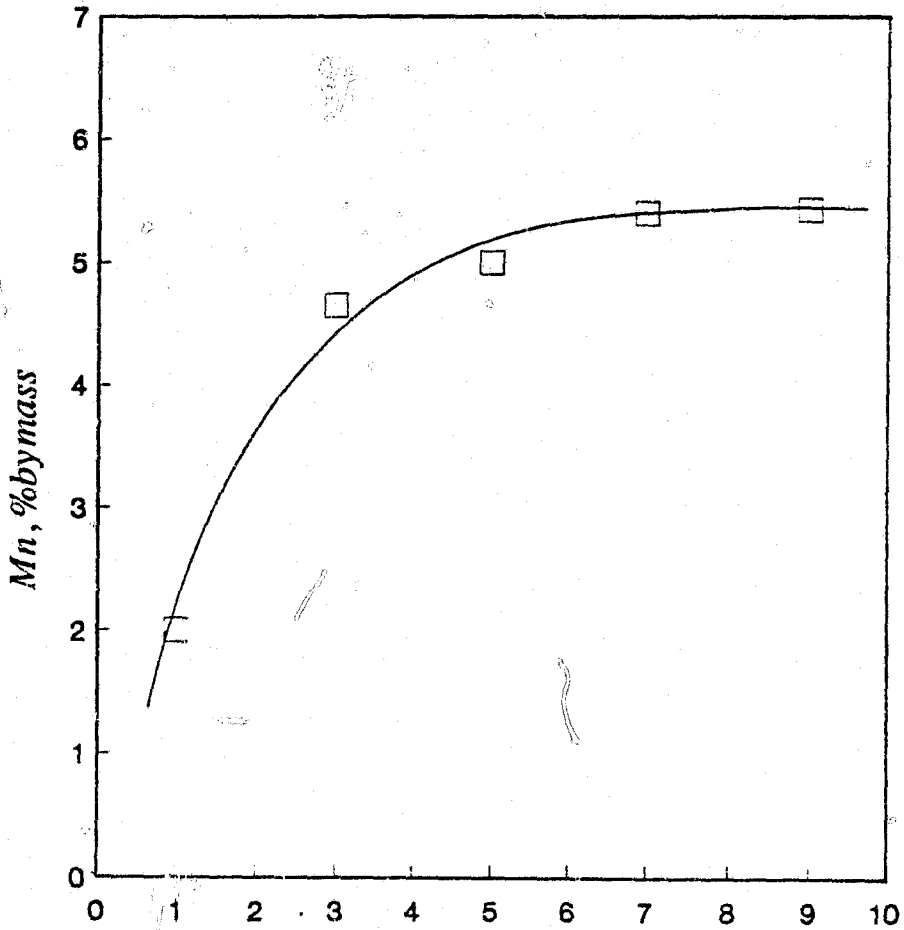

Figure B.1.4. Manganese picked up by platinum from $MnO-CaO-MgO-SiO_2-Al_2O_3$ slag as a function of time at 1500°C.

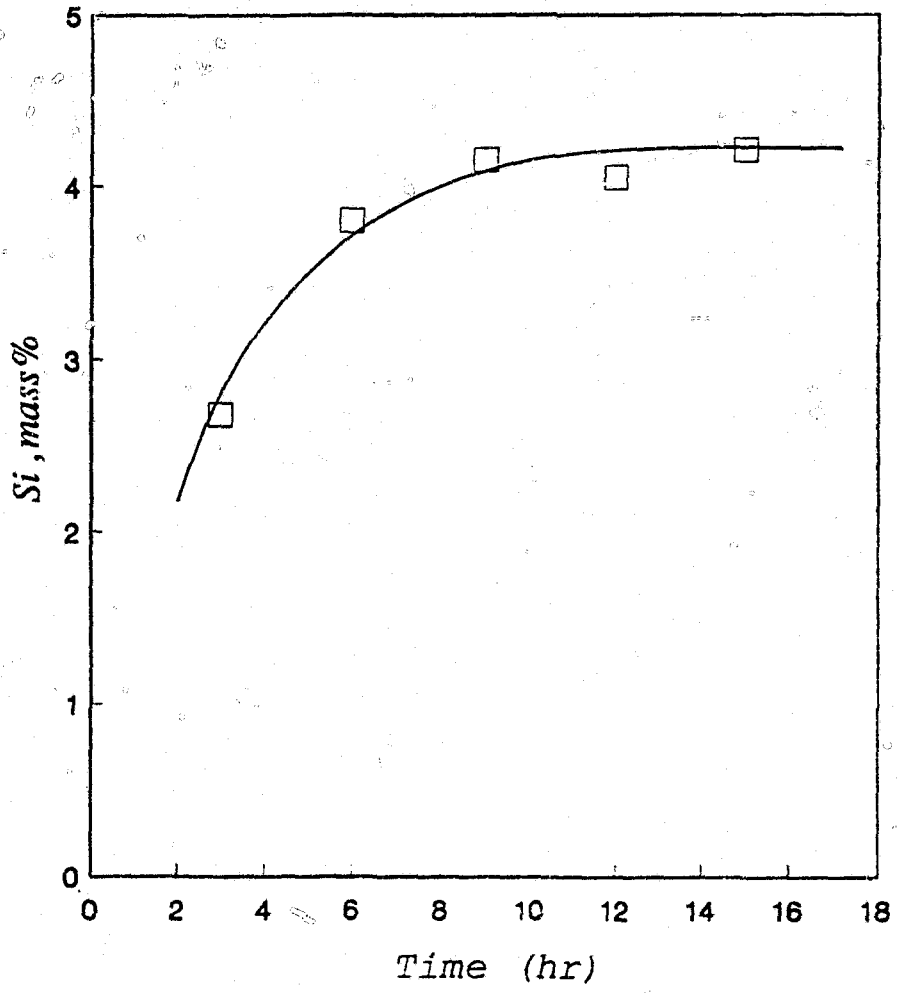

Figure B.1.5. Equilibration time determination experiments for slag-metal equilibria between MnO-CaO-MgO-SiO_2-Al_2O_3 slags and Mn-Si-Fe-C metal phase at 1500°C.

APPENDIX B.2 General

CO gas : Chemically pure grade.

O_2<10 ppm, H_2O<5 ppm, N_2<70 ppm, CO_2<20 ppm, CH_4<100 ppm, H_2<300 ppm, Ar<3 ppm.

CO_2 gas : Chemically pure grade.

99.995% CO_2, O_2<2 ppm, H_2O<4 ppm, N_2<10 ppm, CO<1 ppm, H_2<1 ppm, total hydrocarbons<1 ppm.

Platinum crucibles : 99.98% pure platinum, 7 mm in diameter, 25 mm in dept, 0.125 mm wall thickness.

Platinum specimens : 99,98% pure platinum, 4 mm x 4 mm x 0.025 mm.

Graphite crucibles : High purity graphite electrodes.

Particle size	: 0.074 mm
Density	: 1.7 gr/cm$_3$
Specific resistance	: 0.0010 ohms^{-CM}
Fractional strength	: 2500 N/cm^2
Ash content	: 0.05-0.1%
Porosity	: 27%
Dimensions	: h=44 mm, o.d.=20 mm, i.d.=14 mm

Synthetic MnO-CaO-MgO-SiO_2-Al_2O_3 slags :

Prepared from analytical-reagent grade MnO, CaO, MgO, SiO_2 and Al_2O_3 oxide powders.

Mn-Si-Fe-C alloys :

Prepared from electrolytic manganese, electrolytic iron, high-purity silicon and spectrographic-grade graphite powders.

Chemical analysis :

Atomic absorption method, precision : 2-3% (rel.).

X-ray fusion method; precision : 1.5% (rel.).

Inductively coupled plasma (ICP) method; accuracy for Mn : 0.8%, accuracy for Si : 2.5%, accuracy for Fe : 0.8%.

O-pheantroline colorimetric method; accuracy : 0.01% absolute over range 0.03 to 0.2%, precision : 0.055%.

LECO analyser; accuracy : 0.02-1%, precision : 0.1 ppm.

APPENDIX B.3 Quantitative energy dispersive analysis of X-rays (EDAX) of some Pt-Mn binary alloy samples.

Quantitative energy dispersive analysis of X-rays (EDAX) of some Pt-Mn binary alloy samples are given in this Appendix. The analysis of Pt-Mn strips were determined at ten different points by line scanning accross the Pt-Mn binary alloys.

Table B.3.1 The SEM-EDAX analysis of Pt-Mn alloy sample by line scanning (Pt-Mn system, equilibration time is 48 hours at 1300°C and p_{O_2}=4.17x10^{-9} atm, Mn content determined by chemical analysis is 6.59 mass per cent).

Point	Mn, %	Pt, %
1	6.57	93.43
2	6.61	93.39
3	6.54	93.46
4	6.49	93.51
5	6.52	93.48
6	6.58	93.42
7	6.56	93.44
8	6.56	93.44
9	6.57	93.43
10	6.58	93.42

Table B.3.2. The SEM-EDAX anelysis of Pt-Mn alloy sample by line scanning (Pt-Mn system, equilibration time is 48 hours at 1300°C and p_{O_2}=5.54x10^{-11} atm, Mn content determined by chemical analysis is 10.7 mass per cent).

Point	Mn, %	Pt, %
1	10.71	89.29
2	10.70	89.30
3	10.69	89.31
4	10.67	89.33
5	10.71	89.29
6	10.69	89.31
7	10.70	89.30
8	10.72	89.28
9	10.71	89.29
10	10.71	89.29

Table B.3.3 **The SEM-EDAX analysis of Pt-Mn alloy sample by line scanning (Pt-$MnM_{n5}C_2$ system, equilibration time is 24 hours at 1400°C and p_{O_2}=6.78x10^{-4} atm, Mn content determined by chemical analysis is 6.05 mass per cent).**

Point	Mn, %	Pt, %
1	6.09	93.91
2	6.11	93.89
3	6.07	93.93
4	6.05	93.95
5	6.06	93.94
6	5.89	94.11
7	6.08	93.92
8	6.01	93.99
9	6.06	93.94
10	6.06	93.94

Table B.3.4 **Tha SEM-EDAX analysis of Pt-Mn alloy sample by line scanning (Pt-Mn system, equilibration time is 24 hours at 14[illegible]°C and p_{O_2}=2.35x10^{-10} atm, Mn content determined by chemical analysis is 12.2 mass per cent).**

Point	Mn, %	Pt, %
1	12.25	87.75
2	12.27	87.73
3	12.24	87.76
4	12.23	87.77
5	12.68	87.32
6	13.05	86.95
7	12.70	87.30
8	12.39	87.61
9	12.26	87.74
10	12.23	87.77

Table B.3.5 The SEM-EDAX analysis of Pt-Mn alloy sample by line scanning (Pt-Mn system, equilibration time is 24 hours at 1500°C and p_{O_2}=9.30x10^{-8} atm, Mn content determined by chemical analysis is 10.5 mass per cent).

Point	Mn, %	Pt, %
1	10.49	89.51
2	10.37	89.63
3	10.29	89.71
4	10.45	89.55
5	10.51	89.49
6	10.53	89.47
7	10.59	89.41
8	10.52	89.48
9	10.46	89.54
10	10.51	89.49

Table B.3.6 **The SEM-EDAX analysis of Pt-Mn alloy sample by line scanning (Pt-Mn system, equilibration time $M_{n_3}C_2$ is 24 hours at 1500°C and p_{O_2}=4.76x10^{-7} atm, Mn content determined by chemical analysis is 6.25 mass per cent).**

Point	Mn, %	Pt, %
1	6.37	93.63
2	6.40	93.60
3	6.31	93.69
4	6.34	93.66
5	6.25	93.75
6	6.27	93.73
7	6.26	93.74
8	6.21	93.79
9	6.24	93.76
10	6.28	93.72

Table B.3.7 **The SEM-EDAX analysis of Pt-Mn alloy sample by line scanning (Pt-Mn system, equilibration time is 24 hours at 1500°C and p_{O_2}=4.99x10^{-11} atm, Mn content determined by chemical analysis is 19.5 mass per cent).**

Point	Mn, %	Pt, %
1	19.59	80.41
2	19.47	80.53
3	19.49	80.51
4	19.57	80.43
5	19.59	80.41
6	19.53	80.47
7	19.56	80.44
8	19.52	80.48
9	19.58	80.42
10	19.57	80.43

Table B.3.8 **The SEM-EDAX analysis of Pt-Mn alloy sample by line scanning (Pt-Mn system, equilibration time is 24 hours at 1500°C and p_{O_2}=4.98x10^{-10} atm, Mn content determined by chemical analysis is 14.9 mass per cent).**

Point	Mn, %	Pt, %
1	14.58	85.42
2	14.65	85.35
3	14.86	85.14
4	14.70	85.30
5	14.96	85.04
6	14.80	85.12
7	14.85	85.15
8	14.78	85.22
9	14.81	85.19
10	14.85	85.15

Table B.3.9 **The SEM-EDAX analysis of Pt-Mn alloy sample by line scanning (Pt-Mn system, equilibration time is 24 hours at 1500°C and p_{O_2}=5.19x10^{-6} atm, Mn content determined by chemical analysis is 3.57 mass per cent).**

Point	Mn, %	Pt, %
1	3.56	96.44
2	3.59	96.41
3	3.60	96.40
4	3.54	96.46
5	3.58	96.42
6	3.53	96.47
7	3.49	96.51
8	3.51	96.49
9	3.47	96.53
10	3.57	96.43

Table B.3.10 **The SEM-EDAX analysis of Pt-Mn alloy sample by line scanning ($MnO-CeO-MgO-SiO_2-Al_2O_3$ system, equilibration time is 24 hours at 1500°C and p_{O_2}=5.80x10^{-8} atm, Mn content determined by chemical anelysis is 3.22 mass per cent).**

Point	Mn, %	Pt, %
1	3.23	96.77
2	3.24	96.76
3	3.27	96.73
4	3.20	96.80
5	3.29	96.71
6	3.30	96.70
7	3.32	96.68
8	3.22	96.78
9	3.24	96.76
10	3.25	96.75

Table B.3.11 **The SEM-EDAX analysis of Pt-Mn alloy sample by line scanning ($MnO-CaO-MgO-SiO_2-Al_2O_3$ system, equilibration time is 24 hours at 1500°C and p_{O_2}=4.76x10^{-7} atm, Mn content determined by chemical analysis is 3.20 mass per cent).**

Point	Mn, %	Pt, %
1	3.24	96.76
2	3.23	96.77
3	3.22	96.78
4	3.25	96.75
5	3.26	96.74
6	3.24	96.76
7	3.38	96.62
8	3.33	96.67
9	3.28	96.72
10	3.25	96.75

APPENDIX C Graphical representation of activity of MnO in slags

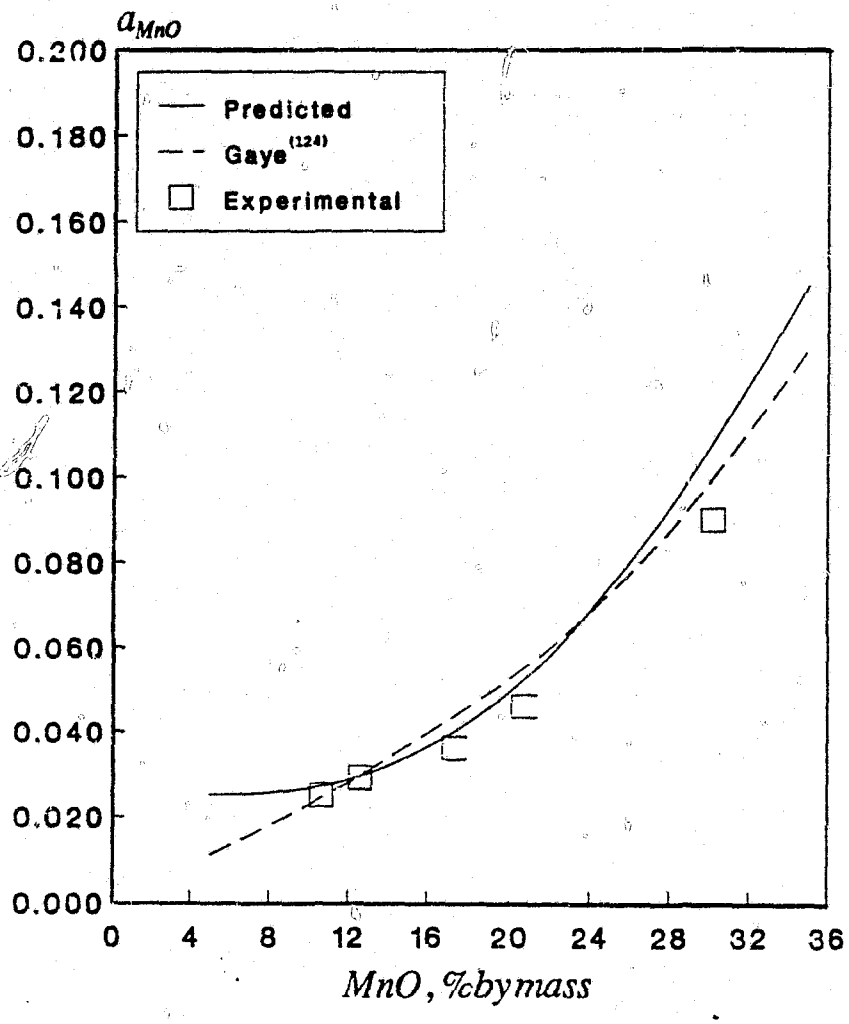

Figure C.1. Activities of MnO in $MnO-CaO-MgO-SiO_2-Al_2O_3$ slags at 1500°C, B=0.65±0.03, CaO:MgO=3.18±0.04, % Al_2O_3=5, optical basicity=0.67.

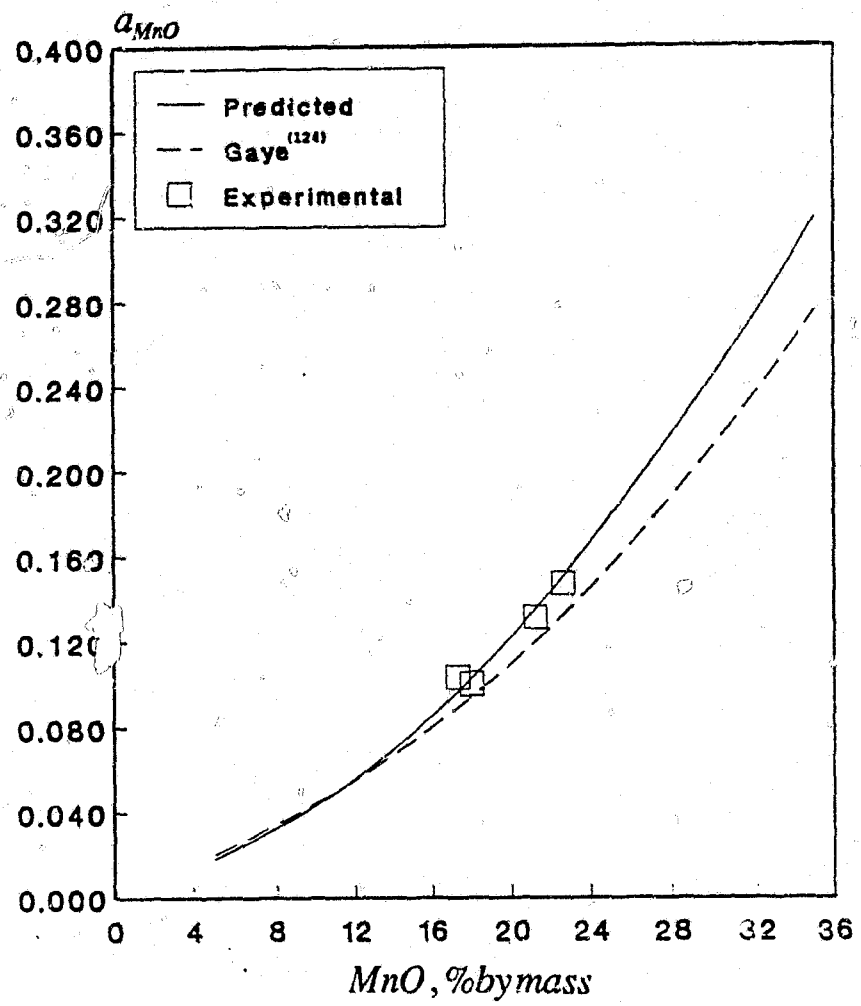

Figure C.2. Activities of MnO in MnO-CaO-MgO-SiO_2-Al_2O_3 slags at 1500°C, B=1.08±0.02, CaO:MgO=3.44±0.07, % Al_2O_3=5, optical basicity=0.72.

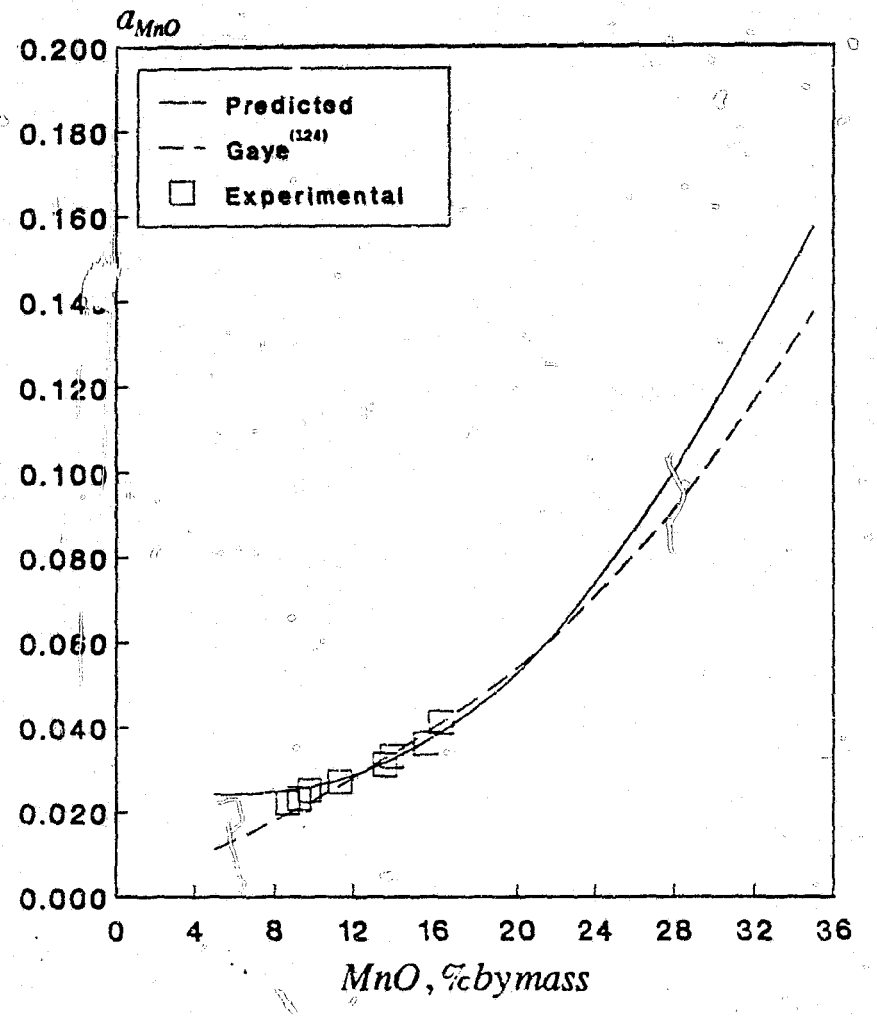

Figure C.3. Activities of MnO in MnO-CaO-MgO-SiO_2-Al_2O_3 slags at 1500°C, B=0.69±0.05, CaO:MgO=1.99±0.06, % Al_2O_3=5, optical basicity=0.65.

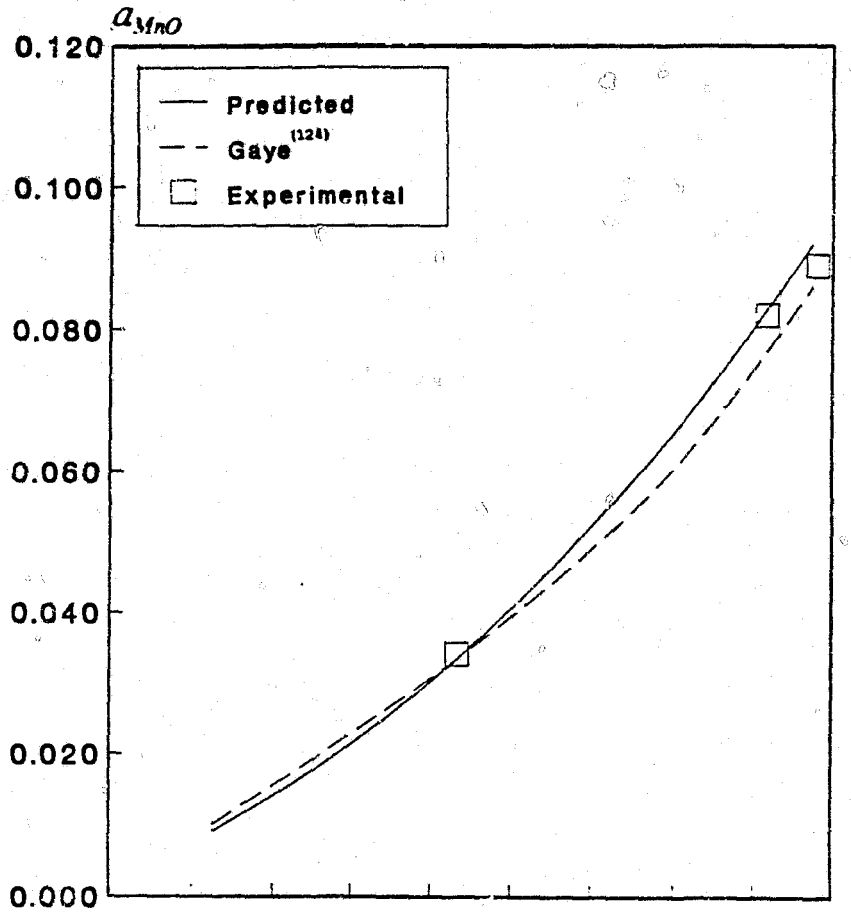

Figure C.4. Activities of MnO in MnO-CaO-MgO-SiO_2-Al_2O_3 slags at 1500°C, B=0.43±0.01, CaO:MgO=2.38±0.04, % Al_2O_3=5, optical basicity=0.67.

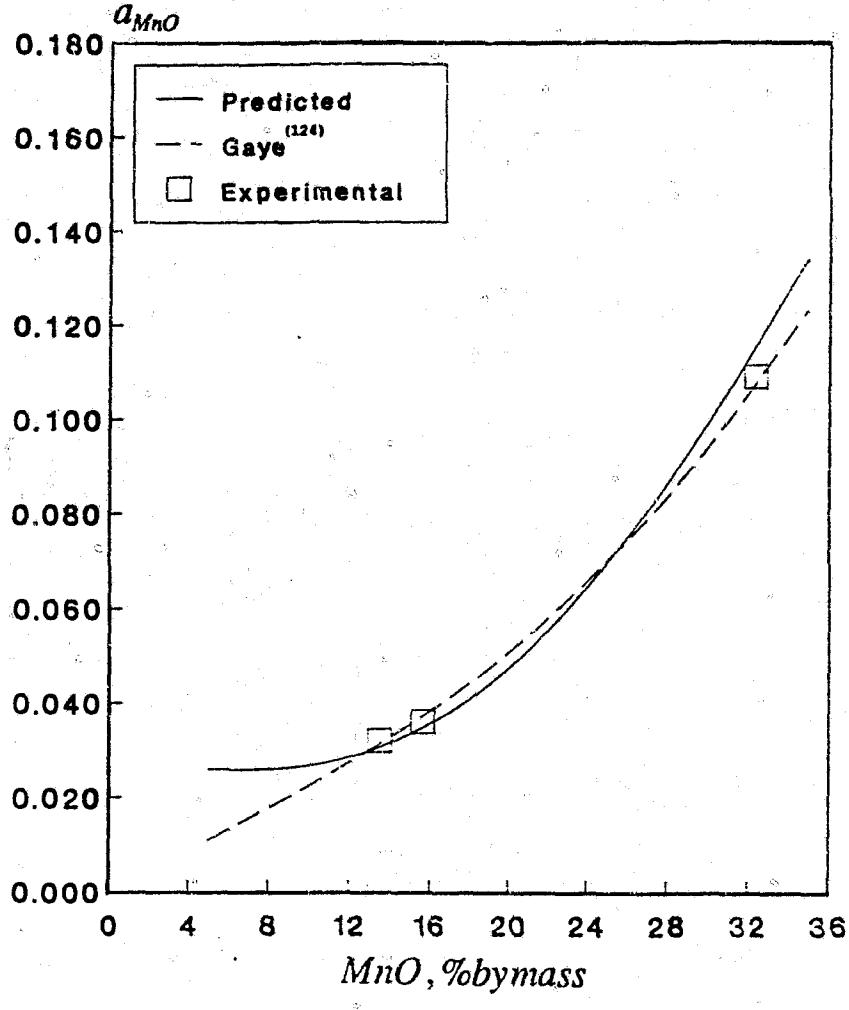

Figure C.5. Activities of MnO in MnO-CaO-MgO-SiO_2-Al_2O_3 slags at 1500°C, B=0.61±0.03, CaO:MgO=5.05±0.04, % Al_2O_3=5, optical basicity=0.67.

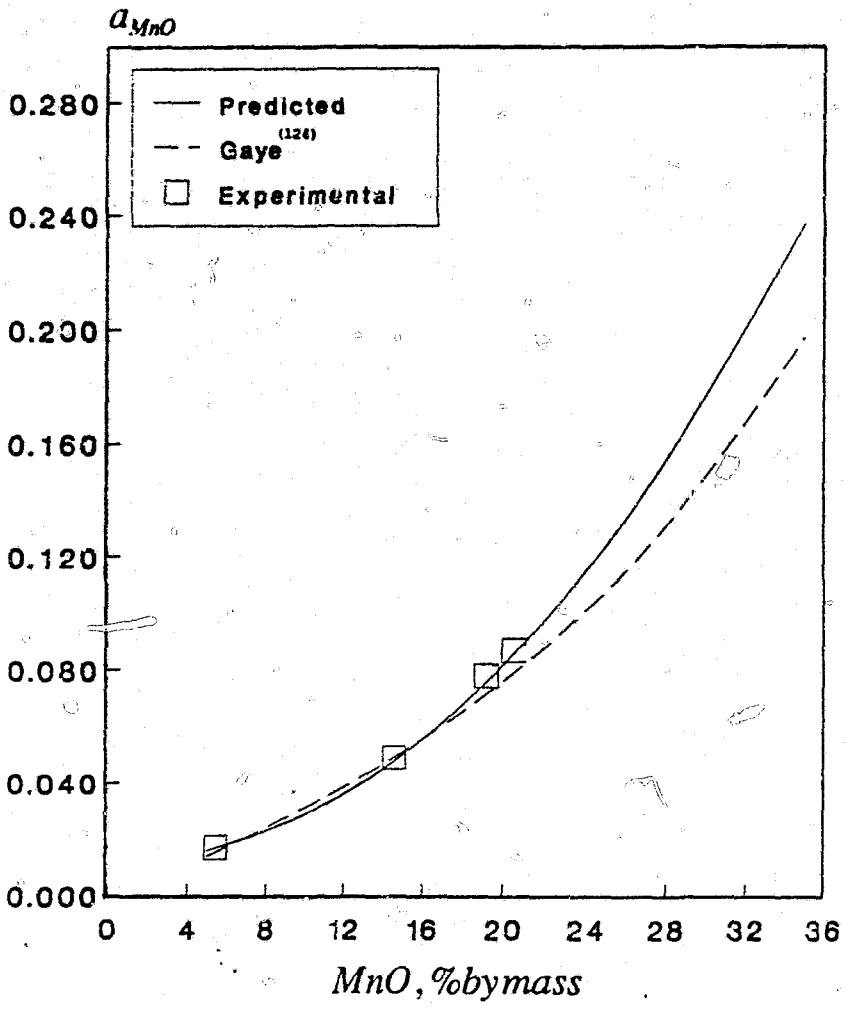

Figure C.6. Activities of MnO in MnO-CaO-MgO-SiO_2-Al_2O_3 slags at 1500°C, B=0.88±0.01, CaO:MgO=2.90±0.05, % Al_2O_3=5, optical basicity=0.68.

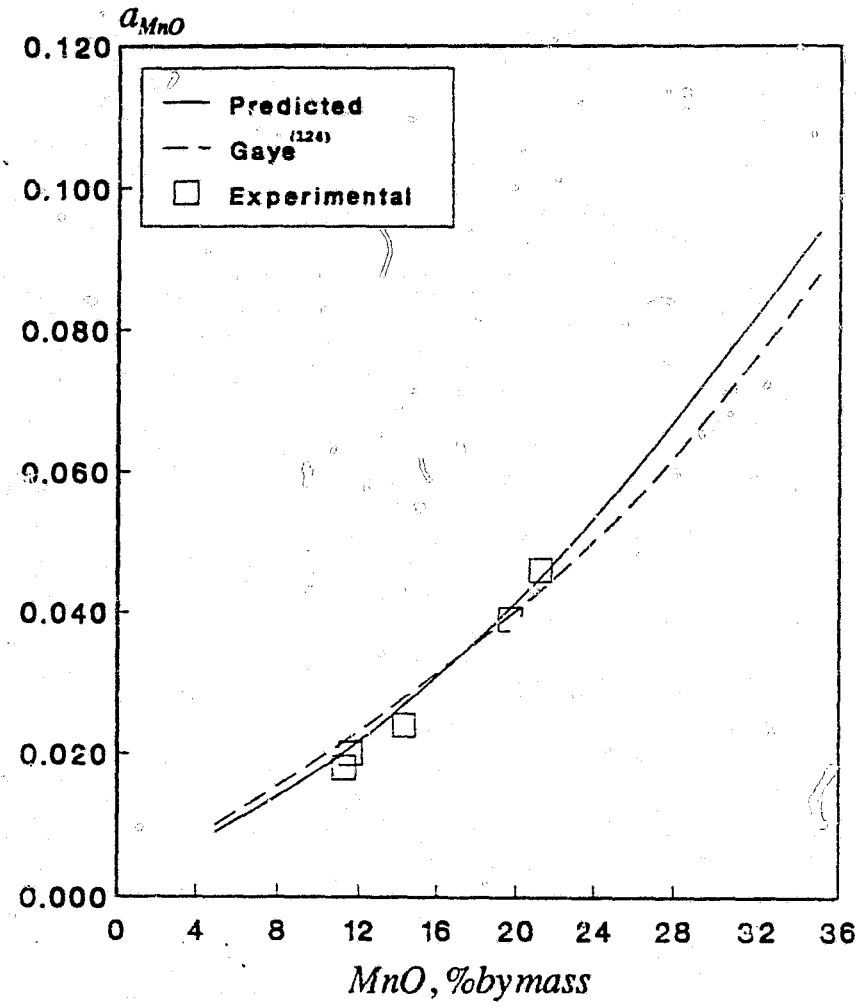

Figure C.7. Activities of MnO in $MnO-CaO-MgO-SiO_2-Al_2O_3$ slags at 1500°C, B=0.43±0.02, CaO:MgO=3.79±0.06, & Al_2O_3=5, optical basicity=0.63.

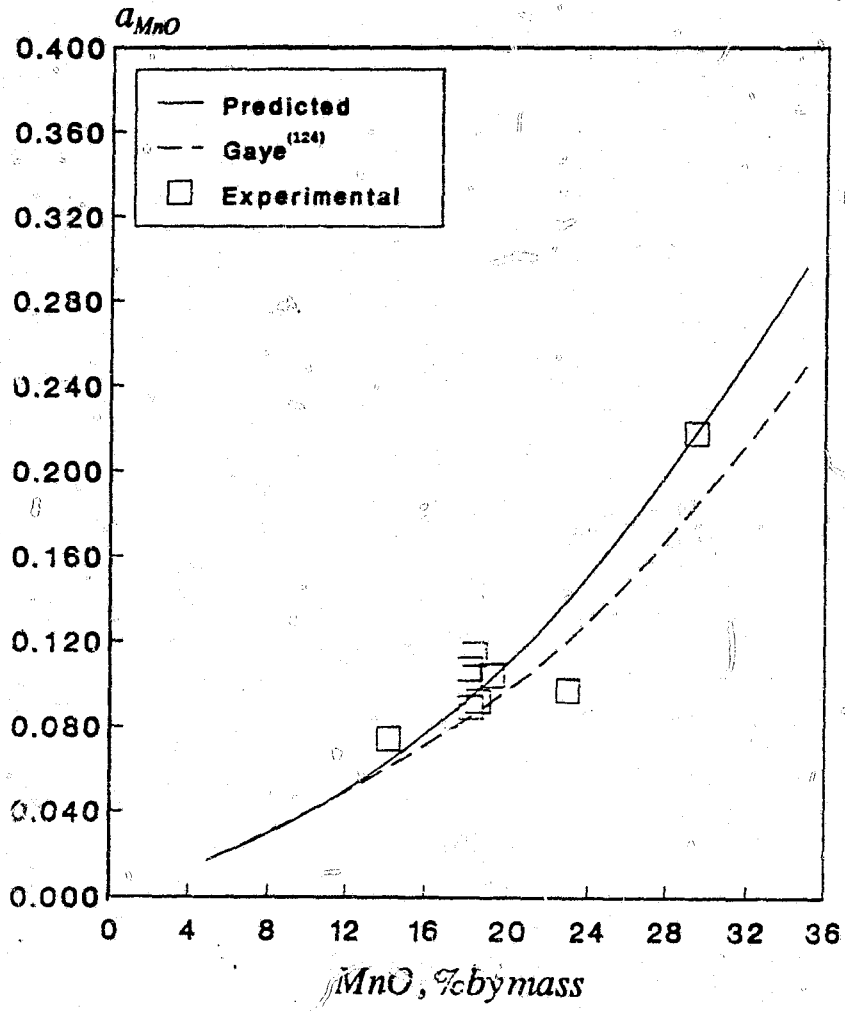

Figure C.8. Activities of MnO in MnO-CaO-MgO-SiO_2-Al_2O_3 slags at 1500°C, B=1.02±0.05, CaO:MgO=2.86±0.07, % Al_2O_3=5, optical basicity=0.71.

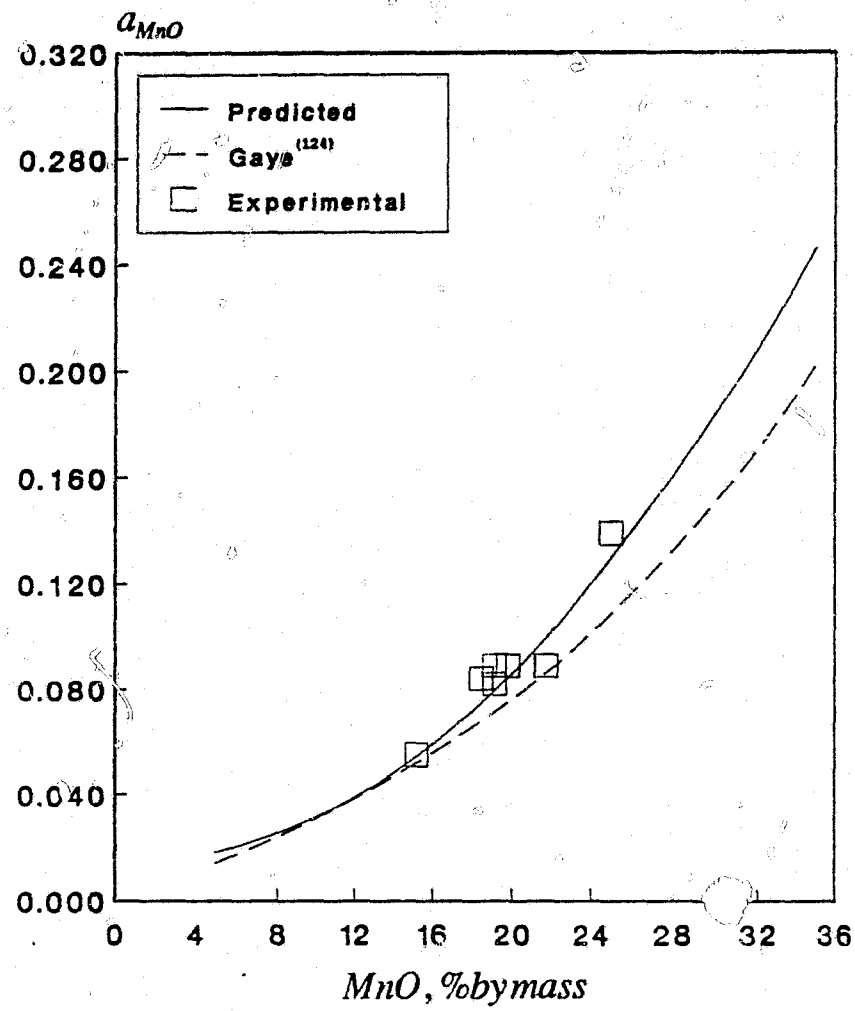

Figure C.9. Activities of MnO in $MnO-CaO-MgO-SiO_2-Al_2O_3$ slags at 1500°C, B=0.91±0.04, CaO:MgO=1.47±0.05, % Al_2O_3=5, optical basicity=0.69.

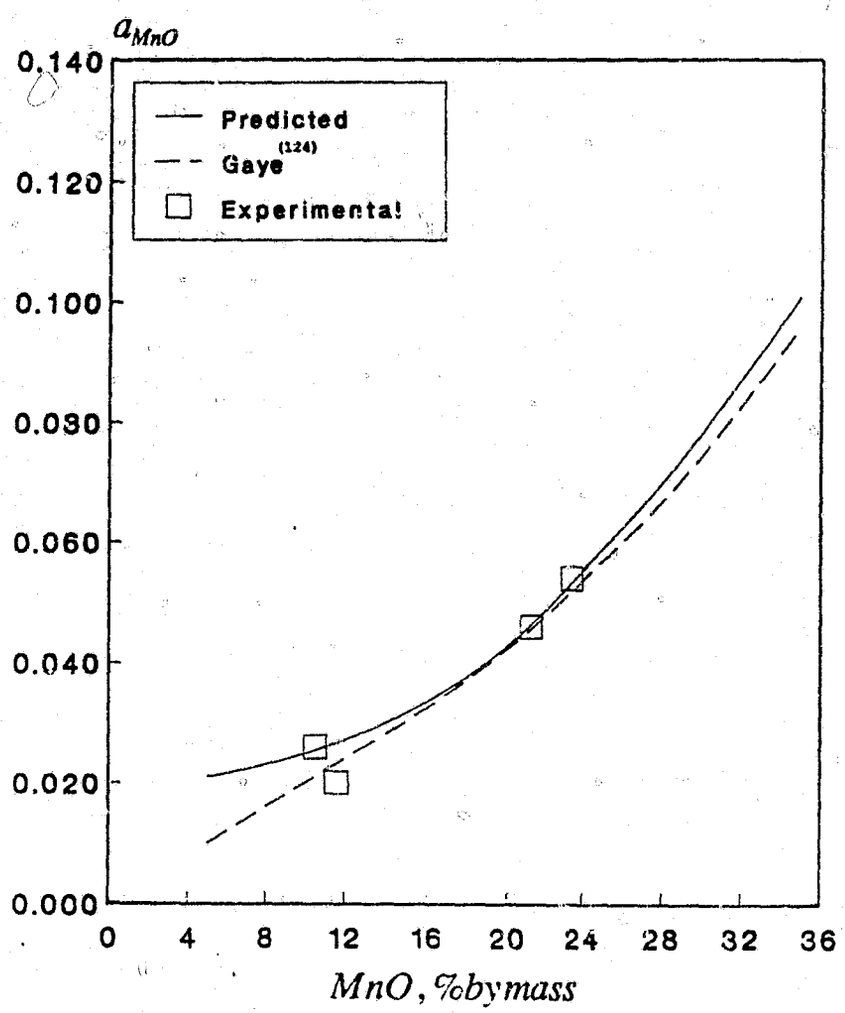

Figure C.10. Activities of MnO in MnO-CaO-MgO-SiO_2-Al_2O_3 slags at 1500°C, B=0.48±0.05, CaO:MgO=4.00±0.05, % Al_2O_3=5, optical basicity=0.64.

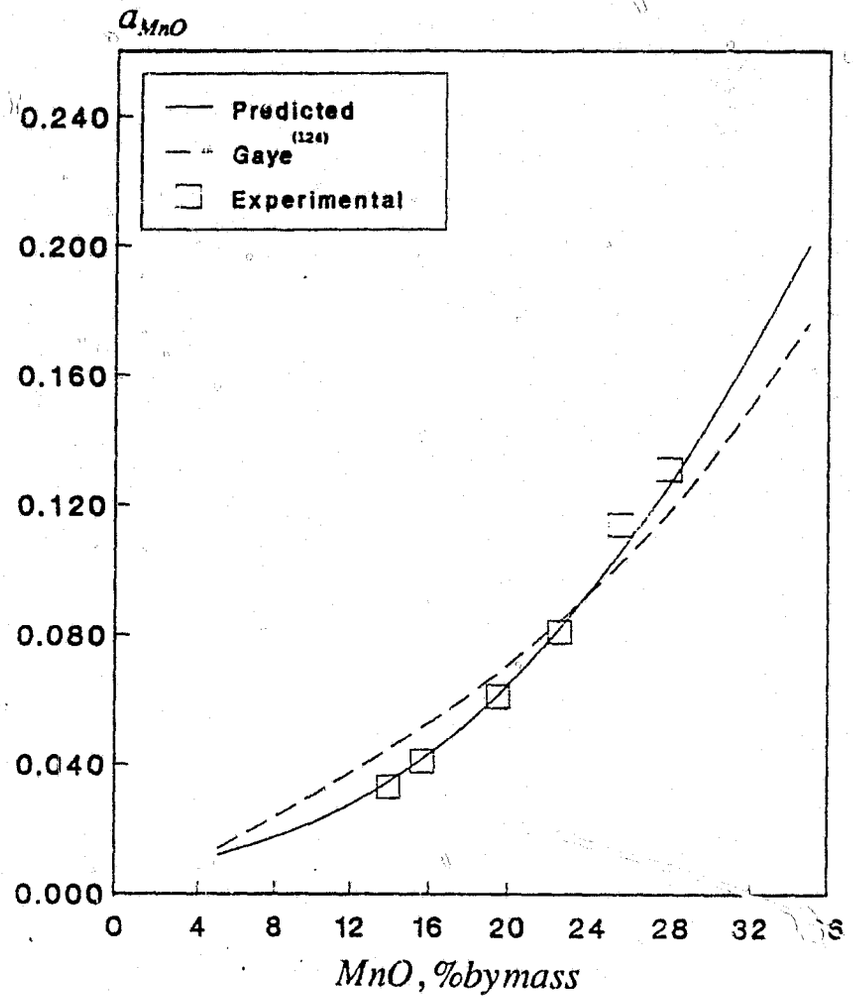

Figure C.11. Activities of MnO in $MnO-CaO-MgO-SiO_2-Al_2O_3$ slags at 1500°C, B=0.78±0.02, CaO:MgO=∞, % Al_2O_3=5, optical basicity=0.70.

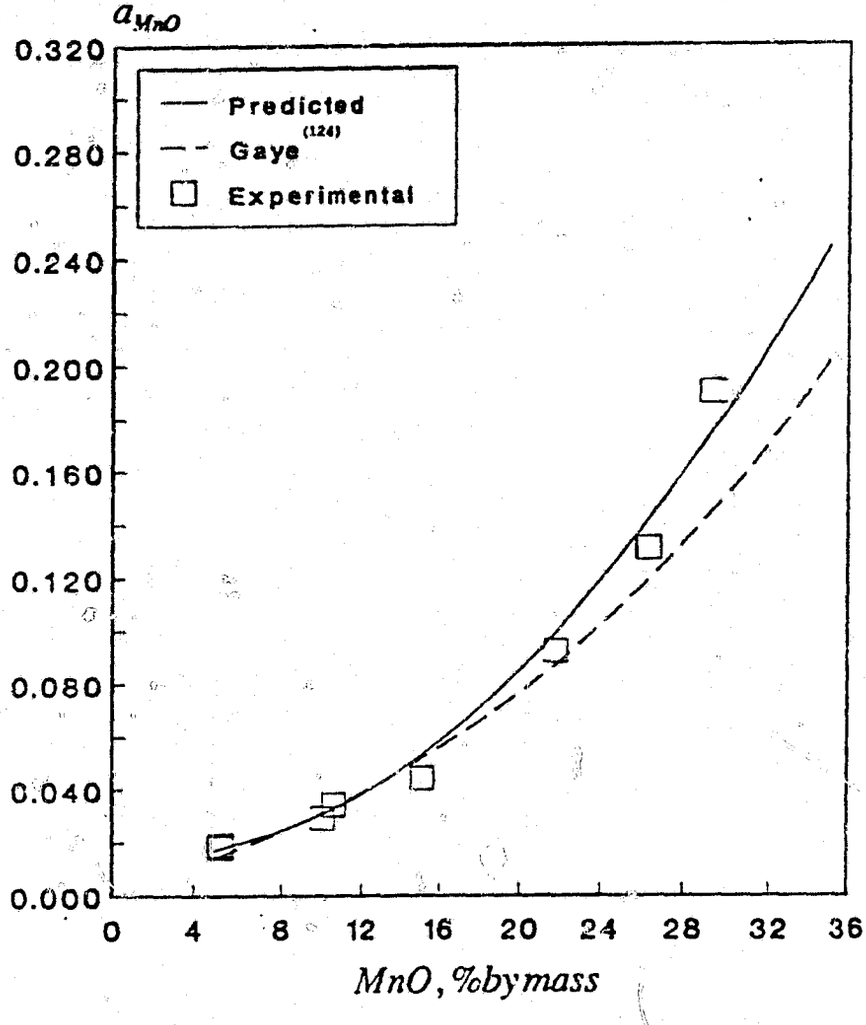

Figure C.12. Activities of MnO in $MnO-CaO-MgO-SiO_2-Al_2O_3$ slags at 1500°C, B=0.90±0.05, CaO:MgO=2.06±0.06, % Al_2O_3=5, optical basicity=0.68.

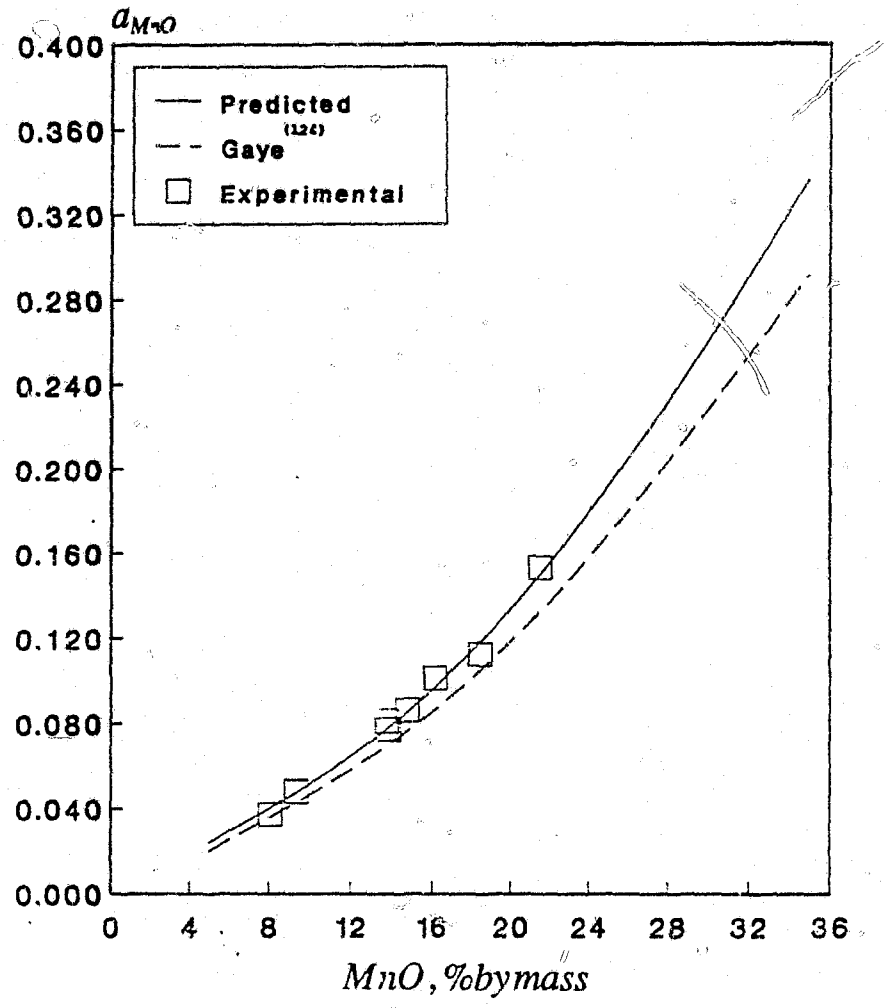

Figure C.13. Activities of MnO in MnO-CaO-MgO-SiO_2-Al_2O_3 slags at 1500°C, B=1.15±0.03, CaO:MgO=1.59±0.04, % Al_2O_3=5, optical basicity=0.69.

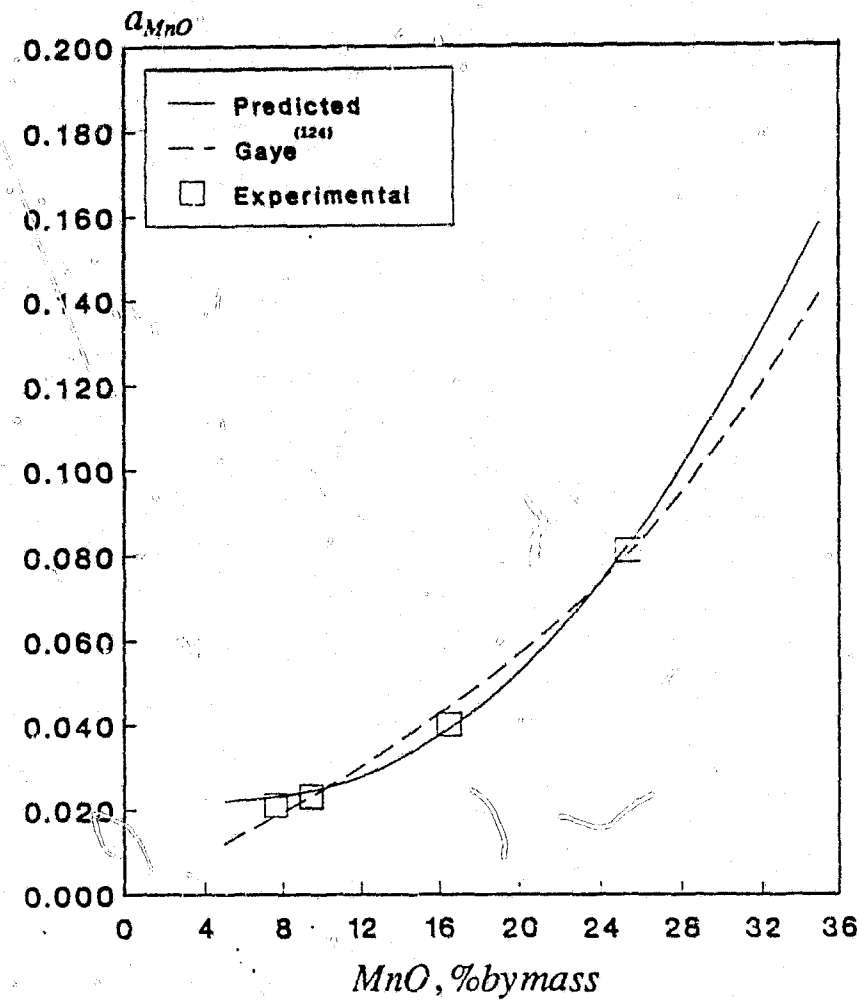

Figure C.14. Activities of MnO in $MnO-CaO-MgO-SiO_2-Al_2O_3$ slags at 1500°C, B=0.68±0.04, CaO:MgO=5.66±0.05, % Al_2O_3=5, optical basicity=0.66.

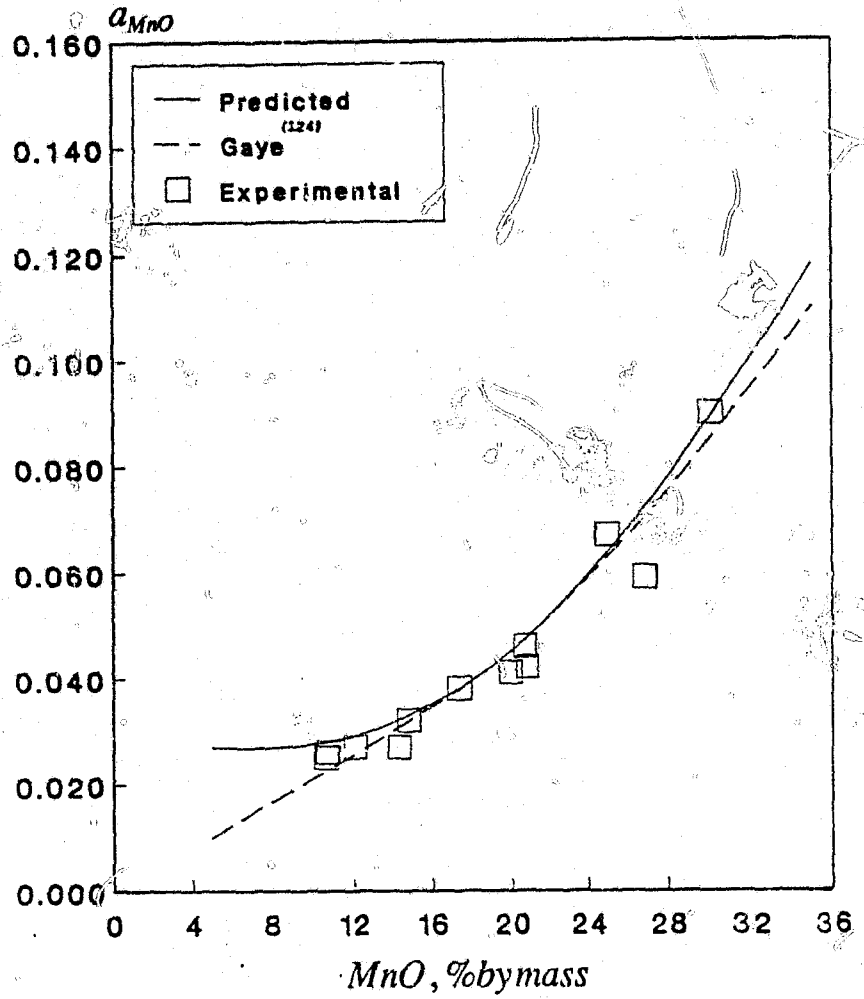

Figure C.15. Activities of MnO in $MnO-CaO-MgO-SiO_2-Al_2O_3$ slags at 1500°C, B=0.56±0.05, CaO:MgO=3.45±0.06, % Al_2O_3=5, optical basicity=0.66.

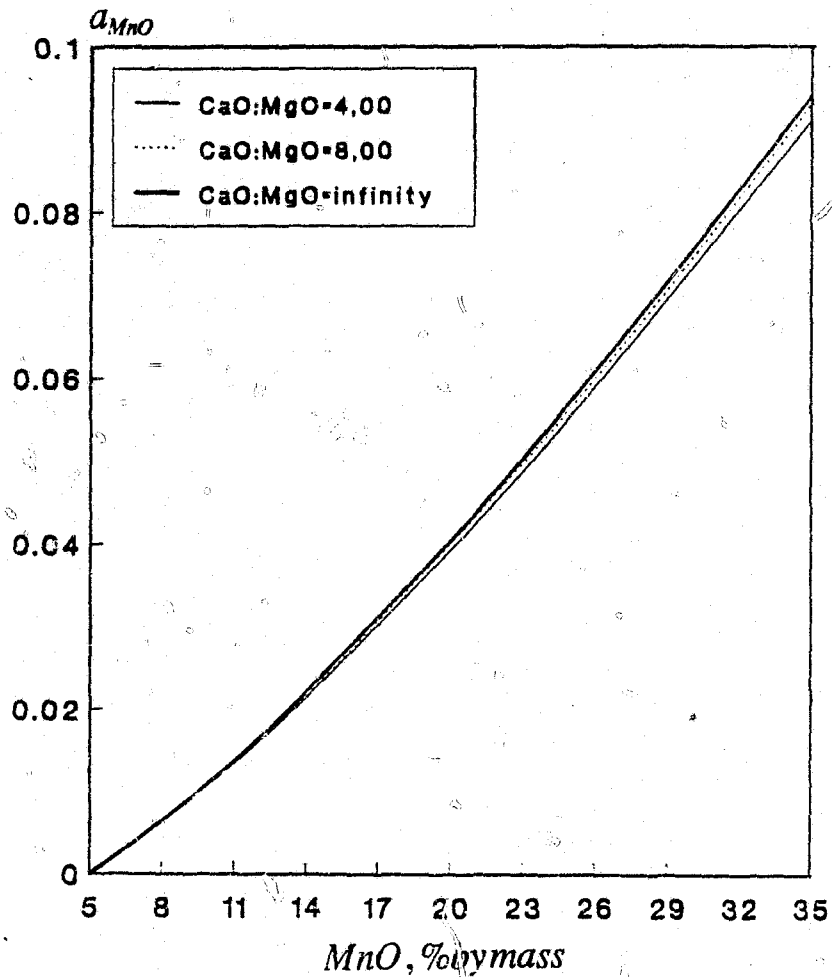

Figure C.16. Activities of MnO in $MnO-CaO-MgO-SiO_2-Al_2O_3$ slags at 1500°C for various CaO-to-MgO ratios with B=0.40.

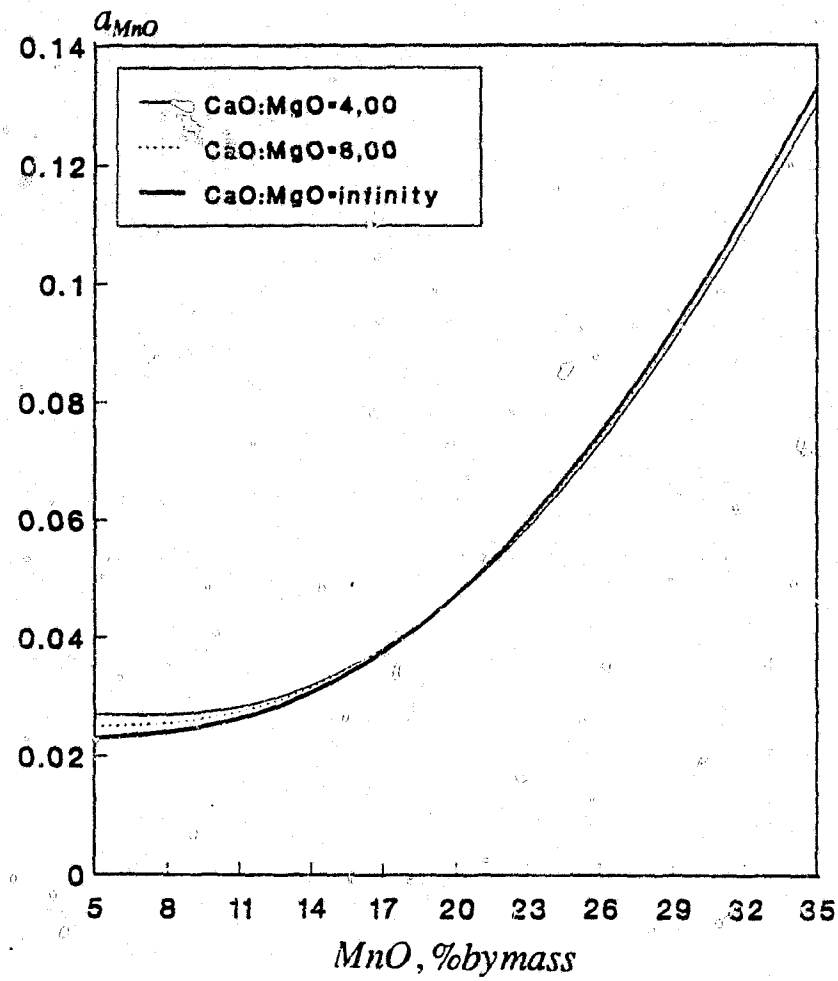

Figure C.17. Activities of MnO in $MnO-CaO-MgO-SiO_2-Al_2O_3$ slags at 1500°C for various CaO-to-MgO ratios with B=0.60.

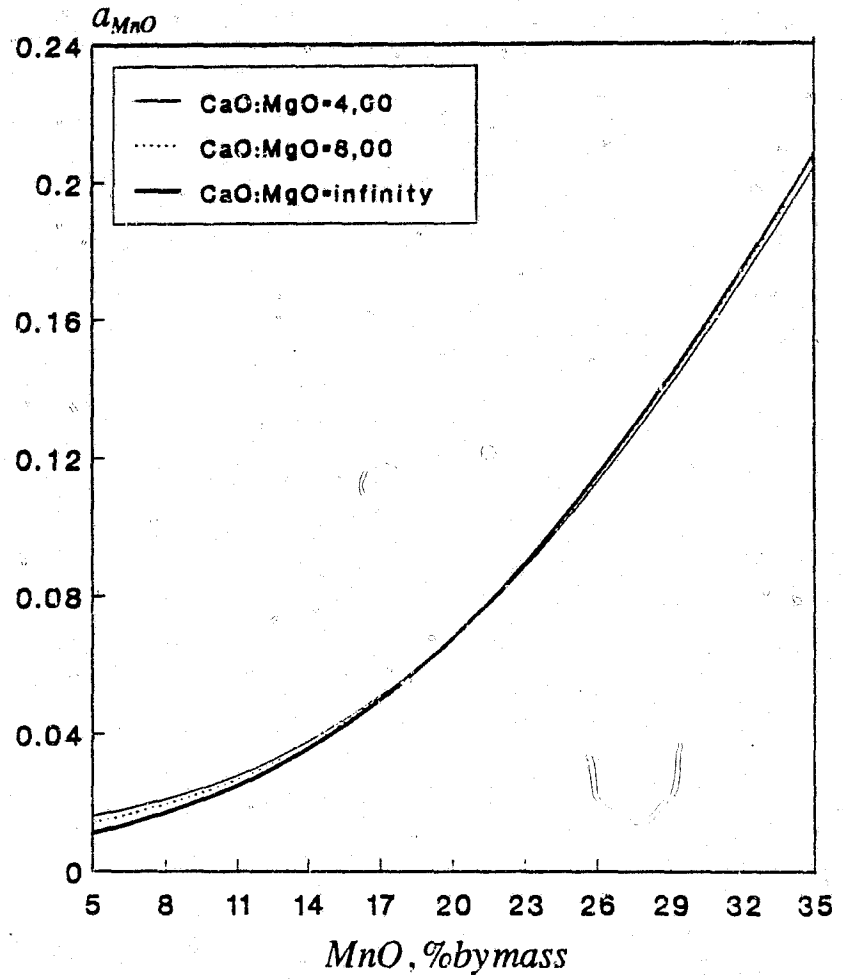

Figure C.18. Activities of MnO in MnO-CaO-MgO-SiO_2-Al_2O_3 slags at 1500°C for various CaO-to-MgO ratios with B=0.80.

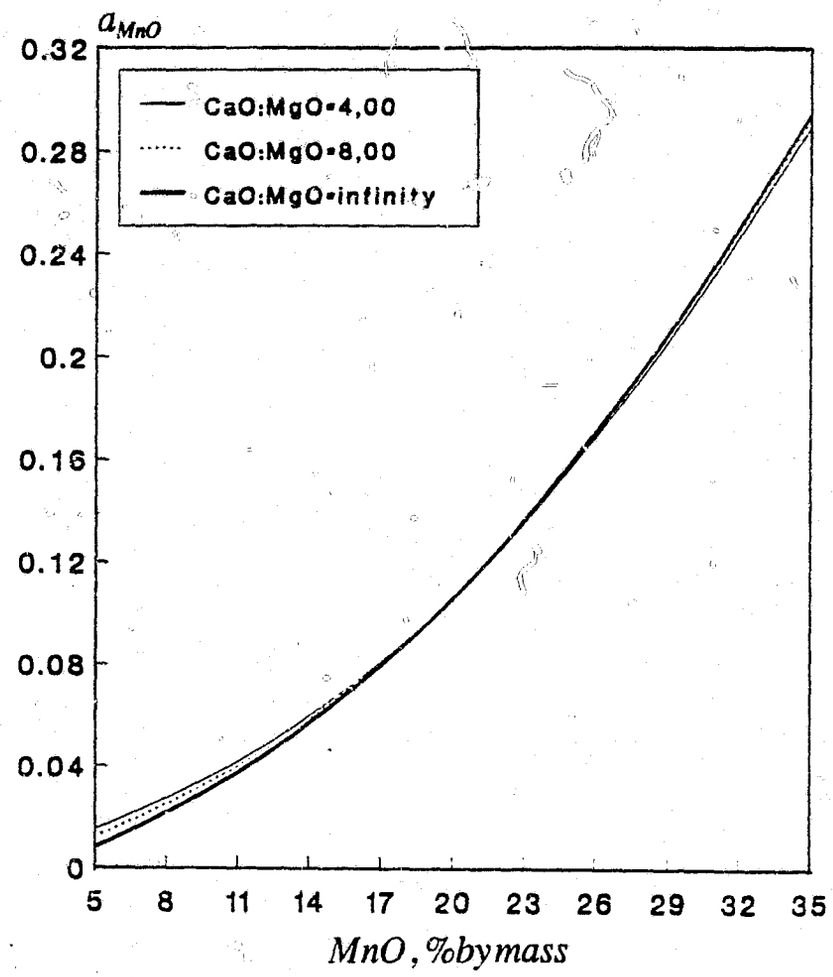

Figure C.19. Activities of MnO in MnO-CaO-MgO-SiO_2-Al_2O_3 slags at 1500°C for various CaO-to-MgO ratios with B=1.00.

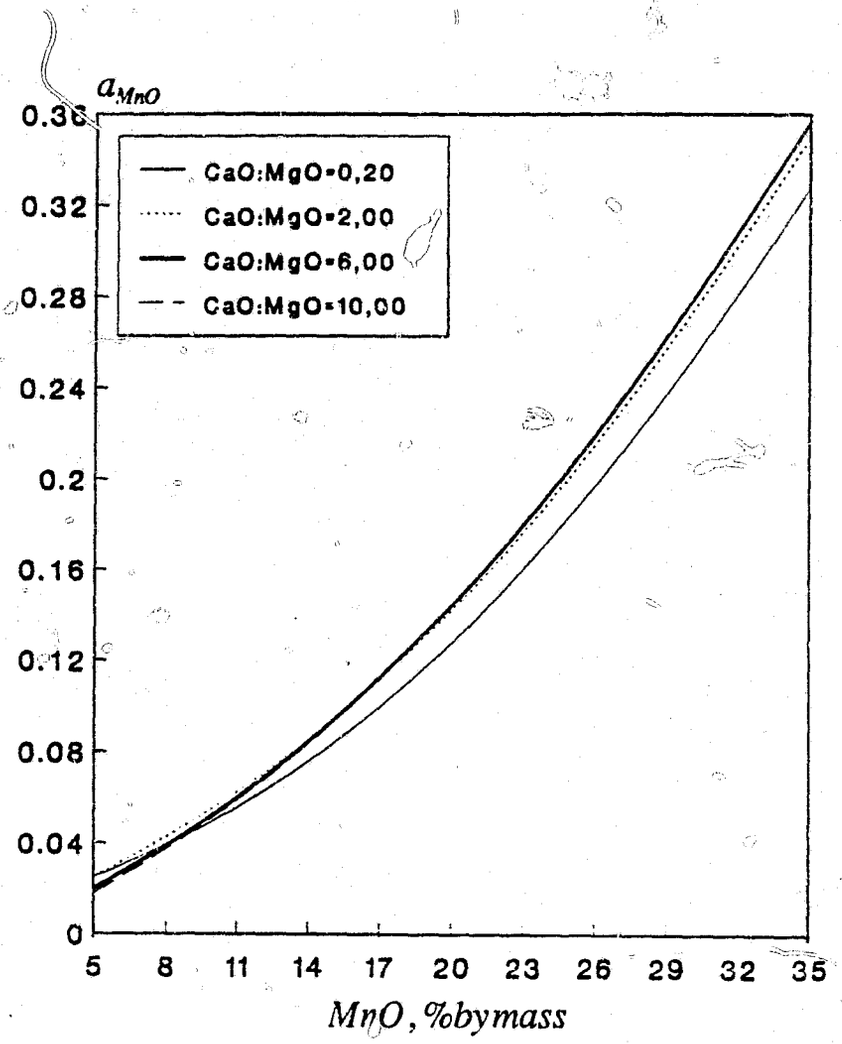

Figure C.20. Activities of MnO in $MnO-CaO-MgO-SiO_2-Al_2O_3$ slags at 1500°C for various CaO-to-MgO ratios with B=1.20.

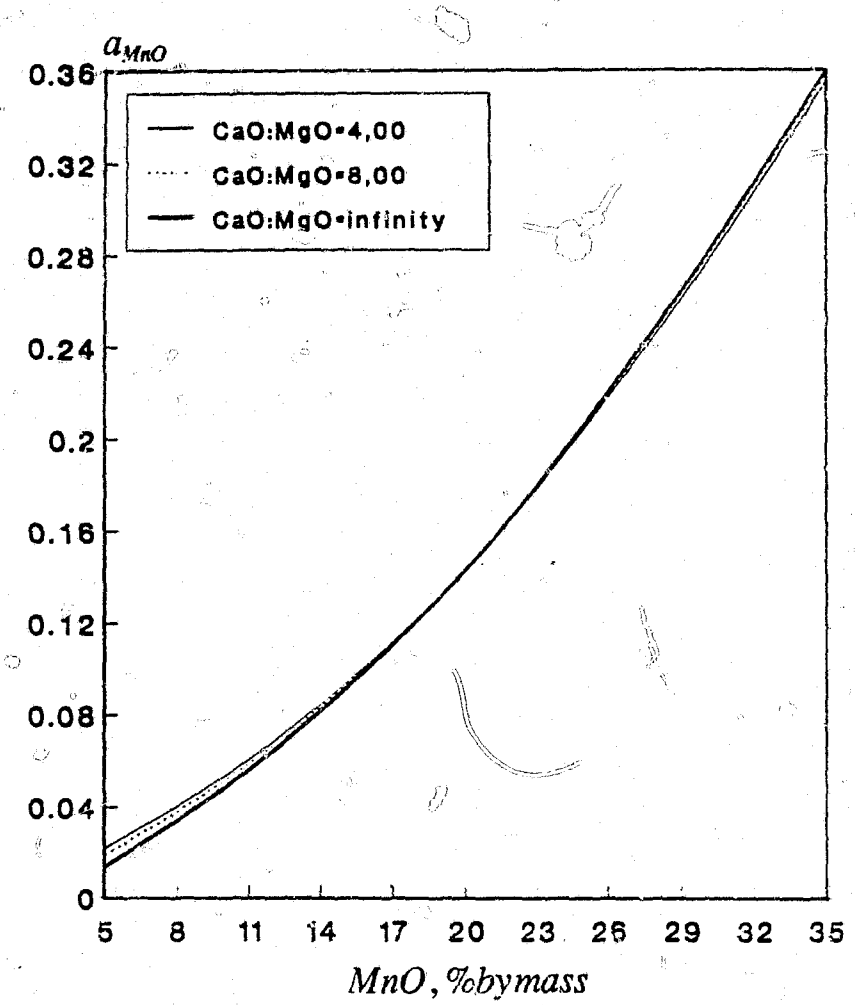

Figure C.21. Activities of MnO in $MnO-CaO-MgO-SiO_2-Al_2O_3$ slags at 1500°C for various CaO-to-MgO ratios with B=1.20.

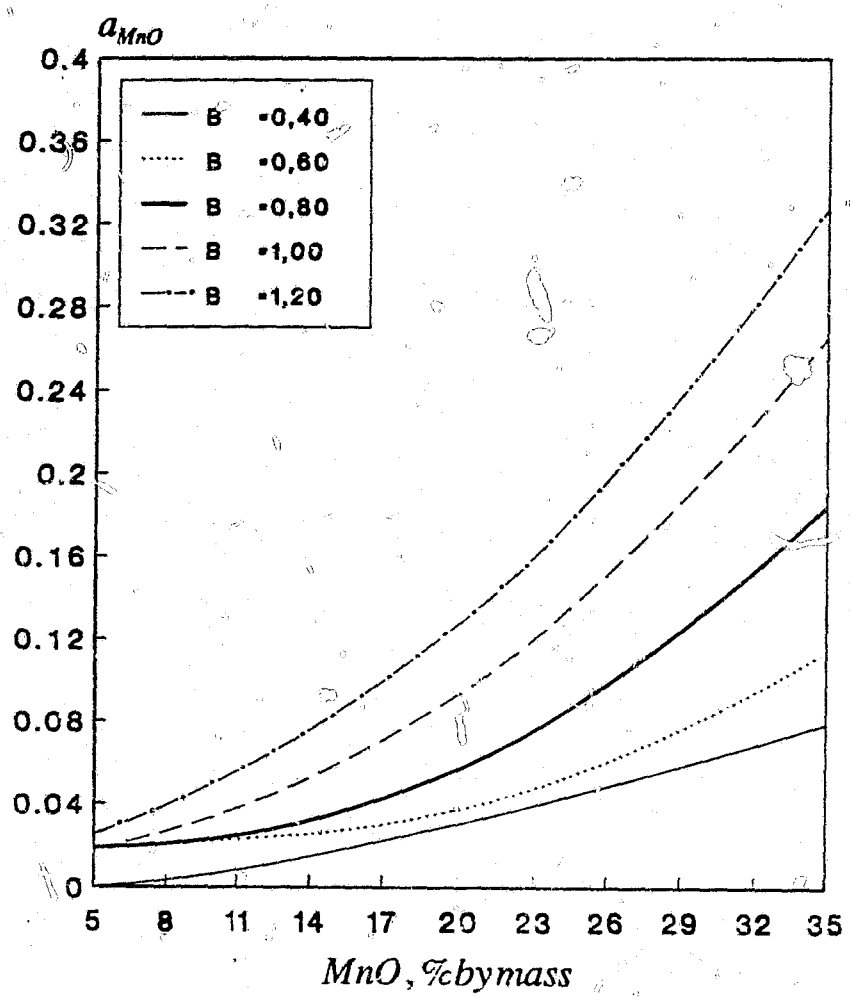

Figure C.22. Activities of MnO in $MnO-CaO-MgO-SiO_2-Al_2O_3$ slags at 1500°C for various basicity ratios with CaO:MgO=8.00.

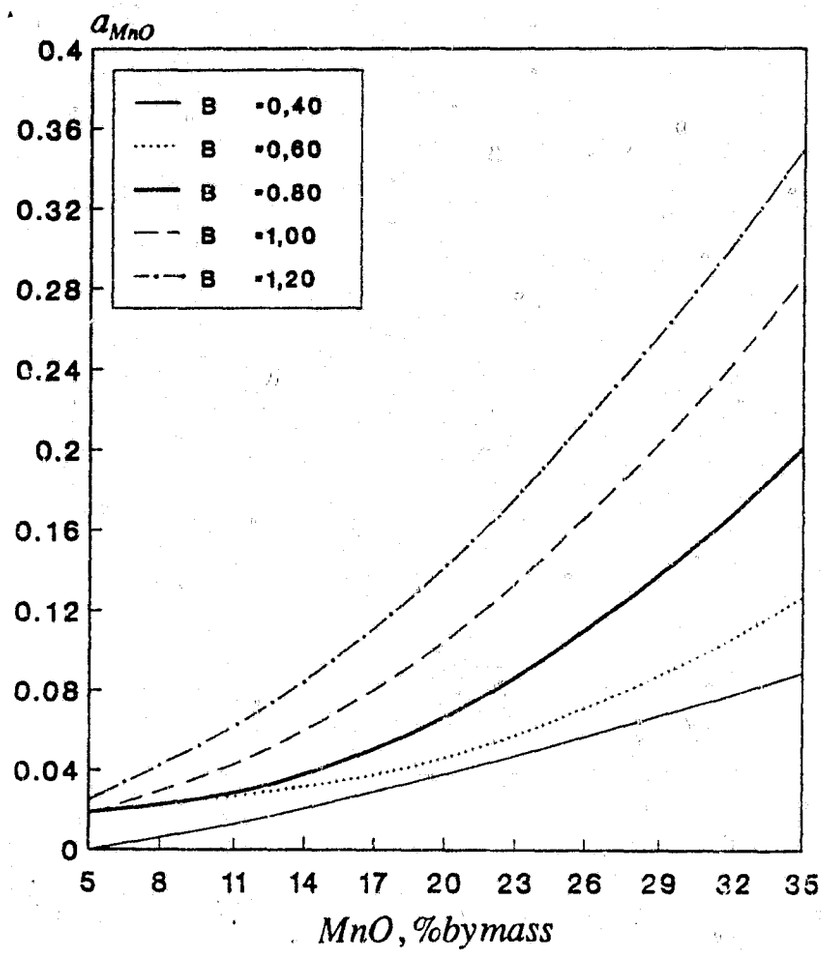

Figure C.2. Activities of MnO in $MnO-CaO-MgO-SiO_2-Al_2O_3$ slags at 1500°C for various basicity ratios with CaO:MgO=10.00.

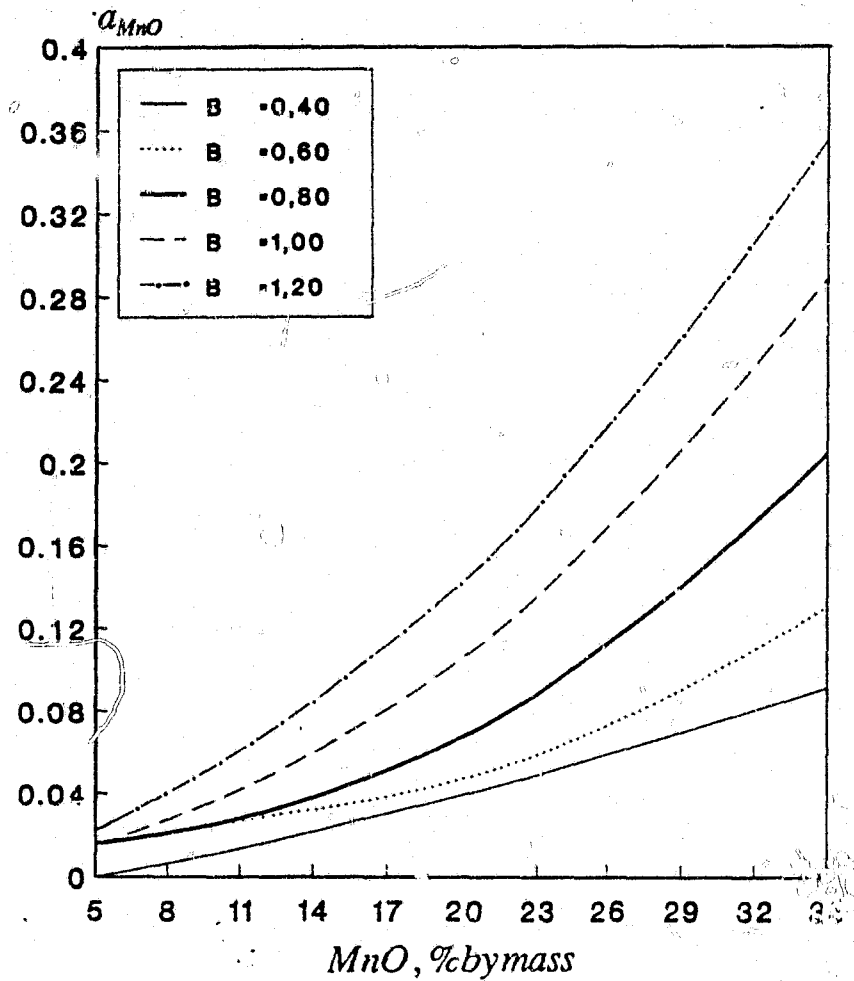

Figure C.24. Activities of MnO in MnO-CaO-MgO-SiO_2-Al_2O_3 slags at 1500°C for various basicity ratios with CaO:MgO=∞.

APPENDIX D Graphical representation of slag-metal equilibria

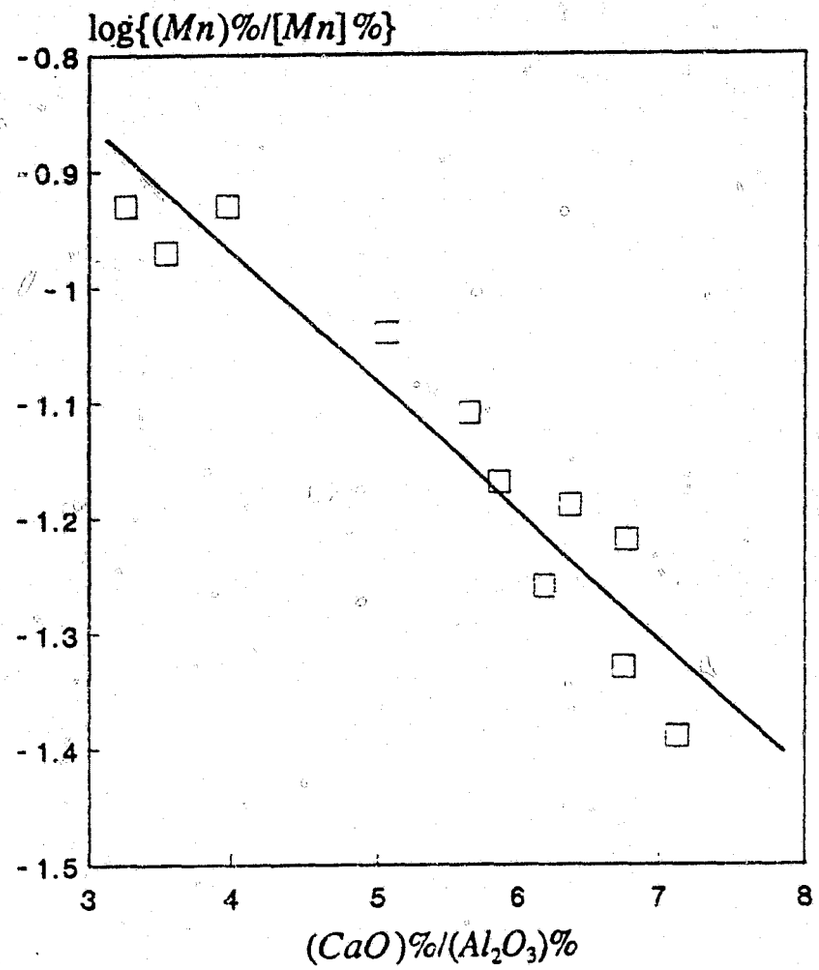

Figure D.1. The effect of the CaO-to-Al_2O_3 ratio of the slag on manganese distribution with Si:Fe≅0.18 in the metal phase at 1500°C under CO atmosphere.